INVESTIGATING THE BIOLOGICAL FUNCTIONS OF THE PROTEIN KINASE WNK1 IN THE REGULATION OF CYTOSKELETAL STRUCTURES AND MEMBRANE TRAFFICKING

APPROVED BY SUPERVISORY COMMITTEE

Melanie H. Cobb, Ph. D.

Katherine Luby-Phelps, Ph. D.

Joseph P. Albanesi, Ph. D.

Luke M. Rice, Ph. D.

DEDICATION

There are many people I would like to express my gratitude to during my study in the United States. First, my mentor, Dr. Melanie Cobb, has always guided me and gave me a lot of support through the entire study. Without her, I will not be able to achieve what I have accomplished today. Second, I would like to express my gratitude to Dr. Kate Luby-Phelps. She has been leading and instructing me for live cell image and microscopy in the past 5 years. I truly thanks for her guidance and help for more than half of data presented in this dissertation. Finally, I also want to thanks Dr. Joseph Albanesi and Dr. Luke Rice for their suggestion and correction for my research and dissertation.

Dr. Wei Chen and so many other lab members' daily help also made this dissertation become possible. Finally, I would like to say thanks to my friends in Dallas and my family in Taiwan for all their love and support. Without their help, I will not have such memorable journey in the United States.

INVESTIGATING THE BIOLOGICAL FUNCTIONS OF THE PROTEIN KINASE WNK1 IN THE REGULATION OF CYTOSKELETAL STRUCTURES AND MEMBRANE TRAFFICKING

by

SZU-WEI TU

DISSERTATION

Presented to the Faculty of the Graduate School of Biomedical Sciences

The University of Texas Southwestern Medical Center at Dallas

In Partial Fulfillment of the Requirements

For the Degree of

DOCTOR OF PHILOSOPHY

The University of Texas Southwestern Medical Center at Dallas

Dallas, Texas

August, 2013

INVESTIGATING THE BIOLOGICAL FUNCTIONS OF THE PROTEIN KINASE WNK1 IN THE REGULATION OF CYTOSKELETAL STRUCTURES AND MEMBRANE TRAFFICKING

Publication No. _____

Szu-wei Tu, Ph. D.

The University of Texas Southwestern Medical Center at Dallas, 2013

Supervising Professor: Melanie H. Cobb, Ph. D.

Abstract: With No Lysine (WNK) 1, a serine/threonine kinase, is a unique kinase to its catalytic lysine residue at a non-canonical position relative to all other kinases. Characterization of endogenous WNK1 distribution by immunofluorescence reveals a perinuclear punctate pattern. I have investigated this perinuclear distribution and how it might relate to the biological functions of WNK1 from two aspects. First, I investigated cytoskeletal structures mainly focused on the microtubules. WNK1 localized on mitotic

spindles during mitosis as well as interphase microtubules. Depletion of WNK1 caused aberrant mitotic spindles, chromosomes and defect of abscission. In interphase cells, disruption of radiating microtubules from microtubule organization center was observed. Centrosomal structure was impaired. Cells showed a migratory defect. Clues from a former student and my mass spectrometry data suggested that dynein and its associated protein-dynactin, centrosomal protein of 70 and 170 kDa might be potential interactors mediating microtubule related phenotypes. Second, I examined WNK1 and membrane trafficking events. Depletion of WNK1 caused higher amount of epidermal growth factor receptors remained at the later step of endocytosis. Lysosomes and lysosome-related organelles were disrupted. Biochemical assay suggested that WNK1 could associate with active Rab 6 or 7 effector complexes. I have identified that the homotypic fusion and vacuole protein sorting (HOPS) complex, one of Rab7 effector complexes could interact with WNK1. Mass spectrometry results showed that WNK1 could pull down clathrin heavy chain and adaptor protein complex-3 (AP-3) β subunit. AP-3 vesicles are also HOPS complex-mediated vesicular trafficking between the Trans-Golgi network and late endosomes. Co-localization analysis suggested that WNK1 co-localized with AP-3 in a high pearson correlation coefficient (0.53). Depletion of WNK1 showed defect of the maturation of autophagosomes. Taken together, WNK1 might affect membrane trafficking through HOPS complex-mediated homotypic (the assembly of phagophores) and heterotypic (late endosomes and lysosomes) membrane fusion.

TABLE OF CONTENTS

PRIOR PUBLICATIONS

Tu SW, Bugde A, Luby-Phelps K, Cobb MH. WNK1 is required for mitosis and abscission. Proc Natl Acad Sci U S A. 2011 Jan 25;108(4):1385-90.

Sengupta S*, **Tu SW***, Wedin K*, Earnest S, Stippec S, Luby-Phelps K, Cobb MH. Interactions with WNK (with no lysine) family members regulate oxidative stress response 1 and ion co-transporter activity. J Biol Chem. 2012 Nov 2;287(45):37868-79.
* equal contribution

LIST OF FIGURES

LIST OF TABLES AND MOVIES

LIST OF ABBREVIATIONS

AI	autoinhibitory
AP-3	adaptor protein complex 3
ARC	Arthrogryposis, Renal Dysfunction and Cholestasis
AT1R	angiotensin II receptor
AtWNK8	Arabidopsis thaliana WNK8
BICD2	Bicaudal-D-2
CD	collecting duct
CDK2	cyclin - dependent kinase 2
Cep 170	Centrosomal protein of 170 kDa
Cep 70	Centrosomal protein of 70 kDa
CNT	connecting tubule
COP	coat protein complex
Co-Smads	common Smads
CS	cardiac steroids
DAG	diacylglycerol
DCT	distal convoluted tubule
DIC	dynein intermediate chain
E13	day 13 of embryonic development
EGF	epidermal growth factor

EGFR	epidermal growth factor receptor
ENaC	Epithelial sodium channel
ER	endoplasmic reticulum
ERK1	Extracellular signal-regulated kinase 1
ERK2	Extracellular signal-regulated kinase 2
Fray	Fly OSR1/SPAK ortholog
GAP	GTPase-activating protein
GLUT	glucose transporters
GPCR	G-protein-coupled receptor
HNF1	hepatocyte nuclear factor 1
HOPS	homotypic fusion and vacuole protein sorting
HPS	Hermansky-Pudlak syndrome
HSANII	hereditary sensory and autonomic neuropathy type II
IGF-1	insulin - like growth factor 1
IP_3	inositol-1,4,5-triphosphate
I-Smads	inhibitory Smads
KCC	K^+ Cl^- co transporter
KS-WNK1	kidney-specific form of WNK1 kinase
LC8	dynein motor protein light chain
LPA	lysophosphatidic acid

M6PR	Mannose-6-phosphate-receptor
MAP2K	Mitogen - activated protein kinase kinase
MAP3K	MAPK kinase kinase
MAP4K	MAPK kinase kinase kinase
MAPK	Mitogen - activated protein kinase
MBP	myelin basic protein
MEK1/2	MAP/ERK kinases 1 and 2
miRs	microRNAs
MTOC	microtubule organization center
MVB	multivescular body
NCC	Na^+ Cl^- co- transporter
Nedd 4-2	Neural precursor cell-expressed developmentally down-regulated gene 4-2
NKCC	Na^+ K^+- $2Cl^-$ co transporter
ORP1L	oxysterol-binding protein (OSBP)-related protein 1L
OSR1	oxidative stress responsive1
PAK1	p21- activated kinase 1
PAS	Periodic acid-Schiff
PASK	proline-alanine-rich Ste20-related kinase
PCT	proximal convoluted tubules
PF2	a second region conserved in PASK and Fray

PHAII	Pseudohypoaldosteronism type II
PI3K	Phosphatidylinositol 3-kinase
PI4K	phosphatidylinositol- 4 kinase
PIP_2	Phosphatidylinositol 4,5-bisphosphate
PKA	cAMP- dependent protein kinase
PKB	protein kinase B
PKC	protein kinase C
PLC β	Phospholipase C β
PLKs	Polo-like kinases
RILP	Rab7-interacting lysosomal protein
ROMK	Renal outer medullary potassium channel
RPE1	retinal pigment epithelial cell line
R-Smads	receptor-activated Smads
SCC	squamous cell carcinoma
SGK1	Serum - and glucocorticoid-induced protein kinase 1
SH 3	Src homology 3
SLC12	solute carrier 12
SM	Sec1/Munc18
SNAREs	soluble N-ethylmaleimide-sensitve factor attachment protein receptors
SOK1	Ste20/oxidant stress response kinase-1

SPAK	Ste20-related proline- alanine-rich protein kinase
Syt 2	synaptotagmin 2
TAL	thick ascending loop of Henle
TBC1D4	Tre-2/USP6-BUB2/Cdc16 Domain family member 4
TGFβ	Transforming growth factor beta
TGN	Trans-Golgi network
TRPC6	transient receptor potential cation channel, subfamily C, member 6
TRPV5	transient receptor potential vanilloid 5 channel
VAMP	vesicle-associated membrane protein
V-ATPase	vacuolar ATPase
VPS	vacuole protein sorting
WNK	With No Lysine

CHAPTER 1

INTRODUCTION

WNK1 is a serine/threonine protein kinase discovered and cloned by Xu et al, 2000 (*1*). It was found using a degenerate primer in a screen for previously unknown members of the mitogen-activated protein kinase kinase (MAP2K) protein family from a rat cDNA library. Two of the resulting clones were similar to a protein kinase reported in a filamentous fungus. Alignment of the sequences of these newly identified kinase domains with other protein kinases domains revealed that the catalytic lysine residue in these enzymes was not in the canonical position. Mutagenesis of lysine residues in the N-terminal domain showed that the catalytic lysine was located in the phosphate anchor ribbon (kinase subdomain I) rather than in beta strand 3 (subdomain II), the position of the catalytic lysine in all other members of the eukaryotic protein kinase (ePK) superfamily. Hence, these enzymes were named "With No Lysine" (WNK) 1 and 2 due to this atypical lysine position. Further cloning and analysis of human WNK protein kinases was performed by Verissimo et al, 2001 (*2*), showing that there were at least 4 human WNK protein kinases located on different chromosomes (Table1-1). Database homology searching of the WNK kinase domain sequence further revealed that WNK protein kinases also existed in *C. elegans, Drophophila*, and plant but not *Saccharomyces* (*1, 2*). Table 1-2 summarizes some of the WNKs currently known in multi-cellular organisms in the NCBI database. The WNK protein kinases are categorized in the human kinome tree as a distinct branch distinct from the MAP2Ks (Ste branch) that were originally sought (*3*).

The first demonstration of relevance of WNKs gene to human health came from Wilson et al, 2001 (*4*) in a study of an inherited form of hypertension (pseudohypoaldosteronism type II,

Table 1-1

gene	genomic DNA length (base pairs)	chromosome location	number of exons
WNK1	158530	12p13.3	32
WNK2	135643	9q22.3	29
WNK3	165820	Xp11.22	24
WNK4	16436	17q21.31	19

Table 1-2

Species	number of WNK genes reported	note
Homo sapiens	4	human
Mus musculus	4	mouse
Rattus norvegicus	4	rat
Drosophila melanogaster	1	fly
Caenorhabditis elegans	1	worm
Arabidopsis thaliana	9	plant
Chlamydomonas reinhardtii	1	green alge with flagella
Giardia lambia	1	a flagellated protozoan parasite

Table 1-1: Summary of the genomic structures of human WNK genes

Table 1-2: Summary of WNK genes in a few selected multi-cellular organisms in NCBI database.

PHAII). Patients often presented with hypertension, hyperkalemia and metabolic acidosis. Through genome wide analysis of linkage, mutations in WNK1 and WNK4 genes were identified as the cause of the disease. Deletions within the first intron of the WNK1 gene increased the expression of WNK1 transcripts. Four missense mutations were found in WNK4 protein coding sequences. More recently, mutations in two additional genes, Kelch-like3 or cullin 3, were also found to cause PHAII (*5, 6*). These two proteins are components of a cullin-RING E3 ligase complex responsible for ubiquitylation-mediated proteolysis (*7*). The link to hypertension suggested the possibility of the involvement of WNK protein kinases in the regulation of ion transports. A wealth of literature regarding WNKs and downstream ion co-transporter effectors will be reviewed later. In addition to ion co-transporters, there are several other cellular signaling pathways and activities reported to involve WNKs, including phosphatidylinositol 3-kinases (PI3Ks), mitogen-activated protein kinases (MAPKs), the transforming growth factor beta (TGFβ) signaling pathway, endocytosis, exocytosis, cell proliferation and migration, angiogenesis and heart development. Here I will review the expression of WNK genes and the structures of WNK protein kinases, followed by more detailed information on proposed roles of WNKs in cellular signaling pathways and activities.

The expression pattern of WNK genes in different tissues

The genomic structure of human WNK1 was first described and identified as containing 28 exons by Verissimo et al., 2001 (*2*). The immediate comparison between the rat WNK1 cloned by Xu et al. (*1*) and the human WNK1 gene revealed the absence of exons 11 and 12 in the rat WNK1 DNA. The WNK1 protein kinase form studied throughout the entire dissertation will be the rat WNK1 protein which is known as rat WNK1 isoform 3 in the NCBI database. The expression of WNK1 mRNA was examined by multiple tissue Northern blot analysis by several

groups (*1, 2, 8, 9*), showing wide distribution in kidney, heart, testis, muscles, lymphocytes, and brain. An alternative internal promoter encoding a kidney-specific form of WNK1 kinase (KS-WNK1) was found by two groups (*9, 10*). KS-WNK1 is a kinase-defective form and expressed highly in the distal convoluted tubule (DCT). The internal initiation site generating KS-WNK1 creates a new 4a exon which is different from the original exon 4 reported in Verissimo et al. (*2, 10*).

A recent comprehensive study of all WNK1 alternative splice variants by RT-QPCR was performed (*11*). A diagram representing the proximal promoter and initiation site producing L-WNK1 and an alternative renal promoter which produces KS-WNK1 is shown in Fig.1-1 A. This study not only confirmed that KS-WNK1 is restricted in expression to the kidney, but also showed that KS-WNK1 is expressed 80-times more than L - WNK1 in the DCT. Splice sites were concentrated in three regions of the gene. Two of them had been reported before- exon 8b, HSN2 and 9 (*11, 12*) (shown in Fig. 1-1 B), exon 11 and 12 (*2, 9-11*) (shown in Fig.1-1 C) and one was a new finding - exon 26, 26a, and 26b (shown in Fig. 1-1 D) reported in Vidal-Petiot et al (*11*). The finding of the splice variant containing exon HSN2 came from a study of hereditary sensory and autonomic neuropathy type II (HSANII) (*12*). HSANII is an inherited autosomal recessive disease. Patients present with clinical symptoms including loss of perception to pain, touch, and heat due to a loss of peripheral sensory nerves. WNK1 has been reported to be a cause of PHAII; the study of HSANII by Shekerabi et al. (*12*) reported a second inherited disease caused by mutations of the WNK1 gene. Specific neuronal WNK1-8b-HSN2 transcripts were found. Though the WNK1-8b-HSN2 transcript was characterized as a neuronal specific form, Vidal-Petiot et al. detected this transcript by RT-QPCR in other tissues including kidney, aorta, colon and lung.

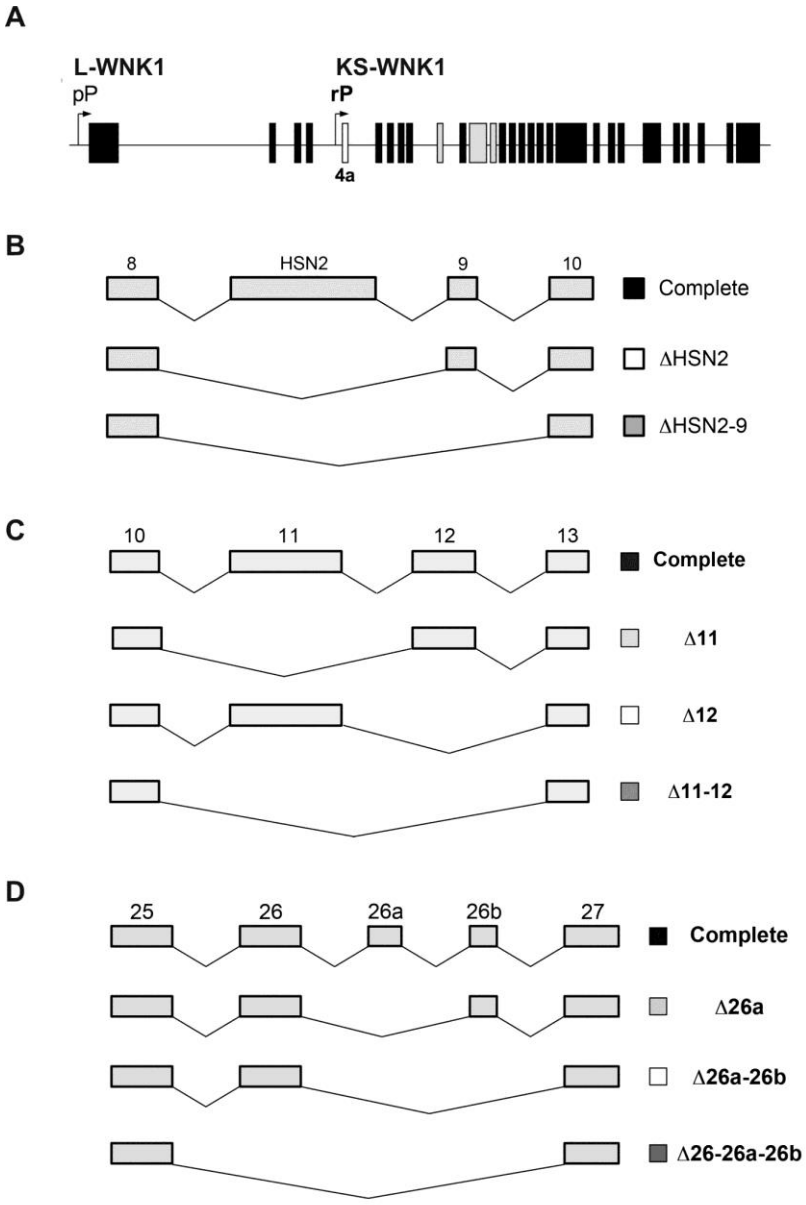

Figure 1-1. Summary of WNK1 isoforms generated by alternative splicing events and an internal initiation site for KS-WNK1.

Figure 1-1 is from Vidal-Petiot E, Cheval L, Faugeroux J, Malard T, Doucet A, et al. (2012) A New Methodology for Quantification of Alternatively Spliced Exons Reveals a Highly Tissue-Specific Expression Pattern of WNK1 Isoforms. PLoS ONE 7(5): e37751.

Figure 1-1 A, B, C and D corresponds to Figure 1A, 2A, 3A and 4A respectively shown in the study of Vidal-Petiot et al. See text for the description.

Exons 11 and 12 were also found alternatively spliced (*9, 10*). The re-examination of three splice variants- Δ 11, Δ12 and Δ11 and 12 (*11*) suggested that each variant was specific to certain tissues. The splice variant containing exons 11 and 12 was only found in heart, skeletal muscle and neural tissues. The Δ11 and 12 variant was the predominant form in aorta. And the Δ11 was a major isoform in the kidney. Δ12 was a rare splice variant in all tissues. The third newly identified alternatively spliced exons found by Vidal-Petiot et al. (*11*) were exons 26a and 26b. Exons 26a and 26b lie within the region of intron 26. This rare splice variant was only expressed in neural tissues and skeletal muscle. While exon 26b can be present alone in the central nervous system, exon 26a is only found together with 26b. The abundance of WNK1 alternative splice variants and their specific tissue distribution suggested that WNK1 may perform different functions through its variants in different physiological settings. The most commonly used cDNA encoding WNK1 is the one isolated by Xu et al. (*1*), a Δ11 and 12 isoform. This isoform was found to be one of the two most widely expressed, along with the complete one (shown in Fig. 1-1 C). As for the expression of WNK2, 3 and 4, little study of alternative splice variants was reported. It has been shown that WNK2 was widely expressed while WNK4 was highly expressed in the kidney (*10*, *13*). There were two splice variants of WNK3 gene expressed in the brain and the expression of WNK3 could be detected in the kidney, neuron, placenta and lung (*14*).

The structures of WNK protein kinases

There are WNK genes in human and at least 8 isoforms for WNK1 (*2, 11*). The protein length ranged from the longest one- WNK1 isoform (2833 amino acids) to the smallest one- WNK4 (1243 amino acids). There is only one WNK but at least 11 and 7 isoforms in *C.elegans* and *Drosophila* respectively. The protein length for *C. elegans* is about 1600 to 1800 amino

acids and about 2400 amino acids in *Drosophila*. In *Arabidopsis*, there are nine WNKs comprising a variety of shorter protein lengths ranging from 490 to 660 amino acids. The most conserved domain in WNK protein kinases is the kinase domain. By using rat WNK1 kinase domain residues 194 to 483 as a query sequence in NCBI Blastp program against human WNK1 to 4 and *Arabidopsis thaliana* WNK8 (AtWNK8), the identity was about 80 to 100 % among rat and human WNKs but a bit lower in *Arabidopsis* (53%) (Fig. 1-2). I compared AtWNK8 because of a study showing that WNK8 could bind and phosphorylate the vacuolar ATPase (*15*), which was related to the mass spectrometry data I obtained for WNK1 interactors. In addition to the kinase domain, an autoinhibitory (AI) segment found by Xu et al. (*16*) C-terminal to the kinase domain was also conserved among WNKs from human, rat, *C. elegans* and *Arabidopsis*. Rat WNK1 residue 490 to 550, previously defined as an AI segment (X. Min - dissertation) is identical to human WNK1, about 60% identical to human WNK2, 3 and 4 and a lower 37% identity with AtWNK8 (Fig. 1-2). Further analysis using the coils program and the information from Xu et al. and X. Min's dissertation suggested several putative coiled-coil regions. Rat WNK1, human WNK1 and WNK4 have a coiled-coil region following the conserved kinase and an autoinhibitory segment. Near the C terminus, lie a string of PxxP motifs and another coiled-coil region. In contrast, human WNK2, 3 and AtWNK8 apparently lack a coiled-coil region C-terminal to the AI segment. However, there was a common coiled-coil region at the end of the C-terminus for all WNKs. Human WNK2 contains the largest number of PXXP motifs between the AI and the coiled-coil region at the C terminus, whereas WNK3 and AtWNK8 possess almost no predicted PxxP motif (Fig. 1-2).

The kinase domain

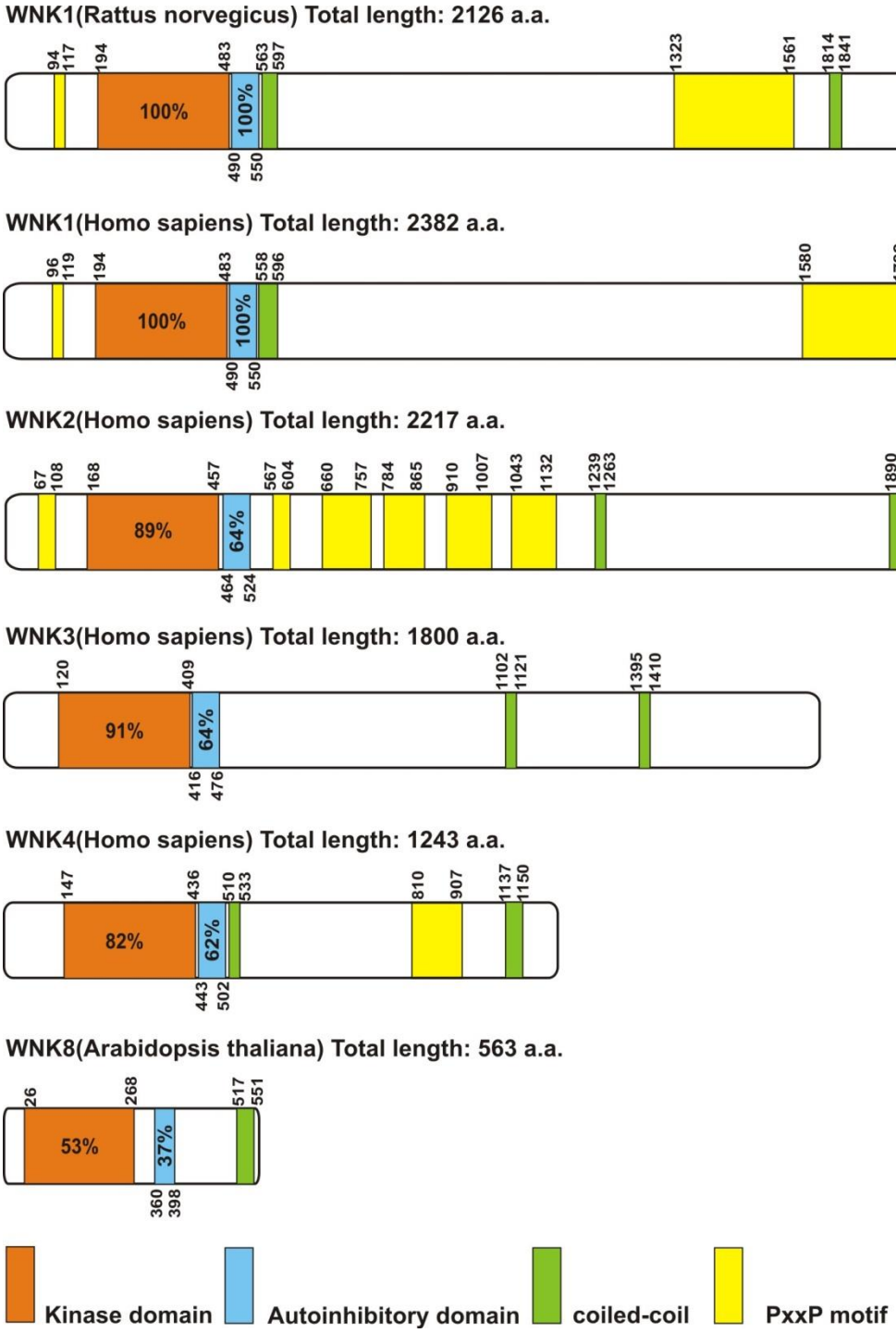

Figure 1-2. Schematic representation of the domain structures of WNK protein kinases among rat, human and plant. See next page for the legend.

The sequences used are AAF74258 (Rat WNK1), NP_061852 (human WNK1), NP_006639 (human WNK2), NP_065973 (human WNK3), NP_115763 (human WNK4) and NP_568599 (Arabidopsis WNK8). The coiled-coil regions and the PxxP motif are predicted by Coils and motif scan programs respectively. See text for the detailed description.

The crystal structure of the WNK kinase domain has been solved in a low activity conformation (*17*). As mentioned above, although the catalytic lysine residue involved in ATP binding and phosphoryl transfer in WNKs was atypically located in beta strand 2, the initial biochemical characterization by Xu et al. (*1*) showed that WNK1 was a bona fide protein serine/threonine kinase. In vitro kinase assays using myelin basic protein (MBP) as a substrate and phosphoamino acid analysis suggested that the kinase domain of WNK was capable of phosphorylating MBP and phosphorylating itself (autophosphorylation) mainly on serine residues. Mutation of the putative magnesium binding residue, aspartate 368, to alanine (D368A) abolished kinase activity. Modeling of WNK1 onto the crystal structure of the catalytic subunit of cAMP-dependent protein kinase (PKA) revealed that all three lysine residues in the N-terminal domain (K233, 256, and 259) could have extended into the active site based on the model alone. Mutagenesis of C250, which occupies the canonical position for the catalytic lysine based on other members of the eukaryotic protein kinase superfamily, and the three lysine residues suggested that K233 was the catalytic residue in WNK1. A multiple sequence alignment of WNKs from other organisms (e.g., Phycomyces) showed conservation of the lysine residue at the position comparable to residue 233 in WNK1. The crystal structure solved by Min et al. (*17*) demonstrated that the side chain of the C250 was pointed away from the active site, whereas the side chain of the K233 was pointed toward the active site, consistent with functioning as the key catalytic residue (Fig. 1-3 A). The overall structure of the WNK kinase domain is similar to most other kinases, which contain two folding domains and a deep cleft between them (*18, 19*). The N terminal domain is associated with nucleotide binding and largely constituted by several anti-parallel beta sheets and an essential alpha helix, alpha C. The C terminal domain of the kinase is mainly helical in structure with beta strands involved in binding peptide substrates and catalysis

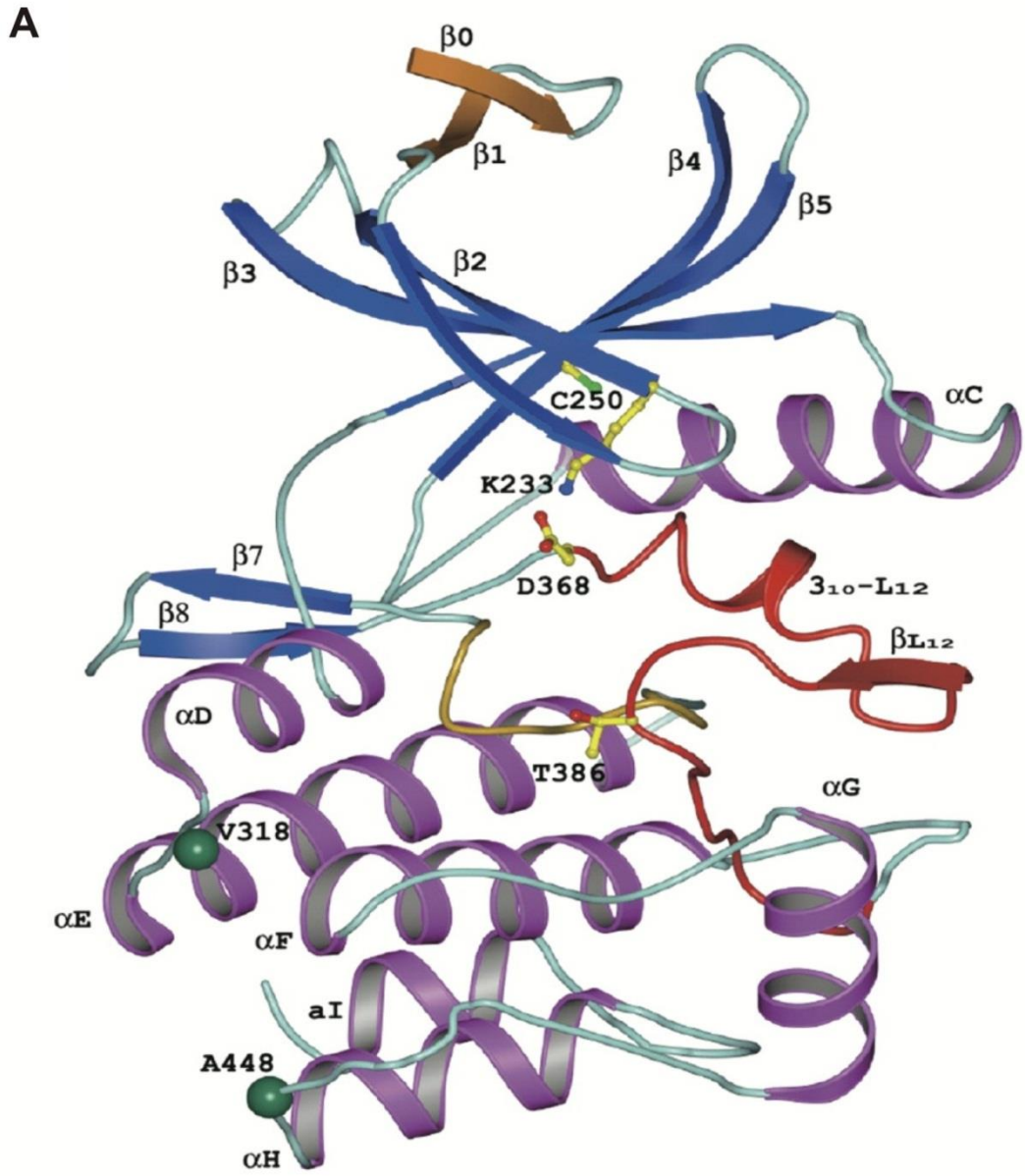

Figure 1- 3 A. The topology of the kinase domain.

Figure 1- 3 is from Min et al. (2004) Structure, Vol.12, p1303-1311 (used with permission from Elsevier). Figure 1- 3 A corresponds to Figure 1C shown in the study of Min et al. The key residues Cys-250, Lys-233, Asp-368 are shown in the ball-and-stick representation. The activation loop is shown in red and the extra N-terminal β strand is shown in Gold.

(*20*). In addition to the novel active site residue, a unique feature of the N terminus of the WNK1 kinase structure is that it contains a beta sheet with six rather than five beta strands, a common arrangement in other protein kinases. The additional beta strand allows the N terminus to form a nearly complete beta barrel (*17*). Because the structure obtained was in a low activity conformation, the activation loop of WNK1 was compared with the structure of a low activity conformation of cyclin-dependent kinase 2 (CDK2) (*21*). Min et al. showed that the N terminus of the activation loop containing a two-turn-310-helix displaced alpha helix C and E268 in that helix from the active site, thereby not forming the catalytic lysine (K233)-glutamate (E268) ion pair. This was a common feature also shown in the kinase structure of CDK2 (*21*). On the other hand, the C terminus of the activation loop adopted a unique inactive conformation, an extensive van der Waals contact with the linker region between helix F and G (Fig. 1-3 B). Finally, from examining the substrate binding site, the authors concluded that the P+1 residue was not a strong specificity determinant for WNK1. This contrasts with many protein kinases that derive some substrate specificity from the residue at the P+1 position; MAP kinases, for example, preferentially phosphorylate substrates containing proline in the P+1 site (*22*).

The autoinhibitory (AI) segment and autophosphorylation

The activity of protein kinases can be regulated by several different mechanisms, one of which is through the release of an autoinhibitory domain, which may sterically or allosterically inhibit the kinase domain. For example, p21-activated kinase 1 (PAK1), a serine/threonine protein kinase is activated by binding GTP- liganded Rac or cdc42 to the autoinhibitory domain in the N terminus of PAK1, thereby releasing the C terminal catalytic core from the inhibition (*23*). In the case of the WNK protein kinases, Xu et al. and X. Min examined N-terminal WNK1 fragments of different lengths and found that truncation near residue 490 resulted in greatly

B

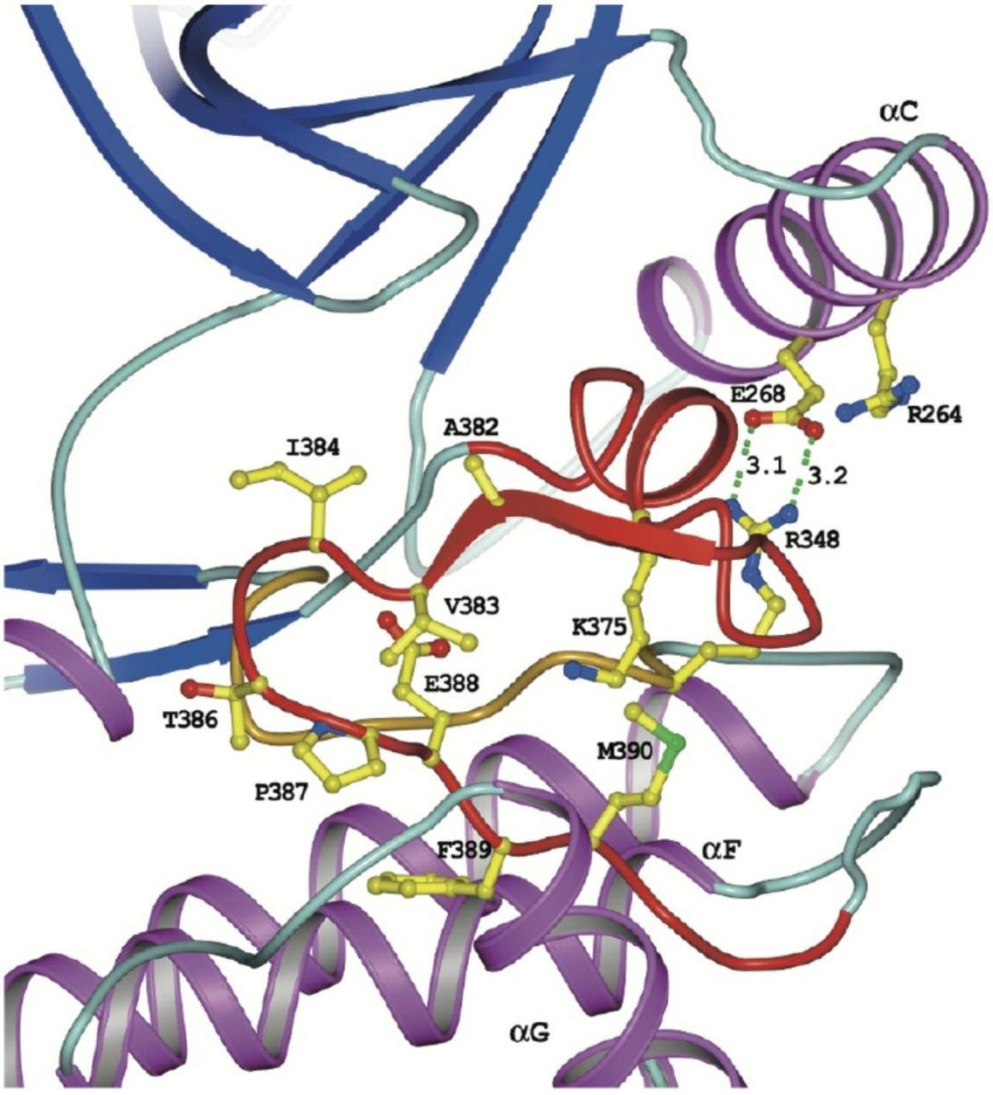

Figure 1- 3 B. The conformation of the C-terminus of the activation loop.

Figure 1- 3 B is from Min et al. (2004) Structure, Vol.12, p1303-1311 (used with permission from Elsevier). Figure 1- 3 B corresponds to Figure 4A shown in the study of Min et al. The C-terminus of the activation loop showed an extensive van der Waals contact with the linker region between helix F and G.

increased kinase activity. Thus, they tested fragments that followed residue 490 for inhibitory activity and found a 70 amino acid fragment, immediately C-terminal to the kinase domain, which can function as an autoinhibitory (AI) segment. The fragment with greatest AI activity was residues 485 to 555, numbers derived from the rat WNK1 protein sequence. The autoinhibitory functionality in this region of the protein will be referred to throughout as the AI. A second related sequence more C-terminal in the WNK1 sequence was found by X. Min in the Goldsmith laboratory (see dissertation) that also has autoinhibitory potential and is discussed further below in a different context. By iterative sequence analysis, Min and Xu proposed that the AI spanned residues 515-569 (*16*). They tested two conserved residues in this region, F524 and F526, important for inhibitory activity. The double mutant F524A/F526A lost inhibitory activity toward a kinase domain fragment of WNK1. The authors also found that if the fragment extended to the first coiled- coil region that followed the AI, the kinase activity was restored about 50%. This was an interesting observation given that human WNK2, WNK3 and Arabidopsis WNK8 apparently lack an adjacent coiled-coil region to the C-terminal AI segment (Fig. 1-2). The finding that WNK1 formed oligomers (*16, 24*) suggested the possibility of cross-regulation among the WNK protein family through the AI segment and hetero-oligomerization.

The solution structure of the AI segment of WNK1 has been solved recently (*25*). The authors concluded that the structure of the AI segment of WNK1 is similar to that of a binding site in a short noncatalytic domain of OSR1 (see below)- called the PF2, a second region conserved in PASK (another name for SPAK-see below) and Fray (the fly OSR1/SPAK ortholog). Two related protein kinases Ste20-related proline- alanine-rich protein kinase (SPAK) and oxidative stress responsive1 (OSR1) are substrates for WNK1. The PF2 domain of OSR1 binds to the RFXV motif(s) in WNK1. The AI segment of WNK1 can also bind RFXV peptides

with micromolar affinities. This raises the possibility that RFXV motifs of WNK1 may bind to its own AI (or AI-related) segment. A second interesting point made by Moon et al. (*25*) was that when they predicted the secondary structure of human WNK1 isoform 3, an additional autoinhibitory-like segment was found from residue 846 to 948, as previously suggested by X. Min. Residues 846 to 948 are only present in certain human WNK1 isoforms (3 and 4) but not others (e.g., 1 and 2). The sequence used in this dissertation was rat WNK1 isoform 3 which is approximately equivalent to human isoform 2.

As mentioned earlier, kinase activity may be regulated by multiple mechanisms. Autophosphorylation within the activation loop of the kinase domain increases WNK1 activity (*1*). By homology searching for the phosphorylation site of the activation loop of the MAP kinase, Xu et al. (*1*) found that two serine residues, S378 and S382 could be important for the kinase activity of WNK1. In fact, WNK1 expressed in bacteria was autophosphorylated on S382, which was confirmed by the mass spectrometry. Mutation analysis of the residue serine 382 to alanine (S382A) resulted in decreased kinase activity, suggesting the important contribution of phosphorylation of the activation loop to kinase activity.

Coiled-coils

Coiled-coils are common structures found in many proteins. Coiled-coil regions imply the possibility of protein-protein interactions through hetero or homo-dimerization. In the absence of structural data, several programs have been developed to predict the likelihood of the existence of coiled coil regions in a given protein sequence (e.g., http://embnet.vital). Such predictions have led to the conclusion that WNK protein kinases have a conserved coiled-coil region near the C terminus. Other regions have also been predicted to be coiled coils; for

example, in rat, human WNK1 and WNK4, an additional coiled-coil region is expected adjacent to the AI segment (Figure 1-2). A recent report by Thastrup et al. (*26*) demonstrated an analysis of the putative coiled-coil region at the end of the C-terminus of four human WNKs mainly by using purified recombinant proteins. They investigated how the coiled-coil region of each WNK isoform affected the status of the dimerization and autophosphorylation, thereby impacting the kinase activity. From a multiple sequence alignment, Thastrup et al. predicted 15 conserved residues. By doing alanine scanning, three residues - histidine, glutamate and glutamine were found to be important for the interaction with other WNK isoforms (Fig. 1-4). The mutant form of WNKs, named HQ mutant were made in the full length context of WNK2, 3 and 4 in HEK 293 cells. WNK2, 3, and 4 HQ mutants all failed to interact with WNK1 but WNK2, 3, and 4 kinase dead mutants were still capable of interacting with WNK1. Gel filtration analysis (*24*, *26*) suggested that endogenous WNK1 or WNK3 was eluted at the fraction representing the molecular weight higher than 670 KDa. When compared the WT and HQ mutant of WNK4 expressed in HEK 293 cells, the WT was eluted at the corresponding fraction as endogenous WNK1 or 3 was but the HQ mutant was eluted at the later fraction representing molecular weight lower than 670 KDa. These data suggested that coiled-coil region at the end of the C-terminus of WNKs was capable of interacting with other isoforms or itself. Whether it was required or not, more experiments will need to be tested. From immuno-precipitation experiments with a WNK1 fragment, residues 1-940, I have observed co-immunoprecipitation of endogenous WNK2 and WNK3; this result was further supported by mass spectrometry. Under the conditions I used, it is possible that WNK1 1-940 interacted with endogenous WNK1; if that is so, the associated WNK2 and 3 may have been captured by full length endogenous WNK1. In the same immuno-precipitation experiment with WNK1 1-940, I failed to detect endogenous WNK1 by Western

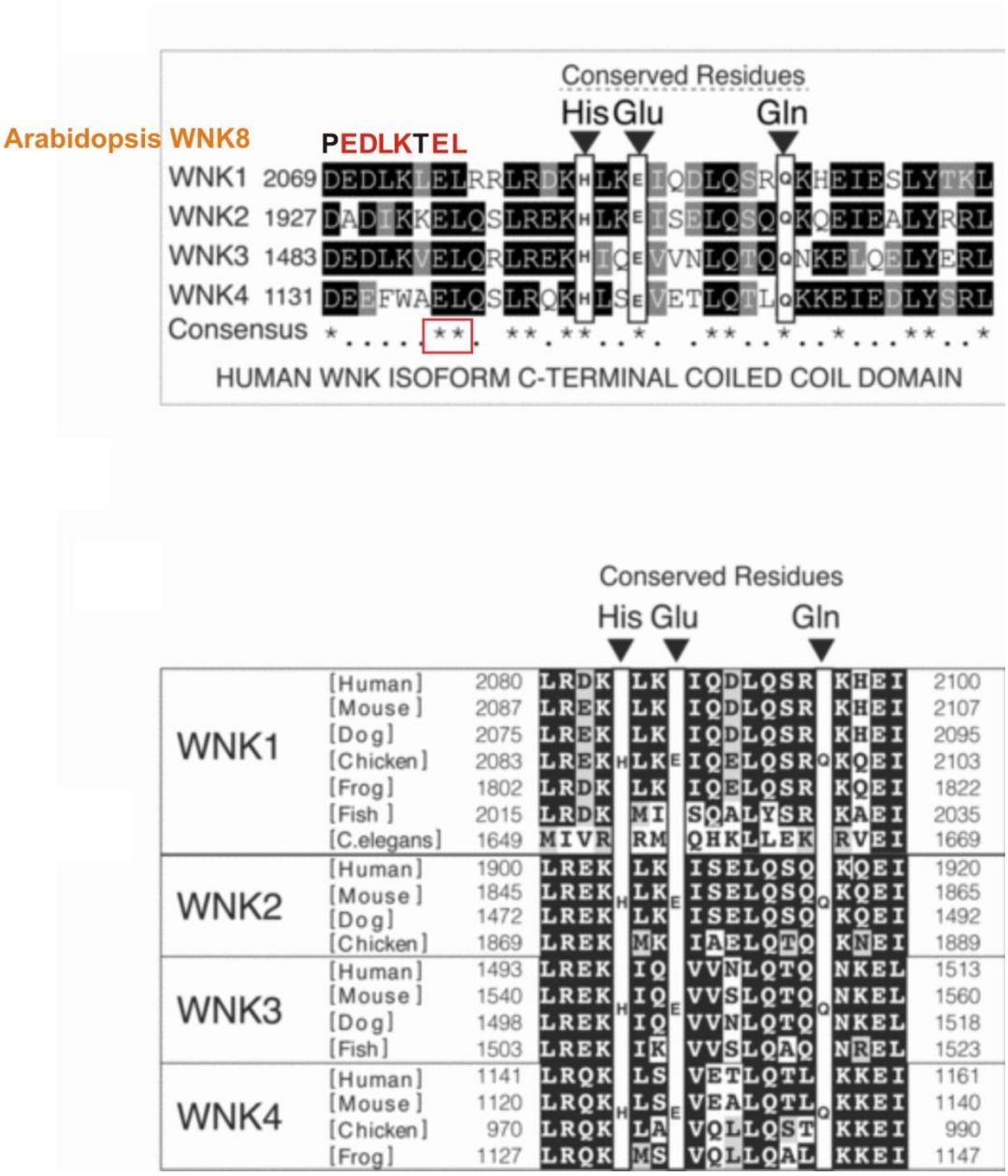

Figure 1- 4. Multiple sequence alignment of the coiled coil region of human WNKs 1 to 4 and WNKs from several other species including Arabidopsis WNK8.

Figure 1- 4 was adapted from Thastrup et al. (2012) Biochem. J. vol. 441, p325-337. This figure originally came from figure 4E and F in the study of Thastrup et al. The C-terminal coiled-coil region sequence of *Arabidopsis* WNK8 was added for the comparison and analysis. The conserved residues -histidine, glutamate and glutamine were shown in human, mouse, dog frog, chicken but not in plant.

blot analysis, whereas WNK1 residues 1800 to 2126 containing the coiled-coil region strongly pulled down endogenous WNK1 (unpublished data). Purified recombinant WNK fragments might be able to clarify the requirement of the coiled-coil region at the end of the C-terminus-mediated interaction with other WNK isoforms.

As discussed earlier, the autophosphorylation of S382 in the activation loop was important for the WNK kinase activity. Thastrup et al. also tested the HQ mutants of WNKs for the phosphorylation state of the conserved serine residue in WNK2, 3 and 4. Both the kinase activity and the phosphorylation of the serine residue greatly diminished in the HQ mutants, suggesting an intermolecular autophosphorylation mechanism for WNK protein kinases. WNK1 was shown to phosphorylate WNK4 on multiple sites (*24*), consistent with this idea.

PxxP motifs

PxxP motifs are common protein binding sites containing proline residues with two intervening residues (X), that may be any amino acid. The importance of this motif became clear once it was determined that it bound Src homology (SH) 3 domains. SH3 domains are 50 to 70 amino acids in length and are often parts of signaling complexes or associated with cytoskeletal proteins such as PI3K regulatory subunits and actin-binding proteins (*27*). He et al. (*28*) reported that intersectin could bind to three N-terminal PxxP motifs of WNK1. Intersectin is an endocytic scaffold protein involved in clathrin-coated vesicle - mediated endocytosis and has five SH3 domains. He et al. demonstrated that the N-terminal PxxP motif of WNK1 binds to the third SH3 domain of intersectin. The N-terminus of WNK1 was sufficient for the binding and the C-terminal PxxP motifs were not involved. Among the four human WNKs, WNK2 possesses the most PxxP motifs (Fig. 1-2). However, this feature has not been studied extensively so far.

In summary, the structure of WNK of protein kinases displays conservation for - the kinase domain, the autoinhibitory segment and the coiled-coil region at the end of the C-terminus. Functions of some conserved residues have also been defined, including the catalytic lysine 233 (K233) in the kinase domain, phenylalanine residues 524 and 526 (F524 / 526) in the autoinhibitory segment, and histidine and glutamine (HQ) at the end of the C-terminal coiled-coil region. The only exception was that *Arabidopsis* WNK8 did not contain the conserved "HQ" residues (Fig.1- 4).

The involvement of WNKs in cellular signaling pathways

Mitogen-activated protein kinase (MAPK) pathways

MAPKs play diverse roles in all kinds of cellular activity, including proliferation, differentiation, cytoskeletal remodeling, cell cycle progression, stress responses, inflammation, and transcriptional regulation (*29, 30*). MAPK pathways are among the clearest examples of multi-kinase cascades in that the activation of the MAPKs is exerted by the upstream kinases, MAP kinase kinases (MAP2Ks), which are activated by the upstream kinases, MAPK kinase kinases or MAP3Ks (Fig. 1-5). The extracellular signal-regulated kinase 1 (ERK1) and ERK2, were identified and purified as kinases activated by insulin and growth factors. Rapidly thereafter, these kinases were shown to be in a pathway regulated by Ras family small G proteins and in a three kinase cascade including– Raf kinases (MAP3K), the MAP/ERK kinases 1 and 2 (MEK1/2) (MAP2K), and ERK1/2 (MAPK). Several other related signaling pathways were found that have parallel organization but respond to some different stimuli (Fig. 1-5) (*29*). As WNK1 was found in a screen searching for novel MAP2Ks, it was speculated that WNK1 might have impact on other existing MAPKs. While the first attempted testing by Xu et al., 2000 did

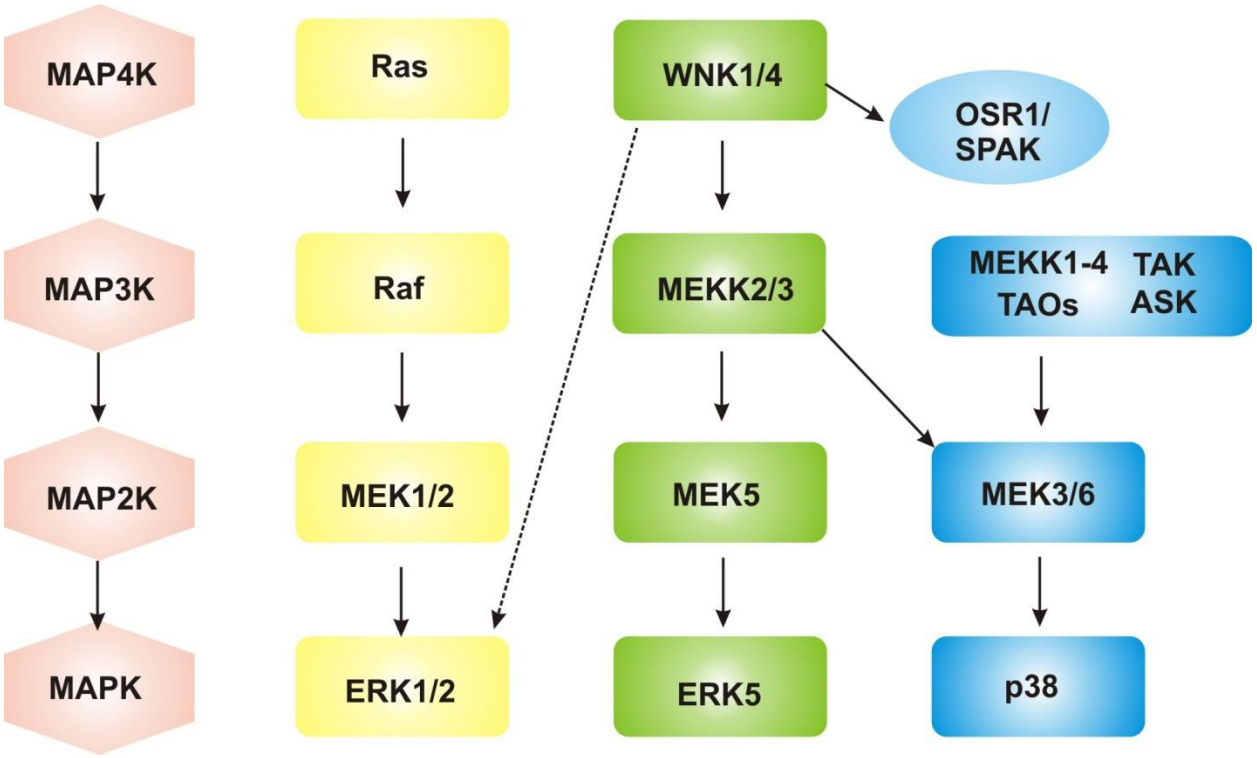

Figure 1- 5. The involvement of WNKs in the MAPKs pathways.

The overview of the three-tiered MAKP cascades is from Raman et al. (2007) Oncogene vol. 26, p3100-3112. The figure was modified from figure 1 in the review article of Raman et al. WNK1 or 4 might act as a MAP4K. Evidence for the dashed line drawn from WNK1/4 toward ERK1/2 is weak and needs further investigation.

not show any effects, the following experiments using WNK1 residues 1 to 490, a fragment without the autoinhibitory segment, revealed an effect on ERK5 but not ERK2 (*31*). ERK5 is a MAPK regulated by the upstream kinases MEK5 (MAP2K) and MAP/ERK kinase kinases MEKK2/3 (MAP3K) forming a distinct MAPK pathway. ERK5 activity is increased in response to growth factors, oxidative stress and hyperosmolarity (*32*). Further analysis suggested that WNK1 activated ERK5 by interacting with MEKK2/3 through a WNK1 kinase activity-independent mechanism. The authors also found that WNK1 was required for ERK5 activation by low concentrations of epidermal growth factor (EGF) as depletion of WNK1 impaired this activation. High concentrations of EGF overcame any requirement for WNK1. Sun et al. (*33*) also observed that if WNK1 was depleted, the activation of both ERK1/2 and ERK5 was suppressed in the presence of EGF. These data suggested that WNK1 might play a role as a MAP4K and modulate related downstream signaling pathways.

WNK2 was also reported to be involved in MAPK pathways. In contrast to WNK1, possibly a positive regulator of MAPK pathways, Moniz et al. (*34*) observed that WNK2 functioned as a negative modulator of ERK1/2 and had no effect on ERK5. Depletion of endogenous WNK2 increased the activation of ERK1/2. Likewise, overexpression of WNK2 slightly suppressed ERK1/2 activity. Phosphorylation of the activation loop S218 / S222 of the upstream kinase MEK1 increased as well as phosphorylation on S298. However, neither GTP-bound Ras nor Raf kinase activity was affected, nor was binding between WNK2 and MEK1 detected. Moniz et al. further investigated the mechanism underlying actions of WNK2 as a negative regulator of MEK1 and suggested that phosphorylation of PAK1 increased in WNK2-depleted cells. PAK1 can phosphorylate MEK1 on S298 (*35*). The activation of PAK1 was correlated with the activation of a small GTPase - Rac, a PAK1 activator. The antagonistic

relationship between Rac and Rho was also reflected in WNK2-depleted cells, which displayed higher Rac activity and lower Rho activity. The subsequent co-immunoprecipitation experiment revealed the striking interaction between WNK2 and a dominant negative form of Rho (T19N). This observation leads to the possibility that WNK2 might exist in a complex with Rho GEFs.

There are no reports to date on WNK3 and MAPK pathways. As for WNK4, two groups showed that WNK4 was a positive regulator of ERK1/2, and perhaps for p38 as well (*36, 37*). Over-expression of wild type WNK4 increased the activity of ERK1/2 and p38 upon stimulation by EGF or NaCl (*36*). WNK4 mutants containing disease-causing mutations had similar effects as wild type in one report (*36*), but no effects in the other (*37*). Suppression of WNK4 by RNAi compromised activation of ERK1/2 by NaCl. These data suggested that WNK4 might play a role in the MAPK pathway.

PI3K pathways

PI3K pathways are among the most studied signaling events in the context of growth factor and function as an effector of insulin signaling. Fig. 1-6 demonstrated the PI3K pathway and showed the involvement of WNK1. The first report indicating WNK1 was a substrate for protein kinase B (PKB)/AKt came from Vitari et al. (*38*). While searching novel substrates for PKB/Akt, they found that a sequence near the N-terminus of WNK1, RRRHTM, was a consensus motif for PKB/Akt substrates. Through biochemical study, T60 of human WNK1 was shown to be phosphorylated both in vitro and in vivo. The phosphorylation of T60 was dependent on PDK1 induced PKB/Akt kinase activity. However, the functional consequence of this phosphorylation event was not clear. The kinase activity of WNK1 did not change. Two subsequent reports also demonstrated the same phosphorylation site of WNK1 T60. Jiang et al.

(*39*) found a 250 KDa band from an immunoprecipitation experiment by using an antibody recognizing the phosphopeptide sites containing the PKB/Akt substrates motif. By mass spectrometry identification, the 250 KDa band corresponded to the WNK1 protein kinase. In our group, Xu et al. (*40*) found this site phosphorylated. WNK1 binds and activates serum- and glucocorticoid-induced protein kinase (SGK1). Activation requires only WNK1 residues 1 to 220; a fragment without the N-terminus of WNK1 is unable to activate SGK1. PI3K inhibitors abolished SGK1 activation by WNK1. Co-expression of PKB/Akt kinase dead and WNK1 impaired the activation of SGK1. These data pointed toward a possibility that the N-terminal residue T58 (rat T58 corresponds to human WNK1 T60) might be important for activation of SGK1. Mutation of threonine 58 to either alanine or aspartate reduced the ability of WNK1 to activate SGK1. However, binding of T58A WNK1 to SGK1 did not change, suggesting that WNK1 binding was required but not sufficient for SGK1 activation (*41*). Xu et al. also found that in additional to PKB/Akt, SGK1 also could phosphorylate T58 and other sites on WNK1. Stimulation of insulin-like growth factor 1 (IGF-1) could activate SGK1 but activation of SGK1 was impaired by depletion of endogenous WNK1. These data provided a positive feedback mechanism for regulation of T58/60 of WNK1. Phosphorylated T58/60 of WNK1 may serve as a scaffold to enhance activation of SGK1. Phosphorylation of WNK1 T58/60 may also be an as yet not understood feedback mechanism (Fig. 1-6).

Effects on SGK1 of the other three WNK protein kinases were investigated by Heise et al. (*41*). They found that N-terminal fragments of all four WNKs could activate SGK1 activity. SGK1 and PKB/Akt also could phosphorylate WNK4 T47, which corresponded to WNK1 T58/60. As was the case with WNK1, the mutant T47A WNK4 conferred a lower ability to activate SGK1, suggesting a common mechanism underlying the action of WNK1 and WNK4 on

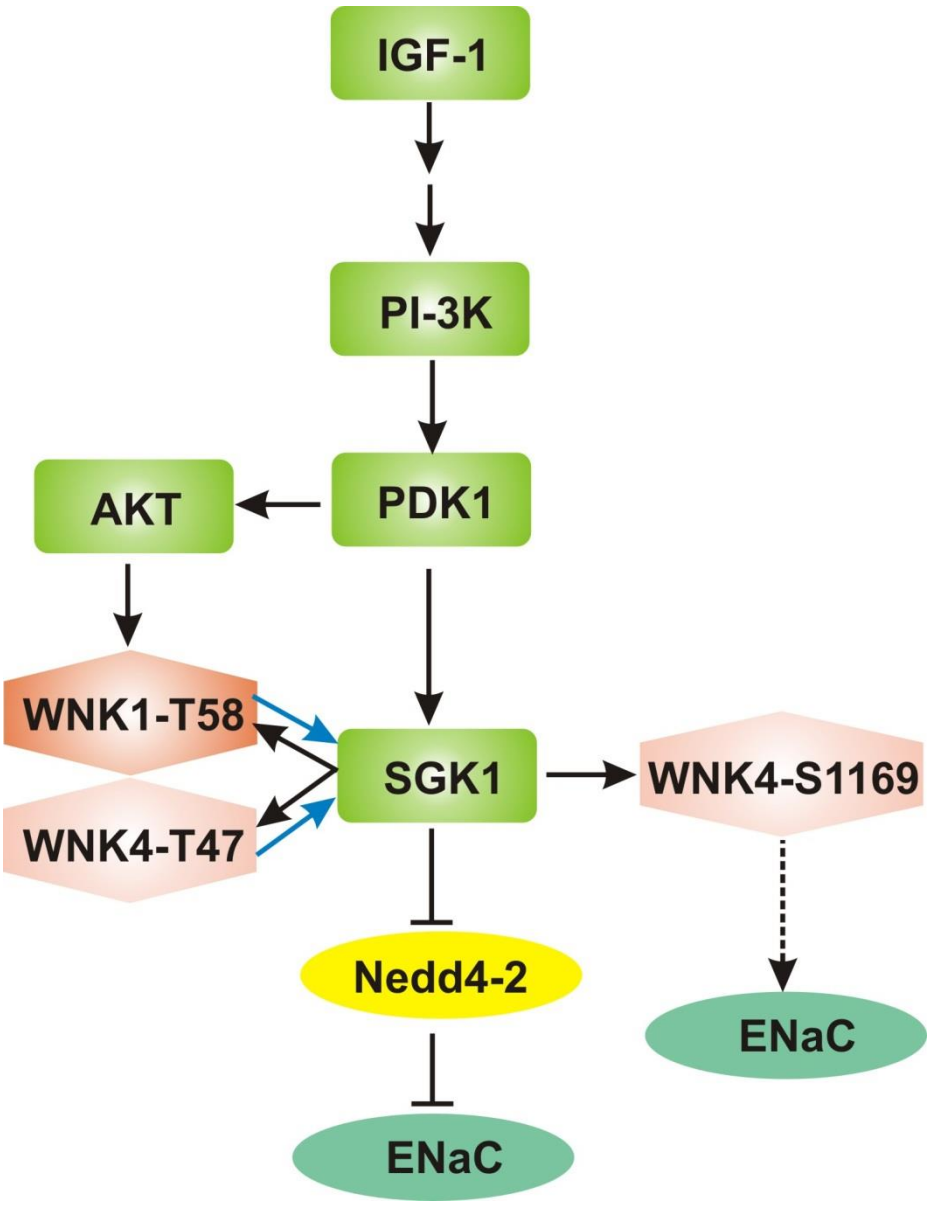

Figure 1- 6. The involvement of WNK1 or WNK4 in the PI3K pathways.

Figure 1- 6 was adapted from Xu et al. (2005) J. Biol. Chem.280, p34218-34223. Following this study, Heise et al. (2011) also suggested that WNK4 could activate SGK1 and ENaC by a similar mechanism. Another group reported that wild type WNK4 inhibited ENaC activity but phosphorylation of serine 1169 by SGK1 relieved the inhibitory effect. Sold blue arrowheads indicate that the activation of SGK1 by WNK1-T58 or WNK4-T47 is through non-catalytic activity.

SGK1 kinase activity. Interestingly, two more groups reported that SGK1 was capable of phosphorylating the C-terminal region of WNK4 (*42, 43*). They mapped the phosphorylation site of WNK4 as S1169, close to R1185, mutated in one of the PHAII kindred. The functional consequence of the phosphorylation of S1169 is not clear.

G-protein-coupled receptor (GPCR) - Gq signaling

GPCRs share a common hydrophobic seven transmembrane- topology and their actions are often mediated by heterotrimeric G proteins. Ligands for GPCRs are diverse and include odorants, neuropeptides, peptide hormones, lipids and photons (*44*). The G protein-coupled angiotensin II receptor (AT1R) was shown to affect ion transport through WNK4, although no mechanism was reported (*45*). More recently, An et al. (*46*) studied the mechanism of WNK1 action in a GPCR signaling pathway. An et al. found that the Gαq signaling pathway was impaired in WNK1-depleted cells. Phospholipase C (PLC) β, a major downstream effector for Gαq signaling, hydrolyzes Phosphatidylinositol 4,5-bisphosphate (PIP_2) and generates two second messengers, inositol-1,4,5-triphosphate (IP_3) and diacylglycerol (DAG) in response to stimulation of a relevant GPCR. Subsequently, DAG can activate the transient receptor potential cation channel, subfamily C, member 6 (TRPC6) and IP3 can stimulate the release of Ca^{2+} from its intracellular storage compartment in the endoplasmic reticulum (ER). In order to sustain the PLCβ signaling, the substrate, PIP_2 must be re-synthesized by phosphatidylinositol- 4 kinase (PI4K) during Gαq signaling (*47*). An et al. examined how WNK1 could affect the Gαq – PLCβ pathway by assaying TRPC6 current as the functional readout. WNK1 1-490 increased current independent of WNK1 kinase activity. PLCβ activity was required for the enhancement of TRPC6 current mediated by WNK1. The synergistic effect of the combined actions of PLCβ and WNK1 suggested that they might act in parallel. It is possible that WNK1 might affect PIP_2

synthesis during activation of Gαq signaling. As PI4KIIIα was the major enzyme responsible for the re-synthesis of PIP_2, silencing of PI4KIIIα by small interfering RNA diminished WNK1-induced TRPC6 current. As mentioned earlier, WNK1 increased the TRPC6 current through a non-catalytic function of the N-terminal region. This non-catalytic function was reminiscent of effects of WNK1 on activation of SGK1 by IGF1 which were enhanced by phosphorylation of WNK1 T58/60. As a result, the authors tested the requirement of WNK1 and the importance of T58 and PI4KIIIα for effects of IGF1 and carbachol. The results suggested that PI4KIIIα and wild type WNK1 and were required for IGF1-induced PI3K and carbachol-induced Gαq signaling and that phosphorylation of WNK1 T58 enhanced the response. How WNK1 enhances the activity of PI4KIIIα is still unknown. No physical interaction between WNK1 and PI4KIIIα has been detected neither could WNK1 phosphorylate PI4KIIIα (*46*).

Transforming growth factor β (TGFβ)-Smad signaling

TGFβ has a major role in the regulation of cell proliferation, differentiation and apoptosis (*48*). Its receptor is a complex of two type II and two type I transmembrane serine/threonine protein kinases which regulate three classes of downstream effectors, receptor-activated Smads (R-Smads), common Smads (Co-Smads) and inhibitory Smads (I-Smads). Phosphorylated R-smads bind Co-Smads and translocate to the nucleus to regulate gene transcription (*49*). Recently, TGFβ signaling has been found to regulate a subset of microRNAs (miRs) including miR-21, miR-192 and 194 (*49, 50*). miR-192 is thought to be expressed exclusively in the kidney (*51*). miR-192 is thought to target at least three genes, zeb1, zeb2 and WNK1 in renal proximal tubular cells (PTC) (*52*). Treating the PTC with TGFβ decreased miR-192 expression. The molecular mechanism underlying repression was through inhibition of binding of hepatocyte nuclear factor 1 (HNF1) and p53 to the promoter region of miR-192 (*50*). Together these reports

may suggest that TGFβ increases the expression of WNK1 by decreasing expression of miR-192. The interaction between WNK1 and TGFβ and Smads came from Lee at al. (*53*). The authors observed that silencing WNK1 decreased the expression of Smad 2 protein and mRNA. Phosphorylated Smad 2 increased in the nuclear fraction in WNK1-depleted cells. These observations were made in the absence of TGFβ, suggesting that effects were TGFβ independent. WNK1 could bind Smad 2 and 3, although this was not detected in cells, and WNK1 phosphorylated Smad 2 in vitro. Lee et al. also tested whether WNK1 could affect TGFβ signaling by examining target gene expression. The results showed that the expression of TGFβ target genes was increased by depletion of WNK1, suggesting that WNK1 acts as a negative regulator of TGFβ signaling. Taken together, these results suggest a negative feedback loop between WNK1 and TGFβ in renal proximal tubular cells.

Exocytosis

Secreted molecules and secretory processes are specialized for different cell types, yet the basic exocytotic protein machinery is a common protein complex named soluble N-ethylmaleimide-sensitve factor attachment protein receptors (SNAREs) (*54*). The SNAREs complex requires accessory proteins to carry out different types of exocytosis. These include the priming proteins (e.g. Munc18, Munc 13, or complexin) and/or the triggering proteins (synaptotagmins, Doc2, or various protein kinases) (*54*). WNK1 has been shown to interact with synaptotagmin (Syt) 2 and Munc 18c by Lee at al. and Oh et al. respectively (*55, 56*). Lee et al. (*55*) conducted a yeast two- hybrid screen and found that Syt 2, 3 and 9 were interactors. Syts are Ca^{2+} sensors that contain two Ca^{2+} - binding C2 domains. Ca^{2+} binding to the C2 domain of Syts facilitate its phospholipid binding to catalyze membrane fusion. The WNK1 kinase domain, residues 180-555, was sufficient to interact with the C2B domain of Syt2. WNK1

phosphorylated T202 in the C2A domain of Syt2. Phosphorylation increased the Ca^{2+} concentration required for Syt2 binding phospholipid vesicles. What can be concluded about WNK1-mediated phosphorylation of Syt2 in physiological settings? In neuronal cells, the ultrafast exocytosis is generally executed by SNAREs and a Syt family member (*54*). The speed of exocytosis is thought to vary dependent on the Syt protein; from fastest to slowest, the speed of the Syt was 2>1> 9 (*57*). The conclusion made by Lee et al., that WNK1 might influence the rate of cycling of Syt2, is consistent with effects on Ca2+- dependent binding to phospholipids during ultrafast exocytosis. Phosphorylation might shorten the time that Syt2 was bound to membranes.

While neuronal SNAREs mediate rapid exocytosis, islet β cells or adipocytes trigger slower exocytosis and are associated with priming proteins such as Munc18 family members (*54*). A yeast two- hybrid screen suggested that Munc 18c is a WNK1 interactor (*56*). Sec1/Munc18 (SM) proteins bind SNAREs and facilitate SNARE-mediated membrane fusion. Munc18c is thought to bind syntaxin4 (a SNARE component) by releasing the inhibitory state of syntaxin4, hence promoting the assembly of a SNARE ternary complex (*58*). Oh et al. (*56*) showed that the kinase domain of WNK1 was sufficient to bind N-terminal residues 1-172 of Munc18c. The kinase-dead mutant of WNK1 had the same binding capacity and WNK1 did not phosphorylate Munc18c. Over-expression of Munc18c in islet β cells actually inhibited exocytosis. Further analysis suggested that over-expression of Munc18c decreased the assembly of the SNARE complex as measured by the binding of syntaxin4 and vesicle-associated membrane protein (VAMP) 2 (*59, 60*). Oh et al. was able to show that over-expression of the binding domain of WNK1 and Munc18c could restore the inhibition of exocytosis and over-expression of a non-binding fragment of WNK1 residues 1-220 and Munc18c did not rescue the

inhibitory effect. However, they failed to demonstrate any effects on the release of human peptide C (a functional readout for exocytosis) when cells were depleted of WNK1 by small interfering RNA.

Mendes et al. (*61*) suggested that WNK1 could promote the surface expression of glucose transporter 1 (GLUT1) by regulating a Tre-2/USP6-BUB2/Cdc16 Domain family member 4 (TBC1D4) – Rab8A complex. The finding of the interaction between WNK1 and TBC1D4 was identified by mass spectrometry. They reported that WNK1 residues 1-538 bound to TBC1D4 and phosphorylated it in vitro. Over-expression of wild type WNK1 in HEK293 cells increased the binding of TBC1D4 with 14-3-3 but over-expression of the kinase - dead mutant did not. TBC1D4 is a Rab GTPase-activating protein (GAP) coupled to Rab2A, Rab8A, Rab10 and Rab14, which have been shown to regulate glucose transporters in different tissues (*62, 63*). Over-expression of wild type but not kinase-dead WNK1 also increased the surface expression of GLUT1 in HEK 293 cells. Depletion of Rab8A impaired the increased surface expression of GLUT1 mediated by WNK1, suggesting that Rab8A was the important downstream effector. These data suggest that WNK1 forms a complex with TBC1D4 and 14-3-3, thereby sequestering the Rab GAP TBC1D4. As TBC1D4 is a negative regulator for Rab8A, the sequestering effect mediated by WNK1 would activate Rab8A activity, promoting the movement of the glucose transporter vesicles containing vesicle-GLUT1 to the plasma membrane.

Endocytosis

Phagocytosis, macropinocytosis, clathrin-coated vesicle -mediated endocytosis and caveolae- mediated endocytosis are all mechanisms to bring materials into cells (*64*). WNKs have been implicated in at least two of these, clathrin-coated vesicle and caveolae - mediated

endocytosis. He et al. (*28*) demonstrated that the N-terminal 220 residues of WNK1 interacted with intersectin, a scaffold and clathrin heavy chain binding partner for clathrin-coated vesicle-mediated endocytosis. Like WNK1, WNK4 also bound to intersectin. The binding region was adjacent to a disease-causing mutation of WNK4 (D561A).The disease causing mutant increased the binding of intersectin and WNK4. In the case of either WNK1 or WNK4, the binding of intersectin enhanced the endocytosis of the renal outer medullary potassium channel (ROMK), hence decreasing its surface expression. WNK1 T58/60, a phosphorylation site for PKB/Akt, was also important for the endocytosis of ROMK (*65*). The authors showed that T58A WNK1 did not decrease ROMK currents as wild type WNK1 did (a result of increased endocytosis shown by their previous study). However, they did not determine how WNK1 T58A affected binding with intersectin.

Two papers showed that WNK4 affected caveolae-mediated endocytosis of the transient receptor potential vanilloid 5 channel (TRPV5) (*66, 67*). TRPV5 is a channel-mediating Ca^{2+} re-absorption in the distal nephron. Protein kinase C (PKC) is thought to increase the surface expression of TRPV5 by inhibiting caveolae-mediated endocytosis (*66*). Following this study, Cha et al. (*67*) observed that over-expression of WNK4 1-584 inhibited the surface expression of TRPV5 comparing biotinylated - surface TRPV5 and its currents. The PHAII-disease causing mutation WNK4 E559K more strongly inhibited TRPV5. To probe the potential mechanism in which WNK4 exerted its positive regulatory role on endocytosis of TRPV5, intersectin was tested for a requirement on WNK4 –mediated regulation of TRPV5 endocytosis. Intersectin interacted not only with clathrin heavy chain but also with dynamin 2, which was required for both clathrin-coated vesicle and caveolae-mediated endocytosis. Knocking down of intersectin or caveolin1 or over-expression of dominant negative dynamin 2 diminished the enhancement of

endocytosis by WNK4, whereas there was no effect when clathrin heavy chain was depleted. These data suggested that WNK4 promotes caveolae-mediated endocytosis of TRPV5 through caveolin1, intersectin and dynamin 2.

Membrane trafficking

Internalized cargo enters early endosomes, the first cargo sorting station. Recycling endosomes transport cargo back to the plasma membrane (anterograde transport). Cargo sorted to late endosomes will eventually be degraded in the lysosomal compartment. The Golgi apparatus also is pivotal in secretory and endo-lysosomal pathways for trafficking of newly synthesized cargo. Clathrin-coated vesicles usually couple the adaptor protein (AP) complex as heterotetramers. The AP-3 complex has been found to travel from the *Trans*-Golgi network (TGN) to late endosomes / lysosomes or early endosomes and from early endosomes back to the TGN (*68*) (Fig. 1-7). Two reports suggested that WNK4 could regulate Na^+ Cl^- co- transporter (NCC) through the AP-3 complex. It has been shown that WNK4 inhibited the surface expression of NCC through a dynamin-independent event (*69, 70*). Consistent with previous study, Subramanya et al. (*71*) observed that the retrograde transport of endocytosis was not affected but the anterograde transport of NCC was reduced in the presence of exogenous WNK4. Subramanya et al. examined the trafficking of NCC from the TGN to the plasma membrane and found that the biosynthesis and the delivery of NCC from the TGN shifted the routes to lysosomal compartment rather than to the plasma membrane. The author found that the cytoplasmic tail of NCC harboring the AP-3 complex recognition signal sequence and bound to the AP-3 complex tighter in the presence of WNK4. Sortilin is one of the VPS10 family receptors and also coupled with the AP-3 complex. Zhou et al. (*72*) reported that sortilin could interact with NCC and WNK4 increased the amount of NCC co-localized with lysosomes. These

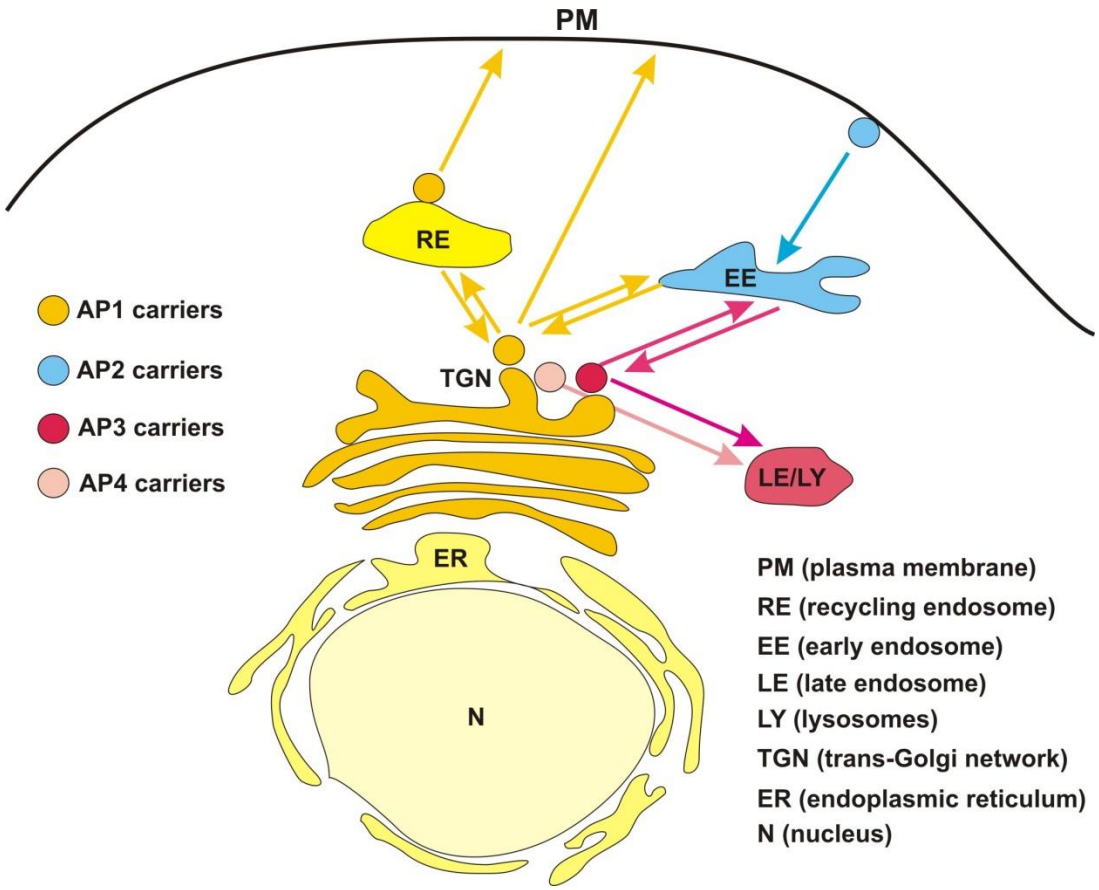

Figure 1-7. Schematic representation of the trafficking of the adaptor protein (AP) complexes in cells. See text for detailed description.

data suggested that WNK4 influenced the intracellular trafficking of NCC by shifting cargoes to lysosomes and probably being degraded, hence less surface amount of NCC.

STE20/SPS1-related, proline alanine-rich kinase (SPAK) / oxidative stress responsive 1(OSR1) pathway.

SPAK and OSR1 are two-close related kinases. SPAK was cloned and characterized by Johnston et al. (*73*). Through sequence alignment, it has been grouped as a member of the SPS1 subfamily of sterile (STE) 20 kinases protein family. OSR1 was identified and cloned by Tamari et al. (*74*). The sequence of OSR1 was highly similar to human Ste20/oxidant stress response kinase-1(SOK1), a molecule that was activated by oxidative stress. They therefore named this novel gene "oxidative-stress-response kinase 1". SPAK and OSR1 shared three highly conserved domains as shown in Fig.1-8 A. The kinase domain had 89% identity, and the PF1 and PF2 domains shared about 78% identity. Through yeast two-hybrid analysis (*75-77*) using the PF2 domain as a bait, they found that interactors with SPAK/OSR1 possessed the common motif- " RFXV " motif (Fig. 1-8 B). The interaction between WNKs and OSR1 / SPAK was characterized by three groups (*77-79*). All of them were able to co-immunoprecipitate endogenous WNK1 and SPAK or OSR1. In vitro kinase assay showed that SPAK or OSR1 was *a bona fide* substrate as compared with non-specific substrate myelin basic proteins and WNK1 had greater ability to phosphorylate the substrate than WNK4 did. Using mass spectrometry for identifying the phosphorylation sites on OSR1, a conserved S325 located within the PF1 domain was found. In addition to S325, Vitari et al. (*78*) also reported that T185, another conserved residue at the activation loop of OSR1 was phosphorylated. When T185 was mutated to alanine, WNK1 was not able to phosphorylate T185A mutant and the kinase activity of T185A was abolished, suggesting that phosphorylation by WNK1 at the activation loop of residue T185 was

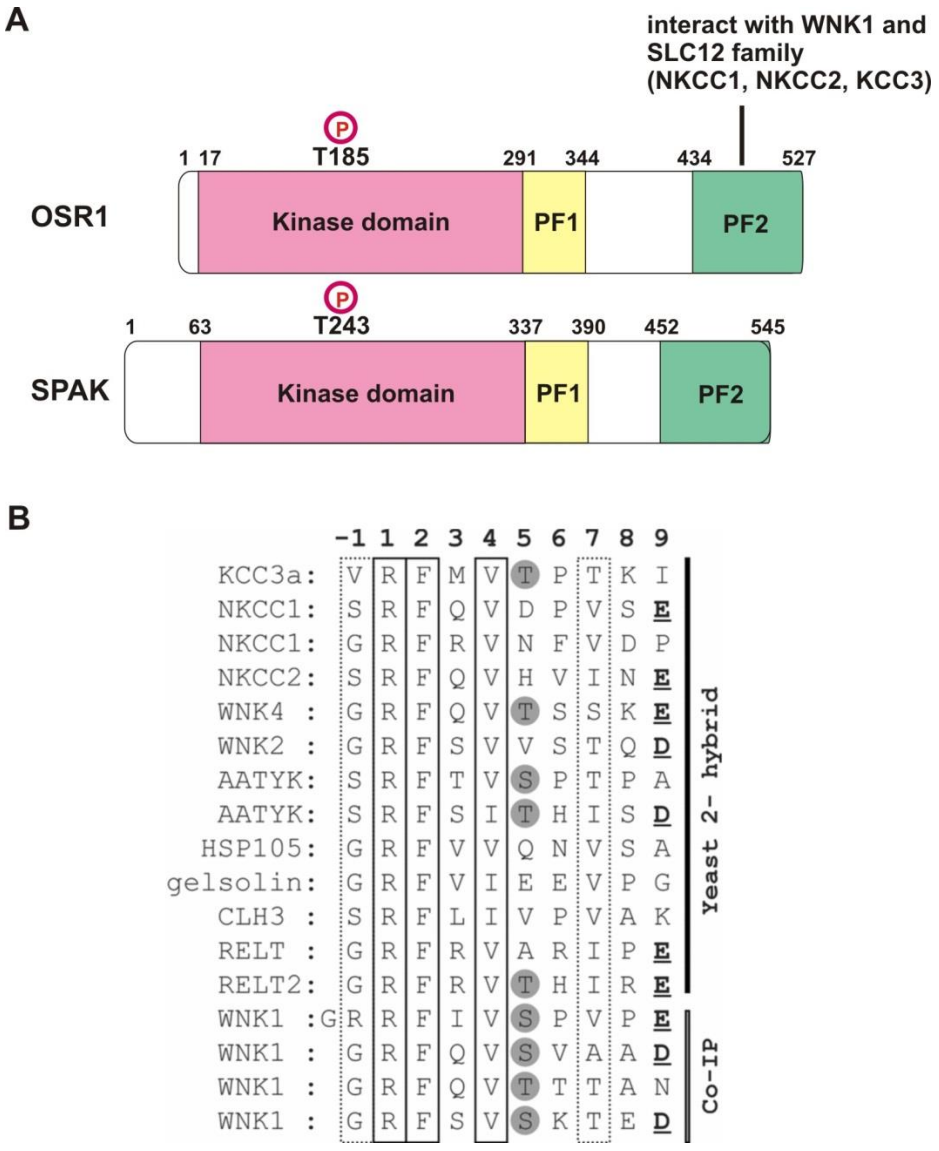

Figure 1- 8. Schematic representation of SPAK and OSR1 domain structures (A) and the SPAK / OSR1 consensus binding motif (B).

The sequences used in Figure 1- 8 A for OSR1 and SPAK are NP_005100 and NP_037365 respectively. Figure 1 - 8 B was from Delpire and Gagnon (2008) Biochem. J. vol. 409, p321-331.

important for the activation of OSR1. Further analysis by small interfering RNA for depletion of endogenous WNK1 demonstrated that WNK1 was required for the activation of OSR1 activity in vivo (*77*). These data established that WNK1 is a positive regulator for the activity of OSR1/SPAK. The downstream effectors / interactors of OSR1/SPAK had been shown to regulate ion co-transporters by Piechotta et al. in 2002 (*76*). It became evidently that WNK1 or WNK4 might influence ion co-transporters at least in part via OSR1/SPAK protein functions.

Ion co- transporters and channels

There are several ion co-transporters and channels in the distal nephron for controlling and balancing ion homeostasis. The anatomy of mammalian nephron segments starting from the glomerular capsule is as following, the proximal convoluted tubules (PCT), the thick ascending loop of Henle (TAL), the distal convoluted tubule (DCT), the connecting tubule (CNT), and the collecting duct (CD) as shown in Fig.1-9 A (*80*). During the formation of urine, a large amount of fluids and salt is filtrated from blood into glomerular capsules. The function of tubules is to reabsorb them back into blood vessel. The inherited gene mutations which caused abnormal blood pressure and other symptoms are mostly expressed in the distal nephron (Fig. 1-9 A). The expression and distribution of several important proteins (e. g. WNKs family), ion co-transporters and channels along nephron segments is summarized in Fig.1-9 B (*81*). Disease – causing mutations of WNK1 or WNK4 reported by Wilson et al. are summarized in Fig.1-10.

Renal outer medullary potassium channel (ROMK)

ROMK is a major potassium excretion channel along the distal nephron (Fig.1-9 B). One of PHAII symptoms is hyperkalemia, implying that less activity of ROMK is presented. The detailed mechanism was investigated by Huang's group as discussed in endocytosis section.

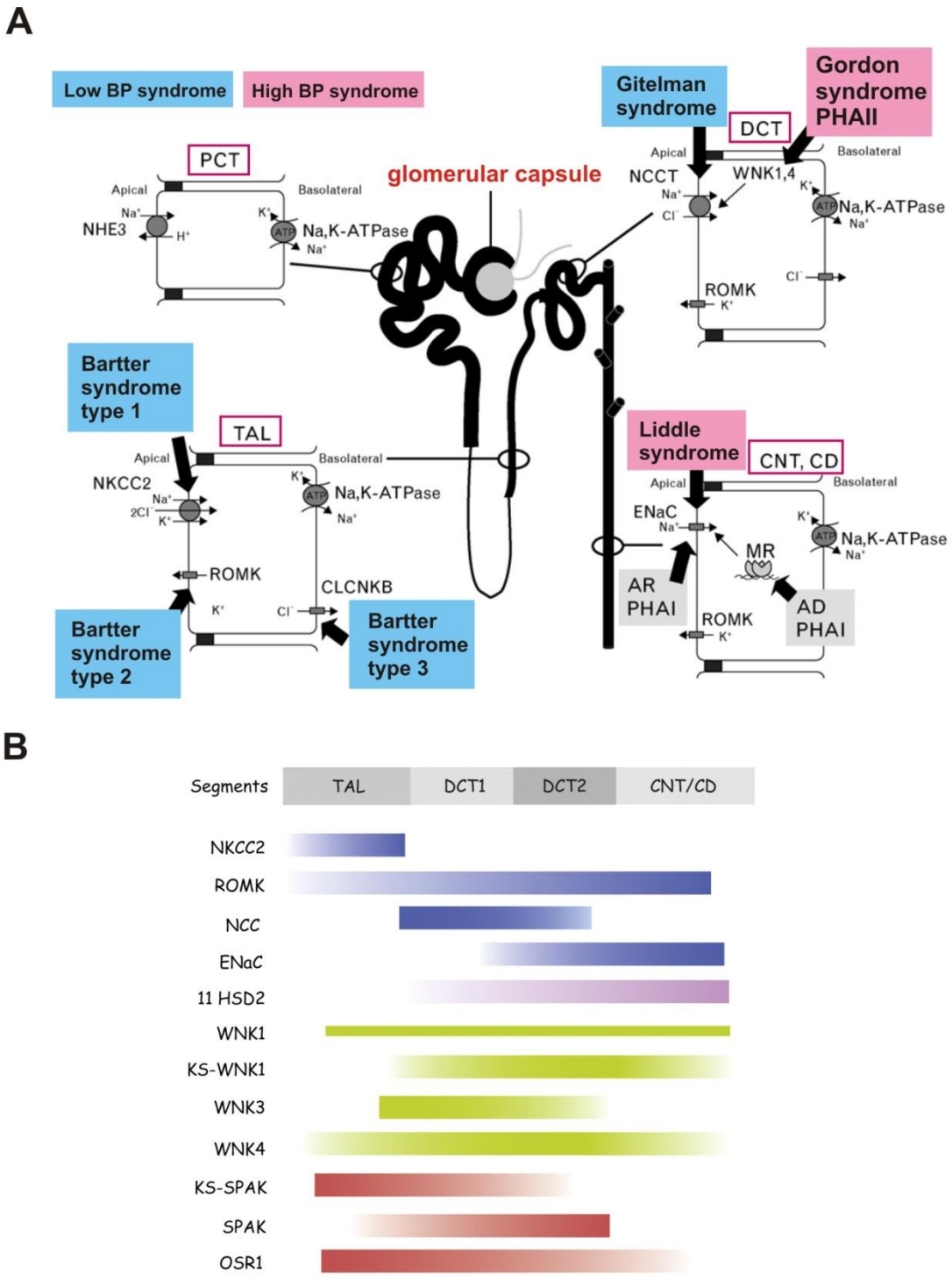

Figure 1-9. Schematic representation of the anatomy of the distal nephron and related inheritable diseases (A) and the distribution of important ion co-transporters, channels and protein kinases along the distal nephron (B).

Figure 1- 9 A was from Glover and O'Shaughnessy (2011) Current opinion in nephrology and hypertension. Vol. 20, p16-22 with permission from Lippincott Williams & Wilkins, INC. Figure 1-9 B was from Hoorn and Ellison (2012) Experimental cell research. vol. 318, p1020-1026 with permission from Elsevier.

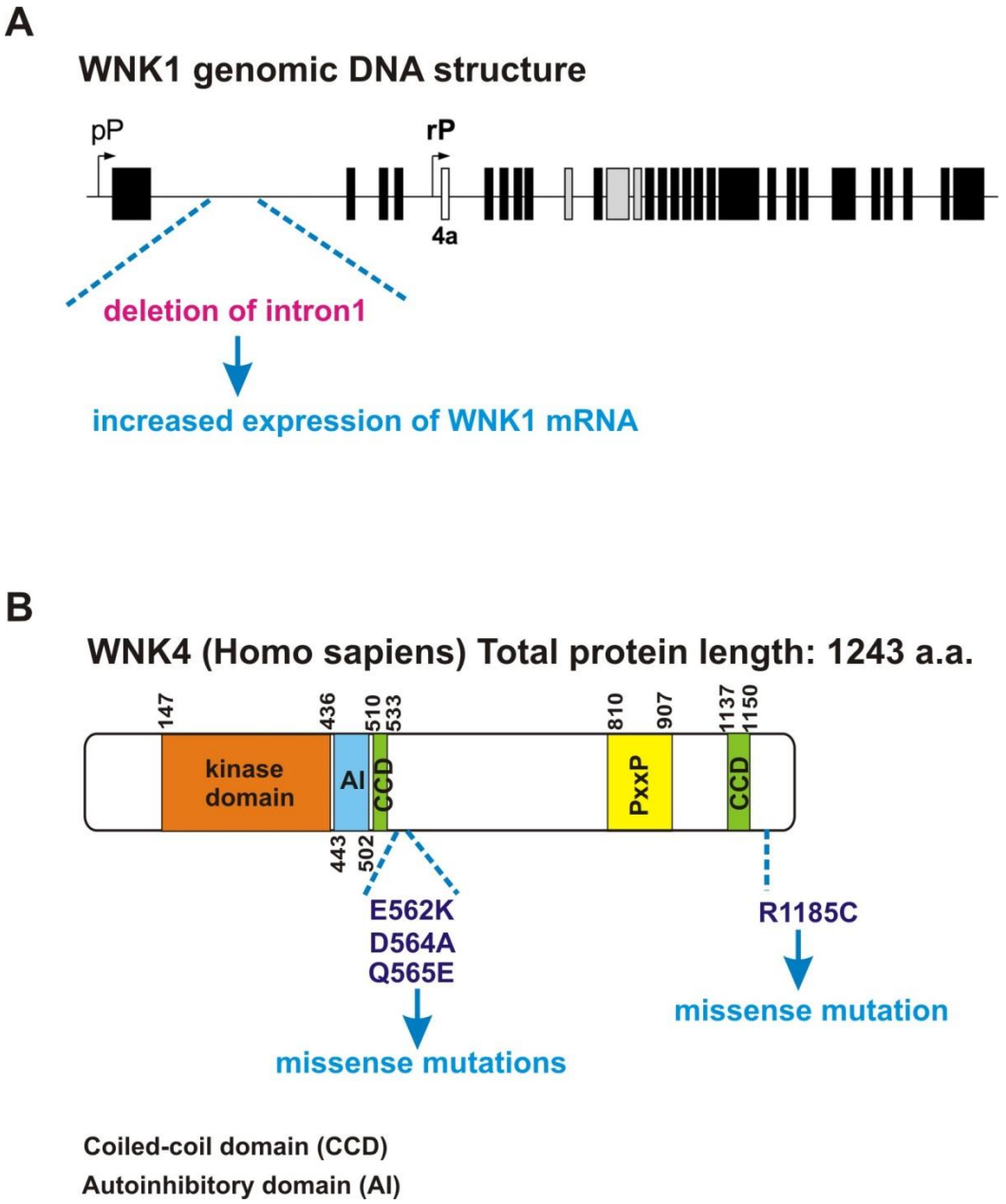

Figure 1-10. Schematic representation of WNK1 (A) or WNK4 (B) mutations in PHAII syndrome.

Figure 1-10 A was modified from Figure 1A shown in Vidal-Petiot E, Cheval L, Faugeroux J, Malard T, Doucet A, et al. (2012) PLoS ONE 7(5): e37751. The original report for mutations shown in Figure 1-10 was from Wilson et al. (2001).

Overexpression of WNK1 was observed in the WNK1 gene mutation patients. Therefore, it seemed reasonable to explain that hyperkalemia could be due to the enhancement of endocytosis of ROMK by overexpression of WNK1. As for the WNK4 mutation genes, there were four different mutations (Fig. 1-10). Huang's group observed (*28*) that WNK4 E559K, D561A or Q562E mutant enhanced endocytosis of ROMK as well. Taken together, these data suggested that mutations of WNK1 or WNK4 could contribute to hyperkalemia, often associated with PHAII syndrome.

Epithelial sodium channel (ENaC)

The expression and distribution of ENaC are more restricted in the late DCT and CNT/CD (Fig. 1-9 B). Neural precursor cell-expressed developmentally down-regulated gene 4-2 (Nedd 4-2) is an E3 ubiquitin ligase regulating the stability of ENaC through ubiquitylation-mediated proteolysis. Nedd 4-2 is also a substrate for a protein kinase-SGK1, which could be activated by WNK1 or WNK4 (discussed in the PI3K pathway). The phosphorylation of Nedd4-2 by SGK1 could result in the adaptor protein 14-3-3 binding, which caused less amount of Nedd4-2 bound to ENaC, hence increasing the stability of ENaC on surface expression of tubule cells (*82*). Therefore, overexpression of WNK1 could enhance ENaC activity through SGK1-mediated stabilization of ENaC, promoting sodium re-absorption, leading to hypertension.

The solute carrier 12 (SLC12) family

The SLC12 family comprises nine genes. Among them, $Na^+ K^+$- $2Cl^-$ co transporter (NKCC) 1, 2 and $K^+ Cl^-$ co transporter (KCC) 3a have been characterized as SPAK/OSR1 binding proteins (Fig. 1-8 B). Along the distal nephron, NKCC2 is mainly distributed and expressed in the TAL and NCC is in the DCT (Fig. 1-9 B). NKCC1 is ubiquitously expressed in

all kinds of tissues. Several studies suggested that SPAK / OSR1 phosphorylated three conserved threonine residues at the N-terminal NKCC1, 2 and NCC proteins (Fig.1-11) (*83-85*). Mutation of the conserved residue T60 at NCC protein inactivated co-transporter activity. WNK1 plays a positive role in the activation of SPAK / OSR1, whose function is also a positive regulator for ion co-transporters (Fig. 1-11). Therefore, overexpression of WNK1 could increase the activity of NCC or NKCC2 via SPAK / OSR1-mediated function in distal nephron, resulting in increased sodium re-absorption (hypertension).

As for WNK4, there are more complicated regulatory events. Though in vitro study suggested that wild type WNK4 could phosphorylate and activate SPAK (*78*), how the PHAII mutations of WNK4 affected the activity of SPAK / OSR1 still remained unknown. Recently, a WNK4 D561A knock-in mice has been reported (*86*). The phosphorylation of SPAK / OSR1 as well as the expression and phosphorylation of NCC was increased in WNK4 D561A mice. Chiga et al. (*87*) performed a genetic cross-mating experiment to generate a WNK4 D561A / SPAK T243A / OSR1T185A triple knock-in mice. The phosphorylation of NCC was abolished in the triple knock-in mice. Moreover, all PHAII symptoms presented in WNK4 D561A mice were corrected in the triple-knock-in mice. These data suggested that increased activity of NCC by WNK4 D561A mutant was mediated through SPAK / OSR1 pathway. The other regulatory effect exerted by WNK4 was the trafficking of NCC by AP-3 / sortilin- mediated lysosomal pathway as discussed before. Together with the phosphorylation and trafficking events, it seemed that mutations of WNK4 increased the activity of NCC through dis-inhibition of surface expression and increased phosphorylation by SPAK / OSR1, hence promoting sodium re-absorption (hypertension).

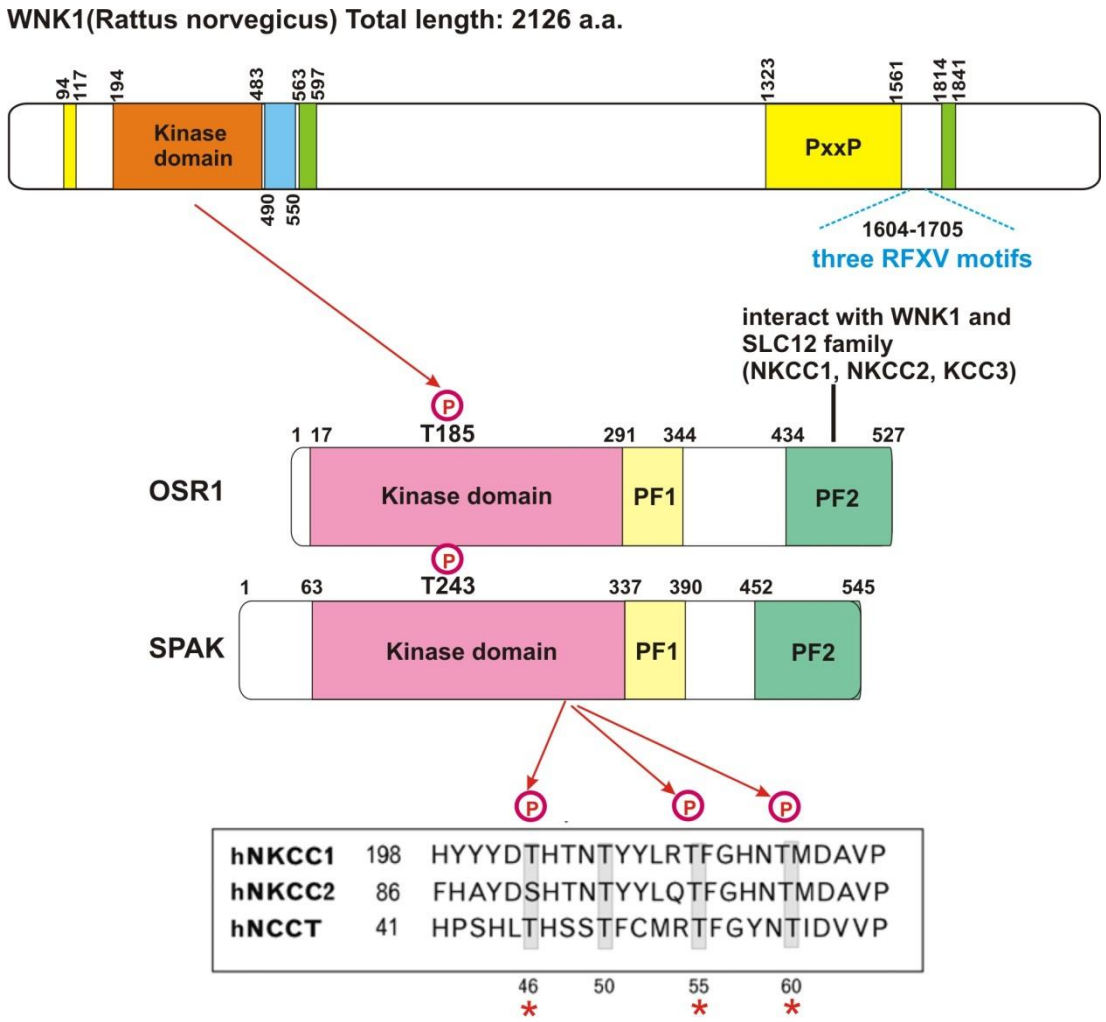

Figure 1-11. Schematic representation of WNK1-SPAK / OSR1- SLC12 ion co-transporter pathway.

The key residues for activation of SPAK (T243) / OSR1 (T185) and human NCC (T46, T55 and T60) are shown. WNK1 is the important upstream kinase that activates the cascade.

WNK1 and cardiovascular development

A heterozygous WNK1 mouse displayed a significant decrease in blood pressure (*88*). A homozygous null WNK1 mouse did not survive after day 13 of embryonic development (E13). These data are the first mouse genetic study regarding the importance of WNK1 gene in the developmental process. Delaloy et al. (*89*) had established WNK1 reporter transgenic mice for monitoring WNK1 expression. The expression of WNK1 was observed as early as E 8.5 in the developing vasculature and primitive heart. This report suggested that WNK1 might be important for the cardiovascular development. Xie et al. (*90*) continued to investigate detailed morphological defects in WNK1 null homozygous mice and found that null mice in E10.5 displayed smaller chambers of hearts and reduced myocardial trabeculation. Further analysis by immunostaining a pan-endothelial cell marker revealed that the density of blood vessels in the head region was reduced. The secondary and tertiary branching was also significantly reduced. Xie et al. went on to establish a tissue –specific knockout mice – an endothelial cell specific WNK1 null mice, displaying similar angiogenesis sprouting and cardiac developmental defects as shown in the global ablation of WNK1 null mice. These data suggested that the function of WNK1 gene in endothelial cells was critical for the maturation of angiogenesis. What are the phenotypes in OSR1 or SPAK knockout mice? Yang et al. (*91*) reported that SPAK knockout mice survived and displayed a decreased expression of phosphorylated and total NCC proteins while total NKCC2, phospho-NKCC2 and phospho-OSR1 were increased. In contrast to survived SPAK knockout mice, Xie et al. (*92*) reported that global ablation of OSR1 mice died in the beginning at E11. The timing was earlier than WNK1 homozygous null mice, suggesting its important downstream role in mediating developmental process. Further analysis suggested that global ablation of OSR1 null mice as well as endothelial specific OSR1 null mice had similar

angiogenesis and cardiac defects as observed in WNK1 homozygous null mice. The constitutively active mutant OSR1 expressed in the endothelial cells rescued phenotypes in global ablation of WNK1 null mice background. These data suggested that WNK1 exerted its function in angiogenesis sprouting mediated through its downstream effector- OSR1.

Cell proliferation and migration

WNK1 and 4 had been shown to involve in the MAPK signaling pathway. The positive regulatory role of WNK1 for ERK1/2 or 5 suggested that WNK1 might act as a positive regulator in proliferation and possibly migration as well. Sun et al. (*33*) examined a neural progenitor cell line- C17.2 for cell proliferation and migration by suppression of WNK1 expression through an antisense WNK1 plasmid. Assays used for cell proliferation and migration are counting cell numbers and wound healing respectively. Cell proliferation was slower and migration was defective in WNK1-supressed cells. In fact, a genome wide RNAi screen for the survival factors in *Drosophila (93)* also suggested that WNK1 was a positive regulator for cell viability. Mausbacher et al. (*94*) performed a phosphoproteomics analysis to study cell migration and proliferation. WNK1 was a prominent phosphoprotein among hits. Moreover, three phosphorylation sites including S382 were found to be up-regulated two fold after 1.5 min lysophosphatidic acid (LPA) treatment. RNAi-mediated WNK1 depletion impaired LPA-induced migration in squamous cell carcinoma (SCC) 9 cells. These data suggested that WNK1 could play a positive regulatory role in EGF or LPA stimulated cell proliferation and migration. On the other hand, depletion of WNK1 in 3T3 - L1 adipocyte increased serum-stimulated cell proliferation shown by Jiang et al. (*39*), suggesting that WNK1 could be a negative regulator in insulin-stimulated mitogenesis. Taken together, WNK1 could play diverse roles in regulating cell

proliferation and migration depending on different cellular types as well as physiological contexts.

WNK2 could be a suppressor for cell growth. Hong et al. (*95*) found that the CpG island of promoter region of WNK2 gene was hyper-methylated in gliomas. Further analysis suggested that the expression of WNK2 was down-regulated in tumors associated with aberrant CpG island methylation but not in normal brain or tumors with non-methylated promoter region. Overexpression of wild type WNK2 or kinase-dead mutant both could suppress the growth of gliomas, suggesting WNK2 acted as a tumor suppressor. Consistent with the negative regulatory role in cell proliferation in human gliomas, HeLa cells depleted of endogenous WNK2 displayed higher ERK1/2 activity and increased G1/S cell cycle progression (*34*). Better understanding of WNKs family in cellular signaling pathways will contribute to the advanced knowledge not only in hypertension but also in the therapeutics of human cancers.

Description of research in thesis

Chapter 1 is the overview of WNKs expression and protein structures. The biological functions of WNKs are also covered by the following areas including cellular signaling pathways, endocytosis, exocytosis, membrane trafficking, ion co-transporters, cardiovascular development and cell survival and migration.

My research for WNK1 function is mainly through the observation of phenotypes caused by depletion of WNK1. I had also observed cell survival and migration defects. This leads to the following research.

Chapter 2 is the investigation of WNK1 and mitosis.

Chapter 3 is the investigation of WNK1 and interphase microtubules.

Chapter 4 is the investigation of WNK1 and membrane trafficking.

Chapter 5 is the conclusion and future directions.

CHAPTER 2

WNK1 AND MITOSIS

Abstract

WNK (with no lysine (K)) protein kinases are found in all sequenced multicellular and many unicellular organisms. WNKs influence ion balance. Two WNK family members are associated with a single gene form of hypertension. RNA interference screens have implicated WNKs in survival and growth, and WNK1 is essential for viability of mice. I found that in resting cells the majority of WNK1 is localized on cytoplasmic puncta. During cell division, WNK1 localizes to mitotic spindles. Therefore, I analyzed mitotic phenotypes in WNK1 knockdown cells. A large percentage of WNK1 knockdown cells fail to complete cell division, displaying defects in mitotic spindles and also in abscission and cell survival. One of the best characterized WNK1 targets is the protein kinase OSR1 (oxidative stress responsive 1). OSR1 regulates ion cotransporters, is activated in response to osmotic stress by WNK family members, and is largely associated with WNK1. In resting cells, the majority of OSR1, like WNK1, is on cytoplasmic puncta. OSR1 is also in nuclei. In contrast to WNK1, however, OSR1 does not concentrate around spindles during mitosis and does not show a WNK1-like localization pattern in mitotic cells. Knockdown of OSR1 has only a modest effect on cell survival and does not lead to spindle defects. I conclude that decreased cell survival associated with loss of WNK1 is due to defects in chromosome segregation and abscission and is independent of the effector kinase OSR1.

Introduction

Microtubules are one of the most important cytoskeletal structures within cells. As microtubules are responsible for so many cellular activities including the transport of proteins and organelles, the establishment of the polarity and the formation of mitotic spindles during mitosis, the regulation and organization of the microtubules radial arrays have been studied for more than 100 years (*96*). Microtubules are consisted of 13 proto-filaments, forming a hallow cyclinder polymers with the polarity. The fundamental building block of each proto-filament is a unit of heterodimer, composed of α and β tubulin. The continuous heterodimer within each proto-filament accounts for the intrinsic polarity of microtubules. Each α and β tubulin has one GTP binding site. The GTP-binding pocket within α tubulin is located at the interface of the heterodimer. Therefore, the GTP in α tubulin is considered as a part of structures and not exchangeable. The GTP binding site of β tubulin, however, is exposed to the surface and could bind with either GTP or GDP. The GTP-bound β tubulin in the tip of the proto-filament is considered as a growing polymer. The GTP would then be hydrolyzed by intrinsic nucleotide hydrolysis activity of β tubulin and switch to GDP bound form. The GDP bound β tubulin is not favorable for the addition of GTP bound heterodimer (most free heterodimer would exist in GTP bound form within cells), causing depolymerization of proto-filaments. The growing and shrinking of proto-filaments thus depend on the rate of hydrolysis of nucleotides and the rate of the addition of GTP bound heterodimer. If the rate of the addition of GTP bound heterodimer is faster than the rate of nucleotides hydrolysis, the tip of filament is keeping in the GTP bound form, thus promoting polymerization. On the other hand, if the rate of nucleotides hydrolysis is faster than the addition of GTP bound heterodimer, depolymerization would occur. At any given time and proto-filaments, the chance of the tip of the proto-filament in GTP or GDP bound form

is random, therefore, the growing and shrinking would happen interchangeably. This unique physical nature of microtubules is called dynamic instability. The more dynamic growing and shrinking end is called the plus end which is the one with the exposure of β tubulin. The other end is called the minus end which is the one with the exposure of α tubulin and is less dynamic (Molecular biology of the cell, fourth edition).

I have published some data regarding WNK1 and mitosis that will be described in this chapter. There are also five unpublished figures related to mitosis. In addition, I will discuss WNK1 and interphase microtubules in the third chapter.

Materials and Methods

Constructs

Rat Flag-WNK1 cDNA was created by PCR using the following forward and reverse primers: GAATTCATGTCTGACGGCACCGCAGAGAAGC and GGATCCCTAGGTGGTCCGTAGGTTGGAACT with Myc WNK1 as cDNA template. PCR products were digested with EcoRI and BamHI and ligated into p3XFlagCMV7.1.

Antibodies and reagents

Antibodies to the following proteins were as indicated: WNK1immunofluorescence, Cell Signaling (#4979) and immunoblotting Q256 (*1*); OSR1 immunofluorescence (Cell Signaling #3729); SPAK (Cell Signaling #2281), α-tubulin (clone DM1A, Sigma Aldrich, or clone YL1/2, Abcam), Flag epitope (clone M2, Sigma Aldrich). Secondary antibodies for immunofluorescence are: goat anti-mouse Alex 488 or 546, goat anti-rabbit Alex 488 or

546, and goat anti-rat Alex 647 (Invitrogen). DAPI, dextran conjugated with Alex488 and 10% normal goat serum were also purchased from Invitrogen.

Cell culture, immunofluorescence, and immunoblotting

Cells were cultured in Dulbecco's modified Eagle's medium with 10% fetal bovine serum and 1% L-glutamine at 37°C under 5% CO2. For imaging, cells were plated on 35 mm or 6-well glass bottom plates (MatTeK Corp.). For immunofluorescence, cells were washed with phosphate-buffered saline (PBS) at 37˚C, fixed with 4% paraformaldehyde in PHEM buffer (60 mM PIPES, 25 mM HEPES, pH 6.9, 10 mM EGTA, 2 mM $MgCl_2$) for 10 min, and washed 2X for 5 min with PBS. Cells were permeabilized with 0.1% Triton X-100 in PBS at 4/ for 5 min, washed as above, incubated with 10% normal goat serum at room temperature for 30 min, and then incubated with primary antibody (1 to 100 dilution) at 4˚C overnight. Cells were then washed with PBS, incubated with Alexa fluor-conjugated secondary antibody at room temperature for 1 h, washed 2X with PBS and imaged by fluorescence microscopy. For immunoblotting, confluent cells were harvested in lysis buffer containing 1% Triton X-100, 50 mM HEPES (pH 7.5), 150 mM NaCl, 1.5 mM $MgCl_2$, 1 mM EGTA, 10% glycerol, 100 mM NaF, 0.2 mM Na_3VO_4, 50 mM β-glycerophosphate, 1 mM dithiothreitol, 1 mM benzamidine hydrochloride, 10 mg/L leupeptin, 0.5 mg/L pepstatin A, and 1.5 mg/L aprotinin. The cells were vortexed for 30 seconds and incubated on ice for 10 min. The lysates were clarified by centrifugation at 16,000 g in a microfuge for 20 min.

Immunoprecipitating kinase assay

HeLa S3 cells were synchronized by nocodazole or taxol for 16 hours. Cells were then be shaken off from 75T- cultural flask and lysed with buffers (0.5% Triton X-100, 50 mM HEPES

(pH 7.5), 150 mM NaCl, 1.5 mM $MgCl_2$, 1 mM EGTA, 10% glycerol, 100 mM NaF, 0.2 mM Na_3VO_4, 50 mM β-glycerophosphate, 1 mM dithiothreitol, 1 mM benzamidine hydrochloride, 10 mg/L leupeptin, 0.5 mg/L pepstatin A, and 1.5 mg/L aprotinin). Cells were vortexed for 30 seconds and incubated on ice for 30 min. The lysates were clarified by centrifugation at 16,000g in a microfuge for 20 min. Immunoprecipitating antibodies (WNK1 Q256 1: 100 ratio (µl antibody / µl lysate)) were added to the 16,000g supernatant and incubated at 4˚C with rotation overnight. Next day, protein A/G agarose beads (30 µl) were added and incubated at 4˚C with rotation for one hour. Beads were washed with lysis buffer with salt concentration 1M NaCl three times, for 10 min each. Kinase assays were performed in 30 µl of kinase buffer (20 mM HEPES, pH 7.5, 10 µM ATP, 10 mM $MgCl_2$, 10 mM β-glycerophosphate, 1 mM dithiothreitol and 1 mM benzamidine hydrochloride) containing 10 µ Ci of γ-^{32}P ATP, incubated at 30˚C for 30 min. Reactions were terminated by the addition of 5X SDS sample buffer and heating for 3 min at 94˚C.

RNAi

HeLa cells were transfected with dsRNA oligonucleotides using Lipofectamine RNAiMAX according to manufacturer's instructions (Invitrogen). After 48 h, protein localization was examined. Oligonucleotides: WNK1- sense, GGAUCAAGUGCGAGAAAUUTT, antisense, AAUUUCUCGCACUUGAUCCTT; OSR1-sense, GGAACAGGUCCGUGGUUAUTT, antisense, AUAACCACGGACCUGUUCCTT; scrambled control- silencer negative control #1 siRNA (Ambion).

Time lapse microscopy

Cells were transfected as above with siWNK1 or scrambled control oligonucleotides. After 24 h, cells were imaged with a Deltavision RT deconvolution microscope (Applied Precision) with an environmental control chamber (Solent). Images were acquired using a 20X phase contrast objective lens every 30 min for 72 h. Data were processed and analyzed with Image J (Rasband, W.S., Image J, U.S. National Institutes of Health, Bethesda, Maryland, USA, http://rsb.info.nih.gov/ij/, 1997-2006).

Microinjection

Cell culture medium was replaced with CO_2-independent medium just before injection. A Transjector 5246 (Eppendorf) on an Eclipse TE300 microscope (Nikon) was used for microinjection. Cells were co-injected with 20 ng /µl dynactin-tdtomato cDNA or 1 mg/ml dextran-Alexa 488 with 20 nM WNK1 or scrambled control siRNA oligonucleotides.

Image analysis

Fluorescent z-stacks were acquired and deconvolved using the Deltavision RT deconvolution microscope. Co-localization and three dimensional models were analyzed using Imaris software (v. 6.4, Bitplane, Zurich). All data shown are displayed as projections through the Z stack. The co-localization channels depicting voxels showing statistically significant co-localization were generated using the Co-Loc module of Imaris, which is based on (*97*).

Cell survival assay

Cells were transfected twice, 24 h apart, with WNK1, OSR1 or scrambled control oligonucleotides. After 72 h, cells excluding Trypan blue were counted. Cell survival was normalized to that for the scrambled control. Three independent experiments were performed. Statistical analysis was by one-way ANOVA with Bonferroni test.

Results

WNK1 displays a punctate localization pattern

I first validated the antibody used for the immunostaining experiment for endogenous WNK1. Peptide blocking using the antigen for WNK1 antibody greatly diminished the WNK1 signal (Fig. 2-1 B). Depletion of WNK1 by small interfering RNA also significantly reduced WNK1 fluorescence, suggesting the specificity of the signals is valid (Fig. 2-1 C, arrows indicate cells with knockdown). Fig. 2-1 A and D indicated that the distribution of endogenous WNK1 in HeLa cells under normal cultural conditions was a perinuclear punctate pattern and a similar pattern was apparent in MCF7 breast and HT29 colon cancer cell lines as well (Fig. 2-1 E and F). Low level expression of GFP-WNK1 also exhibited a punctate distribution (Fig. 2-1 G to I). These data suggested that endogenous WNK1 displays a perinuclear punctate distribution in interphase cells.

WNK1 localizes on mitotic spindles during mitosis

I then started to investigate the localization of endogenous WNK1 during mitosis by co-immnuostaining WNK1 and α tubulin. In early prophase, WNK1 was localized at astral microtubules that were organized from the centrosome (Fig. 2-2 A to C). In metaphase, WNK1 localized at the spindle microtubules with higher signals close to the spindle pole body than at the kinetochore ends (Fig. 2-2 D to F). Fig. 2-2 G to I presents the data from Fig. 2-2 D to F by using a 3D volume rendering method in which the transparency of each voxel varies according to its depth in the volume. Therefore, it could demonstrate the three dimensional structure in a way that human eye could perceive the image better. In anaphase, WNK1 signals still remained in the polar spindle microtubules and some of the signals were detectable in the midzone area (Fig. 2-2

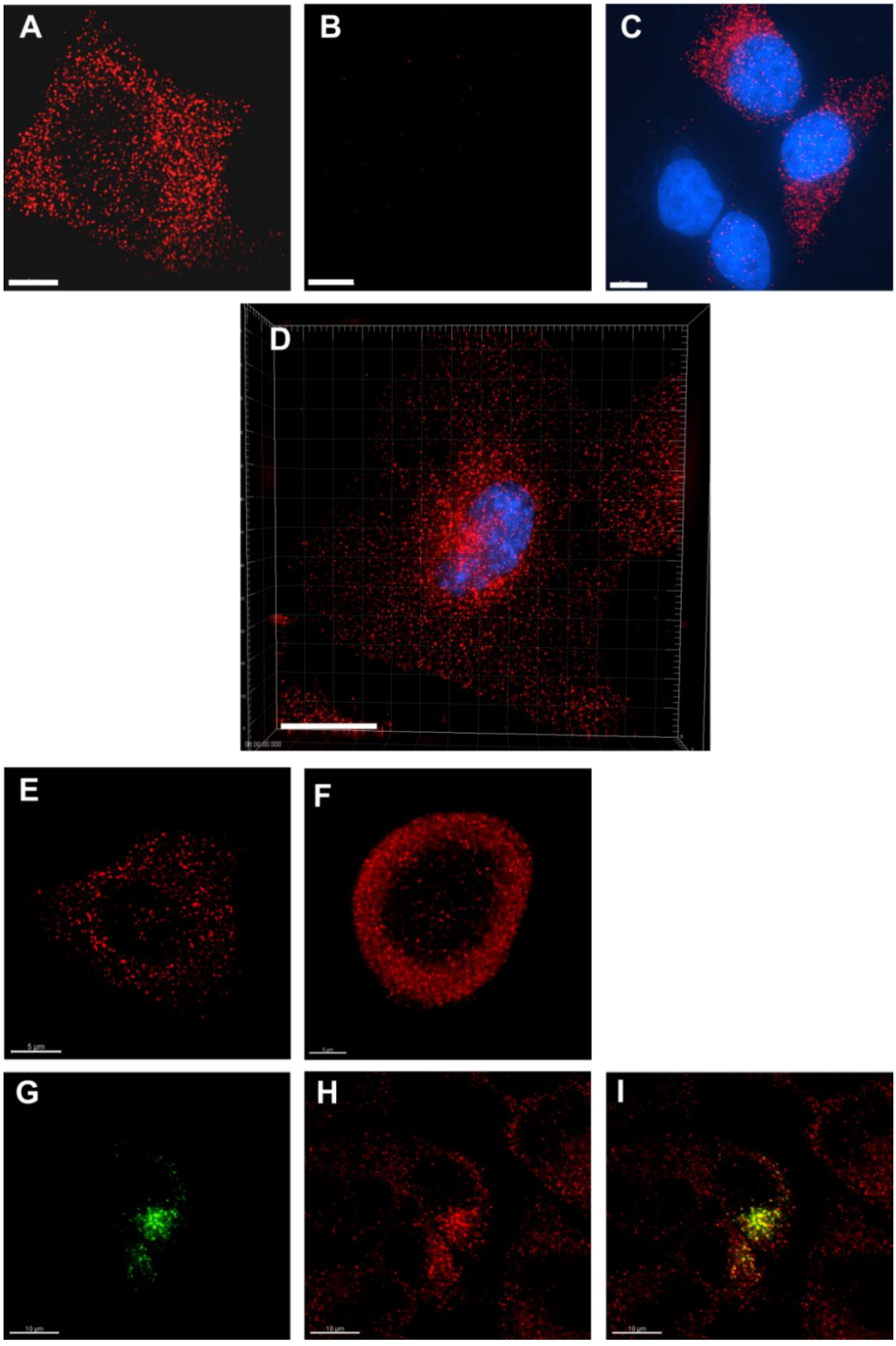

Figure 2-1. WNK1 displays a punctate localization pattern (Tu et al., 2011). See next page for the legend.

Immunostaining of HeLa cells: WNK1 (red) and DAPI (blue). (A) Projected Z-slices of HeLa cells stained for WNK1. The specificity of the WNK1 antibody was verified by peptide antigen block (B) and siRNA knockdown (C). (D) A zoomed in picture emphasizes the perinuclear staining of endogenous WNK1. (E) WNK1 staining in MCF7 cells or (F) HT29 cells. Scale bar: 5 μm. (G) HeLa cells expressing low levels of GFP-WNK1. (H) Immunostaining of endogenous HeLa WNK1 (red). (I) Color merged. Scale bar: 10 μm.

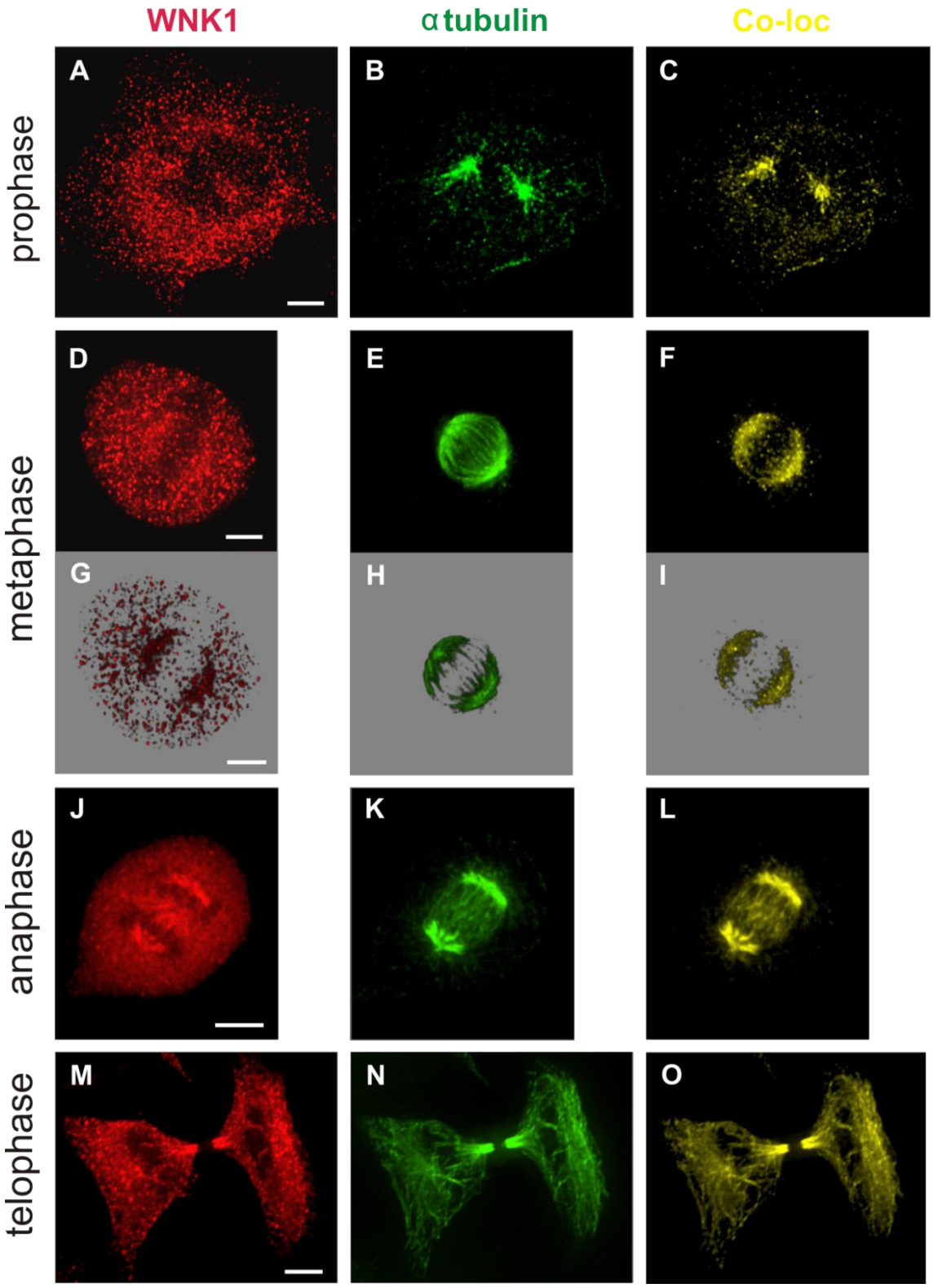

Figure 2-2. WNK1 localizes on mitotic spindles during mitosis (Tu et al., 2011). See next page for the legend.

Immunostaining of HeLa cells: WNK1 (red), tubulin (green). The co-localized channel (yellow) was generated by Imaris 6.4 software. (A-C) Early prophase (D-F) Metaphase (G-I) The same images as in D-F, shown in volume-rendered projection. (J-L) Anaphase (M-O) Telophase. Scale bar: 5μm.

J to L). In telophase, WNK1 still localized at the astral microtubules and stronger signals were evident in the spindle midzone between two daughter cells (Fig. 2-2 M to O). These observations suggested that WNK1 might be involved in mitosis and probably as early as prophase which is when astral microtubules form. In order to explore the possible mechanism underlying how WNK1 could affect mitosis, I mainly employed small interfering RNA to deplete endogenous WNK1 and observed the phenotypic results. There were two major phenotypic defects- one was aberrant mitotic spindles and chromosomes, the other was failure of abscission which is the final step of cutting or separating two daughter cells.

Depletion of WNK1 causes aberrant mitotic spindles

For the mitotic spindle defects, there were several different aberrant phenotypes, including longer and misaligned spindles and chromosomes (Fig. 2-3 D to F), tri-polar spindles and L-shape chromosomes (Fig. 2-3 G to I), tetra-polar spindles and cross shaped chromosomes (Fig. 2-3 J to L) and multipolar spindles with misaligned chromosomes (Fig. 2-3 M to O). Time lapse microscopy experiments also revealed that cells depleted of WNK1 arrested in mitosis and eventually died. The initial time lapse microscopy imaging experiment was done by using a 12 well glass bottom dish. The experimental design was as follows: cells were treated with control non-targeting siRNA in one well and the other well was treated with siRNA targeting WNK1. The microscope was capable of setting multiple positions for imaging cells in each well for 72 hours with controlled CO_2 and 37˚C. The drawbacks for this experiment were that I was doing random imaging and did not know whether cells showing phenotypic defects correlated with the depletion of endogenous WNK1. Therefore, most of cells in the 25 positions I imaged did not show defects. However, there were some cells displaying mitosis defects as they arrested and eventually died, indicated by yellow arrowheads (Fig. 2-4 A to F, movie 2-1). In Fig. 2- 4 (movie

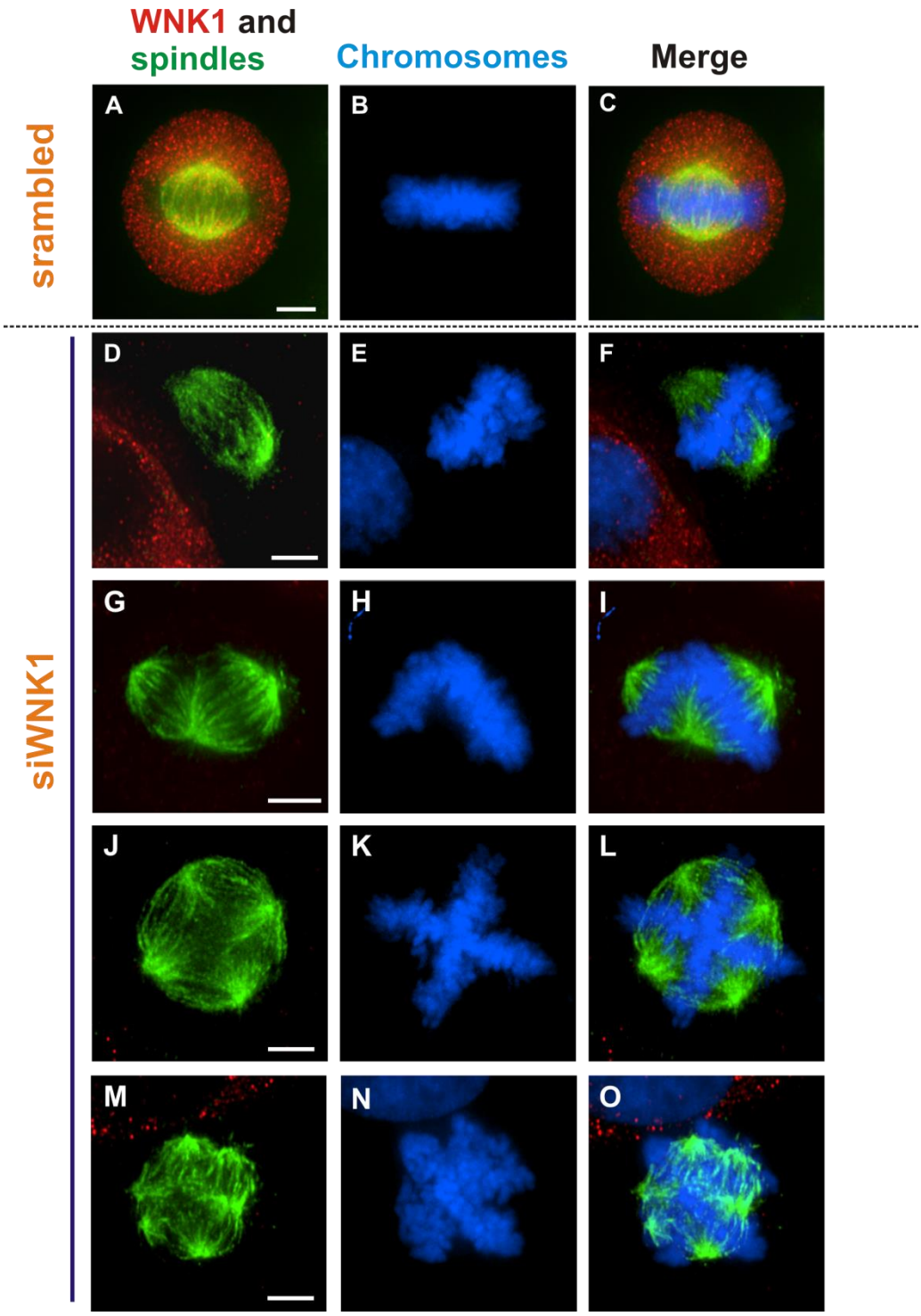

Figure 2-3. Depletion of WNK1 causes aberrant mitotic spindles (Tu et al., 2011)

Immunostaining of HeLa cells 48 hours after transfection with scrambled (A-C) or WNK1 siRNA oligonucleotides (D-O).WNK1 (red), tubulin (green), DAPI (blue channel). Scale bar: 5µm

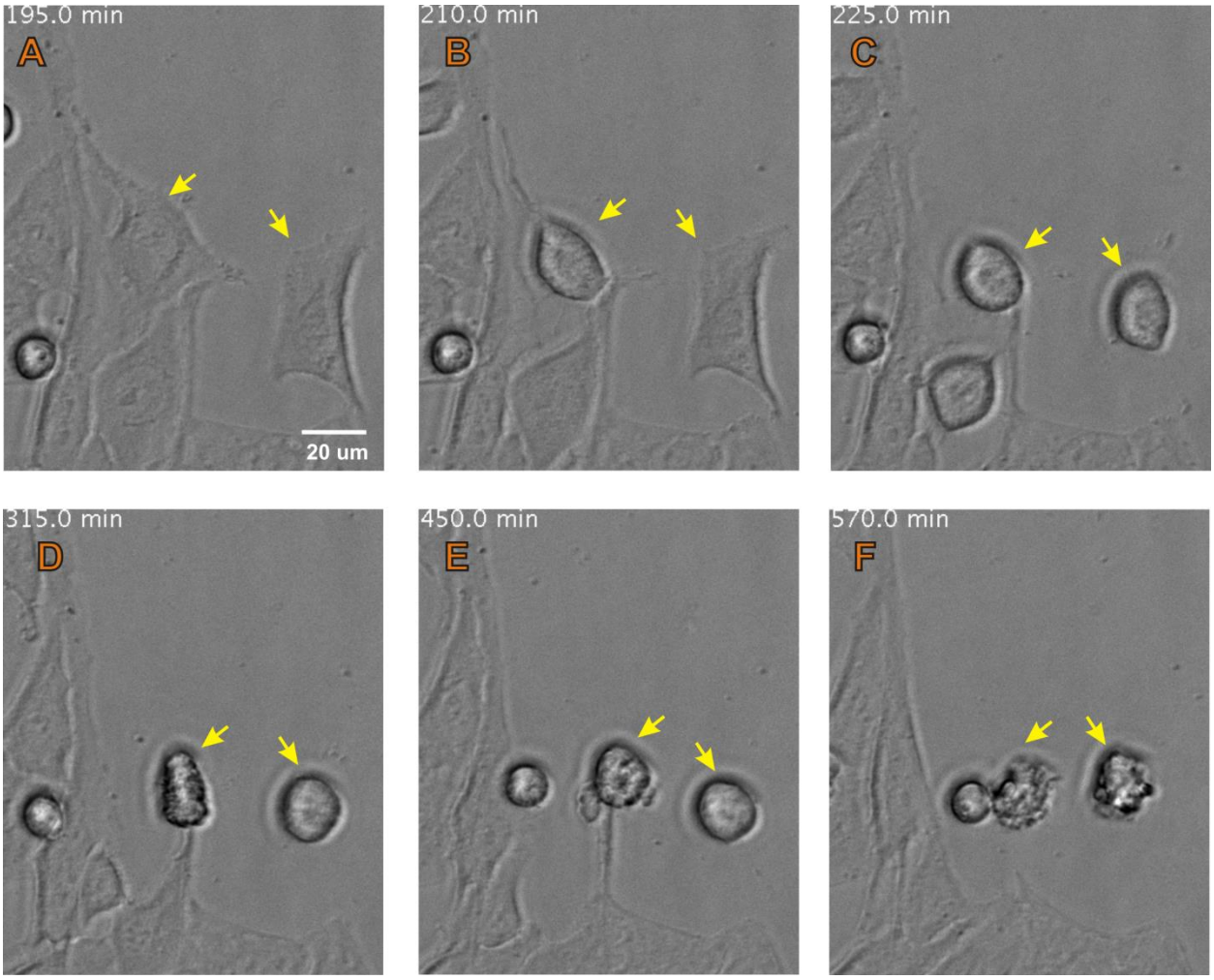

Figure 2-4. Time lapse phase contrast microscopy revealed mitosis defect in WNK1-depleted RNAi dish.

Figure 2-4 corresponds to movie 2-1. Yellow arrowheads indicate that cell arrested in mitosis and eventually died. Time stamper in C to F suggested that cells arrested at least 345 minutes while normal mitosis would just take half to one hour.

2-1), time stamps show that cells arrested for at least 8 hours whereas normal mitosis completed within 30 minutes to one hour. In order to improve the chances of finding WNK1 depleted cells for imaging and increase the efficient delivery of siRNA, I designed a co-injection experiment. A motor accessory protein- dynactin was tagged with a fluorescent protein- tdtomato. I will refer to this construct as tdt-dynactin and discuss this protein later in the third chapter onWNK1 and interphase microtubules. By co-injecting tdt-dynactin and RNAi oligonucleotides (either non-targeting or WNK1), the efficiency was greatly improved and I was able to achieve a statistical sample size. In 50 control cells imaged, only 8% of cells arrested or failed in mitosis whereas in 52 cells imaged in WNK1-depleted condition, 42% of cells arrested in mitosis and died. Fig. 2-5 A to H is a gallery of several image frames from movie 2-2 and demonstrates an example of normal mitosis in the control experiment. Fig. 2-6 and 2-7 are from movie 2-3 and 2-4 respectively and show cells that arrested in mitosis and died in WNK1-depleted condition. It is technically difficult to obtain good images of mitotic cells as they round up and are often out of the focal plane. I tried to observe whether the mitotic spindle defects occur in Fig. 2-6 or 2-7 though the mitotic cells are not well focused. In Fig. 2-6 B, the bottom cell seemed to display an aberrant mitotic spindle similar in Fig. 2-2 D to F. In Fig. 2-7, the bottom cell apparently had tri-polar spindles (Fig. 2-7 F to H) and also died. Though triple division does sometimes happen in HeLa cells, the incidence of tri-polar spindles was much higher in the WNK1-depleted cells. Taken together, these data suggested that depletion of WNK1 indeed affected mitosis and caused aberrant mitotic spindles.

Depletion of endogenous OSR1 does not cause defects in mitotic spindles

As mentioned in Chapter 1, OSR1 is a well characterized WNK1 substrate and affected ion co-transporters. I was prompted to investigate whether WNK1 exerted its mitotic function

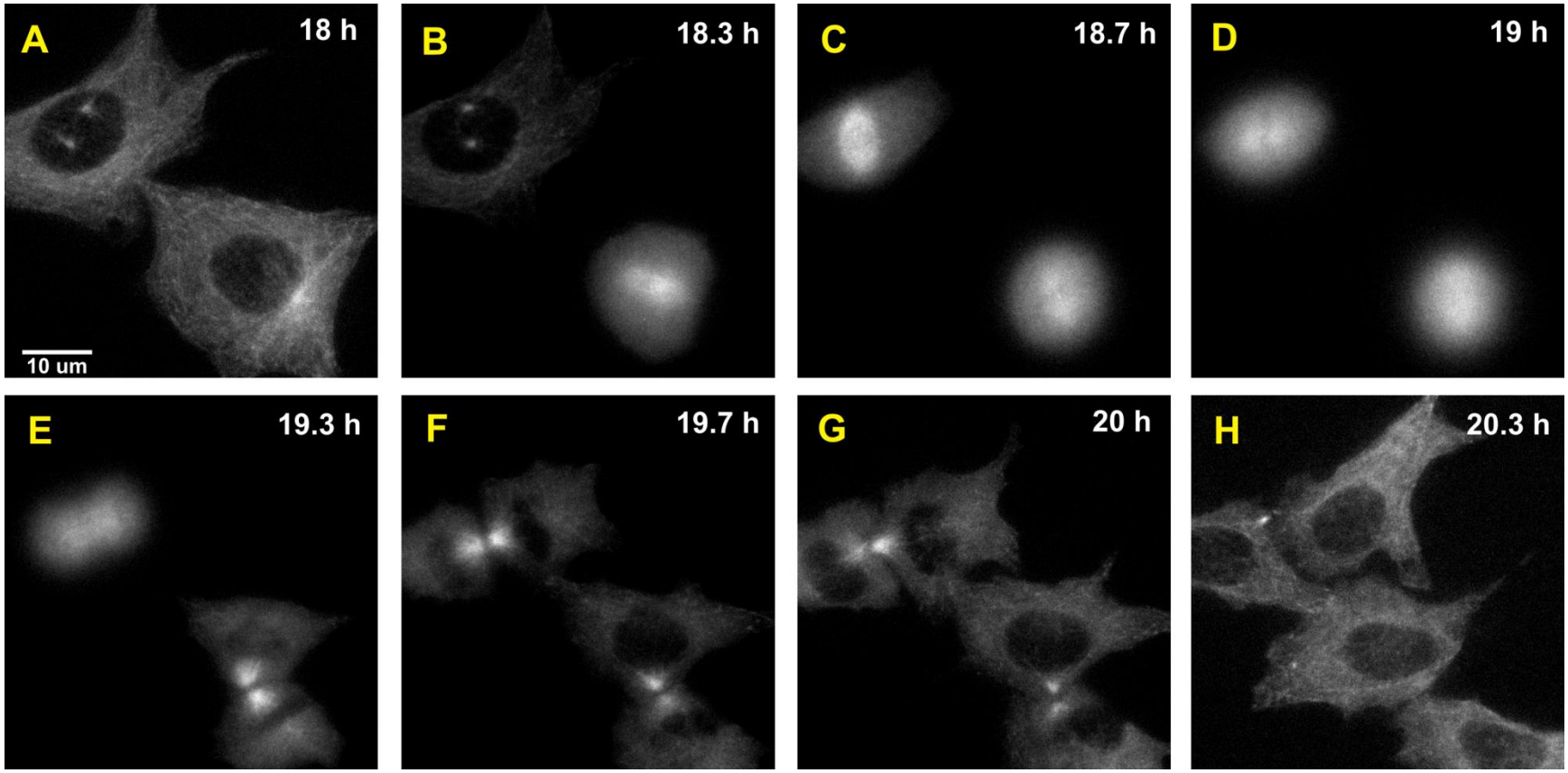

Figure 2-5. Time lapse imaging shows normal mitosis in control cells.

Figure 2-5 corresponds to movie 2-2. Figure A to H show that cells microinjected by tdt-dynactin cDNA and control oligonucleotides displayed normal mitosis.

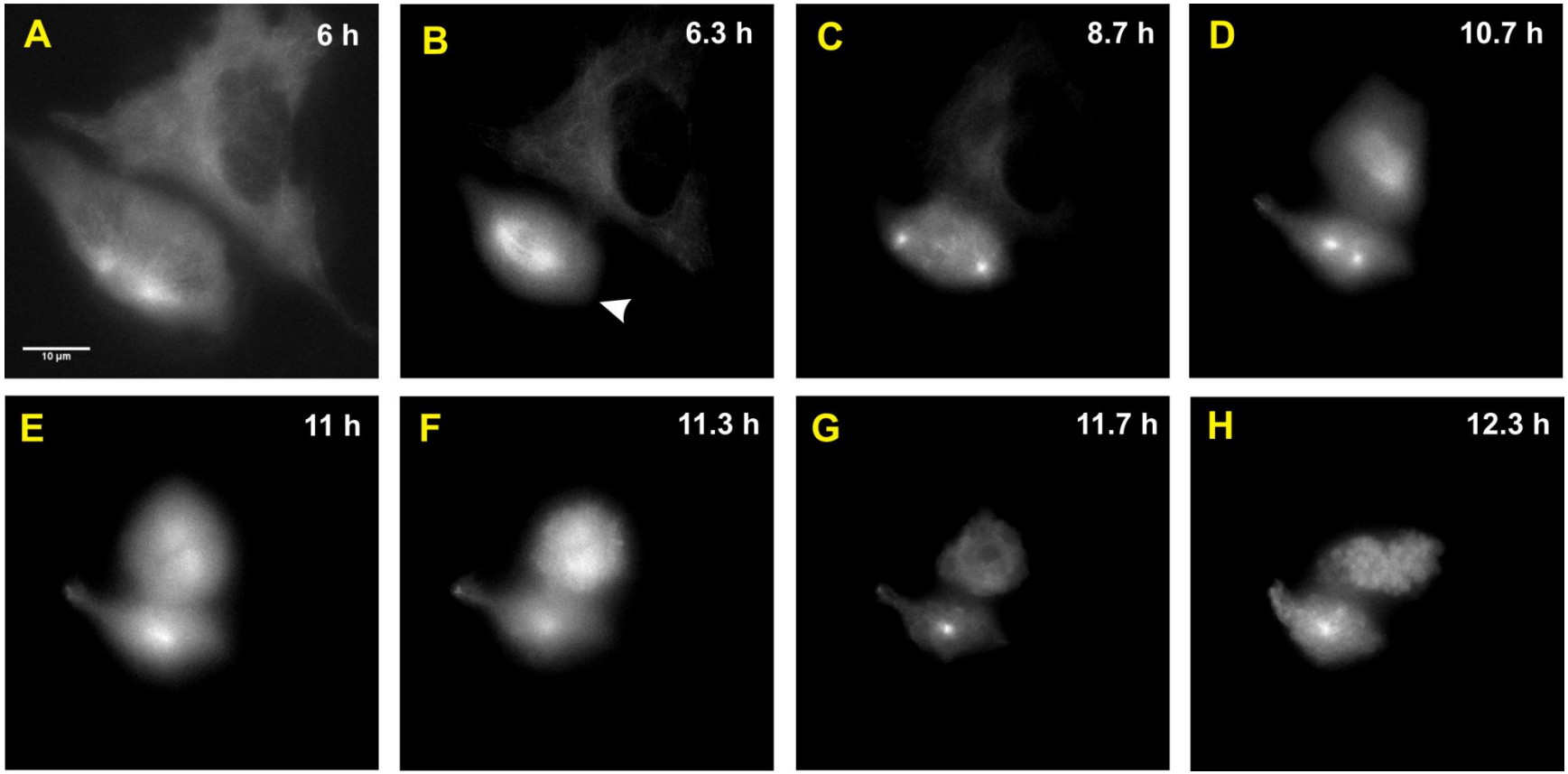

Figure 2-6. Time lapse imaging shows mitosis defect in cells depleted of WNK1.

Figure 2-6 corresponds to movie 2-3. Figure A to H show that cells microinjected by tdt-dynactin cDNA and siWNK1 oligonucleotides displayed mitosis defect. Bottom cell in Figure B (white arrowhead) seemed to have the mitotic spindle defect shown in Fig 2-2 D.

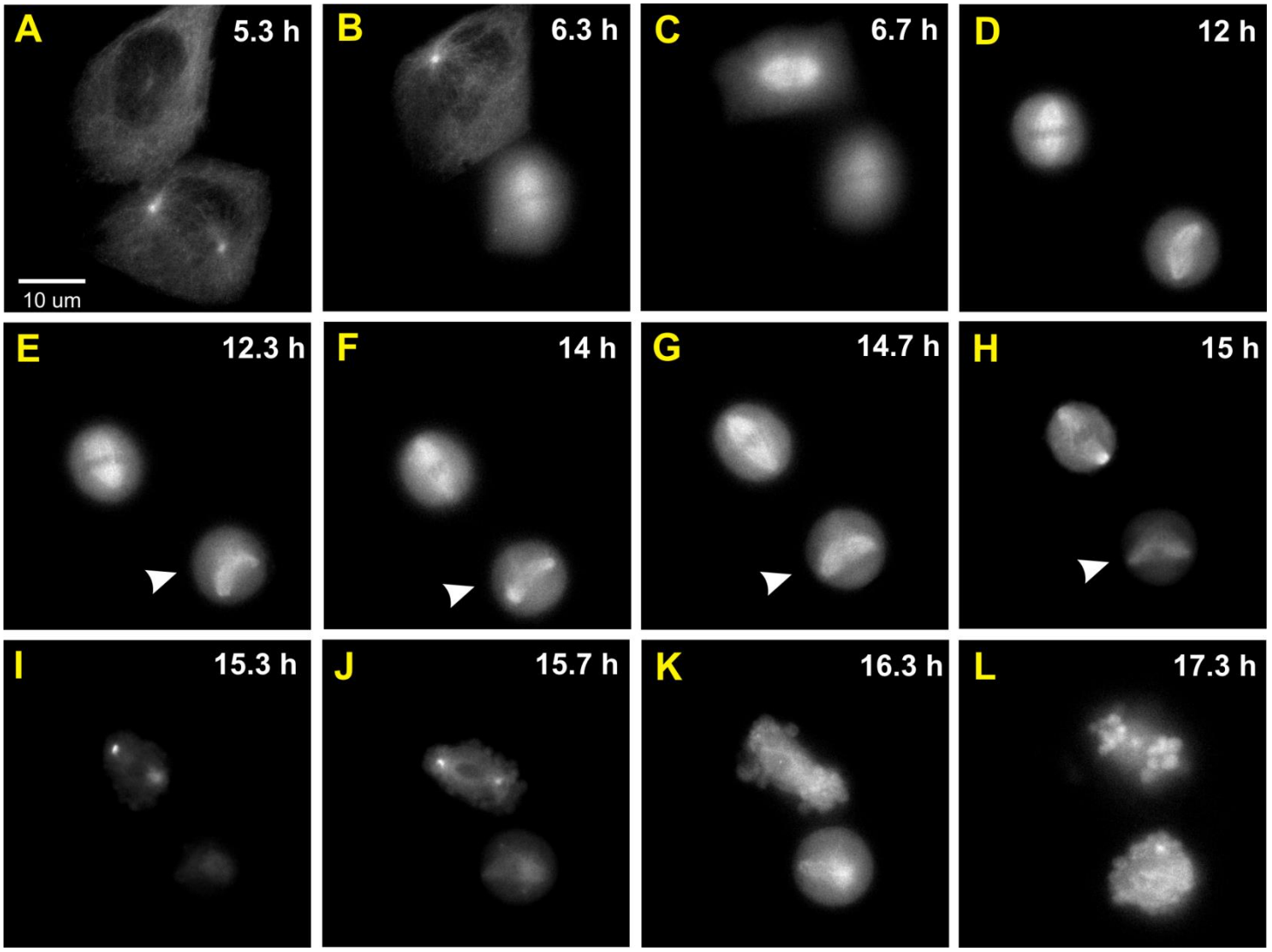

Figure 2-7. Time lapse imaging shows mitosis defect in cells depleted of WNK1. See next page for the legend.

Figure 2-7 corresponds to movie 2-4. Figure A to L show that cells microinjected with tdt-dynactin cDNA and siWNK1 oligonucleotides displayed mitosis defect. The bottom cell had tri-polar spindles (E to H, white arrowheads) and eventually died.

through OSR1. First, the localization of OSR1 during mitosis was examined by co-immnuostaining OSR1 and α tubulin. As shown in Fig. 2-8 A to L, OSR1 was distributed homogeneously within the cell during prophase, metaphase, anaphase and telophase and did not show evidently stronger signals on the mitotic spindles. Second, depletion of endogenous OSR1 by siRNA did not cause aberrant mitotic spindles and chromosomes (Fig. 2-9 A to F) nor did it affect the localization of WNK1 on the mitotic spindles (Fig. 2-9 G to I). Thus, WNK1 might regulate mitosis through other unknown effectors.

WNK1 kinase activity increased in nocodazole or taxol – induced mitotically arrested HeLa S3 cells

To look for WNK1 effectors biochemically, I used mitotic shake off. This experiment was done by using another cell line- HeLa S3. As the cell cycle of HeLa S3 can be synchronized more easily than some other cell types, it is often used for biochemical analysis of cell cycle events. Mitotic-shake off is one of the easiest ways to get mitotically enriched cells. As mitotic cells rounded up and had fewer attachment with the cultural dish, it is not difficult to understand how the shake off could work. Cells were synchronized by treatment with nocodazole or taxol for 12 to 16 hours. Nocodazole is a microtubules depolymerising agent whereas taxol is a microtubules stabilization agent. Nocodazole disrupts interphase microtubules and causes cells to arrest in a prophase to pseudo-metaphase period (*98*). Nocodazole also activates spindle checkpoint which would activate several mitotic kinases. On the other hand, taxol is a drug that preferentially binds covalently to β tubulin and stabilizes the microtubules. It also blocks cells at G2/M transition and causes spindle checkpoint–mediated mitotic arrest (*99*). Though both nocodazole and taxol could cause mitotic arrest, the signaling pathway could be different. Nonetheless, I harvested cells after drug treatment and shake them off for endogenous WNK1

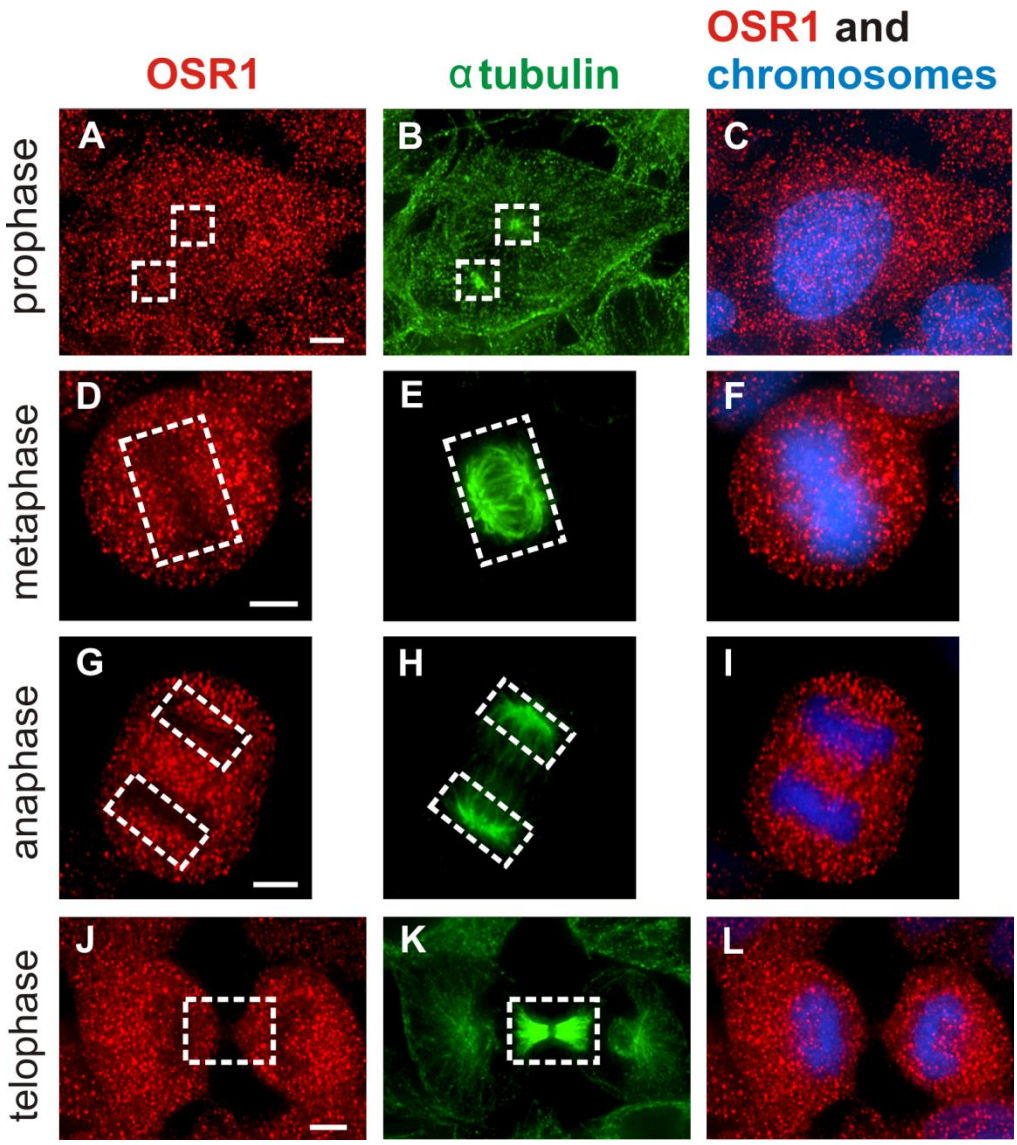

Figure 2-8. OSR1 displays a localization distinct from WNK1 during mitosis (Tu et al., 2011).

Immunostaining of HeLa cells: OSR1 (red), tubulin (green) and DAPI (blue). (A-C) Early prophase. (D-F) Metaphase. (G-I) Anaphase. (J-L) Telophase The broken white lines generally mark mitotic spindles (A,B,D,E,G,H,J,K). Scale bar: 5μm.

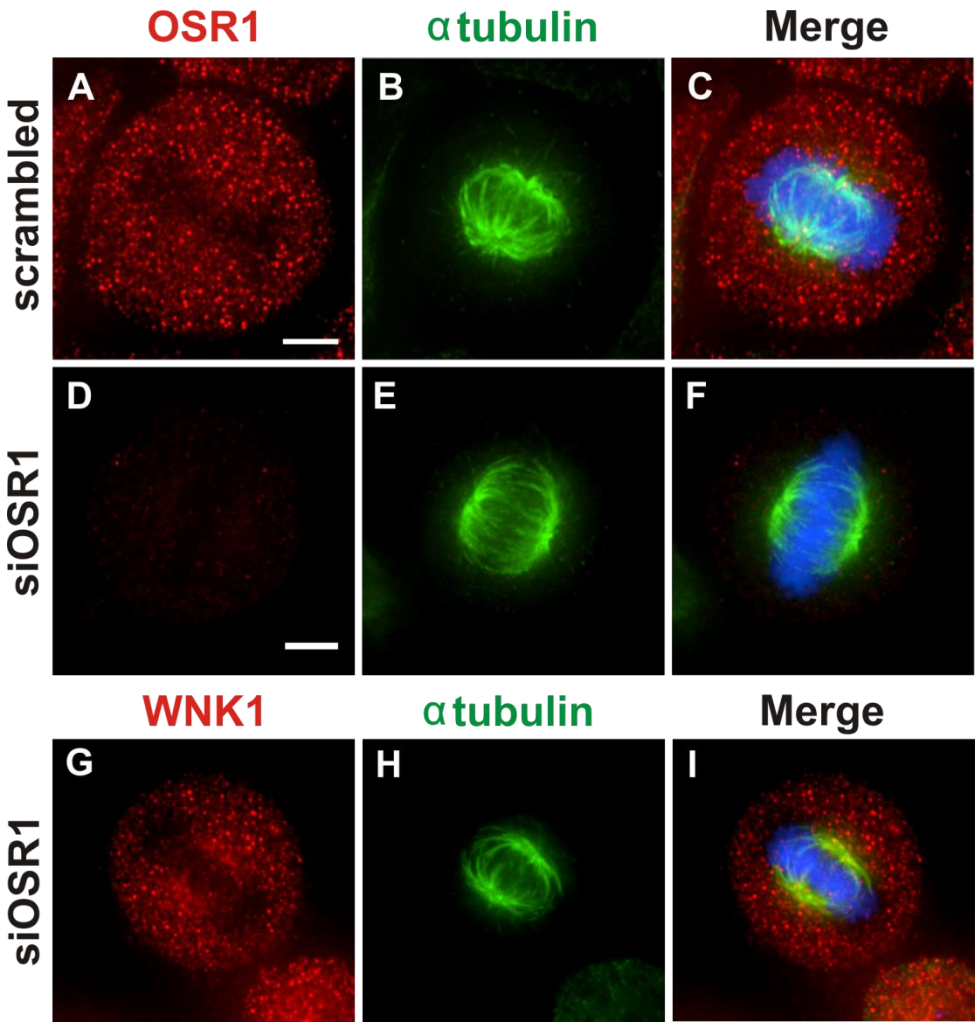

Figure 2-9. Depletion of endogenous OSR1 does not cause defects in mitotic spindles (Tu et al., 2011).

Immunostaining of HeLa cells 48 hours after transfection with scrambled (A-C) or OSR1 siRNA oligonucleotides (D-I). OSR1 (A, D- red) or WNK1 (G- red), tubulin (B, E, H- green), DAPI (C, F, I- blue). Scale bar: 5μm.

immuno-precipitation (IP) kinase assay. As shown in Fig. 2-10, WNK1 kinase activity increased in mitotically cells arrested either by nocodazole or taxol treatment. Green arrowhead indicates that an unknown protein associated with the WNK1 protein complexes and showed an evident radioactivity in nocodazole or taxol treatment.

These results above address how WNK1 might be involved in mitosis mainly in G2 to M phase. Other evidence suggests that WNK1 is also required for later phases of cell division.

RNAi of WNK1 resulted in a defect in abscission

The other phenotypic defect I have observed upon WNK1 depletion was failure of abscission, which is the final step of cutting and separating two daughter cells. In control cells, the length of the bridge between two daughter cells before abscission was 14.1± 0.4 μm, whereas the average length was 31.8 ± 0.9 μm in WNK1-depleted cells (Fig. 2-11 A to C). Time lapse phase contrast microscopy revealed that when two daughter cells moved away from each other after abscission, the un-separated bridge could prevent the crawling movement of two daughter cells, thus causing the bridge and cells to become elongated (Fig. 2-11 D and E). As the experiment shown in Fig. 2-11 D and E was a bright field RNAi experiment, it was not possible to correlate defects in abscission directly with WNK1 depletion. In further experiments, I co-injected Alexa 488 labeled dextran with RNAi oligonucleotides to allow identification of WNK1 depleted cells (movie 2-5). Fig. 2-12 A to J is the gallery of several image frames from movie 2-5. The cell in movie 2-5 showed the same abscission defect as Fig. 2-11 E.

Rescue of mitotic phenotypes by rat WNK1

To show that the phenotypic results I have observed are not due to off-target effect of the RNAi, I did a rescue experiment. Cells were transfected with Rat cDNA WNK1 construct and

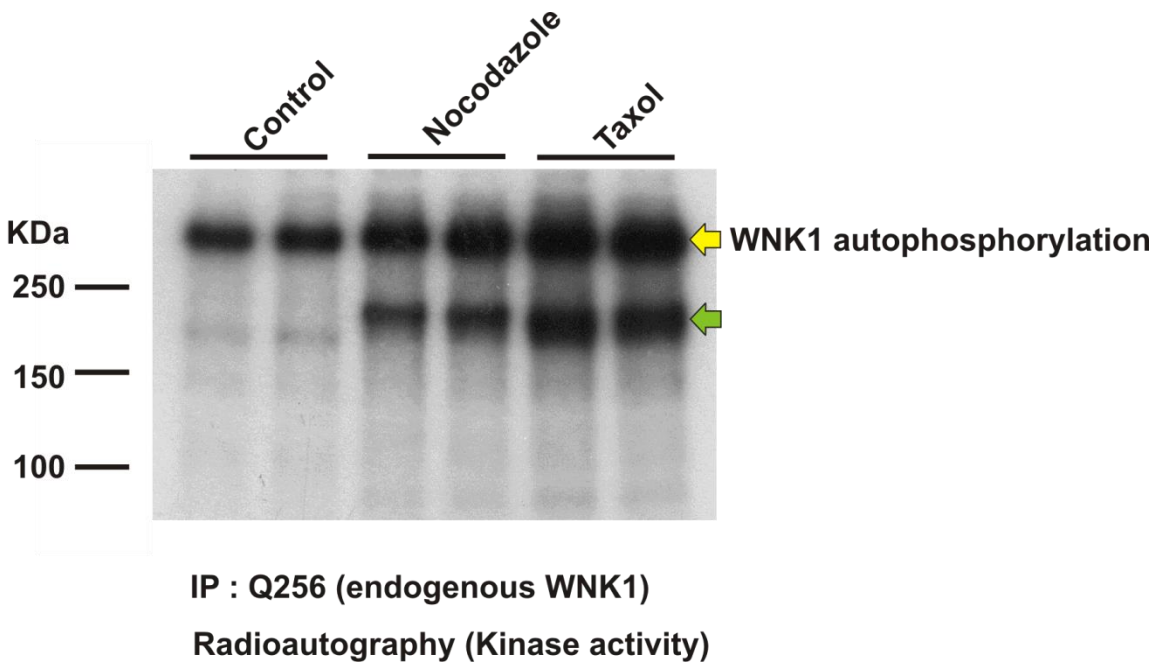

Figure 2-10. WNK1 kinase activity increased in nocodazole or taxol – induced mitotically arrested HeLa S3 cells.

HeLa S3 cells were synchronized by nocodazole or taxol for 16 hours. Cells were then be shaken off from 75T- cultural flask and lysed with buffers (0.5% Triton X-100, 50 mM HEPES (pH 7.5), 150 mM NaCl, 1.5 mM $MgCl_2$, 1 mM EGTA, 10% glycerol, 100 mM NaF, 0.2 mM Na_3VO_4, 50 mM β-glycerophosphate, 1 mM dithiothreitol, 1 mM benzamidine hydrochloride, 10 mg/L leupeptin, 0.5 mg/L pepstatin A, and 1.5 mg/L aprotinin). Cells were vortexed for 30 seconds and incubated on ice for 30 min. The lysates were clarified by centrifugation at 16,000g in a microfuge for 20 min. Immunoprecipitating antibodies (WNK1 Q256 1: 100 ratio (µl antibody / µl lysate)) were added to the 16,000g supernatant and incubated at 4˚C with rotation overnight. Protein A/G agarose beads (30 µl) were added the next day and incubated at 4˚C with rotation for one hour. Beads were washed with lysis buffer with salt concentration 1M NaCl three times, for 10 min each. Kinase assays were performed in 30 µl of kinase buffer (20 mM HEPES, pH 7.5, 10 µM ATP, 10 mM $MgCl_2$, 10 mM β-glyceerophosphate, 1 mM dithiothreitol and 1 mM benzamidine hydrochloride) containing 10 µ Ci of γ-^{32}P ATP, incubated at 30˚C for 30 min. Reactions were terminated by the addition of 5X SDS sample buffer and heating for 3 min at 94˚C.

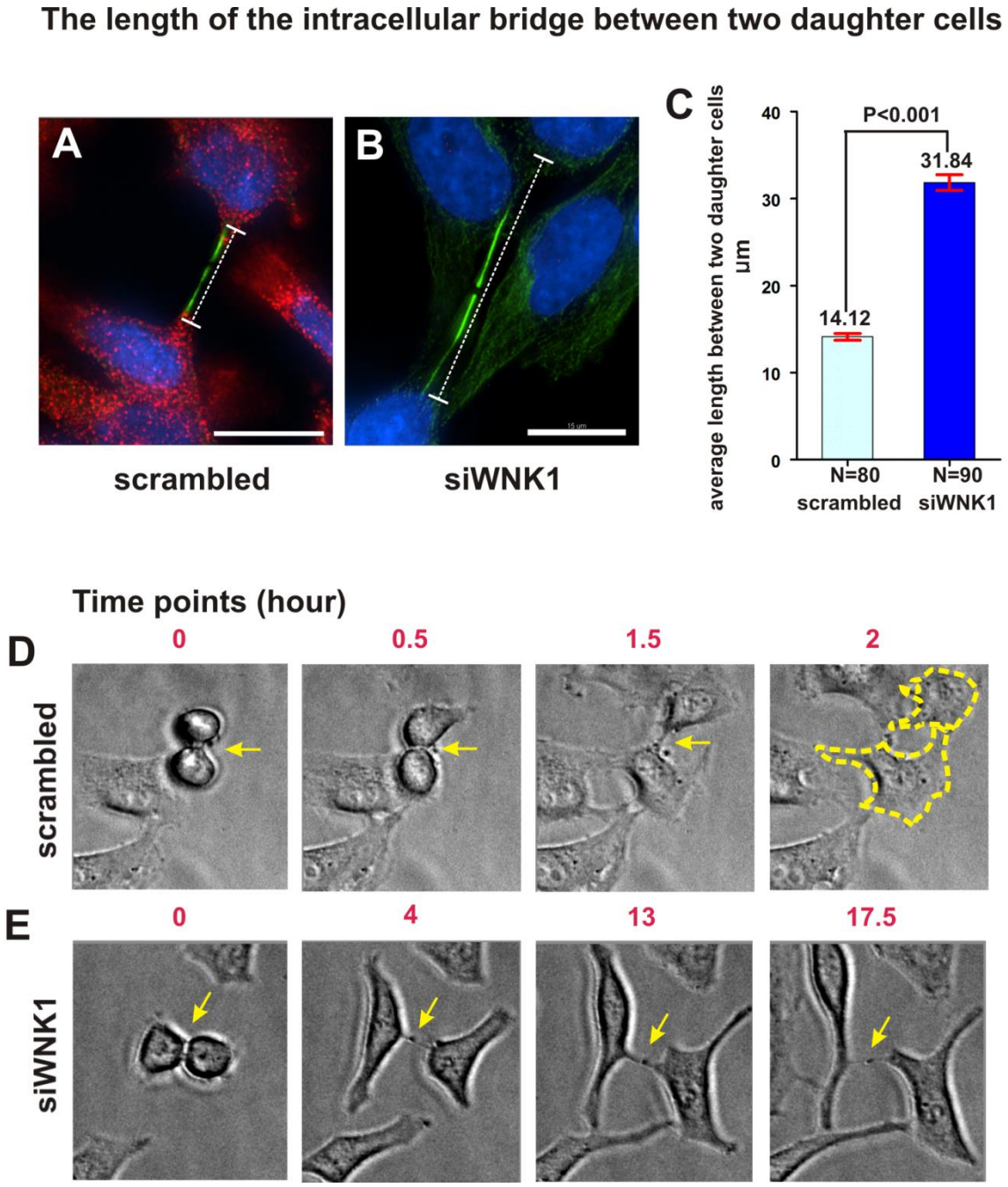

Figure 2-11. RNAi of WNK1 resulted in a defect in abscission (Tu et al., 2011). See next page for the legend.

Immunostaining of HeLa cells 72 h after transfection with scrambled (A) or WNK1 siRNA oligonucleotides (B). WNK1 (red), tubulin (green), DAPI (blue). In A and B, the bridge between two daughter cells is overlaid with a bar indicating length. Scale bar: 15um. (C) The average length of bridges in scrambled control and WNK1 knockdown cells is plotted. Sample images were taken from four independent experiments (scrambled control, N=80; WNK1 knockdown, N=90). Statistical analysis was performed by unpaired t-test. (D, E) Individual frames from time lapse microscopy of (D) scrambled control and (E) WNK1 knockdown cells. Regions between separating cells are indicated by yellow arrowheads. Perimeters of separated daughter cells in the scrambled control are indicated by yellow lines in D.

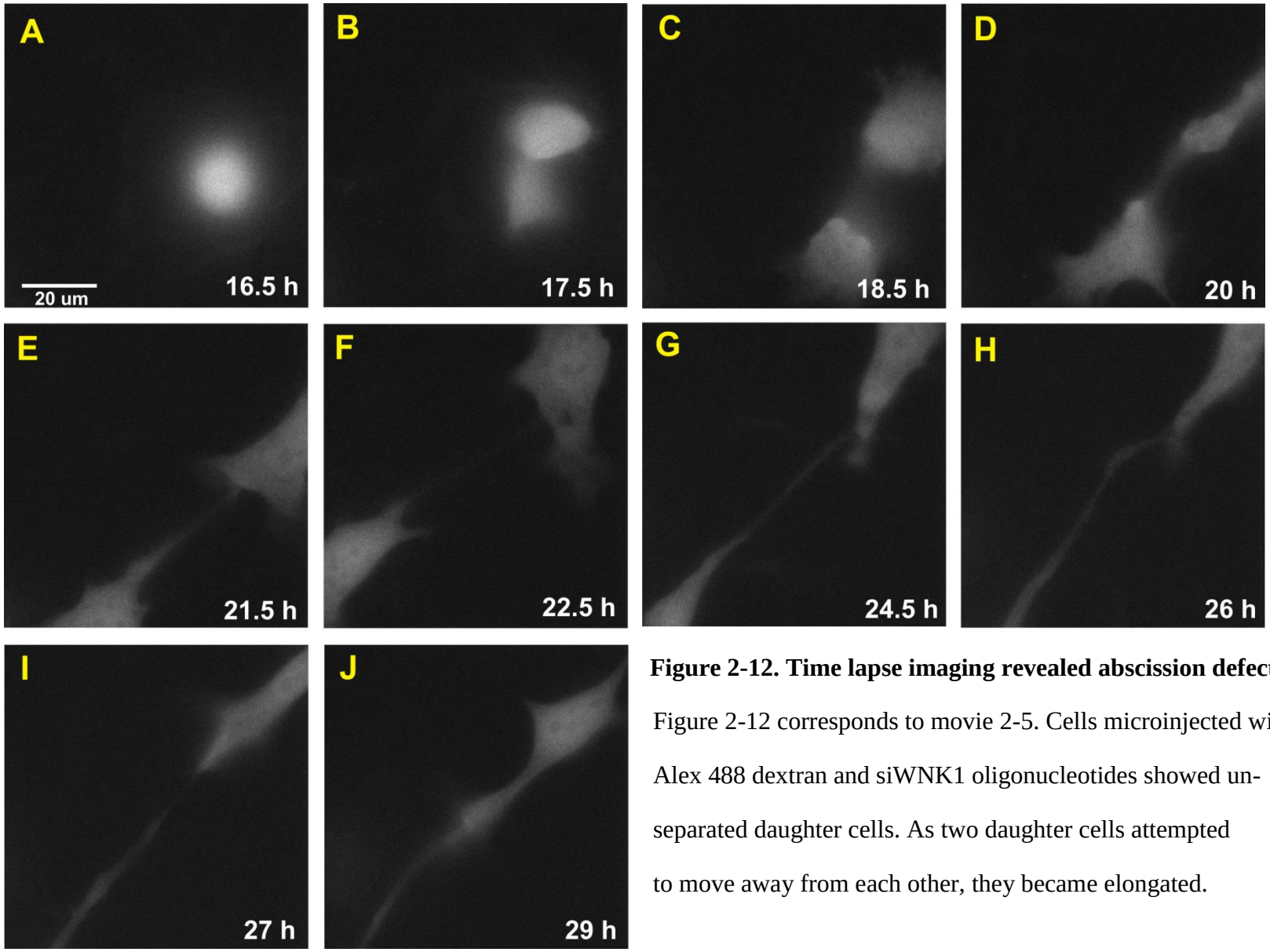

Figure 2-12. Time lapse imaging revealed abscission defect. Figure 2-12 corresponds to movie 2-5. Cells microinjected with Alex 488 dextran and siWNK1 oligonucleotides showed un-separated daughter cells. As two daughter cells attempted to move away from each other, they became elongated.

depleted of endogenous WNK1 by RNAi. The Rat WNK1 sequence has a flag epitope that allows it to be distinguished from endogenous WNK1 by immunofluorescence. By co-immunostaining of endogenous WNK1, exogenous rat WNK1 and α tubulin, I found that cells presented a normal phenotypic result regarding the mitotic spindles and the bridge between two daughter cells in the presence of exogenous rat WNK1 (Fig. 2-13 A to H), suggesting that mitotic and abscission defects were truly caused by the depletion of WNK1.

Effect of depletion of WNK1 or OSR1 on cell survival

From several time lapse microscopy experiments, I often observed that cells depleted of WNK1 would die eventually. I assessed cell survival by trypan blue dye exclusion, as only dead cells could be stained. Cell survival rate was normalized with control RNAi condition. As shown in Fig. 2-14, WNK1-depleted cells had only 34.5% and OSR1-depleted cells had 77.6% survival rate, suggesting that WNK1 and OSR1 might contribute to cell survival through different mechanism.

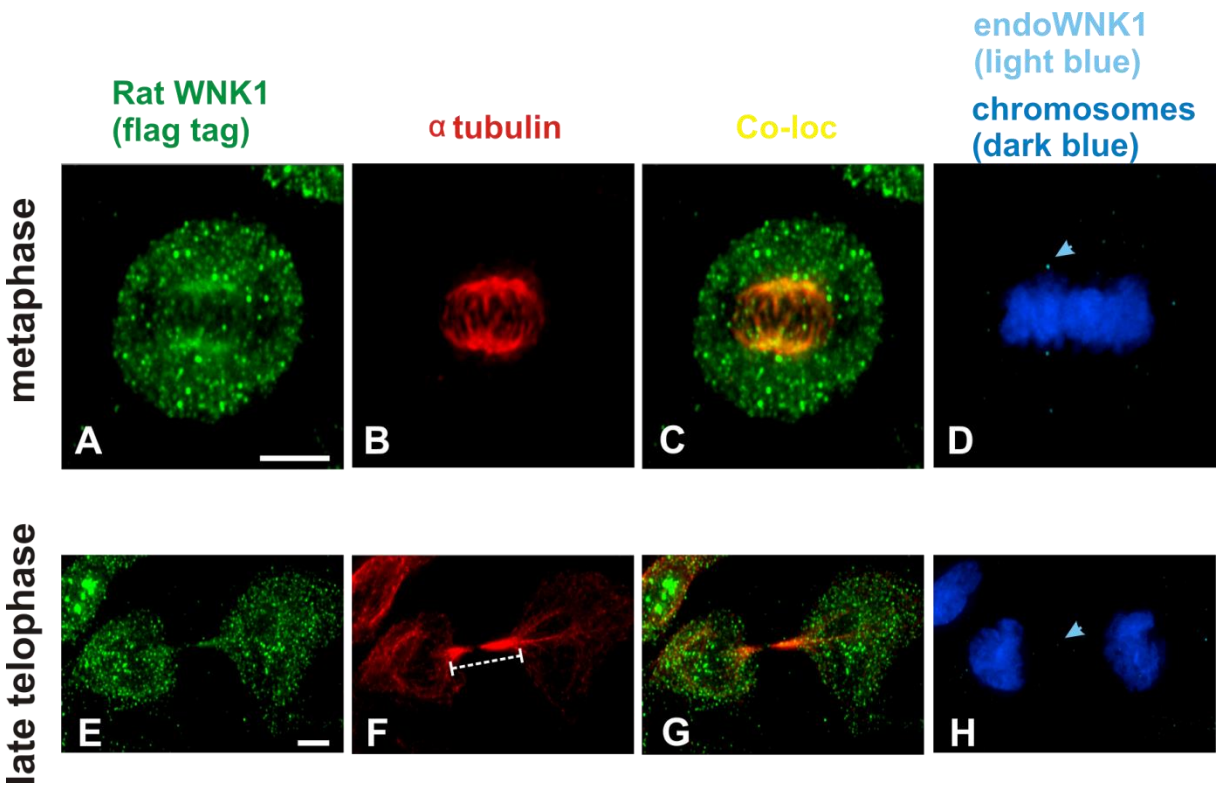

Figure 2-13. Rescue of mitotic phenotypes by rat WNK1 (Tu et al., 2011).

Rat Flag-WNK1 was expressed in cells in which the endogenous protein was knocked down. Rat Flag-tagged WNK1 (green), endogenous WNK1 (light blue), tubulin (red) and DAPI (dark blue). (A-D) Metaphase. (E-H) Late telophase. Scale bar: 5μm

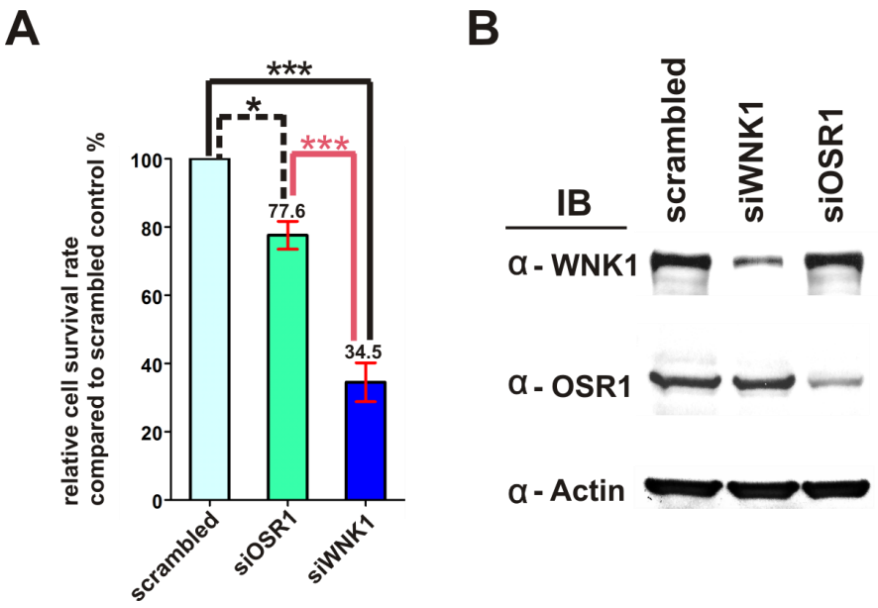

Figure 2-14. Effect of depletion of WNK1 or OSR1 on cell survival (Tu et al., 2011).

(A) The percentage of viable cells remaining following transfection with scrambled, WNK1 siRNA or OSR1 siRNA oligonucleotides is shown as mean ± SEM. Three independent experiments were performed. Statistical analysis was by one-way ANOVA with Bonferroni test. * indicates $P < 0.05$, *** indicates $P < 0.001$. (B) Immunoblotting of HeLa cells transfected with scrambled, WNK1, or OSR1 siRNA oligonucleotides.

Discussion

Here I report a novel property of WNK1, a requirement for localization to spindles during mitosis, not anticipated by any previous biochemical or physiological studies. Depletion of WNK1showed multi-polar spindles, disorganized chromosomes, failed abscission, multi-nucleated cells, and reduced cell survival. WNK1 binds a number of other proteins including protein kinases through its noncatalytic domains (*56, 82, 90*). Thus, WNK1 may exert its mitotic function through either its enzymatic activity or protein-protein associations. Extensive examination of the localizations of endogenous WNK1 and OSR1 reveal punctate, largely cytoplasmic distributions. Although the puncta are too small to be identified unequivocally as vesicles by light microscopy, the data suggest that WNK1 and OSR1 may be on intracellular vesicles in resting cells and support the strong biochemical data showing WNK1-OSR1 association. On the other hand, when GFP-WNK1 was overexpressed, not only did we observe a diffuse rather than punctate staining pattern, but also several intense GFP spots which suggested aggregation. Therefore, it seems unlikely that the diffuse GFP-WNK1 signal is an accurate reflection of WNK1 localization. From live cell imaging I also found that expression of WNK1 had to be carefully titrated. Overexpression caused cell death within several hours post-transfection. As OSR1 is a major WNK1 effector and is bound to WNK1 in resting cells (*77-79, 100*), it was surprising that it was not co-localized on mitotic spindles. Consistent with the distinct mitotic localization of OSR1, knockdown showed that it was apparently not involved in WNK1-dependent mitotic events. The OSR1 homolog SPAK is present at nearly undetectable levels in HeLa cells, making unlikely the possibility that I missed relevant phenotypes due to functional redundancy. The difference in survival between WNK1-depleted and OSR1-depleted cells may simply mean that OSR1 is not involved in WNK1-mediated cell

survival functions. On the other hand, it is possible that WNK1exerts its function on cell survival through multiple downstream targets, of which OSR1 is just one, and the assays used here did not reveal the contribution of OSR1. These findings suggest that WNK1 is a potential mitotic kinase regulating the formation of mitotic spindles and the completion of abscission. WNK1 was found in a shRNA knockdown screen for multi-polar spindle phenotypes among human kinases (*101*), further supporting our discovery of a mitotic function of WNK1. The Aurora and Polo-like kinases (PLKs) play important roles in the formation of mitotic spindles and the completion of abscission (*102, 103*). Although the localization of Aurora A and PLK1 resembles that of WNK1especially on spindle poles, Aurora B localizes differently from WNK1 during mitosis. Knocking down Aurora B results in multi-polar spindles, depletion of PLK1 causes mono-polar spindles, but overexpression of PLK1 or Aurora A results in multi-polar spindles (*102, 104-106*). Given these distinctions, perhaps WNK1 negatively regulates PLK1 or Aurora A kinases. Alternatively, WNK1 may regulate components required for the formation of bipolar spindles independently of PLK1 or Aurora A. Clues to the underlying molecular mechanisms may be obtained from identification of potential WNK1 interactors during mitosis. The present study sets the stage to explore this novel mitotic function of WNK1.

CHAPTER 3

WNK1 AND INTERPHASE MICROTUBULES

Abstract

WNK1, a serine-threonine protein kinase, is involved in a variety of cellular events, including exocytosis, endocytosis, ion transporter regulation, cardiovascular development and mitosis. It is also implicated in signaling through MAPKs, the TGF β pathway, GPCRs, and the PI3K pathway. Spindle microtubules and interphase microtubules originate from the microtubule organization center (MTOC), centrosomes in mammalian cells. To continue the investigation of WNK1 actions on microtubules, I have found that the radial array of interphase microtubules from the MTOC was disrupted and the integrity of the centrosomes was impaired in cells from which WNK1 was depleted. Live cell imaging revealed that GFP-WNK1 1800-2126 could travel along interphase microtubules and mainly toward the plus end. Immunofluorescence studies suggested that WNK1 localizes on interphase microtubules and centrosome-like structures. WNK1 1-940 is sufficient to rescue the interphase microtubules, whereas kinase-dead WNK1 1-940 could not. These data suggest that the microtubules phenotypes observed in WNK1-depleted cells are not due to off-target effects. Three possible WNK1 interactors, dynactin, Centrosomal protein of 70 kDa (Cep 70), and Centrosomal protein of 170 kDa (Cep 170), may contribute to the phenotypic results in WNK1-depleted cells.

Introduction

As I showed previously that WNK1 might regulate mitosis, I followed some clues to investigate the possible mechanism underlying WNK1 actions on spindle microtubules. The first phenotype I noticed was that in some cases WNK1 localized on centrosome-like structures and interphase microtubules. Second, depletion of endogenous WNK1 resulted in disruption of radially arrayed interphase microtubules. Third, a former graduate student in the Cobb lab had found that WNK1 might interact with a dynein motor protein light chain 8 (LC8). Fourth, by performing mass spectrometry analysis, I found potential interactors – Cep 70 and Cep 170. From these clues, I have attempted to construct an explanation for the actions of WNK1 as discussed in this chapter. First, I will introduce background on regulation of the microtubule plus end and then I will discuss regulation of the minus end at the MTOC in the centrosome. The majority of my work on and hypothesis for the regulation of interphase microtubules by WNK1 was based mainly on work from a former graduate student on dynein light chain. A major regulator of the dynein motor complex is dynactin which bundles interphase microtubules (*107*). Dynein is a minus-end directed motor but also has plus end targeting ability mediated through dynactin (*108*). The nature of the plus end targeting ability is not clear, yet the literature suggests that in *Saccharomyces cerevisiae*, dynactin can bring dynein to the plus end of microtubules and the cell cortex where the transport of cargoes is needed (*109*, *110*). During live cell imaging using GFP WNK1 1800-2126 as a reporter, I have observed that GFP WNK1 1800-2126 travels along interphase microtubules mainly toward the plus end. I therefore investigated the possible connection between WNK1 and dynactin. WNK1 also appears to localize to centrosomes. I will present observations for WNK1 and centrosomes and discuss potential mechanisms in the discussion.

Materials and Methods

Constructs

The rat WNK1 splice form with 2126 residues was used (*1*). Fragments were generated by PCR using full length rat WNK1 as a template. PCR products were digested with EcoRI and BamHI and ligated into p3XFlagCMV7.1 or pcDNA3-tdtomato (tdtomato is a gift from Dr. Roger Tsien, UCSD and pc DNA3-tdtomato is a gift from Dr. Richard Anderson, UT Southwestern). The dynactin cDNA is a gift from Dr. Erika Holzbaur, U Penn. Subcloning of dynactin into p3XFlagCMV7.1 or pcDNA3-tdtomato was performed by PCR-based procedures. All mutant constructs were generated by Quikchange (Stratagene).

Antibodies and reagents

The following antibodies were used: anti-dynactin (BD 610473), anti-dynein intermediate chain (Abcam, clone 74.1), and anti-pericentrin (Abcam, ab4448). Other antibodies and reagents were described in chapter 2.

Cell culture, immunofluorescence, and immunoblotting

Human fibroblasts stably expressing mCherry α-tubulin (a kind gift from Dr. Anna Akhmanova, Erasmus Medical Center, Rotterdam, The Netherlands) were cultured in Dulbecco's modified Eagle's medium and Ham's F10 medium (Invitrogen Cat # 11550-043) 1: 1, 10% fetal bovine serum, and G418 (200 µg/ ml) at 37°C under 5% CO_2. HeLa and hTERT-immortalized retinal pigment epithelial cell line (RPE1) cells were cultured as described in chapter 2. Immunofluorescence and immunoblotting were performed as described in chapter 2.

Immunoprecipitation

For immunoprecipitation experiments, cells were harvested in lysis buffer containing 0.5% Triton X-100, 50 mM HEPES (pH 7.5), 150 mM NaCl, 1.5 mM $MgCl_2$, 1 mM EGTA, 10% glycerol, 100 mM NaF, 0.2 mM Na_3VO_4, 50 mM β-glycerophosphate, 1 mM dithiothreitol, 1 mM benzamidine hydrochloride, 10 mg/L leupeptin, 0.5 mg/L pepstatin A, and 1.5 mg/L aprotinin. The cells were vortexed for 30 seconds and incubated on ice for 10 min. The lysates were clarified by centrifugation at 16,000g in a microfuge for 20 min. Immunoprecipitating antibodies (WNK1 Q256 1:100 or dynein intermediate chain (DIC) 1:100 (µl antibody / µl lysate)) were added to the 16,000g supernatant and incubated at 4˚C with rotation overnight. Protein A/G agarose beads (30 µl) were added the next day and incubated at 4˚C with rotation for one hour. Beads were washed with lysis buffer with salt concentrations indicated in the figure legend four times, for 10 min each). Protein was solubilized from beads with 2X SDS sample buffer and heated at 94˚C for 3 min prior to Western Blot analysis. For immunoprecipitating Flag-tagged proteins, anti-flag M_2 agarose beads (Sigma) were added to lysates and incubated and washed as above.

RNAi

HeLa cells were transfected with dsRNA oligonucleotides using Lipofectamine RNAiMAX according to manufacturer's instructions (Invitrogen). After 72 h, protein localization was examined or lysates were harvested for immnuoprecipitation or immunoblotting. WNK1 RNAi was described in chapter 2. Dynein light chain (LC8) oligonucleotides: sense: AUGCGGACAUGUCGGAAGAtt; antisense: UCUUCCGACAUGUCCGCAUtt.

Transfection of cDNA constructs

HeLa or mcherry α-tubulin fibroblasts were transfected with the indicated constructs with Lipofectamine 2000. Cells were imaged or immunostained or immunoprecipitated or immunoblotted at the indicated post-transfection time.

Time lapse microscopy, microinjection, and image analysis

These procedures were described in chapter 2.

Particle tracking analysis

HeLa or mcherry α–tubulin-expressing fibroblasts were transfected with GFPWNK1 1800-2126 using Lipofectamine 2000 for 24 hours. Cells were imaged with a Perkin Elmer Spinning Disk microscope (Ultra view ERS). The lens was 63X oil N/A 1.4 Zeiss plan-Apochromat. 212 time points were captured at 1.76 time points per second; the actual duration was 2 minutes. Data were processed by Image J. (Rasband, W.S., Image J, U.S. National Institutes of Health, Bethesda, Maryland, USA, http://rsb.info.nih.gov/ij/, 1997-2006). Manual tracking analysis was performed with the assistance of the Live Cell Imaging Core Facility at UTSouthwestern.

Results

WNK1 localizes on centrosome-like structures

The microtubule cytoskeleton is a highly dynamic tubular polymer that is dynamically unstable. Imaging the cytoskeleton is sensitive to how well the structures can be preserved. A

solution containing Mg^{2+} in a HEPES based- buffer at 37˚C is useful to preserve microtubules. Using these conditions, I first validated the antibody immunostaining endogenous WNK1 as shown in chapter 2. In some cases, WNK1 signals were concentrated on a centrosome- like structure (Fig. 3-1 A). In dividing cells, the centrosome is duplicated in S-phase. Images of cells in early stages of division are shown in Fig. 3-1 A. At the end of G2, duplicated centrosomes separate to be positioned for formation of astral microtubules. The cell image shown in Fig. 3-1 B appears to be in this state. The white arrowheads in Fig. 3-1 A to E indicate WNK1 localized to centrosome-like structures. The percentage of cells that show the WNK1-centrosome-like staining pattern is small. Perhaps this staining pattern only appears in cells at a specific time in the cell cycle early in mitosis. I performed another time-course experiment without doing cell synchronization. The centrosome-like staining was observed at the time point 53 and 77 hours shown in Fig. 3-1 D and E respectively. GFP-WNK1 expressed at a low level displayed a punctate staining pattern; I observed centrosome-like localization of WNK1 6 to 8 hours post-transfection (Fig. 3-2 A to D) in some cells. Analysis by time lapse microscopy suggested that GFP-WNK1 localized to centrosome-like structures just before these structures duplicated during G2 to M phase. Fig. 3-3 panels A-J show several frames from a time lapse movie (movie 3-1). In this recording, the cell was binucleate and there were two GFP-WNK1 spots indicated by yellow arrowheads in Fig. 3-3 A. At a later time the two spots duplicated once again, yielding the 4 GFP-WNK1 structures shown in Fig. 3-3 B and C. As the cell prepared to undergo the mitosis, it rounded up and one of the spots moved to the opposite side of the cell, vanishing from the focal plane as shown in Fig. 3-3 D and E. The nuclear envelope then broke down. One GFP-WNK1 spot began to extend a filament-like structure, perhaps becoming spindle microtubules (Fig. 3-3 F to J). These data suggested that WNK1 might concentrate on centrosomal microtubules during

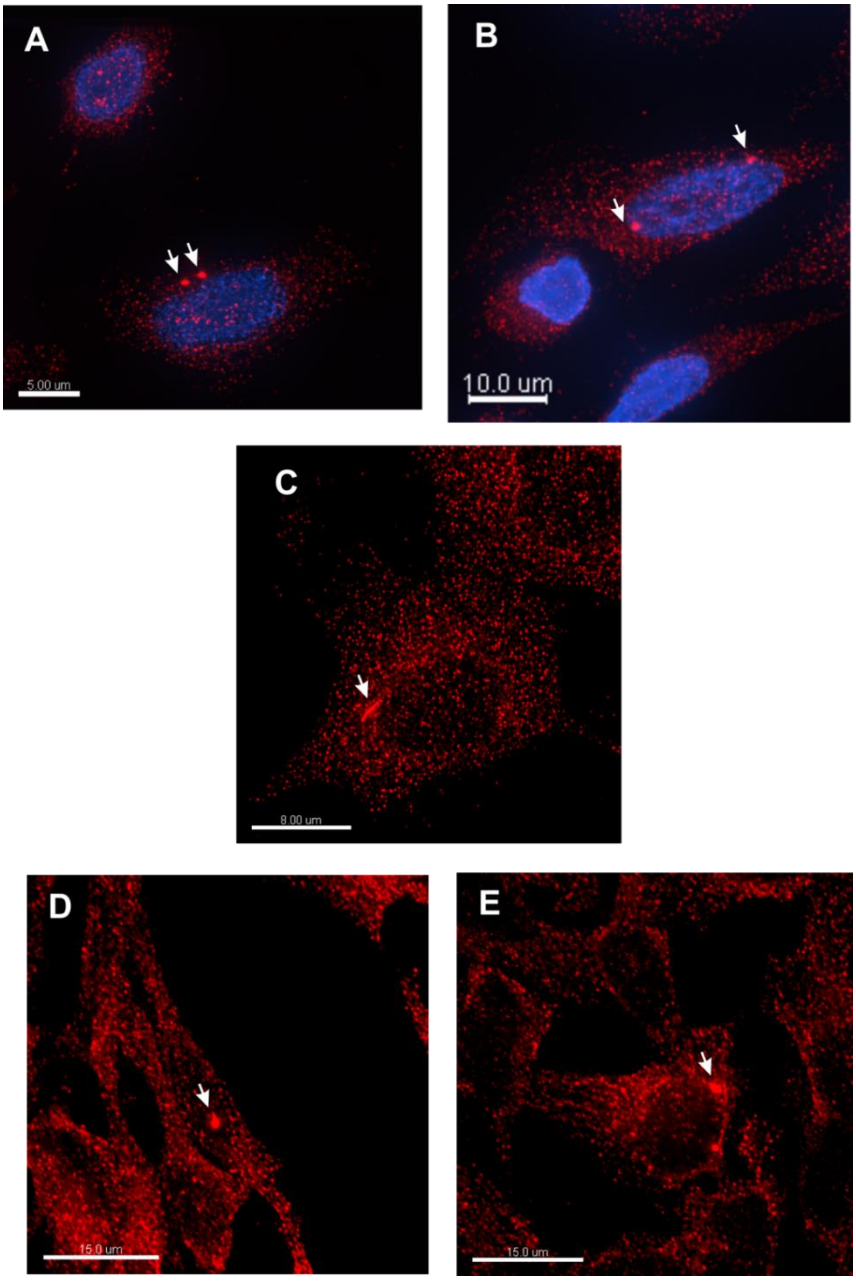

Figure 3-1. WNK1 localizes on centrosome-like structures.

Immunostaining of endogenous WNK1 in HeLa cells (A, B, D, and E) or in MCF7 cells (C). WNK1 (red), DAPI (blue). White arrowheads indicate centrosome-like structures. For the observation of centrosome-like structures shown in Fig. 3-1 D and E, cells were simply plated $3*10^5$ in a 35mm dish and collected for IF at the time point of 32, 40, 46, 53, 67, 77 hours. The centrosome-like staining was observed at the time point 53 and 77 hours shown in Fig. 3-1 D and E respectively.

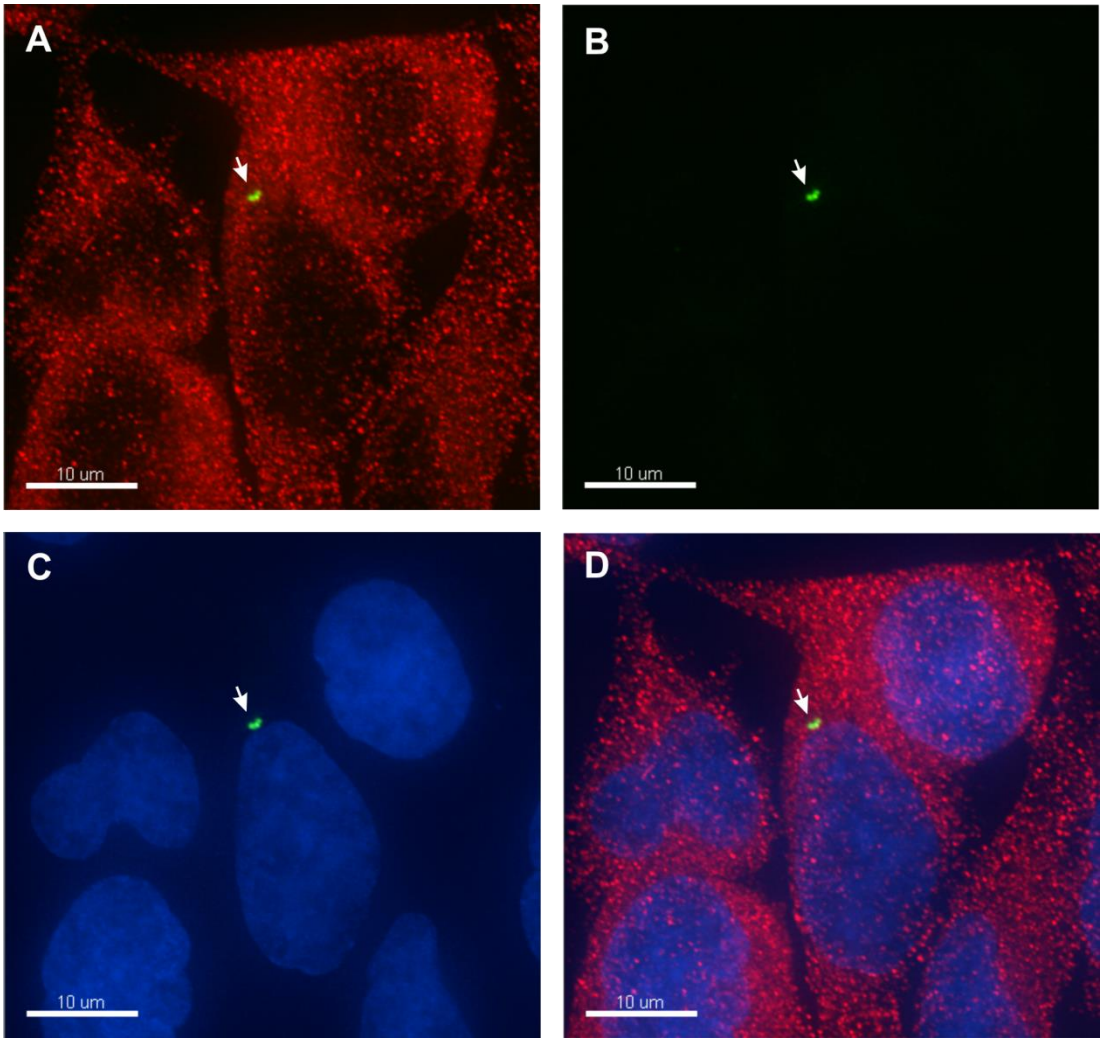

Figure 3-2. GFP-WNK1 localizes on centrosome-like structures at 6 to 8 hours post transfection.

GFP-WNK1 (green), endogenous WNK1 (red), DAPI (blue). HeLa cells were transfected with GFP-WNK1 and immunostained with antibodies against endogenous WNK1 at 6 to 8 hours post transfection. White arrowheads indicate centrosome-like structures.

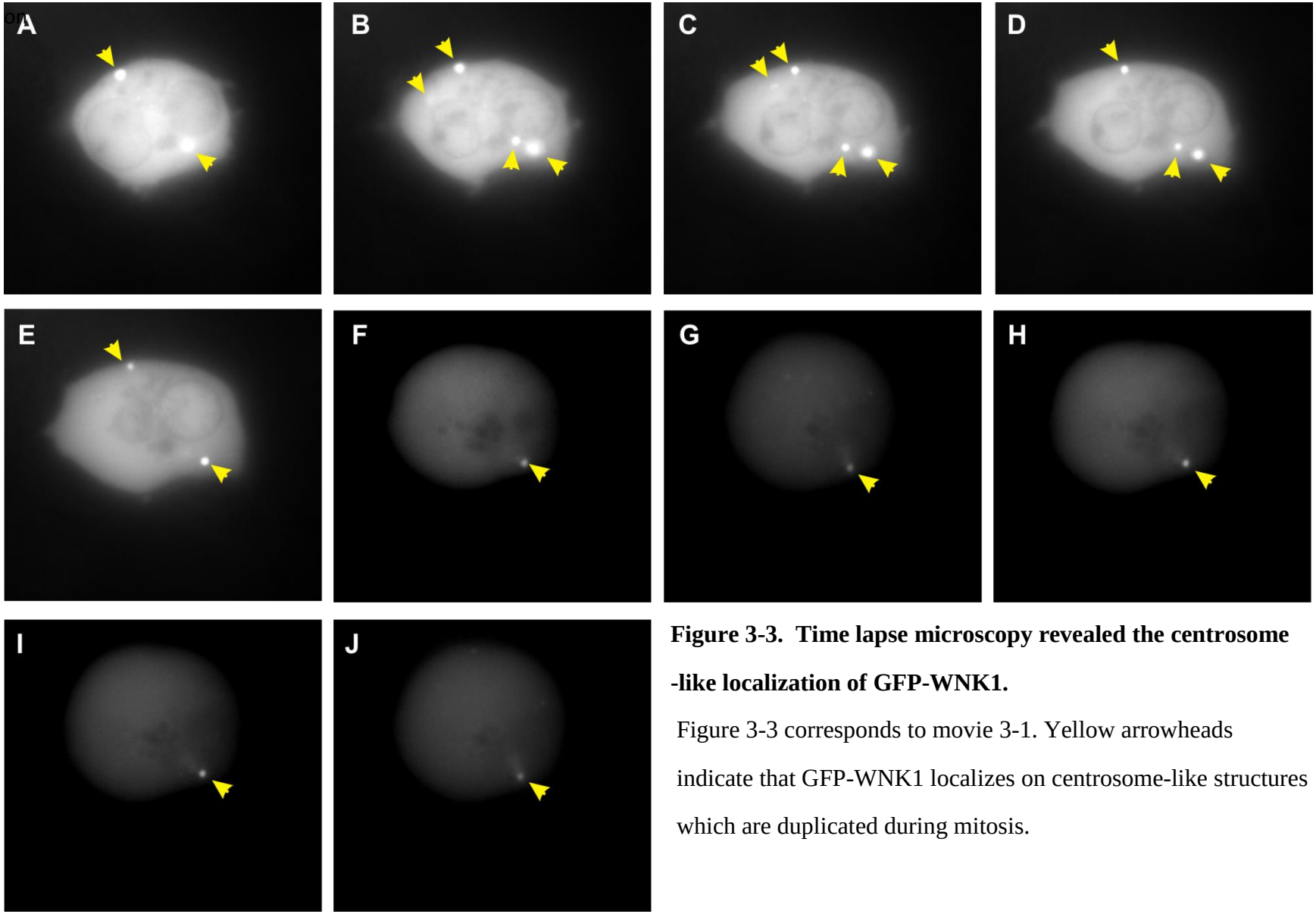

Figure 3-3. Time lapse microscopy revealed the centrosome -like localization of GFP-WNK1.

Figure 3-3 corresponds to movie 3-1. Yellow arrowheads indicate that GFP-WNK1 localizes on centrosome-like structures which are duplicated during mitosis.

the stage of G2 to M phases of the cell cycle. For reasons that are not clear, the results were not reproducible. Therefore, the co-localization of WNK1 and a centrosomal marker did not perform.

The establishment of a live cell image reporter for endogenous WNK1

The idea that live cell imaging could contribute to the functional study of WNK1 originated from movie 3-1 showing GFP-WNK1 could localize on centrosome-like structures. Expression of GFP-WNK1 at a low level displayed a punctate distribution comparable to the endogenous protein only at very early post-transfection. Thereafter, GFP-WNK1 presented a diffuse cytoplasmic distribution as noted by others (*111*). In an effort to identify the region of WNK1 responsible for the punctate distribution, I made a series of rat WNK1 fragments (Fig. 3-4 A). The fluorescent protein tdtomato was attached to the C-terminus of each fragment. As shown in Fig. 3-4 B, WNK1 fragments 1300-2126, 1200-2126 and 1800-2126 displayed a perinuclear punctate localization (Fig 3-4 B bottom panel). Fragments lacking the C-terminus (1-660, 193-1600, and 1300-1600) appeared diffuse (Fig. 3-4 B top panel; residues 193-660 and 193-940 were also diffuse (data not shown)).

As discussed in the first chapter, the C-terminal coiled-coil can mediate homo or hetero dimerization with itself or other WNK isoforms (*24*, *26*). It has been suggested that little WNK3 and WNK4 are expressed in HeLa cells (Wei Chen, personal communication). Expression of WNK2 in HeLa cells has not been investigated yet. Therefore, I tested co-localization of GFP-WNK1 1800-2126 with endogenous WNK1. Using an antibody recognizing an N-terminal sequence of WNK1, I was able to distinguish endogenous WNK1 (Fig. 3-5 A) from GFP-1800-2126 (Fig. 3-5 B). Co- localization analysis by Imaris Co-Loc module suggested that there were

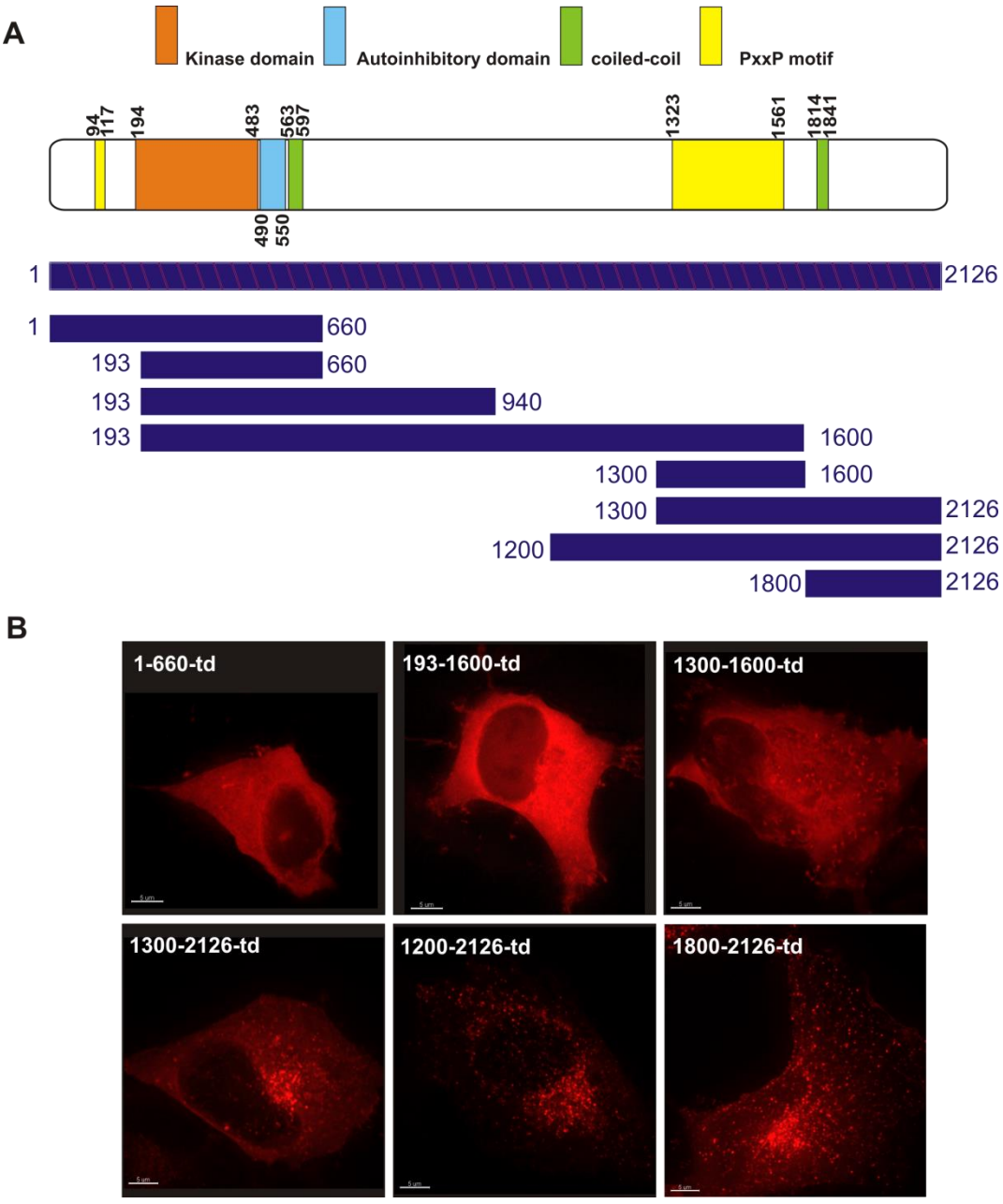

Figure 3-4. The establishment of a live cell image reporter for endogenous WNK1 (published in (*112*)).

WNK1 fragments tested are shown in (A) and have been tagged at the C-terminus with tdtomato. Fragments with the C-terminal coiled coil display perinuclear punctuate staining similar to the pattern of endogenous WNK1 (B, bottom panels) whereas fragments without the C-terminal coiled coil display a diffuse pattern (B, top panels).

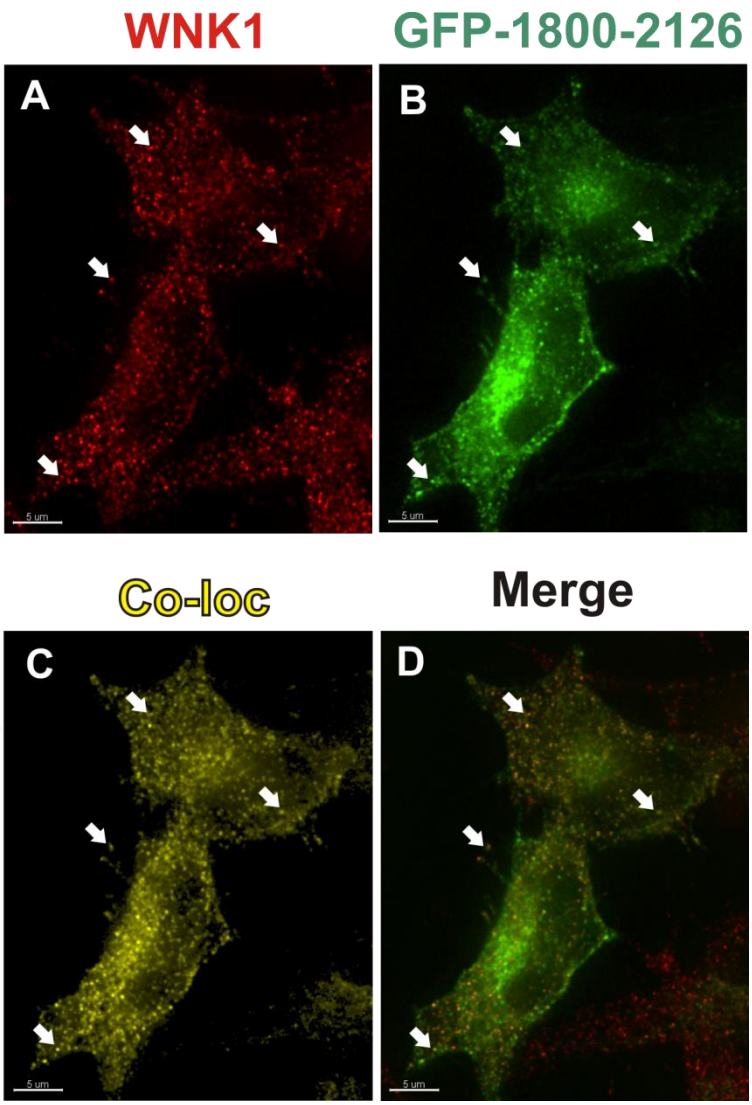

Figure 3-5. GFP- WNK1 1800-2126 co-localizes with endogenous WNK1 (published in (*112*)).

GFP- WNK1 1800-2126 (green), endogenous WNK1 (red), co-localized spots (yellow, generated by Imaris, Co-Loc module).

a subset of GFP-1800-2126 could co-localize with endogenous WNK1. (Fig. 3-5 C and D, published in (*112*)). WNK1 1800-2126 can associate with endogenous WNK1 based on co-immunoprecipitation (see Fig. 4-15 B). These data suggest that GFP-1800-2126 can report on the localization of endogenous WNK1 in live cell imaging experiments. I have collected data from two such live cell imaging experiments. One examined WNK1 traveling along interphase microtubules and the other one examined cell polarity and migration.

GFP-WNK1 1800-2126 particles travel along interphase microtubules

I expressed GFP-WNK1 1800-2126 in a fibroblast cell line stably expressing mcherry-α tubulin and investigated the possible movement of this reporter on interphase microtubules. Using spinning disk confocal microscopy, I found that GFP-WNK1 1800-2126 can travel along microtubules (Fig. 3-6). Fig. 3-6 B to I are zoomed in pictures from Fig. 3-6 A (shown in the white box). White arrowheads indicate the beginning position of the particle and yellow arrowheads indicate the ending position of the moving particle along interphase microtubules (B to I). The movement of GFP- WNK1 1800-2126 appeared more rapid in HeLa cells than in mcherry-α tubulin fibroblasts. I therefore analyzed 15 particle tracks from HeLa cells (movie 3-3); Fig. 3-7, 3-8 and 3-9 are representative tracks. Fig. 3-7 shows two short tracks. Panels B to I are zoomed in pictures from panel A (shown in the white box). Red and yellow arrowheads indicate the beginning position of the particles. As the particles move, the blue lines grow and generate two short tracks (Fig. 3-7 B to I). Fig. 3-8 shows a long track. Orange arrowheads indicate the beginning position of the particle. As the particle moves, the red line grows and generates a long track (Fig. 3-8 B to I). Fig. 3-9 A to I is another example for long tracks. The average total traveling distance is 4.64 μm and the mean velocity is 0.38 μm / sec (Fig. 3-10). The travel direction is generally toward the plus-end of microtubules.

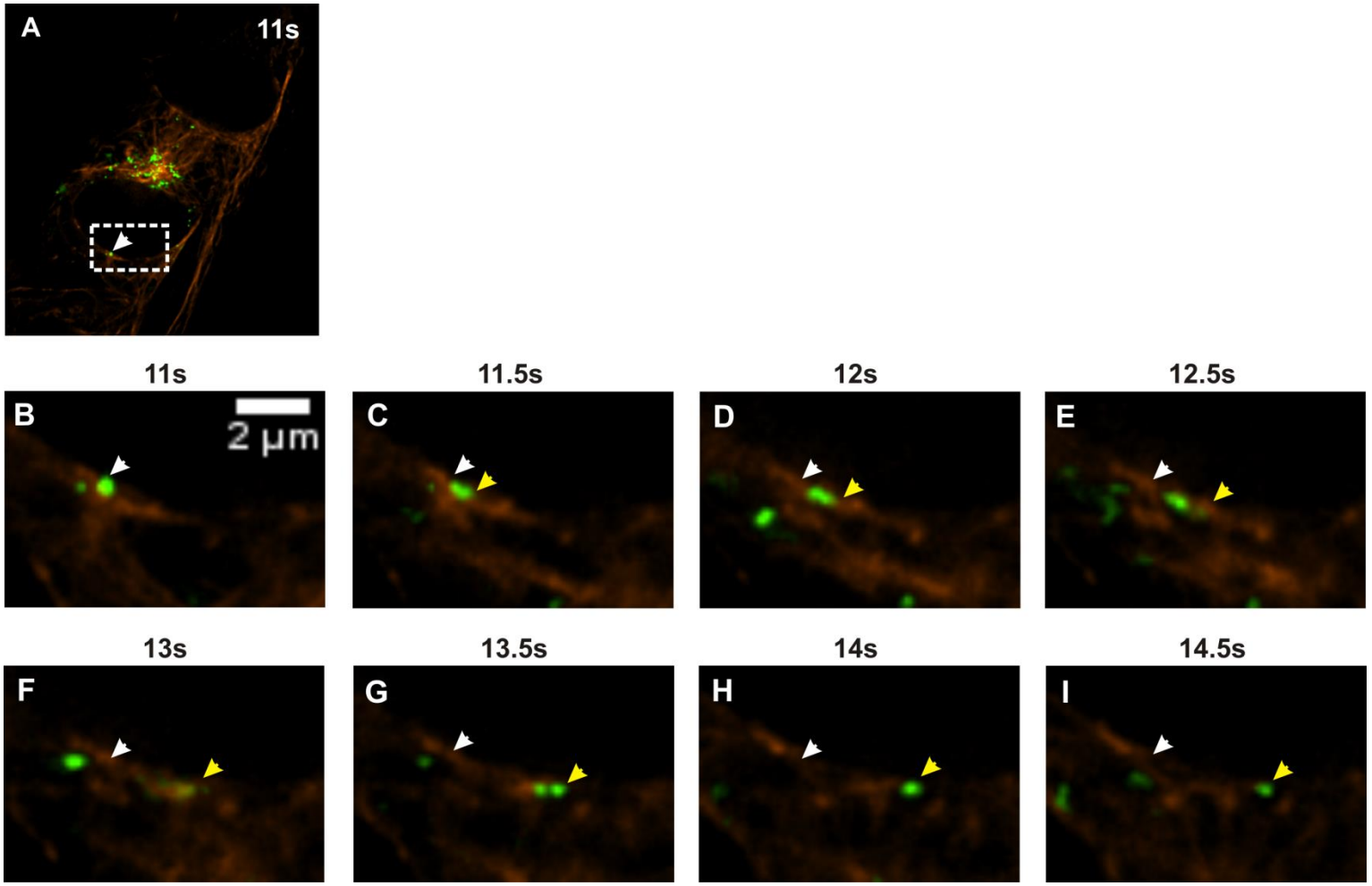

Figure 3-6. GFP-WNK1 1800-2126 particles travel along interphase microtubules. See next page for the legend.

Figure 3-6 corresponds to movie 3-2, beginning with time frame 11s (shown in A). GFP-WNK1 1800-2126 was transfected into fibroblasts stably expressing mcherry- α tubulin for 24 hours. Particle movement was imaged by spinning disk confocal microscopy. Panels B to I are zoomed in pictures from an area of the cell (shown in the white box in panel A). White arrowheads indicate the beginning position of the particle (B) and yellow arrowheads indicate the ending position of the moving particle (C to I).

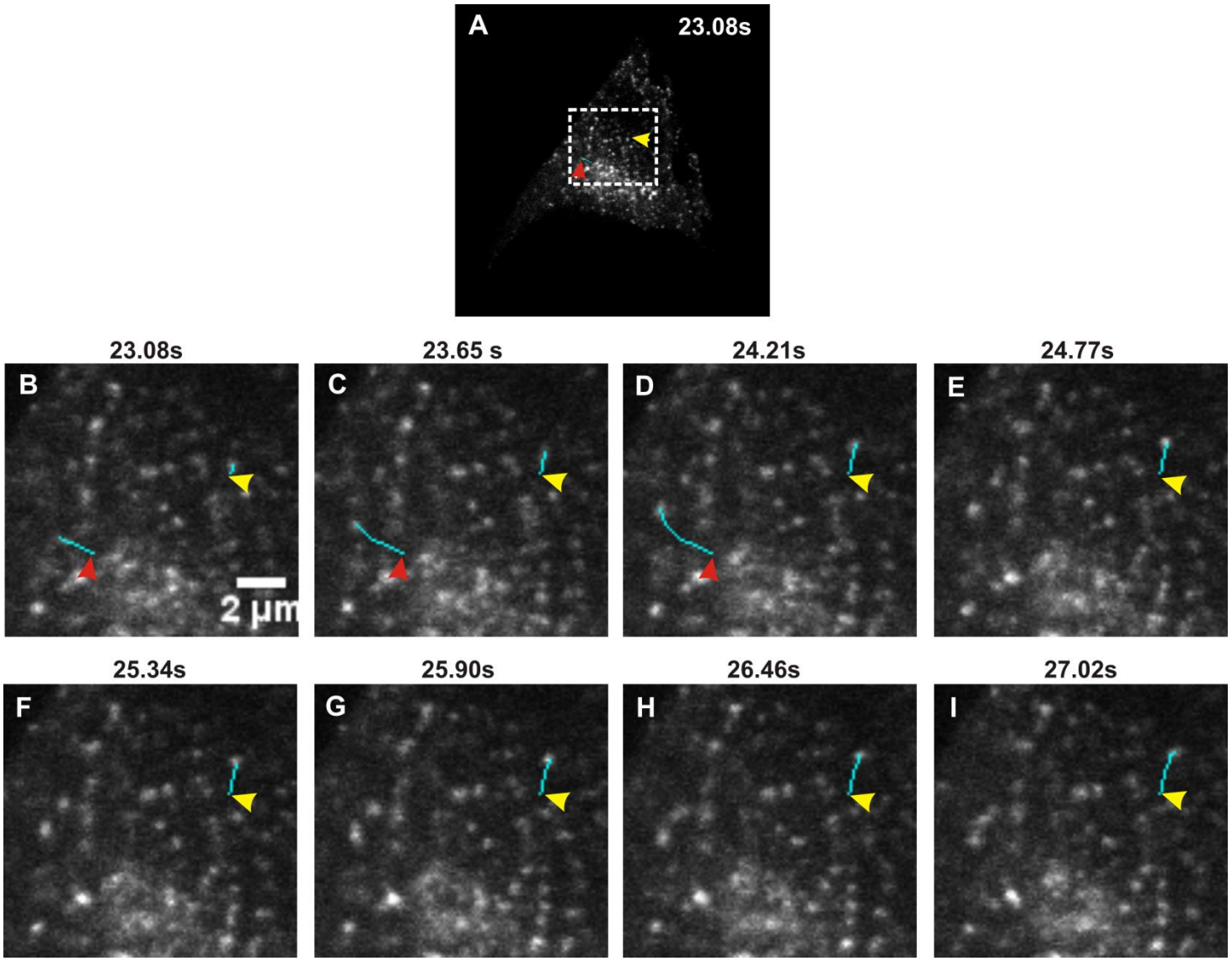

Figure 3-7. Particle tracking analysis of GFP-WNK1 1800-2126. See next page for the legend.

Figure 3-7 corresponds to movie 3-3, beginning with time frame 23.08s (shown in A). GFP-WNK1 1800-2126 was transfected into HeLa cells for 24 hours. Particles were imaged by spinning disk confocal microscopy. Panels B to I are zoomed in pictures from an area of the cell shown in the white box in panel A. Two tracks are shown (blue lines B to I). Red and yellow arrowheads indicate the beginning position of the particles (B to I). In B to D, one particle begins at the position where red arrowheads mark and continues to move (as indicated by the growing blue line), finally vanishes in E (probably due to moving into another focal plane). The other particle begins at the position where yellow arrowheads mark (B) and continues to move (indicated by the growing blue line from C to I). Both of particles movement is toward the plus-end of microtubules.

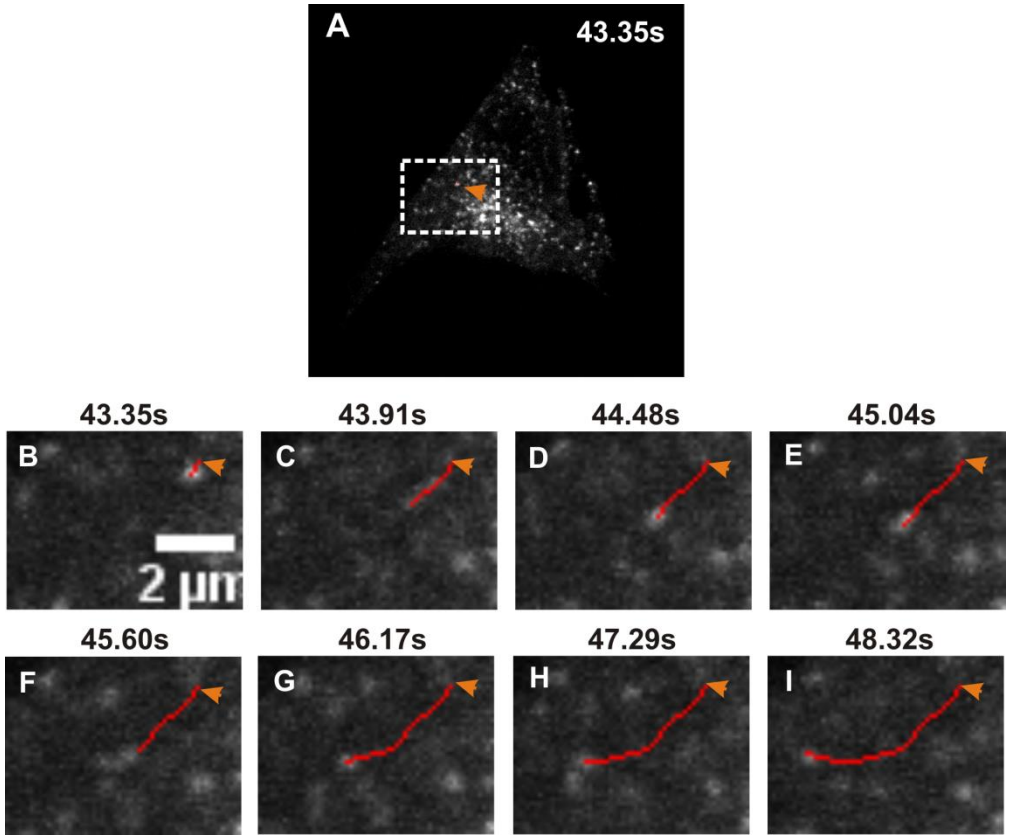

Figure 3-8. Particle tracking analysis of GFP-WNK1 1800-2126.

Figure 3-8 corresponds to movie 3-3, beginning with time frame 43.35s (shown in A). A long track is indicated by the red line. Panels B to I are zoomed in pictures from panel A (shown in the white box). Orange arrowheads indicate the beginning position of the particle (B to I). As the particle moves, the red line grows and generates a long track (C to I). This long track shows that the direction of particle movement is toward the plus-end of microtubules.

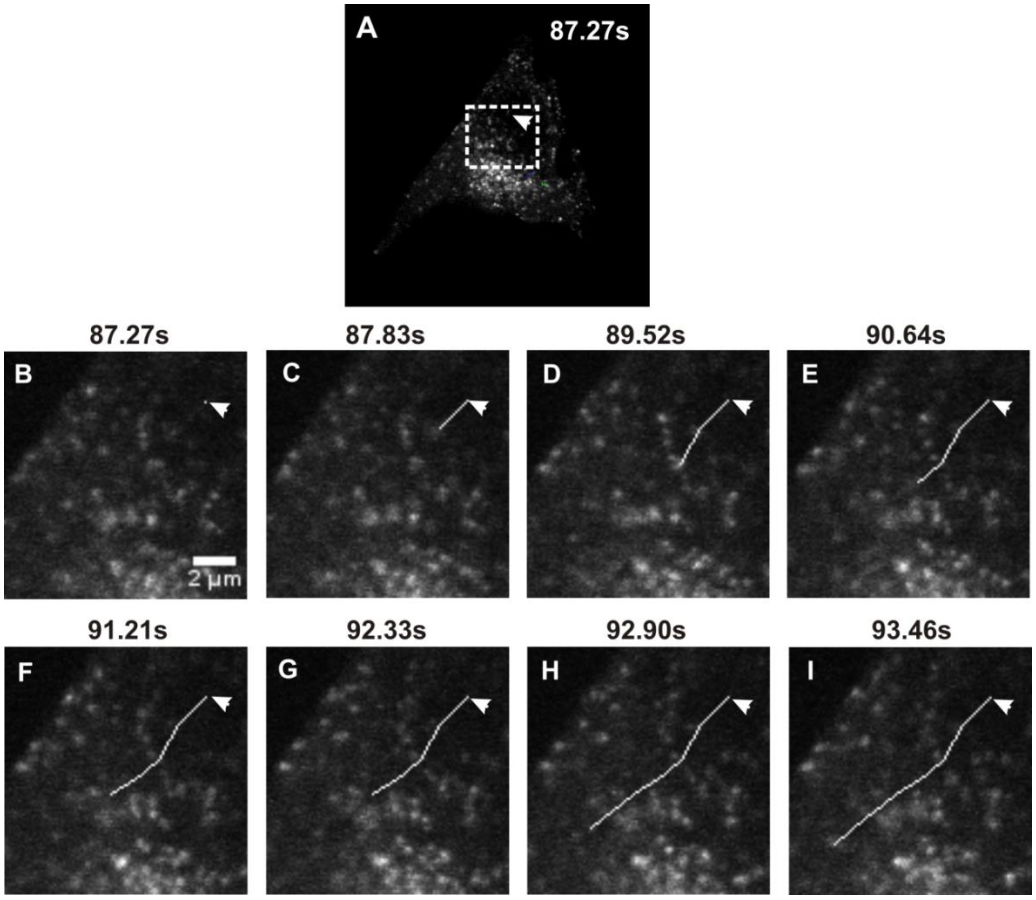

Figure 3-9. Particle tracking analysis of GFP-WNK1 1800-2126.

Figure 3-9 corresponds to movie 3-3, beginning with time frame 87.27s (shown in A). Panels B to I are zoomed in pictures from panel A (shown in the white box). White arrowheads indicate the beginning position of the particle (B). As the particle moves, the white line grows and generates a long track (C to I). This long track also shows the direction of the movement toward the plus end of microtubules.

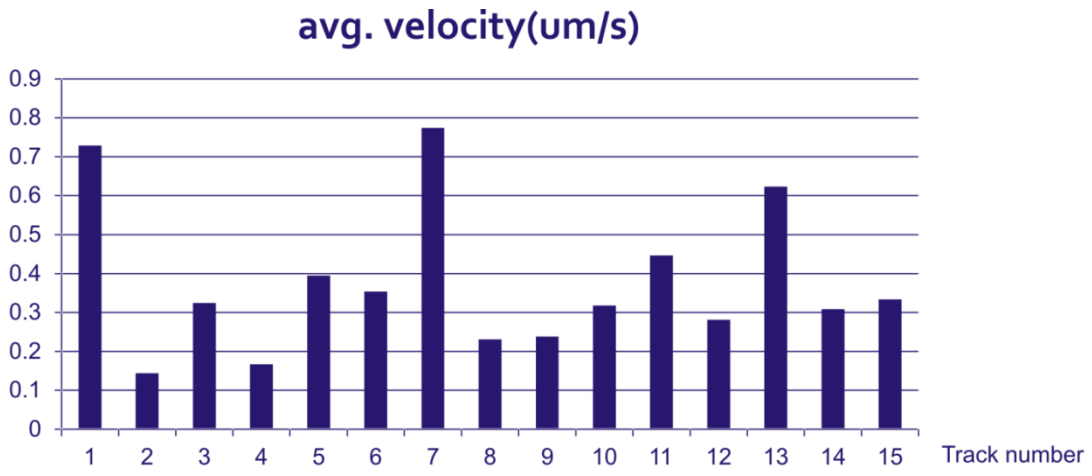

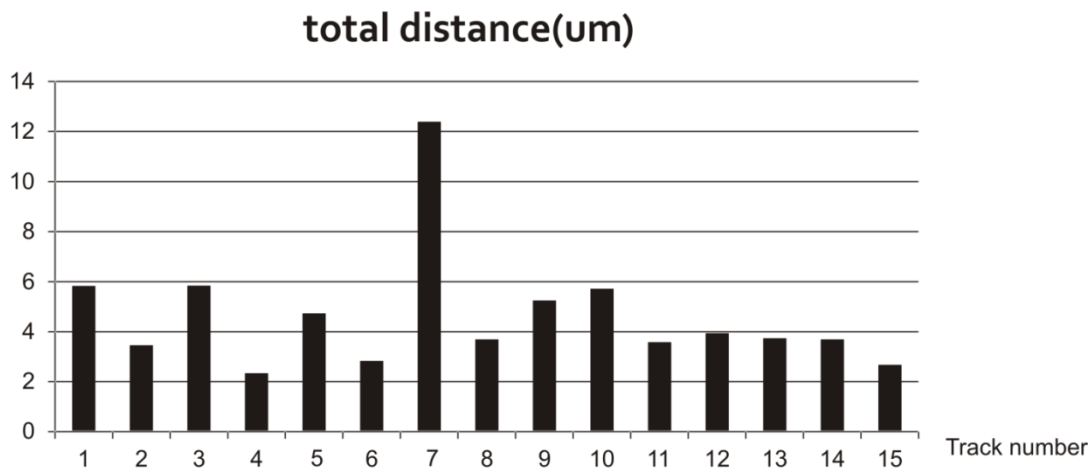

	total distance	Speed(um/s)
Avg	4.64	0.38
Max	12.39	0.77
Min	2.34	0.14

Figure 3-10. Statistical results for 15 particles tracked analyzed from movie 3-3.

The average speed of cargo movement by dynein or kinesin motors is about 1 to 2 μm / sec. The speed shown by GFP 1800-2126 particles seems slower.

WNK1 localizes on interphase microtubules and affects the organization of interphase microtubules

Immunolocalization of endogenous WNK1 (green, shown in Fig. 3-11 B) in mcherry-α tubulin (red, shown in Fig. 3-11 A) cells suggested that a subset of WNK1 co-localized with interphase microtubules (yellow, shown in Fig. 3-11 C). Fig. 3-11 E was zoomed in from Fig. 3-11 D, showing clearly co-localized material (yellow) generated by Imaris Co-Loc module. Similar results were obtained by immunolocalization of WNK1 and α tubulin in HeLa cells (Fig. 3-11 F to I). WNK1 appears on interphase microtubules and is perinuclear near the MTOC and the centrosome (Fig. 3-12 A, HeLa cells, Fig. 3-12 D, RPE1 cells). Depletion of endogenous WNK1 resulted in the disintegration of the MTOC and loss of asymmetrical radial microtubule arrays around the MTOC. As a result, cells are flattened out and display no polarity (Fig. 3-12 B, C, E and F).

Centrosomal structures are impaired in WNK1-depleted cells

Immunostaining for a centrosome marker pericentrin and α-tubulin suggested that centrosomal integrity might be compromised in cells from which WNK1 has been depleted. Pericentrin is an important scaffolding protein of the centrosome. In control RNAi cells, pericentrin staining showed one or two closely spaced spots, representing an integral centrosome consisting of two centrioles (Fig. 3-13 A, B). Strong α tubulin signals emanated from the pericentrin-positive MTOC. Depletion of WNK1 resulted in two well separated pericentrin

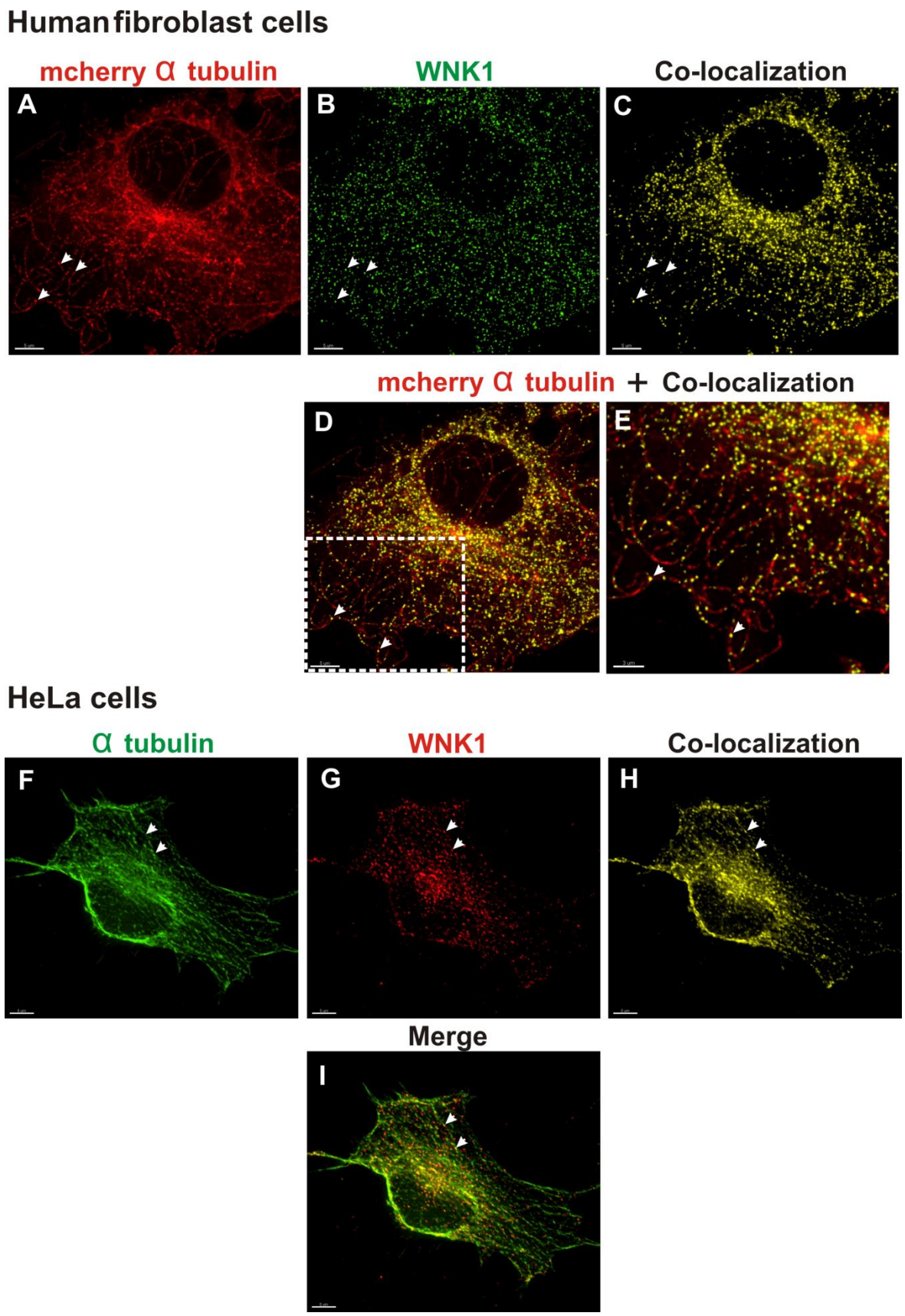

Figure 3-11. WNK1 localizes on interphase microtubules. See next page for the legend.

Immunostaining of endogenous WNK1 (green, shown in B) and mcherry α-tubulin (red, shown in A) in fibroblasts. Co- localized spots (yellow, shown in C) were generated by Imaris Co-Loc module. Only a subset of WNK1 co-localizes with microtubules (shown in D). Fig. 3-11 E is a zoomed in picture from an area of the cell (shown in the white box in D) and clearly shows the co-localized spots (white arrowheads). The Pearson correlation coefficient is 0.17 analyzed from the image above.

HeLa cells were immunostained with anti-WNK1 (red, shown in G) and anti-α-tubulin (green, shown in F) antibodies. Co-localized spots were generated by Imaris Co-Loc module. White arrowheads indicate the co-localized structures. The Pearson correlation coefficient is 0.52 analyzed from the image above.

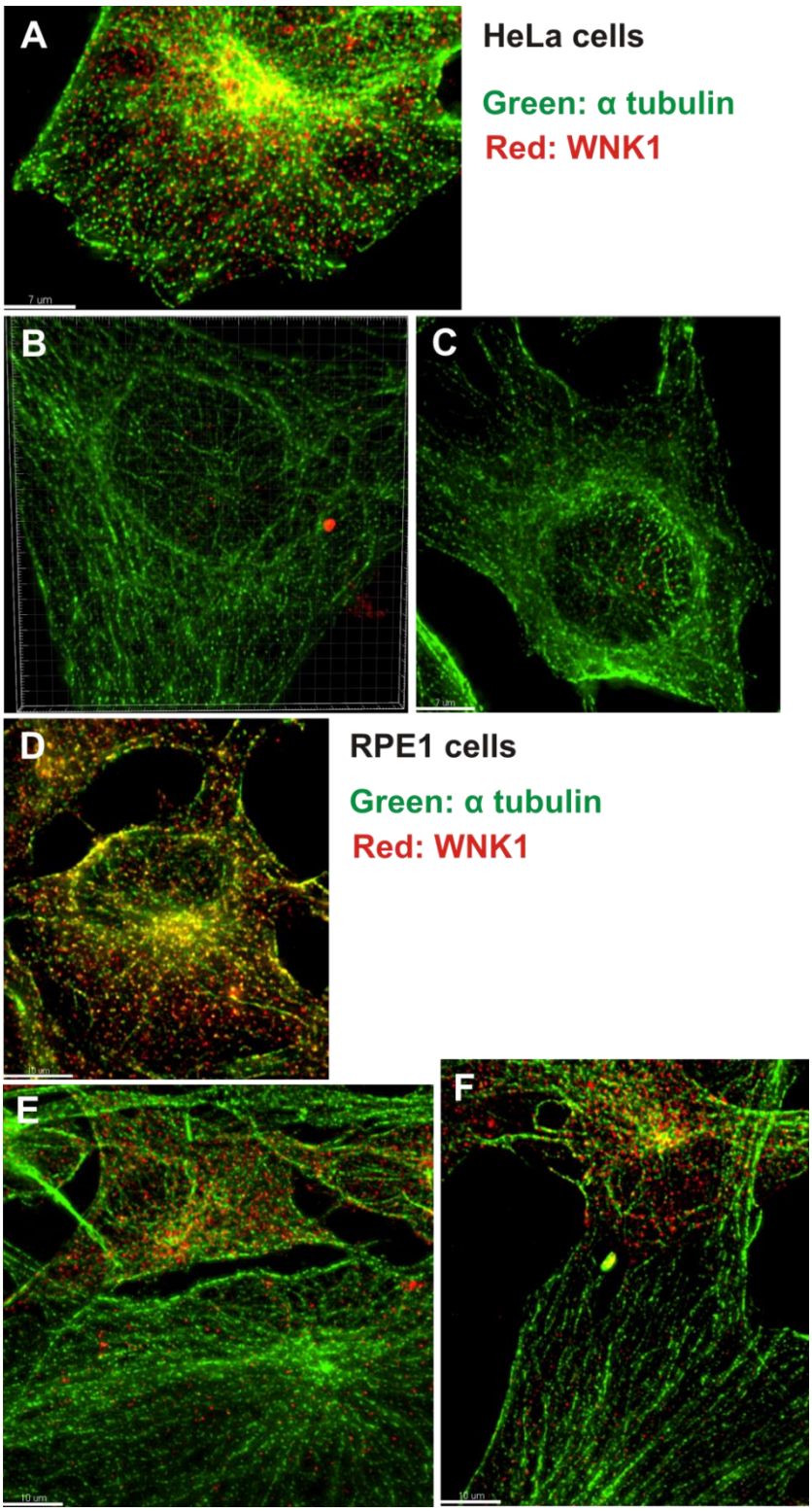

Figure 3-12. WNK1-depleted cells display microtubules that have been disrupted and radiate asymmetrically from MTOCs. See next page for the legend.

Immunostaining of WNK1 (red) and α tubulin (green) in HeLa (A to C) or RPE1 (D to F) cells. WNK1 perinuclear signals co-localize with MTOCs in the control cells (A and D). In WNK1-depleted cells, the asymmetric radial arrays of microtubules are disrupted and cells become flat (B, C, E, and F).

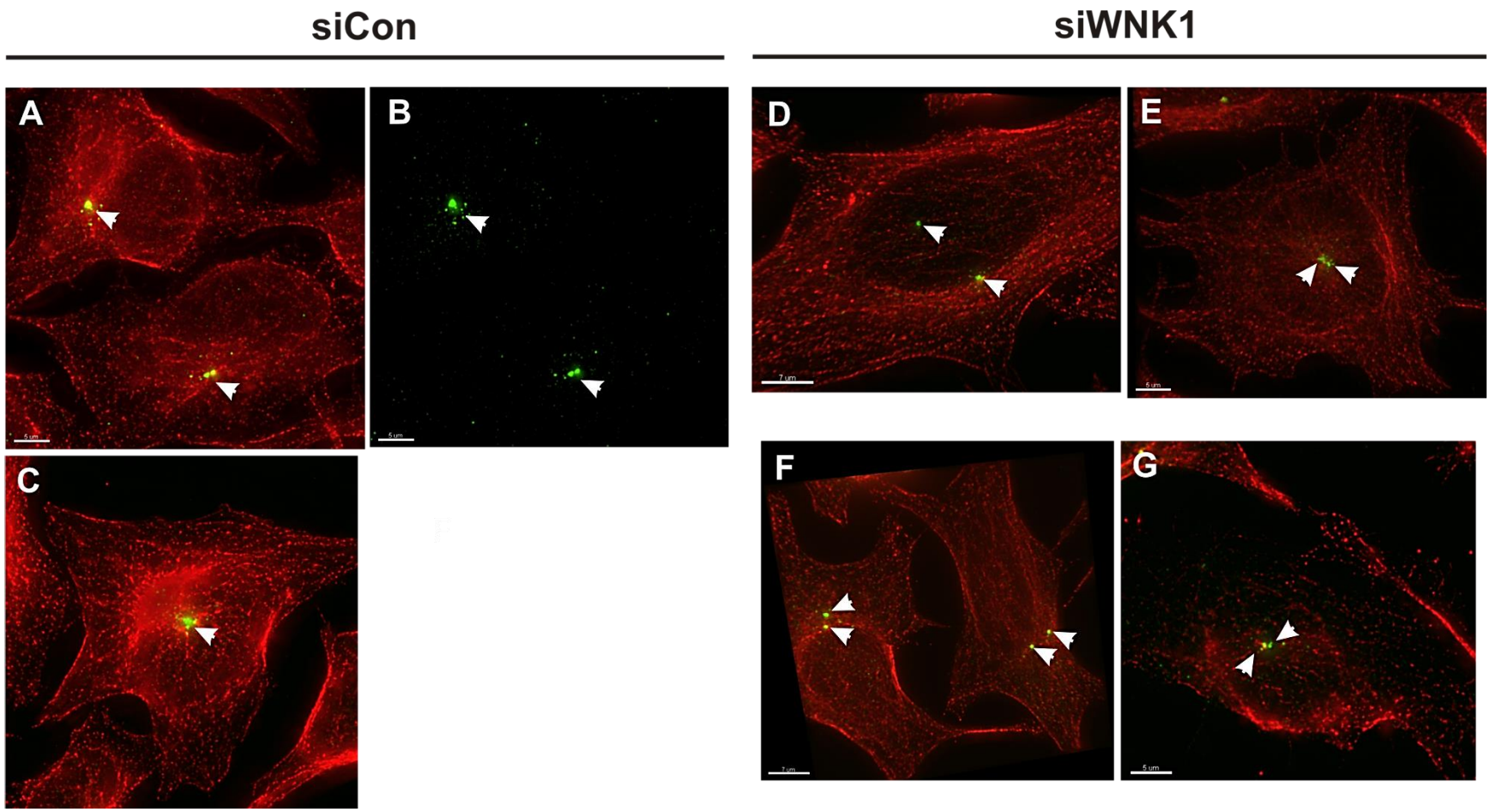

Figure 3-13. Centrosomal structures are impaired in WNK1-depleted cells.

Immunostaining of a centrosomal marker, pericentrin (green) and α tubulin (red) in HeLa cells. Centrosomes are composed of a pair of centrioles in RNAi control cells (A to C, white arrowheads). In WNK1-depleted cells, pericentrin staining appears as two well-separated signals, suggesting the separation of a pair of centrioles (D to G).

signals (white arrowheads in Fig 3-13 D to G). Coupled with the disorganized radial arrays of microtubules from the MTOC, these findings suggest that centrosomal integrity was impaired.

Rat WNK1 rescues interphase microtubule phenotypes

To verify that the microtubule disruption in WNK1-depleted cells was not due to an off-target effect, rescue experiments were performed. Radial arrays of microtubules appeared to be rescued in cells expressing full length rat WNK1 (Fig. 3-14 A, B, cell on the right). In contrast, microtubules remained defective in the cell on the left, which had been depleted of WNK1 and did not express rat WNK1 (Fig. 3-14 A, B, dotted line). In Fig. 3-14, the α tubulin antibody was more dilute (1/5 relative to Fig. 3-12), which reduced microtubule intensity to below the limit of detection in WNK1-depleted cells. A WNK1 fragment 1800-2126 was also tested for its ability to rescue microtubules. Interestingly, cells expressing WNK1 1800-2126 caused the recovery of a few microtubules radial arrays, but the cells seemed smaller and the microtubules were shorter (Fig. 3-14 D) than those in control cells (Fig. 3-14 E). Kinase-dead WNK1 caused microtubules to distribute around the periphery (Fig. 3-14 C), suggesting that kinase activity might also be involved in the formation of interphase microtubule arrays. I investigated which regions of WNK1 were sufficient to restore interphase microtubules. Cells were immunostained for WNK1 (green), the heterologous WNK1 fragment (blue) and α tubulin (red). Fig. 3-15 shows that WNK1 has been depleted in all cases shown. WNK1 1-940 rescued the microtubules phenotype (Fig. 3-15 A and B), while the comparable kinase-dead fragment did not (Fig. 3-15 C and D). WNK1 1-660 also caused some microtubule rescue, but less than the longer fragment (Fig. 3-15 E and F). WNK1 1-490 was more nuclear and did not rescue (Fig. 3-15 G and H). Thus, WNK1 1-940 and kinase activity were required for the proper organization of interphase microtubules.

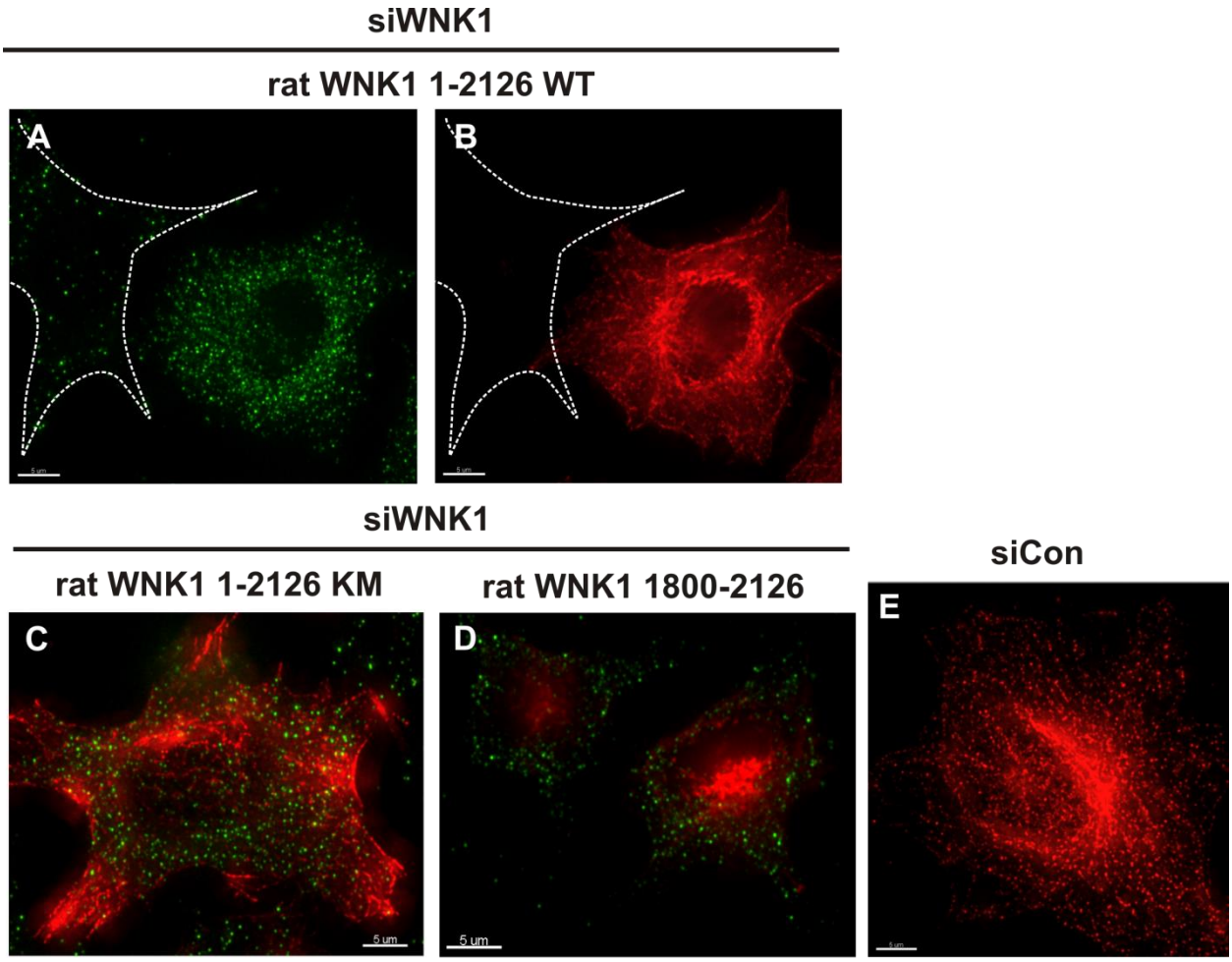

Figure 3-14. Full length rat WNK1 rescues interphase microtubule phenotypes.

Immunostaining of exogenously expressed WNK1 (anti-flag antibody, green), α tubulin (red) and endogenous WNK1 (blue). The intensity and organization of microtubule arrays are rescued by wild type exogenous rat WNK1 (A and B) but not kinase-dead WNK1 (C). A C-terminal fragment used as a reporter for live cell imaging is also not sufficient to rescue (D).

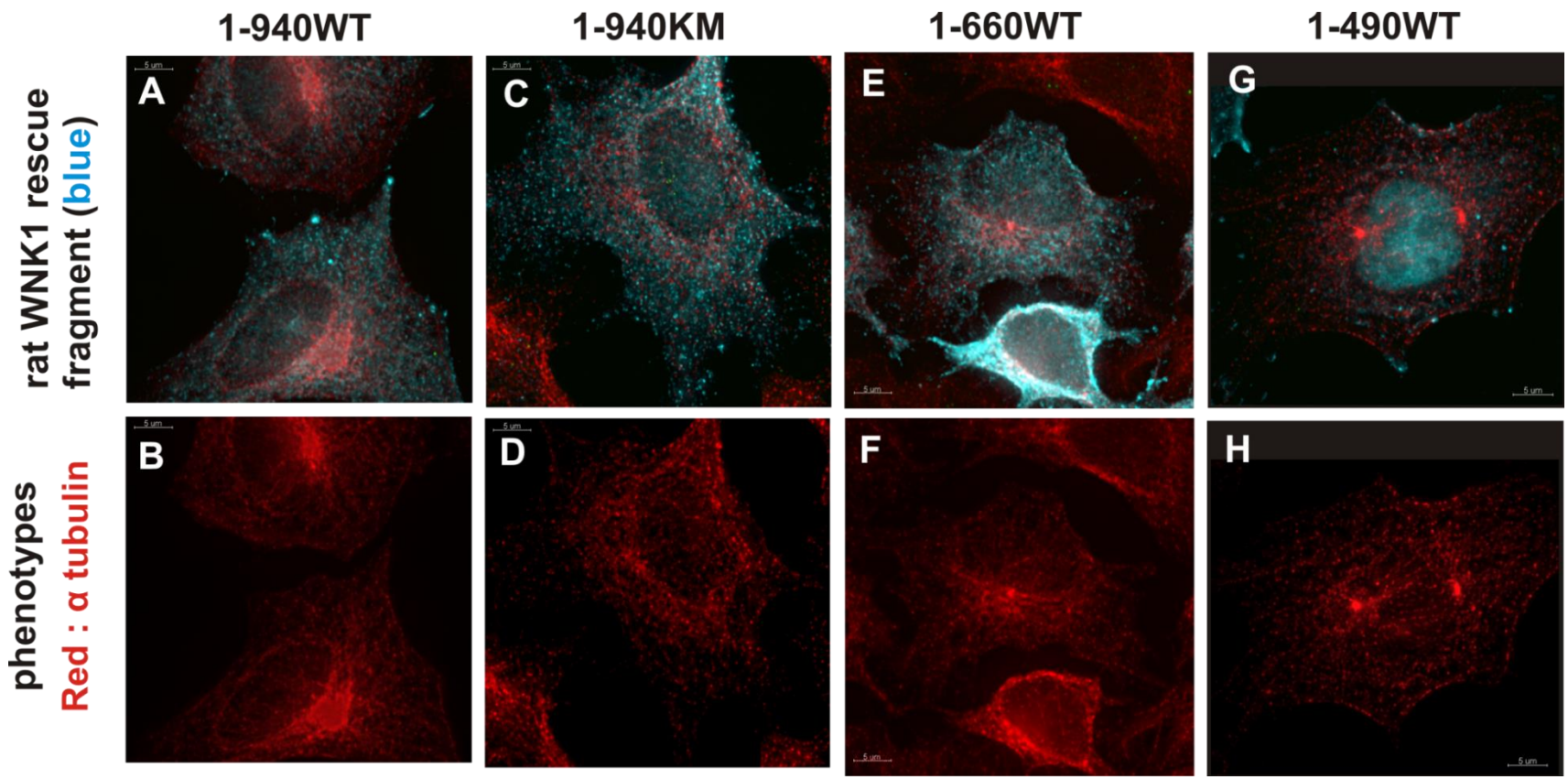

Figure 3-15. Regions of WNK1 sufficient to rescue microtubule phenotypes

Immunostaining of exogenous WNK1 fragment (anti-flag antibody shown in blue), α tubulin (red) and endogenous WNK1 (green). HeLa cells were transfected with indicated rescue fragment for 48 hours. Cells were trypsinized and transfected with WNK1 RNAi oligonucleotides for 48 hours. Cells were then transfected with indicated rescue fragment again for 24 hours and RNAi of WNK1 for another 24 hour. Cells were harvested for immunofluorescence as described in methods.

Depletion of WNK1 caused a migratory defect

The third phenotype I have observed in WNK1-depleted cells is a cell migration defect. Through live cell imaging using a WNK1 1800-2126-tdtomato reporter, I noticed that the reporter is always positioned between the nucleus and the leading edge of migrating cells (Fig. 3-16 A to H, movie 3-4, yellow arrowheads indicate cell migratory direction). WNK1 depleted cells were often unable to migrate. While the leading edge of such cells moved forward, the trailing edge remained in its original position (Fig. 3-17 A to J, movie 3-5, indicated by yellow arrowheads). These cells eventually died. Co-injecting Alexa 488 dextran and RNAi WNK1 oligonucleotides also demonstrated this migratory defect (Fig. 3-18 A to J, movie 3-6, yellow arrowheads indicate migratory direction). In Fig. 3-18, the imaged cell attempted to migrate away from the imaged optical field (Fig. 3-18 D), I manually re-positioned the optical field (Fig. 3-18 E) and re-positioned again (Fig. 3-18 G). In Fig. 3-18 G-I, the cell became elongated and eventually died (Fig. 3-18 J). Thus, the elongated cell shape often shown in the WNK1-depleted cells could result from the abscission defects as discussed in chapter 2 or migratory defects.

WNK1 co-immunoprecipitates with dynactin and dynein intermediate chain

The mechanism underlying the phenotypic defects caused by depletion of WNK1 in interphase cells is unknown. I evaluated the possible WNK1 interactors dynactin, DIC and LC8 by immunoprecipitation and immunofluorescence. Overexpressed dynactin was present in immunoprecipitates of endogenous WNK1 (Fig. 3-19 A). However, the reciprocal immunoprecipitation failed (data not shown). Overexpressed WNK1 full length or 1-940 did not capture enough endogenous dynactin to detect by mass spectrometry. In addition, dynactin appeared in precipitates using both pre-immune serum or anti-WNK1 antibody (Q256) (Fig. 3-19 B, left panel). If precipitates were washed with 0.3 M NaCl, the amount of dynactin in pre-

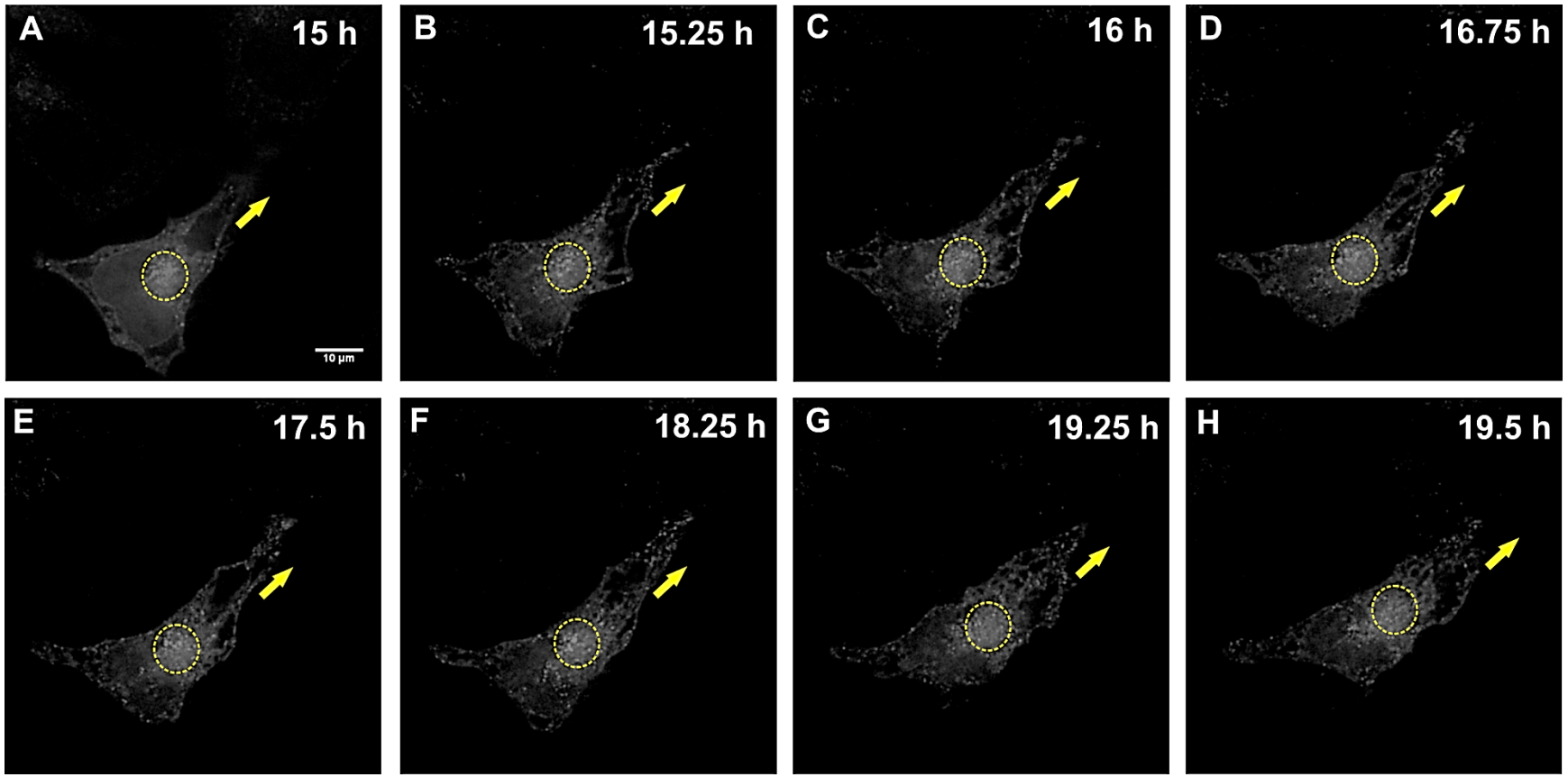

Figure 3-16. Live cell images reveal that WNK1 1800-2126-tdtomato faces the leading edge of migratory cells.

Figure 3-16 corresponds to movie 3-4. Dotted yellow circles indicate the MTOCs in which WNK1 1800-2126 tdtomato is localized. Yellow arrowheads indicated the direction of cell migration and the protusion of the leading edge.

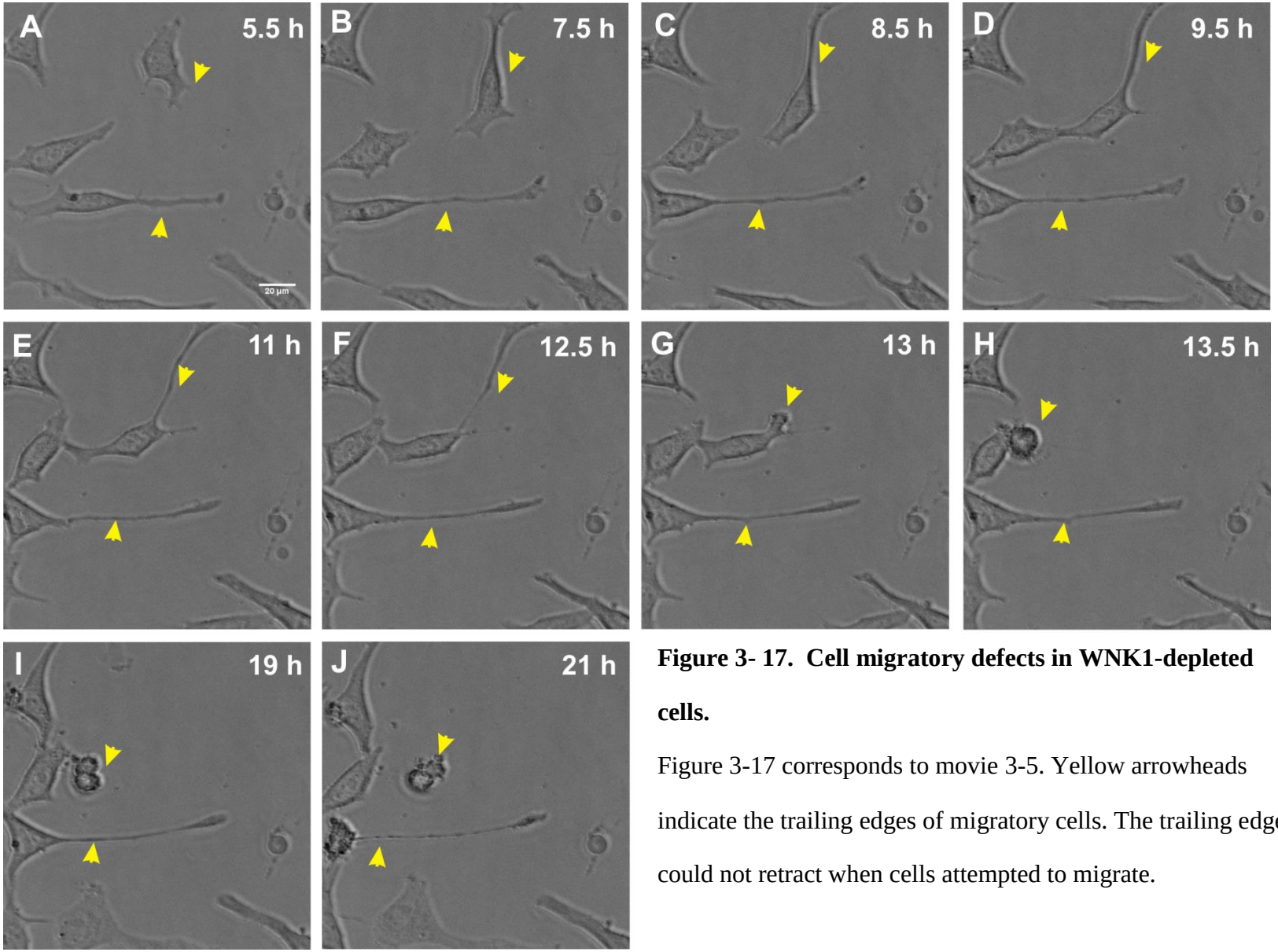

Figure 3- 17. Cell migratory defects in WNK1-depleted cells.

Figure 3-17 corresponds to movie 3-5. Yellow arrowheads indicate the trailing edges of migratory cells. The trailing edges could not retract when cells attempted to migrate.

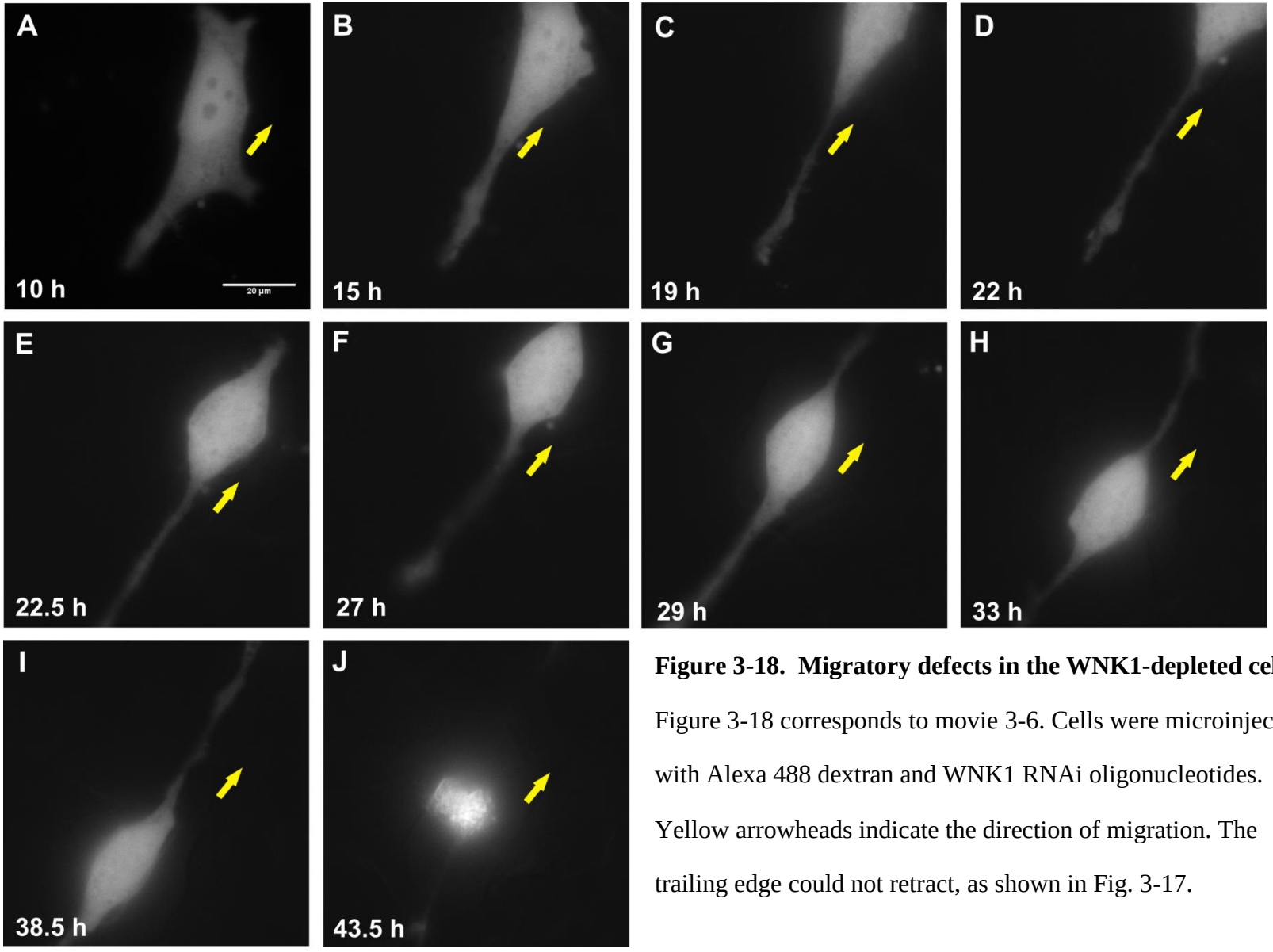

Figure 3-18. Migratory defects in the WNK1-depleted cells.

Figure 3-18 corresponds to movie 3-6. Cells were microinjected with Alexa 488 dextran and WNK1 RNAi oligonucleotides. Yellow arrowheads indicate the direction of migration. The trailing edge could not retract, as shown in Fig. 3-17.

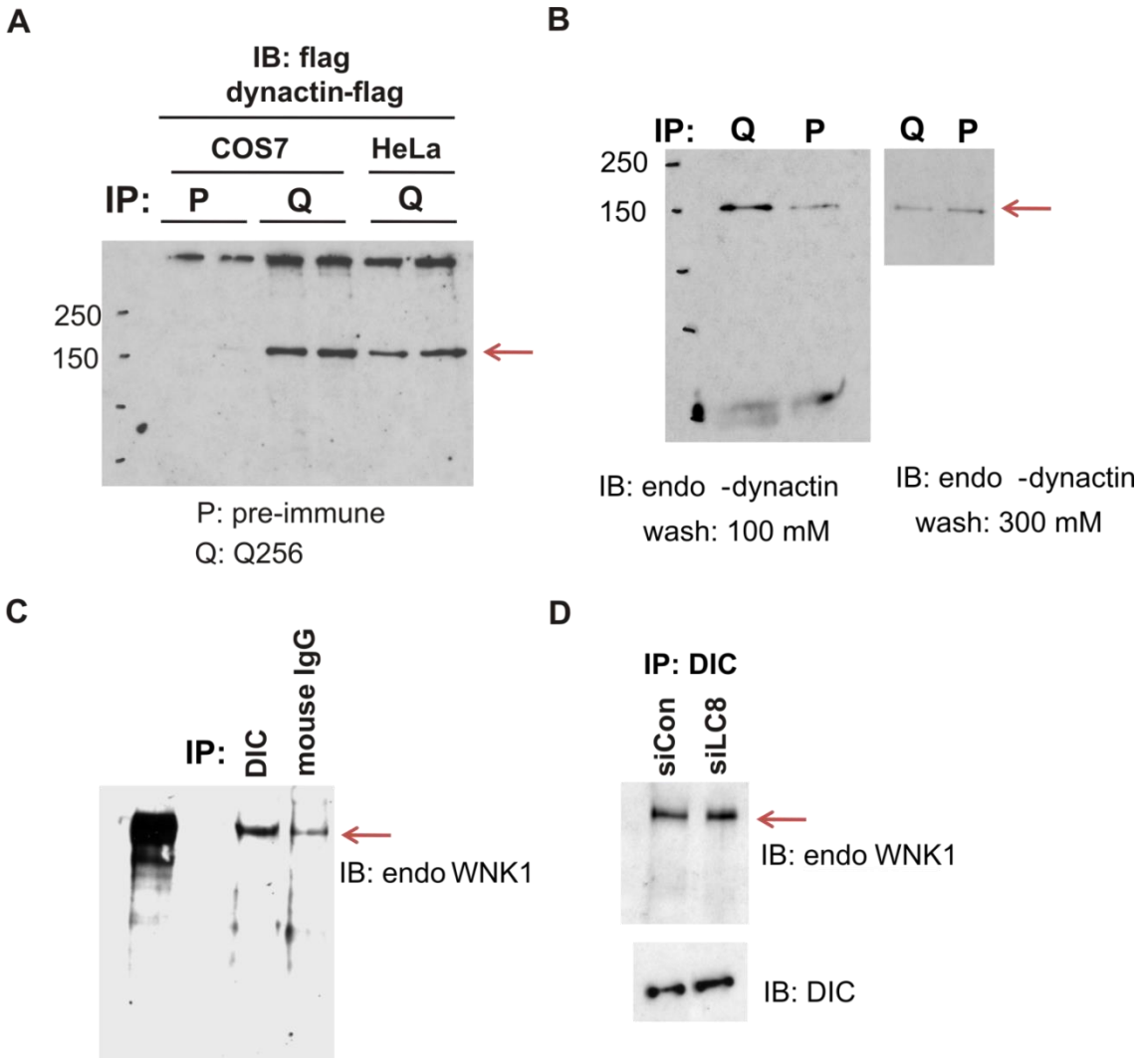

Figure 3-19. WNK1 co-immunoprecipitates with dynactin and dynein intermediate chain.

HeLa or COS7 cells were transfected with dynactin-Flag for 24 hours and harvested. Proteins were immunoprecipitated with anti-WNK1 (Q256) or pre-immune serum followed by Western blotting with anti-Flag. (A) Proteins were immunoprecipitated from HeLa cells with anti-WNK1 or pre-immune serum. Dynactin was immunoprecipitated after low (100 mM) or high (300 mM) NaCl wash (B). Proteins immunoprecipitated from HeLa cells with antibodies to dynein intermediate chain or normal mouse IgG antibody and were immunoblotted with anti-WNK1 (C). HeLa cells were depleted of dynein light chain (LC8) or control for 72 hours. Cells were then harvested and immunoprecipitated with DIC and immunoblotted with WNK1 (D).

immune or Q256 immune complexes was equal (Fig. 3-19 B, right panel). WNK1 was detected in dynein intermediate chain (DIC) immune complexes but also in the mouse IgG control at a lower intensity (Fig. 3-19 C). I depleted the WNK1 binding protein LC8 by RNAi and precipitated dynein motor complexes with anti-DIC. WNK1 co-immunoprecipitated with dynein intermediate chain in both control and LC8-depleted cells (Fig. 3-19 D). WNK1 did co-localize with endogenous dynactin by immunofluorescence (Fig. 3-20 A to C). Co-localization with WNK1 is also observed with dynein intermediate chain (Fig. 3-20 D to F).

A comparison of movements of GFP-WNK1 1800-2126 and tdt-dynactin

GFP WNK1 1800-2126 particles generally move toward the plus-end of microtubules. This leads me to test whether GFP WNK1 1800-2126 movement is the same as tdt- dynactin, one of plus-end tracking proteins. As shown in movie 3-7 and Fig. 3-21, tdt- dynactin displays comet-like movement (white arrowheads shown in Fig. 3-21 A) whereas GFP WNK1 1800-2126 shows a movement that is shorter (Fig. 3-21 B to C). GFP-WNK1 1800-2126 particles hardly encounter tdt-dynactin particles at the tip of microtubules. Therefore, it seemed that GFP WNK1 1800-2126 could move along microtubules but not display a tracking behavior.

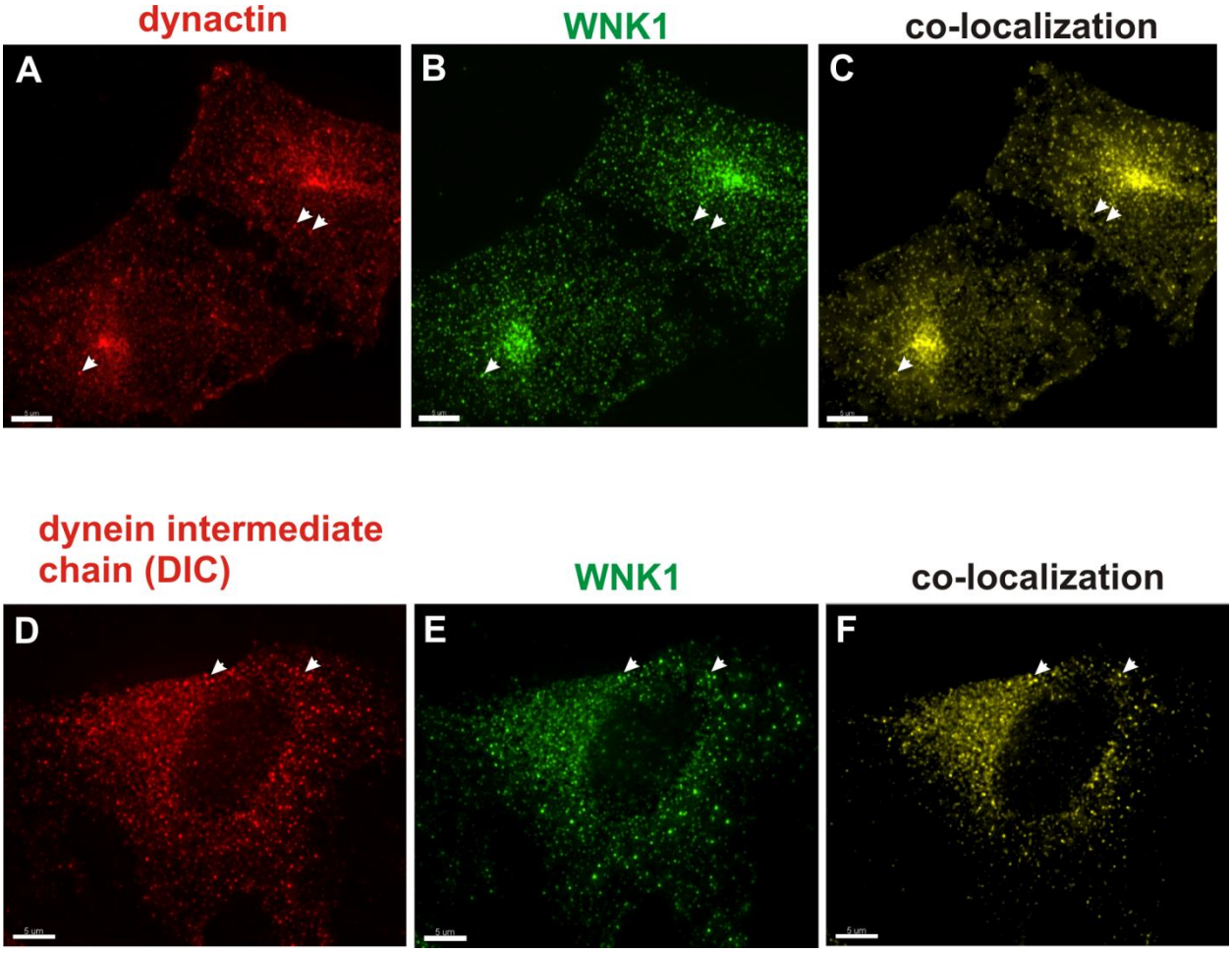

Figure 3-20. WNK1 co-localizes with dynactin or dynein intermediate chain.

Immunostaining of WNK1 (green) and dynactin (red) in HeLa cells (A and B). Co-localized yellow spots generated by Imaris Co-Loc module shown in (C). White arrowheads indicate the co-localized structures. The pearson correlation coefficient is 0.53 analyzed from the image above.

Immunostaining of WNK1 (green) and DIC (red) in HeLa cells (D and E). Co-localized yellow spots generated by Imaris Co-Loc module shown in (F). White arrowheads indicate the co-localized structures. The pearson correlation coefficient is 0.46 analyzed from the image above.

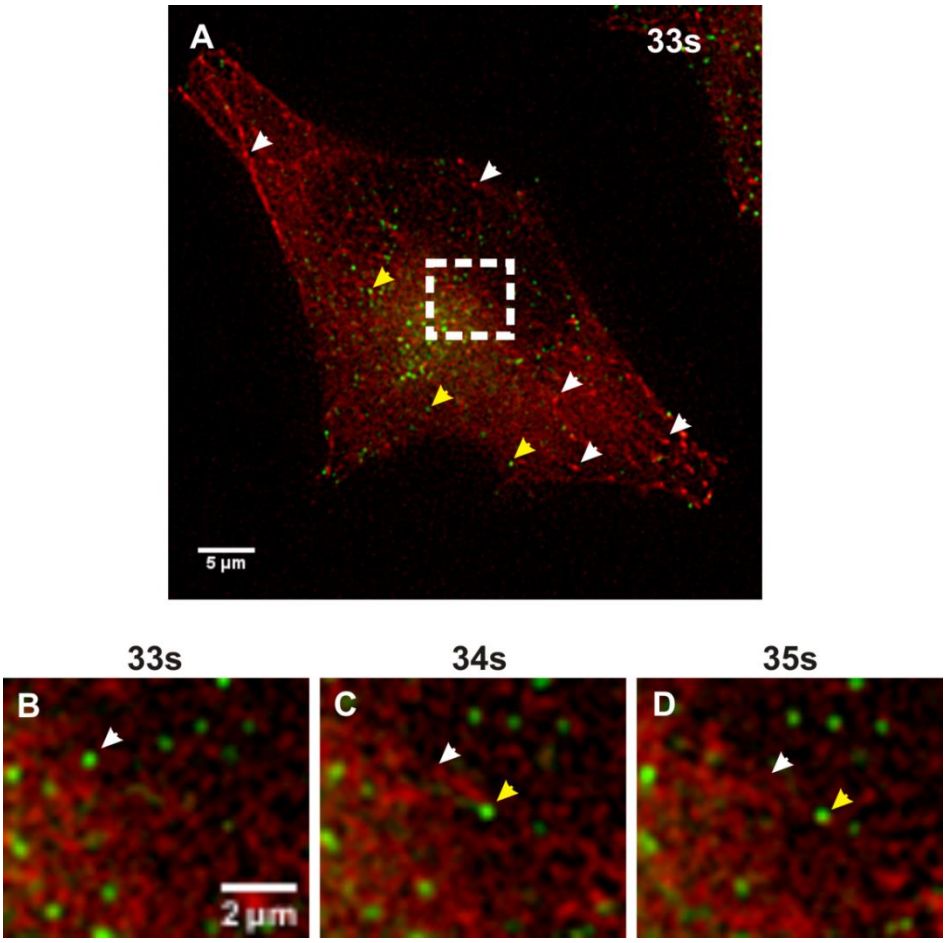

Figure 3-21. A comparison of movements between tdt-dynactin and GFP WNK1 1800-2126.

HeLa cells were co-transfected with tdt-dynactin and GFP-WNK11800-2126 for 24 hours. Images were taken at 1 second time interval. Figure 3-21 corresponds to movie 3-7. The movement of tdt-dynactin exhibits a comet-like dash (white arrowheads shown in A). GFP WNK1 1800-2126 particles (yellow arrowheads shown in A) hardly encounter tdt-dynactin comet-like particles.

Panels B-D are zoomed in pictures from A (shown in the white box). White arrowheads indicate the beginning position of GFP WNK1 1800-2126 particle and yellow arrowheads indicate the ending position of the particle. It seemed that GFP WNK1 1800-2126 particle encounters tdt-dynactin from time frame 33s to 34s (B and C). This is a very rare event where I could observe throughout the entire movie 3-7.

Discussion

Determining the localization of proteins in a cell presents a number of challenges. A fluorescently tagged protein may not always reflect the distribution of the endogenous protein and overexpression of proteins may also cause their mislocalization. Fixation and permeablization also influence results of immunofluorescence (IF) experiments. The attempt to consistently observe WNK1 on the centrosome-like structures did not succeed. Several factors may contribute to this inconsistency. First, WNK1 might localize on the centrosome-like structure in a particular cell cycle stage (e.g., G2 to M phase). A heterogeneous population of cells decreased the chance of this observation. Therefore, it may be worthwhile to perform cell synchronization procedure to capture a specific stage of cell cycle. Second, WNK1 may localize on centrosome-like structures very transiently. Third, WNK1 distributed in the cytoplasm not only on the centrosome-like structures. The wide distribution of WNK1 localization might mask the signal from the centrosome-like structure.

WNK1 is on mitotic spindles during mitosis (Chapter 2). While I observed mitosis defects, I found that interphase microtubules are also compromised and centrosomal structures are impaired. Using a reporter, I found that WNK1 is capable of traveling along microtubules mainly toward the plus end. Immunolocalization revealed that WNK1 localizes on the interphase microtubules. These observations and previous work implicating a dynein light chain suggested that WNK1 might bind dynein motor components or dynactin. Dynactin displays a plus-end tracking ability and bundles microtubules (*107, 109, 110*). Co-localization of WNK1 and dynactin suggested a *bona fide* co-localization between the two proteins. Less compelling are results of co-immunoprecipitation experiments which show protein binding with some conditions but failure with others. With the assistance by Dr. Luby-Phelps in the Live Cell Imaging Core

Facility, I performed co-injection of tdt-dynactin cDNA and WNK1 RNA oligonucleotides, and found no defect in the plus-end tracking ability of dynactin (data not shown). In this particular set of experiments, 43% of cells died due to mitosis defect in RNAi of WNK1 oligonucleotides injected cells while only 8% cells died in control cells (chapter 2). I therefore examined the surviving cells for plus-end tracking ability at the end of 72 hours- time lapse microscopy experiment. It is possible that the remained cells had certain level of expression of WNK1. Therefore, cells I examined may not represent WNK1-depleted condition. Future study might be improved by post-live cell imaging immunofluorescence for checking the expression level of endogenous WNK1. The plus-end tracking ability is visualized as movement of "comet-like" dashes. A comparison of movements of GFP-WNK1 1800-2126 and tdt-dynactin also suggested a difference rather than a similarity in plus-end tracking behavior. Tdt-dynactin displayed typical comet-like dashes while GFP-1800-2126 traveled along microtubules. These data tentatively suggest that the plus-end of microtubules may not be affected by WNK1.

There are other possible effects WNK1 might exert on the dynein motor complex. The literature suggests that motor activity of the dynein complex is not activated until it reaches the microtubule plus end and the cell cortex where cargo transport is needed (*108*). Therefore, WNK1 might affect the motor activity considering the data showing the association of WNK1 and dynein intermediate chain. The functional readout for the in vivo experiment is usually carried out by imaging the GFP- dynein intermediate chain (DIC). However, GFP-DIC (a kind gift from Dr. Kevin Pfeiffer, University of Virginia) would only work in neuron cells by observing the particles traveling on axonal neuritis. The GFP-DIC expression in HeLa cells is cytoplasmic diffusive. Therefore, the investigation of the effect of WNK1 on dynein motor activity might be worth carried out by GFP-DIC in neuronal cells.

What are other possible mechanisms underlying the regulation of interphase microtubules by WNK1? Two possible candidates from the mass spectrometry results are the centrosomal proteins Cep 70 and Cep 170 (Table 3-1). Because WNK1 appears to localize on centrosomes during G2, depletion of WNK1 may not only disrupt radial microtubules arrays from the MTOC but may also impair centrosomes. Rescue experiments with WNK1 1-940 showed a strong MTOC localization. Cep 70 localizes at centrosomes in interphase microtubules and at the spindle pole body during mitosis (*113*). Silencing of Cep 70 disrupts interphase microtubules and causes mitotic spindle defects. Cep 70 might affect the formation of astral spindle MTs, thereby causing spindle pole microtubules defects. Cep 70 binds to centrosomes through γ tubulin, a nucleating center for interphase microtubules as well (*113*). In the WNK1-depleted cells, similar phenotypic defects were also observed as shown in the Cep 70-depleted cells. Shi et al. (*114*) demonstrated that Cep 70 contributes to angiogenesis sprouting by regulating the orientation of the centrosomes during cell migration. Cep 70 has been implicated in activation of Cdc42 and Rac1 in migrating cells. WNK1 has been shown to play a vital role in cardiovascular development and may also be involved in angiogenesis sprouting (*90*). Therefore, it will be interesting to determine if there is a functional relationship between WNK1 and Cep 70. Another candidate is Cep 170. Depletion of Cep 170 resulted in disrupted interphase microtubules and cell shape (*115*). Taken together, both Cep 70 and Cep 170 may bind WNK1 and contribute to both the mitotic spindle and interphase microtubules defects observed in the WNK1-depleted cells.

			Spectral counts		
	Description	mw (Da)	1-2126-1	1-940-1	LIS1-1
1st	CEP70_HUMAN Centrosomal protein of 70 kDa	67632.9	10.81	9.83	
	B7Z1R5_HUMAN V-type proton ATPase catalytic subunit A	68440.6	4		
	B7Z3U6_HUMAN ATPase, Na+/K+ transporting, alpha 1 polypeptide	113130	17.78	13.88	
	COPB_HUMAN Coatomer subunit beta	107344	8.99	3	
	COPG1_HUMAN Coatomer subunit gamma-1	97907.6	2.5		
	GOGA3_HUMAN Golgin subfamily A member 3 (Golgin 160)	156002		5	
2nd	B7ZKR7_HUMAN AP-3 complex subunit beta-2	119309	2	3	
	F5H569_HUMAN V-type proton ATPase 116 kDa subunit a isoform 1	96771.4	3	4	
	COPA_HUMAN Coatomer subunit alpha	139596	13		
	GOGA3_HUMAN Golgin subfamily A member 3 (Golgin 160)	156002	28	26	
	CLH1_HUMAN Clathrin heavy chain 1	188257	22	11	11
	H0Y2V6_HUMAN Centrosomal protein of 170 kDa	175655	10.84	10.84	3.96

Table 3-1. Mass spectrometry results.

HEK 293 cells were transfected with WNK1 1-2126 myc or WNK11-940 myc or LIS1-myc construct for 48 hours. Cells were harvested and lysed in the buffer (20 mM HEPES, 100 mM NaCl, 5 mM $MgCl_2$ pH 7.5, 0.5 % Triton X-100, 0.01% CHAPS, 1 mM DTT, and protease inhibitors) at 4˚C for one hour. Cells lysates were spun at 16,000 g for 20 min. The 16,000 g supernatant was incubated with anti-myc antibody (1 to 100 ratio, µl antibody: µl lysate) at 4˚C rotator for 16 hours. Next day, lysates were added 30 ul protein A/G agarose beads and incubated at 4˚C for one hour. The beads were washed by lysis buffer 4 times, 10 min per time. Proteins were eluted from the beads by addition of 2X SDS sample buffer and heated at 94˚C for 3min. The elution was subjected for running the SDS- polyacrylamide gel. Right after the front dye run 10 mm from the separation gel, gel was stained with Coomassie Brilliant Blue staining and destained. The 10 mm band was cut and diced into $1mm^3$. Samples were ready to submit to the mass spectrometry core facility for protein complexes identification. I have done the experiment twice. (1^{st} was the first time result, 2^{nd} was the second time result).

CHAPTER 4

WNK1 AND MEMBRANE TRAFFICKING

Abstract

Endogenous WNK1 has a perinuclear punctate distribution (*116*). It is not clear if punctate staining is due to localization of WNK1 on vesicles. Depletion of WNK1 decreased the rate of EGF receptor degradation and caused the accumulation of receptors at later steps of endocytosis. Lysosomes and lysosome-related organelles were disrupted in WNK1-depleted cells. Biochemical studies suggested that WNK1 interacts with active Rab6 and Rab7 effector complexes. In screening Rab7 effectors for possible WNK1 binding, I found that WNK1 could associate with the homotypic fusion and vacuole protein sorting (HOPS) complex, the most important tethering complex for membrane fusion between late endosomes and lysosomes or autophagosomes and lysosomes. The HOPS complex also mediates trafficking of adaptor protein complex 3 (AP-3) vesicles between the TGN and late endosomes. Immunofluorescence studies showed that WNK1 co-localizes with AP-3 vesicles with a high Pearson correlation coefficient (0.53). Clathrin heavy chain and the AP-3 β subunit were found in a preliminary mass spectrometry experiment (Table 3-1). WNK1 may regulate membrane fusion mediated by vacuole protein sorting (VPS) 33 and the soluble N-ethylmaleimide-sensitve factor attachment protein receptors (SNAREs) complex rather than membrane recognition by Rab GTPases. Consistent with this observation, cells depleted of WNK1 displayed phenotypes similar to those caused by the depletion of vesicle associated membrane protein (VAMP) 7, one of the SNARE complex subunit. Phenotypes due to depletion of VAMP7 include defective abscission and failed assembly of pre-autophagosome structures, also observed in WNK1-depleted cells. Taken

together, these data suggested that WNK1 modulates membrane trafficking through HOPS complex-mediated membrane fusion events.

Introduction

WNK1 has been implicated in endocytosis and exocytosis (*28, 55, 56, 61*). The perinuclear punctate distribution of WNK1 raised the possibility–that WNK1 may be associated with a subset of vesicles mediating membrane trafficking events. Two of the clues I had before I began to study the impact of WNK1 on membrane trafficking were potential WNK1-interacting proteins, identified in different two-hybrid screens by students who worked on WNK1 previously: 1) VPS4, an AAA ATPase protein that is important for multivescular body formation and 2) dynein light chain 8 (DLC8 aka PIN1), a component of the dynein motor complex which is responsible for transporting cargoes along microtubules. To investigate whether WNK1 influences endocytic pathways, I employed the epidermal growth factor (EGF) receptor degradation assay. In many cell types including HeLa, removal of EGF receptor ligands, by eliminating serum from the culture medium, results in accumulation of the EGF receptor on the cell surface, mainly through early or recycling endosomes. The addition of EGF triggers clathrin-coated vesicle-mediated endocytosis of the ligand-receptor complex. The internalized receptor vesicles are uncoated and fuse with early endosomes. Most of the receptors then move to late endosomes, the multivescular body (MVB), and lysosomes where they are degraded (*117*). Therefore, the EGF receptor degradation assay is a classic assay to assess whether a molecule affects endocytic pathways and warrants further investigation.

As cargoes can be delivered to several intracellular destinations, accurate vesicle trafficking requires Rab GTPases, central coordinators of membrane trafficking between organelles. In mammalian cells, there are more than 60 Rab GTPases. Each of them resides in one or two membrane domains (*118*). For example, Rab 4 and 5 exist in early endosomes and vesicles from plasma membranes. Rab7 mainly resides in late endosomes, lysosomes, and

autophagosomes. Rab1, 6, 8, and 33 are key in Golgi trafficking (Fig. 4-1). A specific active Rab GTPase binds several different effectors for downstream signaling events. The general mechanistic contribution of Rabs to vesicular trafficking has been studied extensively. Fig. 4-2 (*118*) illustrates a five step model for how active Rabs modulate vesicular transport from one membrane domain to another. I have investigated the possibility that WNK1 is involved in motility, tethering and fusion.

Motility of vesicular transport has been extensively studied. As cargoes could be transported by motor proteins-dependent or independent fashion, some studies suggest that motor-dependent transport is for long range-cargo delivery. Two examples of dynein motor-dependent vesicular transport complexes are described: dynactin- Rab7-interacting lysosomal protein (RILP) -oxysterol-binding protein (OSBP)-related protein 1L (ORP1L) - Rab7 and dynactin- Bicaudal-D-2 (BICD2) –Rab 6. The dynactin- RILP-ORP1L-Rab7 complex is important for positioning of perinuclear localization of lysosomal compartments (*119*). The dynactin-BICD2-Rab 6 is important for perinuclear positioning of the Golgi apparatus (*120, 121*). I have examined WNK1 and its potential link to these two complexes.

Tethering is mainly executed by a variety of tethering complexes and fusion is mediated by SNARE complexes. Tethering complexes also could be effectors for active Rabs. There are several different tethering complexes. As shown in Table 4-1 (*122*), each tethering complex has its function between two membrane domains and consists of Rab GTPases or Rho GTPases and interacting with the SNAREs complex. Rab7 plays an important role in late endosomes and

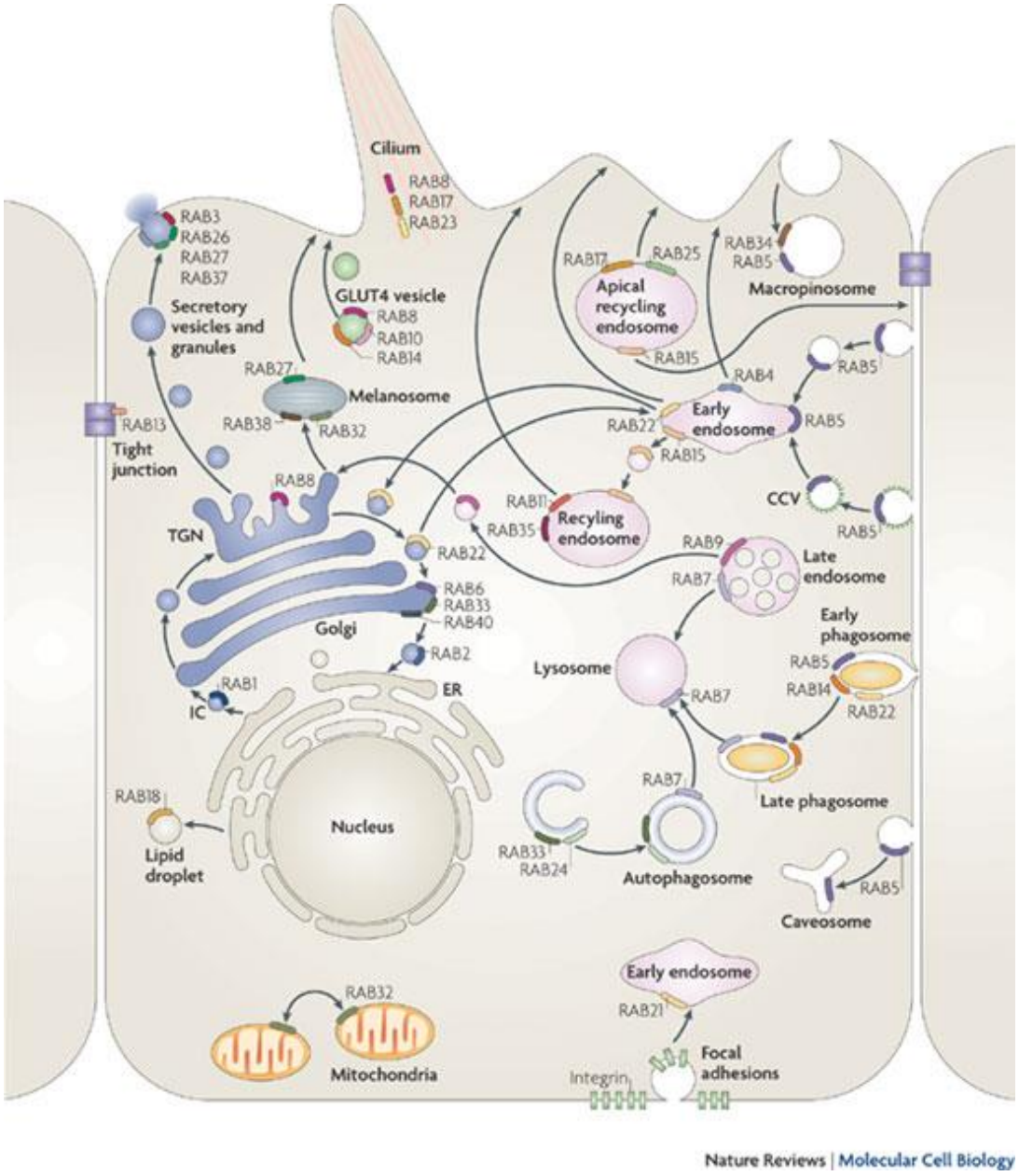

Figure 4-1. Localization and function of Rab GTPases.

Reprinted by permission from Macmillan Publishers Ltd: H. Stenmark, Rab GTPases as coordinators of vesicle traffic. *Nature reviews. Molecular cell biology* **10**, 513 (Aug, 2009). Figure 4-1 corresponds to Figure 2 in Herald Stenmark' review article.

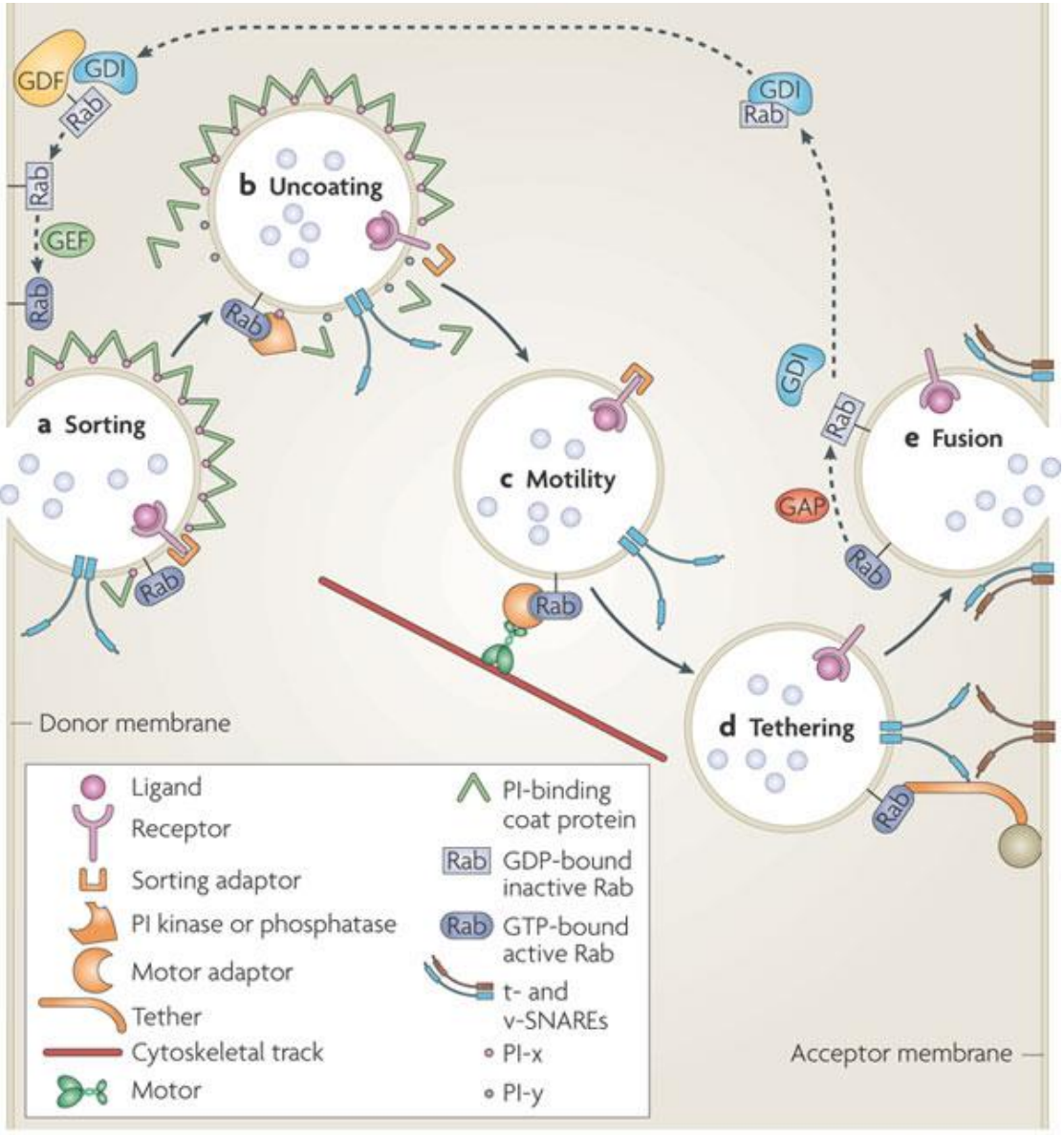

Figure 4-2. Rab GTPase functions in vesicle trafficking.

Reprinted by permission from Macmillan Publishers Ltd: H. Stenmark, Rab GTPases as coordinators of vesicle traffic. *Nature reviews. Molecular cell biology* **10**, 513 (Aug, 2009). Figure 4-2 corresponds to Figure 3 in Herald Stenmark' review article.

Table 4- 1. Properties of tethering complexes.

Tethering complex	Localization	Functions between	Subunits	Rab or Rho GTPase	Interacting SNAREs	Interacting coat/ AP complex	Lipid interaction
Dsl1p	ER	Golgi/ ER	Dsl1 Dsl3 (Sec39) Tip20	Ypt1 (?)	Use1, Sec20	COPI	
COG	Golgi	Endosome / cis Golgi	Cog1 Cog2 (Sec35) Cog3 (Sec34) Cog4 Cog5 Cog6 Cog7 Cog8	Ypt1	Sec22 Gos1 Sed5 Ykt6	COPI	
GARP	TGN	Endosome / TGN	Vps51/Ang2 Vps52 Vps53 Vps54	Ypt6	Tlg1		
Exocyst	Plasma membrane	Vesicle/ plasma membrane	Sec3 Sec5 Sec6 Sec8 Sec10 Sec15 Exo70 Exo84	Sec4 RalA Rho1 Rho3	Sso1,2 Snc1,2 Sec9		Sec3, Exo70
CORVET	Endosome/	TGN early endosomes	Vps8 Vps3 Vps11 Vps16 Vps18 Vps33	Vps21 (Rab5)			
HOPS	Vacuøle	MVB vacuole, and vacuole / vacuole	Vps41 Vps39 Vps11 Vps16 Vps18 Vps33	Ypt7 (Rab7)	Vam3 Vam7 Vti1 Nyv1	d-subunit of AP-3	
TRAPPI	Golgi	ER/ Golgi	Bet3 (2x) Bet5 Trs20 Trs23 Trp31 Trs33	Ypt1		COPII	
TRAPPII	Golgi	Endosome / Golgi	TRAPPI + Trs65 Trs120 Trs130 Tca17	Ypt1, Ypt31/ 32		COPI	
TRAPPIII	Phagophore /	Golgi lysosome	TRAPPI + Trs85	Ypt1			

Subunits that bind SNAREs are indicated in italics and Rab effectors are shown in bold. For TRAPP, the subunits required for GEF activity are underlined. Blank boxes for interactions of tethers with SNAREs, coats or lipids indicate that no data have been reported, to our knowledge.

Table 4-1. Properties of tethering complexes.

Reprinted by permission from Elsevier Ltd: C. Brocker, S. Engelbrecht-Vandre, C. Ungermann, Multisubunit tethering complexes and their role in membrane fusion. *Current biology : CB* **20**, R943 (Nov 9, 2010). Table 4-1 corresponds to Table 1 in Brocker et al., review article.

lysosomes fusion. Several Rab 7 effectors were found. One of them is motility complex-dynein-dynactin-RILP-ORP1L-Rab 7, the other one is the HOPS complex which is responsible for tethering and fusion (*123*). Some evidence I have observed suggested that WNK1 might interact with the HOPS complex.

The HOPS complex consists of six subunits- VPS33, VPS16, VPS18, VPS11, VPS41 and VPS39, originally discovered in the yeast *Saccharomyces cerevisiae* for mutant strains deficient in the vacuole morphology and vacuole protein sorting (VPS) (*124-126*). VPS41 and VPS39 are responsible for active Rab 7 binding and tethering the HOPS complex to late endosome membranes. VPS33 is responsible for the binding with the SNARE complex, mediating final fusion. In the metazoan, there are two VPS33 isoforms - VPS33A and B. Genetic studies suggest that these two proteins are not functionally redundant in *Drosophila (127).* In human, the genetic diseases also suggest that human VPS33A and VPS33B have distinct functions: The Hermansky-Pudlak syndrome (HPS) and Arthrogryposis, Renal Dysfunction and Cholestasis (ARC) affect VPS33 A and VPS33 B respectively. In mice, mutations of AP-3 protein and VPS33A result in decreased coat colors, prolonged bleeding and defects in lysosomal protein targeting (*128, 129*). Mass spectrometry data also suggested that WNK1 could pull down clathrin heavy chain and AP-3 β subunit (Table 3-1). WNK1 might contribute to membrane trafficking through modulating late endosomes and lysosomes fusion or the TGN and late endosomes trafficking.

Materials and Methods

Constructs

All WNK1 fragments cDNA constructs were described in chapter 2 and 3. VPS33A (NM_022916), VPS33B (NM_018668), VPS41 (NM_014396), Rab6 (NM_198896.1) were purchased from OriGene Technologies, Inc. VPS11 (BC065563), VPS16 (NM_022575), Rab 9A (NM_004251) and Rab7 (BC013728) were purchased from Open Biosystems. Rab5 and 11 cDNA constructs were a gift from Dr. Richard Anderson (UTSouthwestern). Mammalian VPS expression constructs were generated by PCR based procedures and subcloned into pCMV5-HA vector. Mammalian Rab GTPases expression constructs were generated by PCR based procedures and subcloned into pCMV7.1 3XFLAG vector. Bacterial Rab GTPases expression constructs were generated by PCR based procedures and subcloned into pGST-parallell (AF097411) vector. All mutant constructs were generated by Quikchange (Strategene).

Antibodies and reagents

Antibodies and reagents used were described in chapter 2, 3 and addition of the following: Rab7 (cell signaling 9367), Rab5 (BD Pharmingen, 610724), clathrin-heavy chain (BD Pharmingen, 610500), mannose 6 phosphate receptor (cation independent) (Abcam, ab2733), VPS4 (Santa Cruz, sc-133122), Golgin 97 (Molecular Probes, A-21270), ORP1L (Abcam, ab131165), BICD2 (Sigma-Aldrich, HPA023013), Lamp1 (BD Pharmingen, 555798), VPS41 (Santa Cruz, sc-377046), VPS11 (Bethy Laboratories, Inc., A311-300A), VPS 33A (GeneTex, GTX119416), anti-HA (clone 16B12, Covance), Adaptin δ (AP-3) (BD Pharmingen, 611328), EGF receptor for immunofluorescence (Oncogene clone 13), for Western blotting (Santa Cruz clone F4, sc-53274), GAPDH (Santa Cruz, sc-25778).

Cell culture

HeLa and HEK293 cells were cultured as described in chapter 3.

RNAi

HeLa cells were transfected with dsRNA oligonucleotides using Lipofectamine RNAiMAX according to manufacturer's instructions (Invitrogen). WNK1 and OSR1 RNAi were described in chapter 2. VPS4A RNAi : sense: GGGAUAAUCCGGAGAAAAAtt ; antisense: UUUUUCUCCGGAUUAUCCCag , VPS4B RNAi : sense : GGGCAAAGUGUACAGAAUAtt ; antisense : UAUUCUGUACCACUUUGCCCtt , BICD2 RNAi: sense: GGAGCUGUCACACUACAUGtt ; antisense : CAUGUAGUGUGACAGCUCCtt.

EGF receptor degradation assay

Immunofluorescence and immunoblotting procedures for EGF receptor degradation assay were the same as described in chapter 3 except using cold PBS as washing buffers and stopped the receptor degradation at each time point indicated. HeLa cells were transfected with indicated small interfering RNA oligonucleotides at the final concentration 25 nM for 48 hours and repeated the same procedure again for another 24 hours. Cells were then replaced with no serum DMEM medium for 8 hours and added EGF at the final concentration 10 ng / ml. Cells were harvested at the indicated time point for immunofluorescence or immnuoblotting. For the immunoblotting, the recipe of the lysis buffer (RIPA) was as following: 50 mM Tris (pH7.4), 150 mM NaCl, 0.25% sodium deoxycholate, 0.5% NP-40 and protease inhibitors (as described in chapter 3). Equal amount of total proteins was loaded for Western blot analysis.

For the rescue experiment, WNK1 fragment 1-940 wild type (WT) or kinase dead (KD) was transfected by lipofectamin 2000 by 1 to 3 ratio of plasmids (µg) to lipofectamine 2000 (µl) for 48 hours. Cells were then treated with the same RNAi procedure as described above for 48 hours and the rescue construct was transfected again for 24 hours in the middle of 48 hours

RNAi treatment. Cells were then treated with RNAi again for another 24 hours and performed 8 hours serum starvation. The subsequent procedures were the same as described above.

Purification of recombinant GST- Rab GTPases

pGST- parallel Rab GTPase WT, QL or TN construct was transformed into Rosetta (DE3). A 50 ml LB culture was grown overnight at 37˚C bacteria shaker and added to a new 1L LB culture for 1 to 100 dilutions. The induction of 500 µM isopropyl β-D-1-thiogalactopyranoside (IPTG) at the final concentration of the LB culture was done at the bacteria density reaching 0.8 (measured by optical density wave length 600) and induced at 16˚C for 16 hours. Bacteria lysates were harvested and resuspended in the extraction buffer (150 mM Tris pH 8.0, 50 mM NaCl, 10 % glycerol, 1 mM dithiothreitol, 1 mM benzamidine hydrochloride, 200 µM phenylmethanesulfonyl fluoride (PMSF), 10 mg/L leupeptin, 0.5 mg/L pepstatin A, and 1.5 mg/L aprotinin). Lysates were then snap frozen by liquid N_2 and kept at -80˚C freezer until the day of purification performed. Bacteria lysates were thawed and added lysozymes at the concentration 50 µg/ ml in room temperature for 30 min. Chromosomal DNA were then sheered by sonication procedure and the lysates were spun by Beckman rotor type Ti 45 at 96,000 g for 3 hours at 4˚C. The supernatants were incubated with 1 ml of GST beads (pre-equilibration with the extraction buffer) at 4˚C for an hour. The beads were loaded onto a column and let the beads settled down to the bottom of the column. The loaded supernatants were flowed through and the column was washed by 20 times column volume of the extraction buffer. The elution buffer (150 mM Tris, 50 mM NaCl, 10 % glycerol, 10 mM glutathione pH 8.0) was incubated with the beads in room temperature for 15 min and repeated twice. The eluted proteins were dialyzed in the extraction buffer overnight at 4˚C. Next day, proteins were concentrated and stored at -80˚C freezer until needed.

Loading of GTPγS or GDP onto Rab GTPase wild type proteins

As Rab GTPase had intrinsic GTP hydrolysis activity, proteins purified from bacteria were usually GDP-bound form. In order to get both active and inactive Rab GTPases, the loading of GTPγS or GDP was performed. Recombinant proteins were washed twice in the nucleotide exchange buffer (20 mM HEPES, 100 mM NaCl, 10 mM EDTA, 5 mM $MgCl_2$, pH 7.5) containing 10 μM GTPγS for active Rabs or 10 μM GDP for inactive Rabs at room temperature for 10 min. Proteins were then incubated with the nucleotide stabilizing buffer (20 mM HEPES, 100 mM NaCl, 5 mM $MgCl_2$ pH 7.5) containing 1 mM GTPγS for the active Rabs or 1 mM GDP for inactive Rabs at room temperature for 30 min. Proteins then could be used for the following GST pull-down experiments.

GST- Rab GTPases pull-down experiments

WNK 1 fragment 1- 1200 or 1- 940 cDNA or other indicated constructs was transfected into HEK 293 cells for 48 hours. Cells were harvested in the lysis buffer (the nucleotide stabilizing buffer containing 0.5 % Triton X-100, 0.01% CHAPS, 1 mM DTT, and protease inhibitors) for 30 min at 4˚C. Lysates were spun at 16000 g, 4˚C for 20 min. The supernatants were then incubated with indicated GST- Rab GTPases for 2 hours at 4˚C. The beads were washed with the lysis buffer 4 times, 10 min per time. The beads were eluted by 2X SDS sample buffer and ready for Western blot analysis.

Measurement of the lysosomal enzyme activity

HeLa cells were transfected with indicated small interfering RNA oligonucleotides as described in the EGF receptor degradation assays. Cells were lysed in the buffer (10 mM sodium phosphate pH 6.0, 0.5% Triton X-100, 150 mM NaCl) for 30 min at 4˚C. Lysates were spun at

16,000 g at 4˚C for 20 min and the supernatants were ready for the assay. Equal amount of total proteins (10 µg) in 200 µl of the supernatants were incubated with 50 µl of 10 mM 4-methylumbelliferone- α-D-mannopyranoside (Sigma N-2127) at 37˚C for an hour in 0.1 M sodium acetate buffer pH 4.4. Reaction was stopped by the addition of 200 µl of 0.5 M $NaHCO_3$, pH 10.7. The fluorescence intensity was measured at 365 nm excitation and 448 nm emission. A standard curve with different concentrations of free 4-methylumbelliferone (Sigma M1381) (0, 200, 400, 600, 800, 1000 and 2000 pM) was also performed.

Transmission Electron Microscopy

HeLa cells were grown on MatTek glass bottom dishes and RNAi was performed as described in the EGF receptor degradation assay. Cells were serum starved with 0% FBS for 8 hours. One set of dishes was used for immunofluorescence for checking the expression of endogenous WNK1. The other set of dishes were rinsed to remove the media and then fixed in 2.5% glutaraldehyde in 0.1 M sodium cacodylate buffer pH 7.4 overnight at 4˚C. Dishes were rinsed with 0.1M cacodylate buffer to remove the glutaraldehyde and then post-fixed in buffered 2% osmium tetroxide containing 0.8% potassium ferricyanide for 60 minutes, followed by 5 washes with dH_2O and en bloc staining in 4% uranyl acetate in 50% ethanol for 60 min. All dished were then dehydrated with a graded series of ethanol and embedded in EMbed-812 resin. A Beem capsule containing fresh Epon resin was placed over the coverslip. Resin was polymerized overnight in an oven at 70˚C. Coverslips were removed from the resin by immersing the capsule in liquid nitrogen. Thin sections were cut on a Leica Ultracut UCT ultramicrotome and then stained with 2% uranyl acetate and lead citrate. Images were acquired on a FEI Tecnai G^2 Spirit electron microscope equipped with a LaB_6 source, Gatan CCD camera and operating at 120 kV.

Lysotracker staining and quantification of image analysis

HeLa cells were grown on MatTek glass bottom dishes with glass coverslips etched with an alphanumberic grid and RNAi was performed as described in the EGF receptor degradation assay. Cells were serum starved with 0% FBS for 12 hours or no starvation. Cells were replaced with medium containing 50 nM lysotracker (Invitrogen, L-7528) at 37˚C for an hour. Cells were washed with PBS twice and the fixation step was performed as described in chapter 2. Cells were then kept in PBS buffer and imaged by Deltavision RT deconvolution microscope (Applied Precision) by using an objective lens 40X air N/A 1.35. The location of each image was also recorded. Cells were then permeablized and stained with anti-WNK1 antibody and DAPI as described in chapter 2. Images were taken again according to previous recorded positions for checking the expression of endogenous WNK1. Images were analyzed by using Image J. The background was subtracted and threshold was selected using the default algorithm. The mean value of the lysotracker intensity was calculated and plotted by Graphpad prism 6. Statistics was performed by unpaired t-test with Welch's correction.

Results

WNK1 affects degradation of EGF receptors

The EGF receptor degradation assay is a classic assay for investigating endocytic pathways. I have observed that accumulation of EGF receptors on the cell surface by 8 hours serum starvation in WNK1-depleted cells is the same as in control cells (Fig. 4-3 A and E, red signals and I). Upon addition of EGF, the internalization of EGF receptors occurred in WNK1-depleted and control cells (Fig. 4-3 B and F). At time 60 min, the intensity and amount of EGF receptors decreased in control cells whereas that of receptors remained high in WNK1-depleted

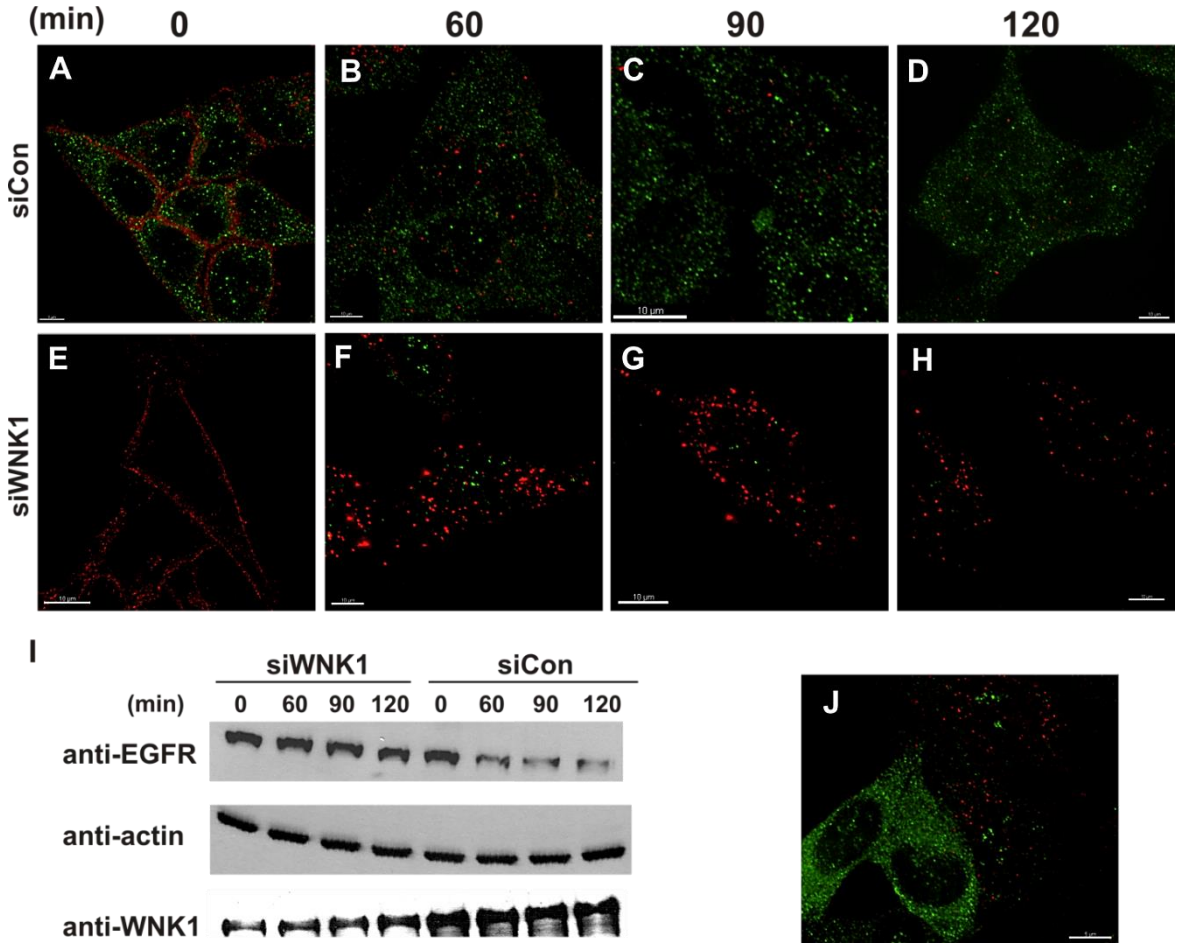

Figure 4-3. Loss of WNK1 slows degradation of the EGF receptor.

HeLa cells were transfected with WNK1 RNAi or scrambled control oligonucleotides twice. After 8 hours of serum starvation, cells were stimulated with 10 ng /ml EGF. At the indicated time, cells were lysed with RIPA buffer (see methods) for Western blot analysis or fixed and stained for immunofluorescence. (A to H). Cells were immunostained for endogenous WNK1 and the EGF receptor shown in the green and red channels, respectively. The EGF receptor accumulated on the plasma membrane at time 0 in both control and WNK1-depleted cells (A and E). Upon EGF stimulation, the EGF receptor was internalized into the cytosol (B and F). At 90 and 120 min, the intensity of EGF receptor staining was weaker in the control cells (C and D), but was sustained in WNK1 knockdown cells (G and H). (J) Cells expressing WNK1showed little or no EGF receptor staining compared to neighboring cells in which WNK1 had been silenced (J). (I) Cell lysates were immunoblotted with anti-EGF receptor, anti-WNK1, and anti-actin antibodies.

cells (Fig. 4-3 B, F red signals and I). At time 90 and 120 min, almost all receptors were degraded in control cells but there were noticeable amount of receptors in WNK1-depleted cells (Fig. 4-3 C, D, G, H and I). In the WNK1-depleted dish, cells still having expression of WNK1 had very little amount of receptors remaining while cells with no WNK1 expression retained a high level of receptors (Fig. 4-3 J). These data suggested that WNK1 might affect endocytic pathways in the later step. As I tried to perform rescue experiments for the receptor degradation phenotype, full length WNK1 did not express well enough in HeLa cells. I therefore used WNK11- 940 wild type (WT) or kinase dead (KD) to test the sufficiency. As shown in Fig. 4-4 B, the WT 1-940 fragment appeared to rescue the phenotype. The 1-940 KD fragment displayed a partial rescue effect: receptor was degraded but the degradation was slower than WT. I have only done this rescue experiment once and more investigation is still needed. Thus far, it tentatively implies that the EGF receptor degradation phenotype caused by depletion of WNK1 may not be due to off-target effect.

WNK1 affects degradation of EGF receptors independent of OSR1 and VPS4

Two possible interactors for WNK1-mediated receptor degradation phenotype could be OSR1 and / or VPS4. OSR1 is a well characterized WNK1 downstream effector, it was therefore examined. I have shown that WNK1 co-localized with OSR1 (Fig. 4-5 A to C, published in Sengupta et al., 2012). Silencing OSR1 expression did not affect the receptor degradation (Fig. 4-5 D). Knocking down of VPS4 did not affect the expression of WNK1 and vice versa (Fig. 4-6 B). To test whether VPS4 is involved in WNK1-mediated receptor phenotype, silencing VPS4 expression was performed and assayed for the same phenotype. As shown in Fig. 4-6 A, the initial amount of EGF receptors was less in VPS4-depleted cells and degradation of receptors did not get affected. Immunofluorescence study showed that the antibody used for the

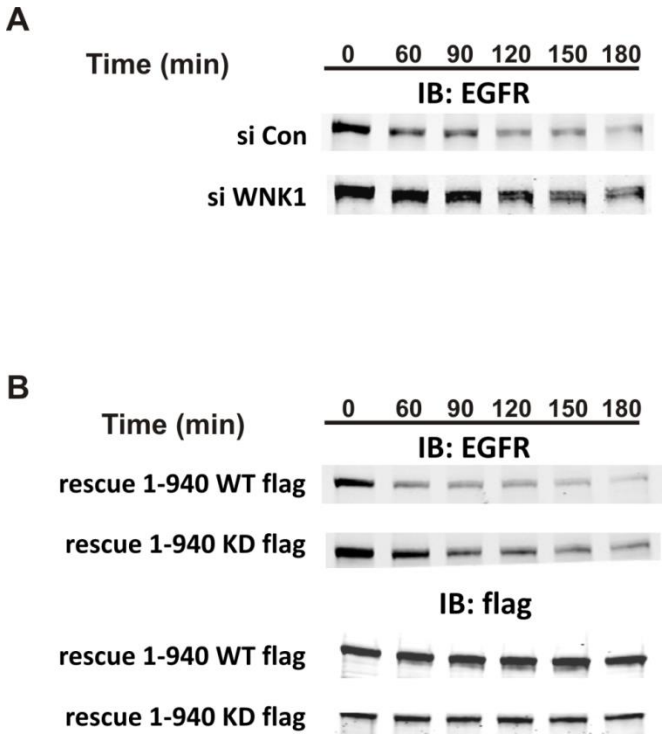

Figure 4-4. WNK1 1-940 may be sufficient to rescue the EGF receptor degradation phenotype.

(A) HeLa cells were transfected with WNK1 siRNA or control oligonucleotides same as described in Fig. 4-3 and cells were harvested with additional 2 time points (150 and 180 min). siCon blot was one representative of twice experiments and siWNK1 blot was also one representative of twice experiments. These two blots were not the same time experiment.

(B) For rescue experiments, a cDNA encoding Flag-WNK1 1-940 wild type (WT) or a kinase-dead (KD) mutant was transfected into cells for 48 hours. Cells were then treated with the same RNAi procedure as described in the methods for 48 hours and the rescue construct was transfected again for 24 hours in the middle of 48 hours RNAi treatment. Cells were then treated with RNAi again for another 24 hours and performed 8 hours serum starvation. The subsequent procedures for harvesting and lysing were the same as described in the methods. Western blots showed the expression of EGF receptor and Flag WNK constructs. Blots shown in (B) were one time experiment.

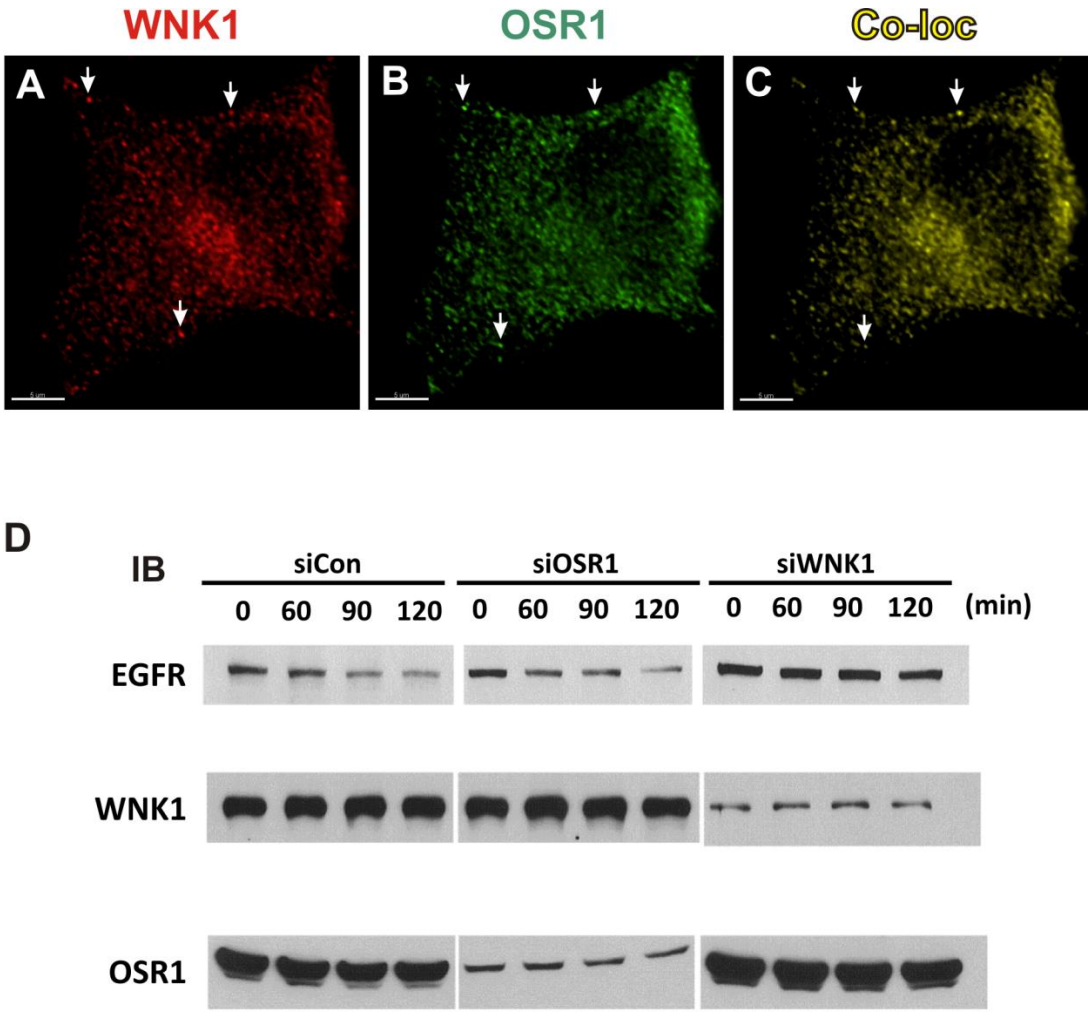

Figure 4-5. WNK1 affects EGFR degradation independent of OSR1.

Cells were transfected with OSR-1 flag construct for 24 hours. Cells were immunostained with anti-WNK1 (A, shown in red) and anti-flag (B, shown in green) antibodies. The co-localized yellow spots (C) were analyzed by Imaris Co-Loc module as described in chapter 2. (Fig. 4-5 A to C was published in Sengupta et al., 2012). White arrowheads indicate co-localized structures. The Pearson correlation coefficient is 0.54 analyzed from the image above.

(D) HeLa cells were treated with WNK1 or OSR1 or control oligonucleotides as described in Fig. 4-3. Subsequent procedures for the treatment of serum starvation, cell lysates harvesting and samples processing were the same as described in Fig. 4-3. Western blot showed the expression of EGFR, WNK1 and OSR1. The experiment was done once.

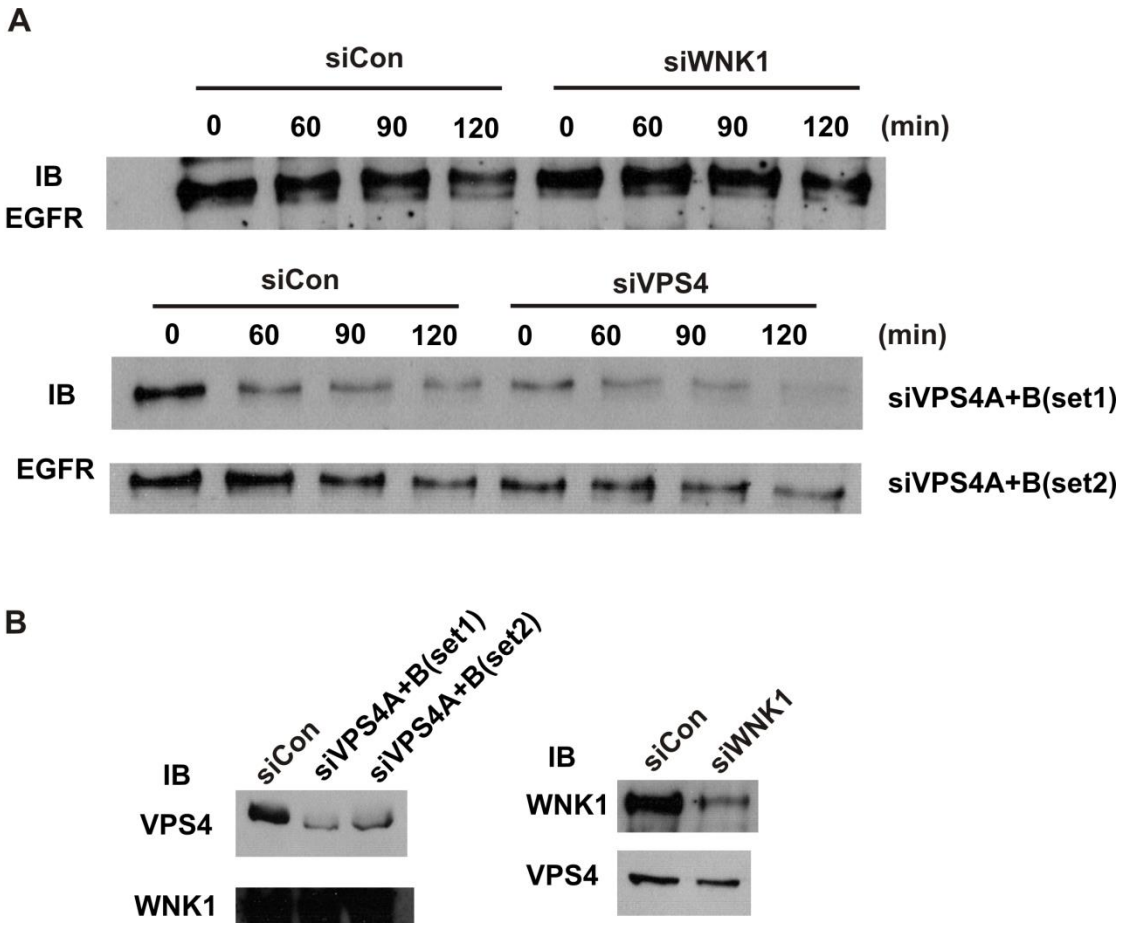

Figure 4-6. WNK1 affects EGFR degradation independent of VPS4.

HeLa cells were treated with WNK1 or control oligonucleotides. For VPS4A and VPS4B, cells were treated with the combination of VPS4A and VPS4B oligonucleotides for 2 sets shown in the legend (siVPS4A+B (set1) or siVPS4A+B (set2)). The subsequent procedures were the same as described in Fig. 4-3. (A) Western Blot showed the expression of EGFR. (B) Cell lysates from (A) time 0 were immunoblotted with anti-WNK1 or anti-VPS4 antibodies. The experiment was done once.

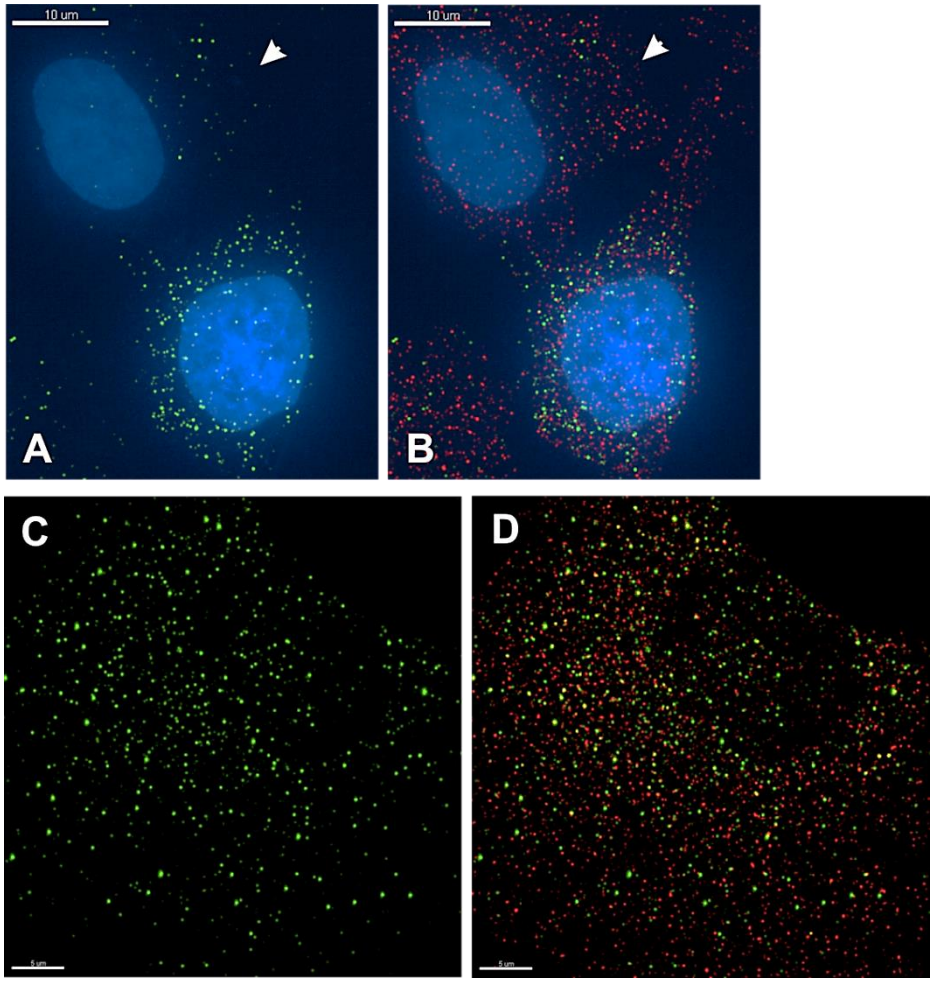

Figure 4-7. WNK1 did not co-localize with VPS4.

Co- immunostaining of HeLa cells with anti- VPS4 (green) and anti-WNK1 (red) antibodies. DAPI staining (blue). VPS4 antibody was validated by treating cells with VPS4A and B (set1) oligonucleotides for 48 hours and immnuostained with anti-VPS4 and anti-WNK1 antibodies (A and B); White arrowheads indicate that VPS4 fluorescent intensity (green) was diminished in VPS4-depleted cells and the WNK1 fluorescent intensity (red) was not affected (B). The distribution of VPS4 pattern was shown in (C). By Imaris Co-Loc module analysis, there is no significant co-localization between VPS4 and WNK1 (D). The Pearson correlation coefficient is 0.1 analyzed from the image above.

immunoblotting specifically recognized VPS4 (Fig. 4-7 A and B). Co-immunostaining by anti-WNK1 and anti-VPS4 antibodies was performed. The results demonstrated that there was no significant co-localization between two proteins (Fig. 4-7 D). Taken together, these data suggested that WNK1 might affect the EGF receptor degradation phenotype through unidentified effectors other than OSR1 or VPS4.

Disruption of proper organization and positioning of lysosomes and the Golgi in WNK1-depleted cells

Higher amount of EGF receptors remained at later time of the receptor degradation assay suggested that WNK1 might affect lysosomal compartment. Lamp1 is a trans-membrane protein residing in lysosomes. In control cells, the staining pattern of Lamp1 and Rab7 was perinuclear localization (Fig. 4-8 A to C) whereas dispersion of Lamp1 and Rab7 was observed in WNK1-depleted cells (Fig. 4-8 D to F), suggesting that the EGF receptor degradation defect could be due to disruption of lysosomal structures. The other important organelle, Golgi, was examined because most newly synthesized lysosomal enzymes are sorted to lysosomes from the TGN. Golgin 97 is one of the Golgin proteins residing in the TGN. In control cells, the staining pattern of Golgin 97 was also perinuclear and in closely-connected tubular structures (Fig. 4-8 G). In WNK1-depleted cells, both the staining patterns of Golgin 97 and Rab 7 were dispersed (Fig.4-8 J to L), suggesting that WNK1 affected both the TGN and lysosomal structures and positioning.

WNK1 does not co-localize with Rab 5, M6PR and Lamp1

As WNK1 displays a perinuclear punctate staining shown in chapter 2, I have tried to characterize the nature of the staining pattern. Rab 5 is an early endosomes marker. Mannose-6-

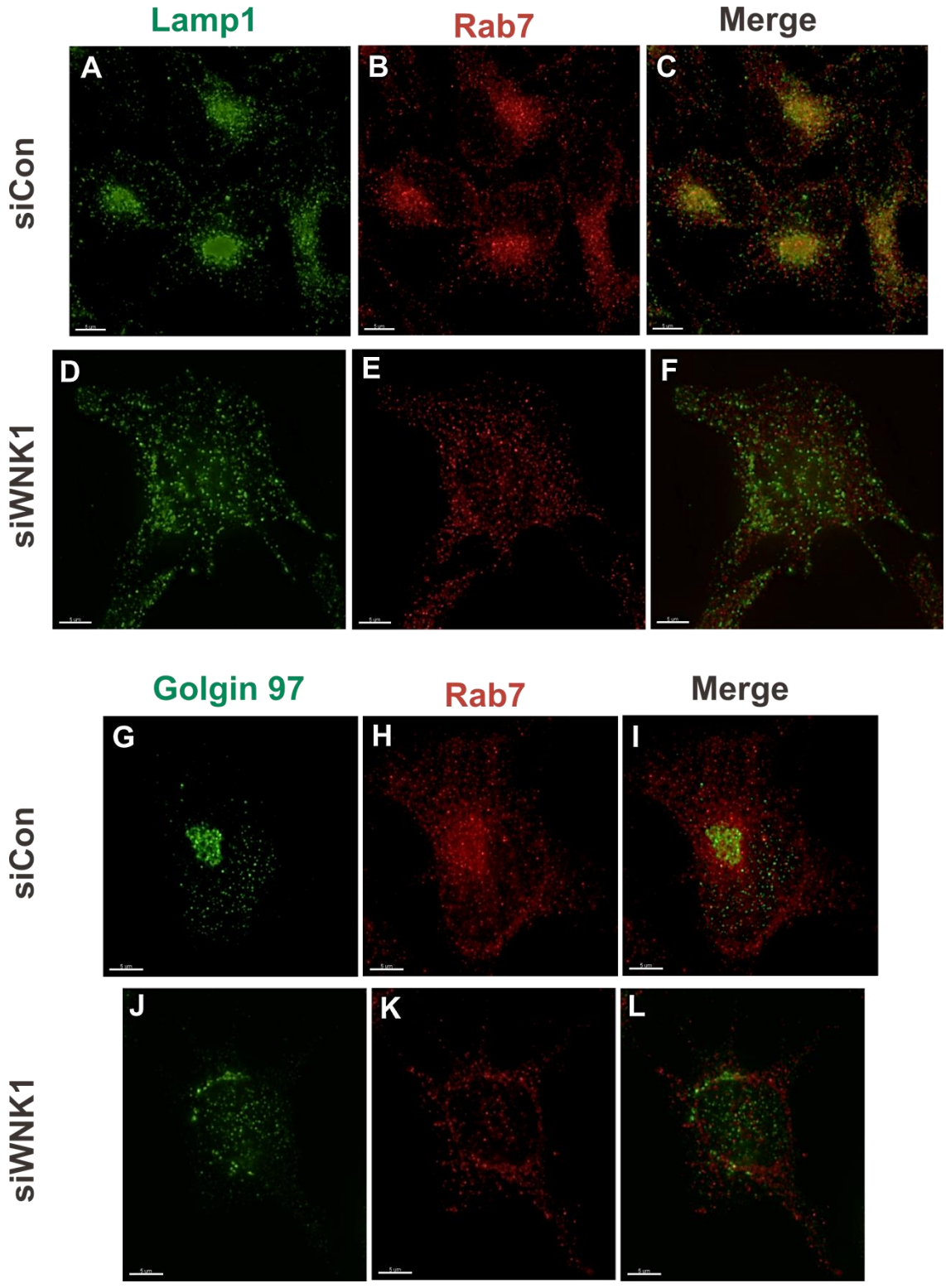

Figure 4-8. Disruption of proper organization and positioning of lysosomes and the Golgi in WNK1- depleted cells. See next page for the legend.

HeLa cells were transfected with WNK1 or control oligonucleotides for 72 hours. Cells were immunostained with the following antibodies:

Co – immunostaining of HeLa cells with anti-Lamp1 (green) and anti-Rab7 (red) antibodies (A to F). The perinuclear staining pattern of Lamp1 and Rab7 was shown in control cells (A to C) whereas dispersion of both Lamp1 and Rab7 was shown in WNK1-depleted cells (D to F). Co - immunostaining of HeLa cells with anti-Golgin 97 (green) and anti-Rab7 (red) antibodies (G to L). Golgin 97 is a marker for the TGN. The perinuclear and reticular-tubular staining pattern of Golgin 97 was shown in control cells (G). Silencing WNK1 expression caused dispersion of the reticular-tubular staining of Golgin 97 (J).

phosphate-receptor (M6PR) is a trans-membrane protein in vesicles traveling between the TGN and late endosomes. Co-immunostaining with WNK1 and a marker protein showed no significant co-localization (Fig. 4-9 A to I). M6PR and Lamp1 are trans-membrane protein receptors and represent a specific membrane organelle whereas Rab GTPases represent vesicles trafficking between different organelles. I then took another biochemical approach to ask whether WNK1 could interact with vesicles. This approach might compensate the problem that some Rab GTPase antibodies are not good enough for immunofluorescence experiment.

WNK1 could exist in GST- active Rab 6 or 7 pull down complexes

Recombinant protein GST- Rab GTPases were made. Glutamine to Leucine (QL) mutant is considered as a constitutively active Rab GTPase. Fig. 4-10 E shows that the amount of recombinant proteins is equal by Coomassie Brilliant Blue staining. Indicated construct, for example, WNK1 1-1200 FLAG was overexpressed in HEK 293 cells as input lysates. Recombinant GST Rab proteins were coated in GST beads and incubated with cell lysates for pull-down experiments. As shown in Fig. 4-10 A, WNK1 1-1200 could be pulled down in active Rab6 or Rab7 complexes, but not Rab5QL or 9QL. OSR1 did not seem to interact with any of the tested recombinant Rabs (Fig. 4-10 C). To show that recombinant Rab 5QL and 9QL are also active, well characterized effectors were used as a positive control. As shown in Fig. 4-10 B and D, NDEL1 myc could interact with Rab 6 and 9 QL and Vps34 FLAG preferred to interact with Rab5 and 9 QL, suggesting that recombinant Rab 5, 6, and 9 QL proteins are active.

WNK1 co-localized on constitutively active Rab6 or Rab7- induced vacuolar - tubular structures

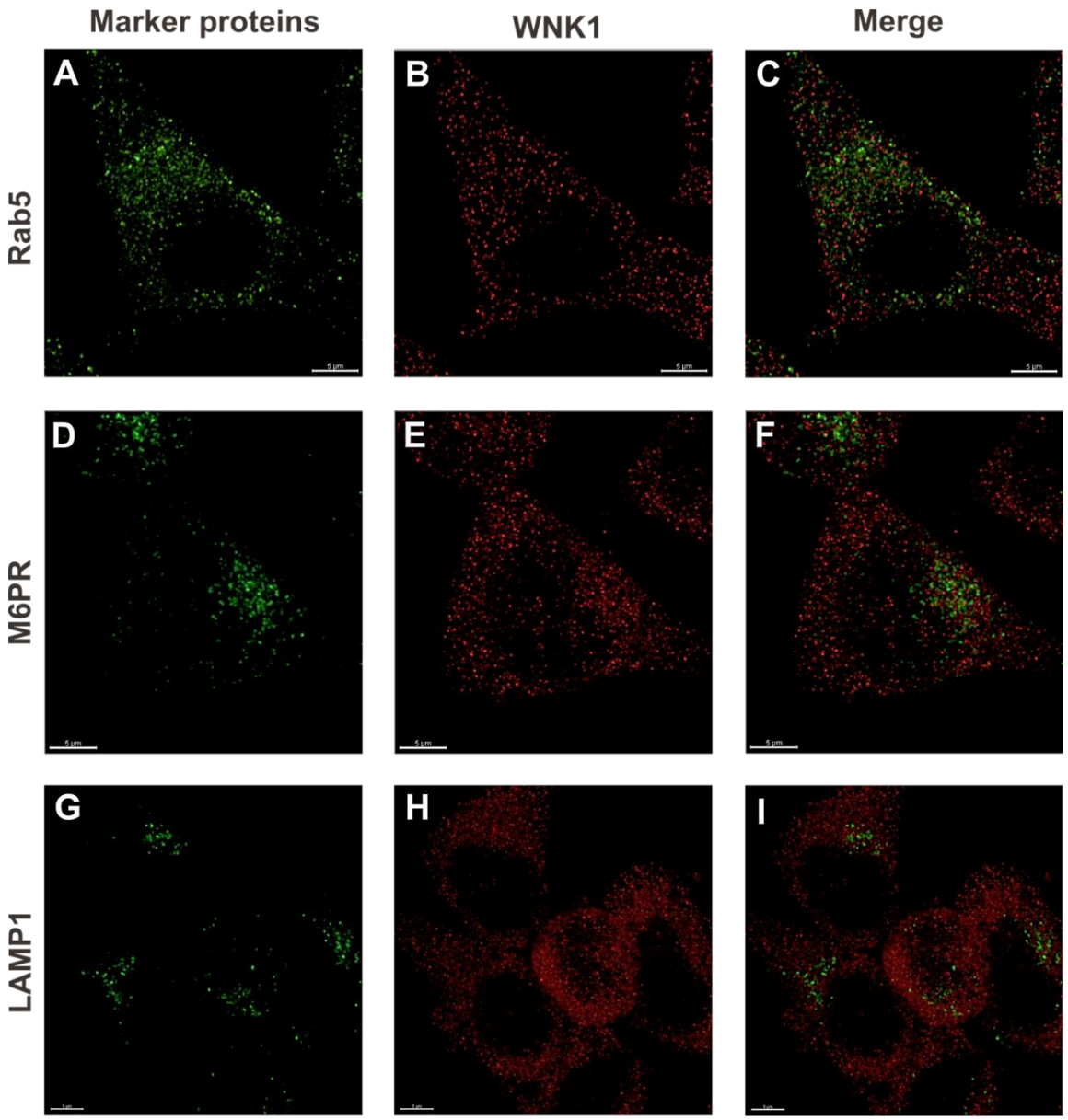

Figure 4-9. WNK1 does not co-localize with Rab 5, M6PR and Lamp1.

Endogenous WNK1 was shown in the red channel and all marker proteins were shown in the green channel. The co-localization of WNK1 with early endosome marker, Rab5 (A to C); the co-localization of WNK1 with late endosome marker, mannose-6-phosphate receptor (M6PR) (D to F); the co-localization of WNK1 with lysosomal marker, LAMP1 (G to I). The co-localization was analyzed by Imaris Co-Loc function. There is no strong evidence showing that WNK1co-localizes with Rab5, M6PR, LAMP1 after software analysis. The Pearson correlation coefficient is 0.2 for Rab 5, 0.17 for M6PR and 0.11 for Lamp1 analyzed from the image above.

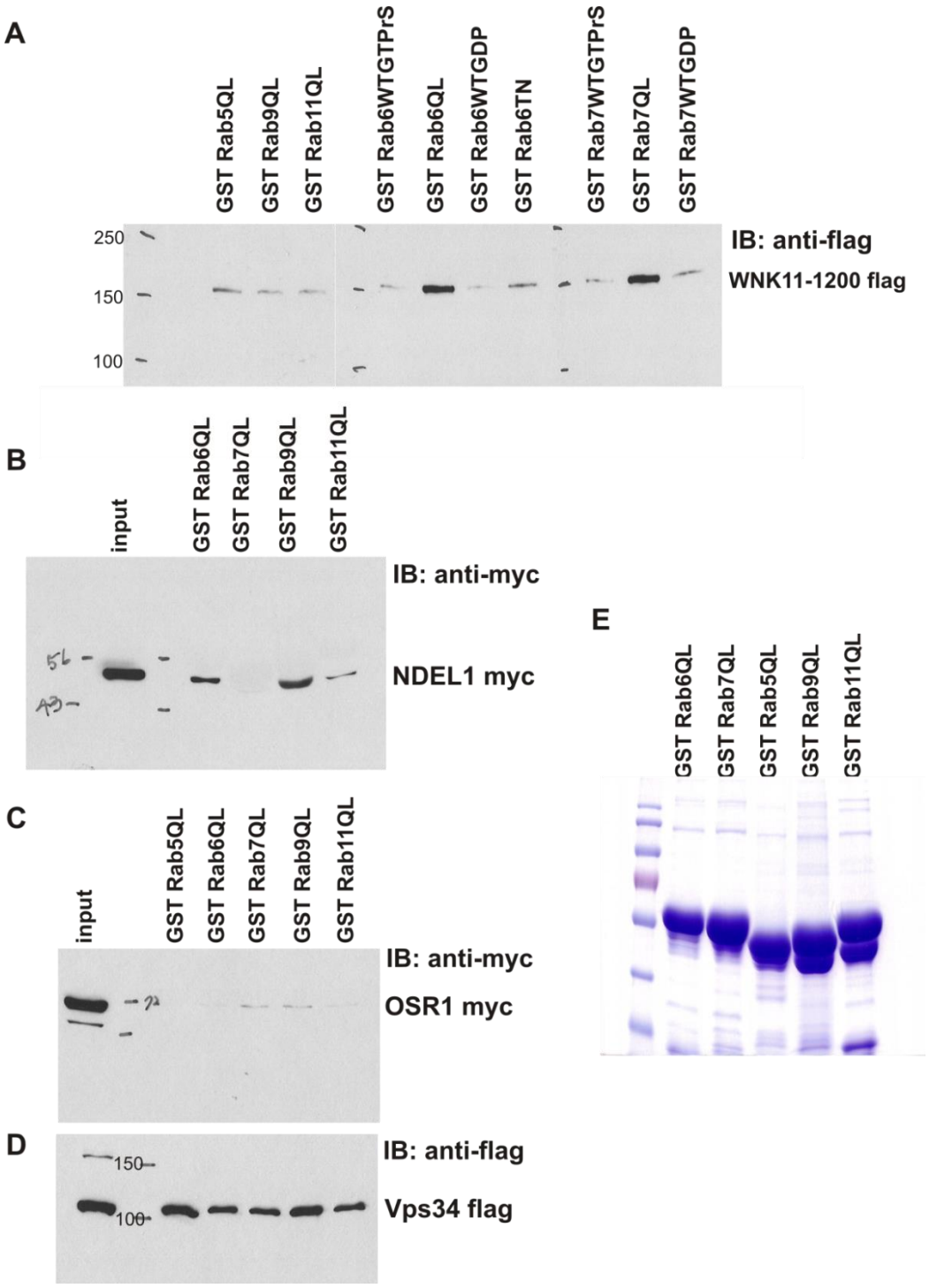

Figure 4-10. WNK1 could exist in active Rab6 or Rab7 effector complexes. See next page for the legend.

Recombinant GST- Rab GTPases were purified from bacteria (shown in E, Coomassie Brilliant Blue staining). HEK 293 cells were transfected with the indicated construct for 48 hours. Cells

were lysed and cleared by the centrifugation (see methods). The supernatants were incubated with indicated proteins coated on GST beads for 2 hours at 4˚C. The beads were washed 4 times with the lysis buffer and eluted by 2X SDS sample buffer for Western blot analysis. Flag-tagged proteins were immunoblotted by anti-flag antibody and myc-tagged proteins were immunoblotted by anti-myc antibody. (A) WNK1 1-1200 flag could associate with Rab6 QL or Rab7 QL-effector complexes. (B) NDEL1-myc could associate with Rab 6 or 9 QL- effector complexes and used as a control to show that purified GST Rab6 and 9 QL are active. (C) OSR1-myc did not seem to associate with recombinant GST- Rab GTPases tested. (D) VPS34-flag could interact with Rab5 QL-effector complexes and used as a control to demonstrate that purified Rab5 QL is active.

HeLa cells were transfected with Rab6 QL flag or Rab7 QL flag construct. Cells were immunostained with endogenous WNK1 and anti-FLAG antibodies. The localization of endogenous Rab6 and 7 has been shown to be in the TGN and lysosomes respectively. Overexpression of Rab 6QL or Rab7QL could result in vacuolar- tubular structures (Fig. 4-11 A and D, white arrowheads). The localization of Rab 6QL was highly concentrated in the TGN and in vacuolar structures. Co- localization analysis suggested that endogenous WNK1 could co-localize with active Rab6 vesicles which decorates vacuolar structures (Fig. 4-11 B and C, white arrowheads). The Pearson correlation coefficient calculated by Imaris Co-Loc module yields a high correlation- mean 0.45 from 5 images analyzed. In Fig. 4-11 D, the tubular structures formed by constitutively Rab 7QL were shown (white arrowheads). When examining the localization of endogenous WNK1, it was interesting to notice that endogenous WNK1 co-localized at the end of the tubular structures (Fig. 4-11 E, F, and G, white arrowheads). These data suggested that WNK1 could localize on active Rab6 or Rab7- induced vacuolar and tubular structures.

The possible cross-regulation between the TGN and lysosomes

The above data suggested that WNK1 could interact with at least two membrane organelles, Rab6- mediated TGN and Rab7-mediated lysosomes. As shown above, the TGN and lysosomes were disrupted in WNK1-depleted cells (Fig. 4-8). Lysosomal enzymes are synthesized and delivered from the TGN. Lysosomal enzyme activity could be measured by 4-methylumbelliferone-conjugated substrates. Hydrolysis of these artificial substrates at acidic pH leads to the formation of 4-methylumbelliferone, which is highly fluorescent at a pH above 10. Examining the activity of one of the lysosomal enzymes - α mannosidase demonstrated that enzyme activity was lower in WNK1 or BICD2-depleted cells (Fig. 4-12 B). BICD2 is one of

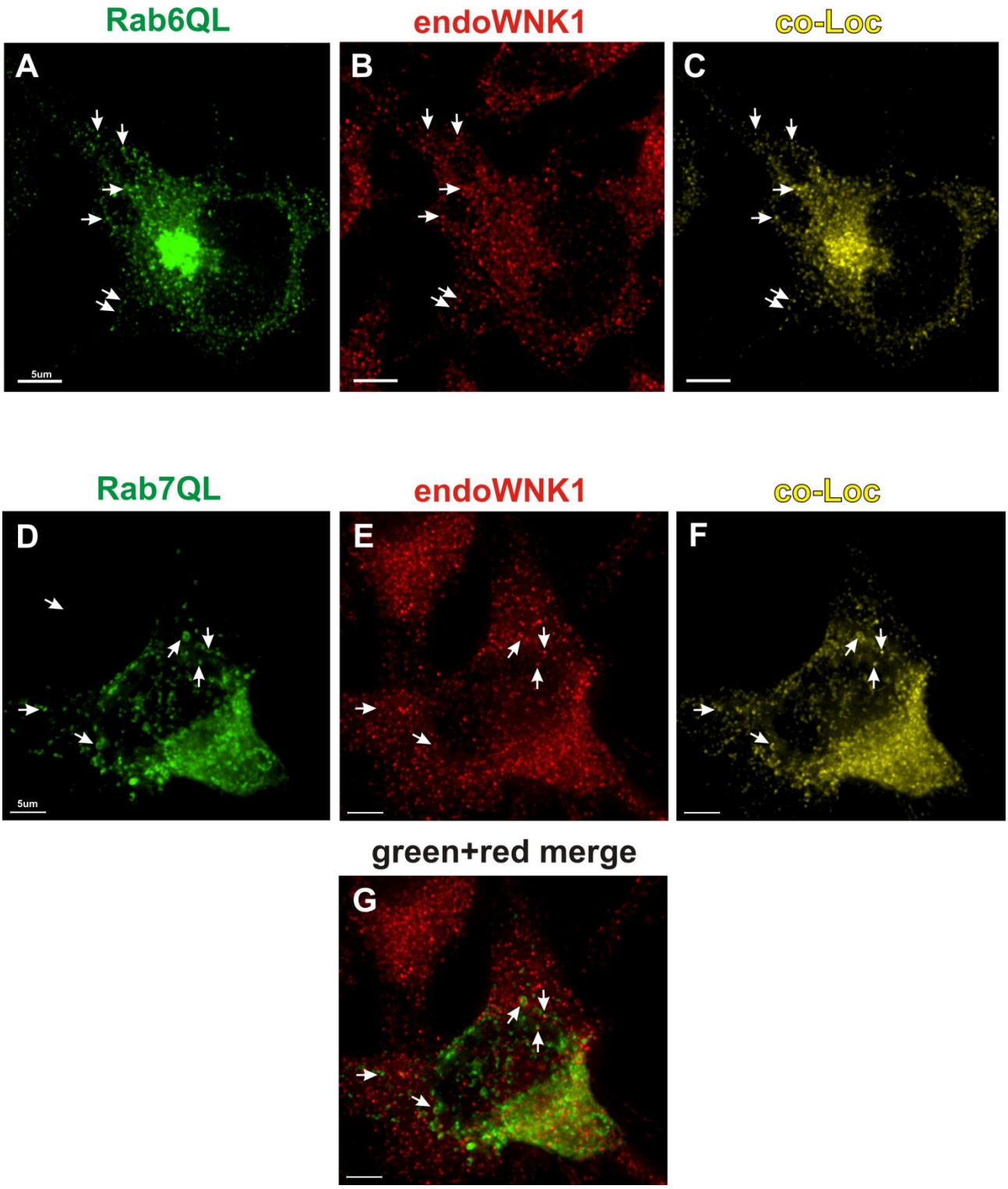

Figure 4-11. WNK1 co-localized on constitutively active Rab 6 or Rab7- inducing vacuolar - tubular structures. See next page for the legend.

HeLa cells were transfected with Rab6 QL or Rab7 QL flag construct for 24 hours. Cells were co- immunostained with anti-flag (green) and anti-WNK1 (red) antibodies. Co-localized yellow spots were generated by Imaris Co-Loc module.

Overexpression of constitutively Rab6 QL mutant could induce several vacuolar structures (shown in A, white arrowheads). Co-localization analysis suggested that WNK1 could localize on vacuolar structures induced by Rab6 QL (B and C, white arrowheads). The Pearson correlation coefficient yields a high correlation - 0.45 from 5 images analyzed.

Overexpression of constitutively Rab7 QL mutant could induce tubular structures in HeLa cells (shown in D, white arrowheads). Co-localization analysis suggested that WNK1 could localize on the end of the tubular structures induced by Rab7 QL (E, F and G, white arrowheads). The Pearson correlation coefficient is 0.5 analyzed from the image above.

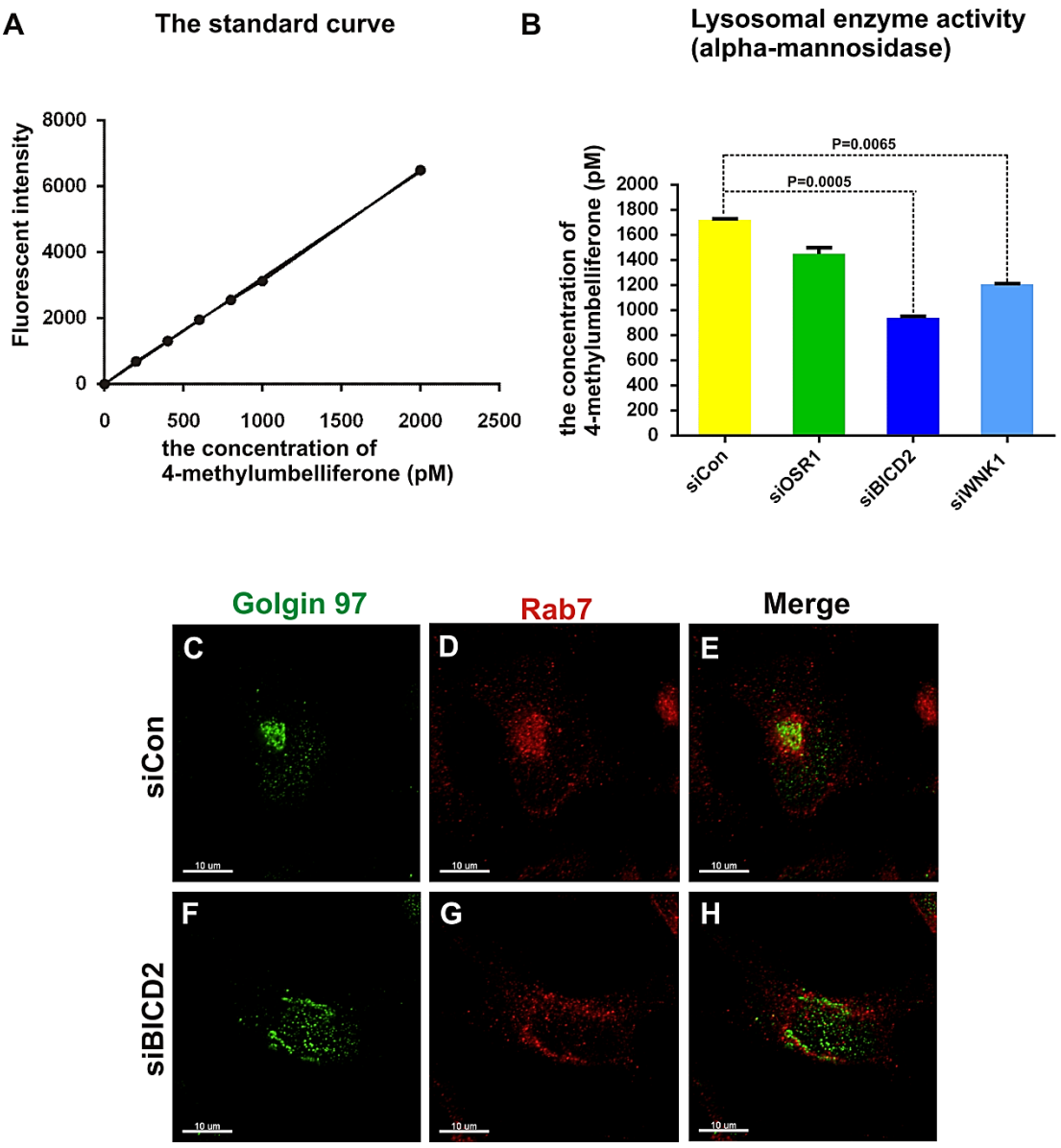

Figure 4-12. Depletion of WNK1 or BICD2 caused the impairment of lysosomal enzyme activity and dispersion of Rab7- perinuclear staining.

HeLa cells were transfected with WNK1, OSR1, BICD2 or control oligonucleotide for 48 hours and repeated the same procedure one more time. Cell lysates were assayed for one of the lysosomal enzymes, α-mannosidase by using 4-methylumbelliferone-α-D-mannopyranoside as a substrate. Detailed assay procedures were described in the methods.

(A) The standard curve was performed by measuring free 4-methylumbelliferone fluorescent intensity at 365 nm excitation and 448 nm emission. (B) The releasing amount of 4-

methylumbelliferone from α-mannosidase under each condition was calculated and plotted by Graphpad prism 6. Statistics was performed by unpaired-t test with Welch's correction. The difference between control and RNAi of OSR1 was not significant whereas the difference between control and RNAi of BICD2 or WNK1 was significant (p value < 0.05). This experiment was done once with duplication for each condition.

HeLa cells were transfected with BICD2 or control oligonucleotides for 72 hours. Cells were co-immnuostained with anti-Golgin 97(green) and anti-Rab7 (red) antibodies (C to H).

active Rab 6 effectors. RNAi of BICD2 could lead to dispersion of Rab7 perinuclear staining similar to depletion of WNK1 (Fig. 4-12 G). These data implied that the TGN could affect endolysosomal compartments probably due to the impairment of protein sorting from the TGN.

Dynactin-BICD2 or dynactin-RILP-ORP1L complex could not be detected in WNK1 immunocomplexes

WNK1 might be in active Rab6 or Rab7 effector complexes shown in Fig. 4- 10. The candidates, dynactin-BICD2-Rab6 and dynactin-RILP-ORP1L-Rab7, were tested. I performed a co-immunoprecipitation assay to see whether WNK1 could associate with BICD2 or ORP1L (RILP antibody is not available). Immunoprecipitated lysates from cells overexpressing WNK1 1- 1200 FLAG proteins were used for immunoblotting endogenous BICD2 or ORP1L. Both proteins were not detectable (Fig. 4-13 B and C). These data implied that WNK1 might associate with Rab6 or Rab7 effector complexes other than dynactin-BICD2 and dynactin-RILP-ORP1L.

The HOPS complex was present in WNK1 immunocomplexes

In an effort to investigate other possible effector complexes, one of the important Rab 7 effector complexes is the HOPS complex. I therefore used commercially? available antibodies to test whether the subunits of HOPS complex existed in WNK1-immunocomplexes. As shown in Fig. 4-14 A, VPS41 and VPS11 were detectable in WNK1 immunocomplexes (yellow arrowheads). Fig. 4-14 B shows the amount of different WNK1 fragments being precipitated. Judging from Fig. 4-14 A and B, it appeared that WNK1 1-940 fragment was sufficient for the binding with the HOPS complex and fragment 1200-2126 was also capable of this interaction.

WNK1 interacted with VPS33 more strongly than VPS 41

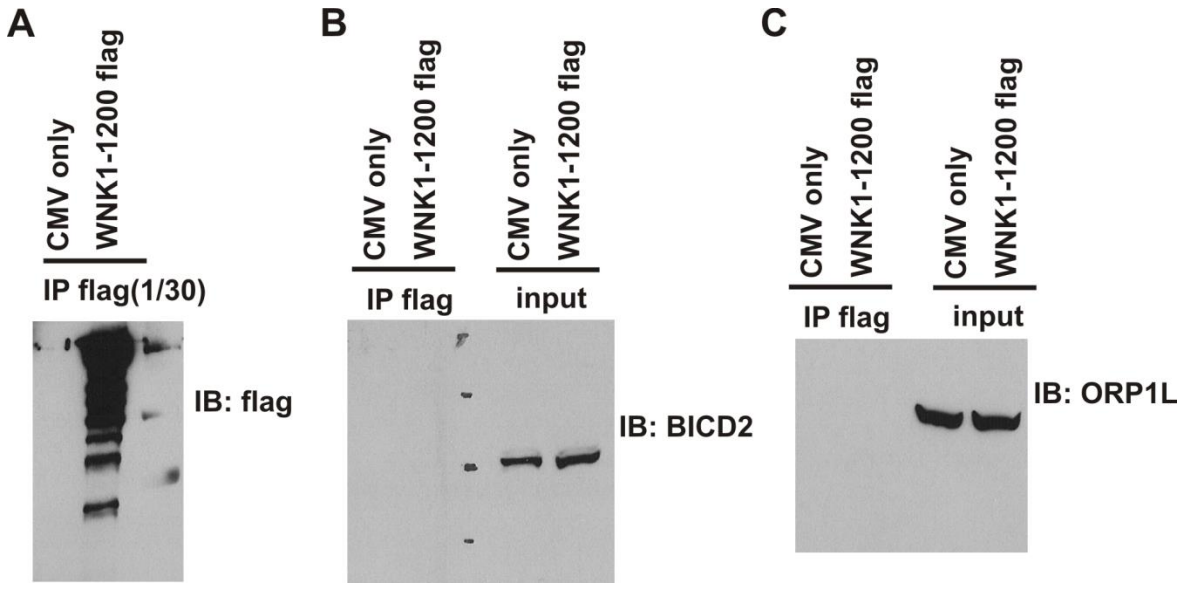

Figure 4-13. Dynactin-BICD2 or dynactin-RILP-ORP1L complexes could not be detected in WNK1 immunocomplexes.

HEK 293 cells were transfected with WNK1 1-1200 flag for 48 hours. Cell lysates were harvested and prepared as described in the method section of GST-Rab GTPases pull down assay. Anti-flag WNK1- immunocomplexes were immunoblotted with anti-flag (A) or anti-BICD2 (B) or ORP1L (C).

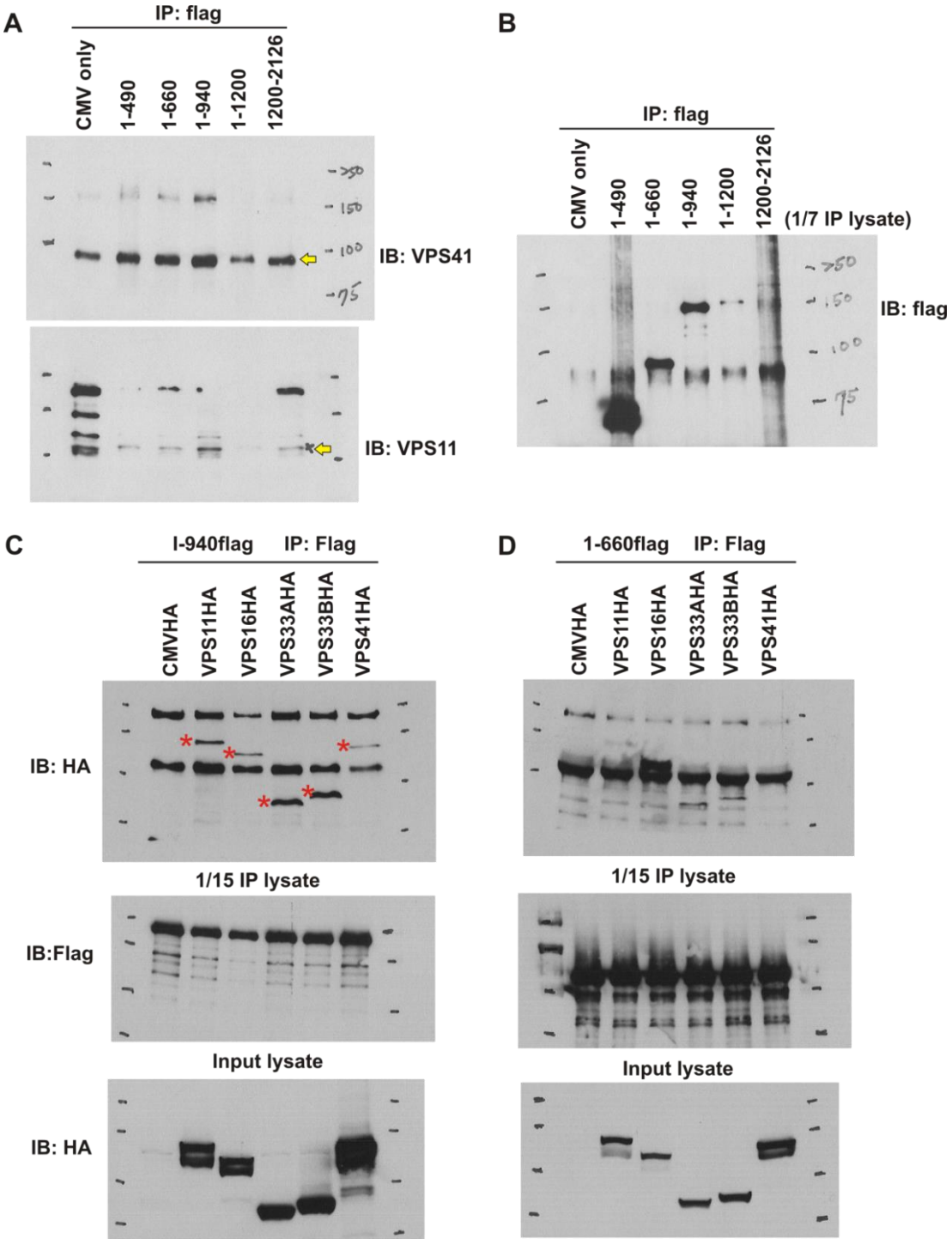
A
IP: flag
CMV only
1-490
1-660
1-940
1-1200
1200-2126
IB: VPS41
IB: VPS11
B
IP: flag
CMV only
1-490
1-660
1-940
1-1200
1200-2126
(1/7 IP lysate)
IB: flag
C
I-940flag IP: Flag
CMVHA
VPS11HA
VPS16HA
VPS33AHA
VPS33BHA
VPS41HA
IB: HA
1/15 IP lysate
IB:Flag
Input lysate
IB: HA
D
1-660flag IP: Flag
CMVHA
VPS11HA
VPS16HA
VPS33AHA
VPS33BHA
VPS41HA
1/15 IP lysate
Input lysate

Figure 4-14. The HOPS complex could exist in WNK1-immunocomplexes. See next page for the legend.

HeLa cells were transfected with indicated WNK1 cDNA fragments for 48 hours. Cell lysates were immunoprecipitated with anti-flag antibody. Anti-flag WNK1-immunocomplexes were immunoblotted with anti-VPS41 or anti-VPS11 antibody (A, yellow arrowheads). 1/7th of anti-flag WNK1- immunocomplexes was blotted with anti-flag antibody to show the immnunoprecipitation efficiency (B). WNK1 1-940 flag (C) or 1-660 flag (D) construct was co-transfected with indicated plasmids encoding VPS subunits for 48 hours in HEK293 cells. Cell lysates were immunoprecipitated with anti-flag antibody and immnoblotted with anti-HA or anti-flag or anti-WNK1 antibodies. (C) Red stars indicate the interaction of the HOPS complex with WNK1 1-940 and WNK1 preferred to interact with VPS33 A and B rather than VPS41. It seemed that WNK1 1-660 is not sufficient to interact with the HOPS complex shown in (D).

The HOPS complex serves as late endosomes and lysosomes tethering and fusion complex. The tethering is involved in membrane recognition which is mediated by VPS41-active Rab 7. The fusion is mediated through VPS33-SNAREs complex. I therefore examined the interaction of WNK1 with each subunit. Co-expression of WNK1 1-940 with indicated VPS subunit was performed. It appeared that WNK1 preferred to interact with VPS 33A and B rather than VPS 41 as compared with the input lysates that the amount of VPS41 is greater than VPS 33A and B (Fig. 4-14 C). The same experiment by using a shorter fragment WNK1 1-660 suggested that WNK1 1-660 is not as efficient as WNK1 1-940 (Fig. 4-14 D). As shown earlier in Fig. 4-14 A, WNK1 fragment 1200-2126 is capable of pulling down the HOPS complex. This fragment includes the C-terminal coiled-coil region. To test whether the interaction is through the association of the C-terminal coiled-coil with endogenous WNK1, I performed another co-transfection experiment. WNK1 1-940, 1800-2126, or 1-490 was co-transfected with each VPS subunit. The ability of fragment 1800-2126 to pull down the HOPS complex is the same as that of fragment 1-940 (Fig. 4-15 A and B, red stars). Further examination revealed that fragment 1800-2126 could strongly pull down endogenous WNK1 but fragment 1-940 or 1-490 could not (Fig. 4-15 A, B and C). It appeared that fragment 1-490 was capable of pulling down VPS16 but not sufficient for VPS 33A or B (Fig. 4-15 C). Taken together, these data suggested that WNK1 could interact with the HOPS complex probably through VPS33 and VPS16.

WNK1 co-localized with clathrin heavy chain and AP-3

Not only the HOPS complex governs membrane fusion between late endosomes and lysosomes, it also mediates clathrin and AP-3 coated- vesicle trafficking between late endosomes and the TGN. Mass spectrometry data suggested that WNK1 could pull down clathrin heavy chain and AP-3 subunit β. Co-immunolocalization experiment for WNK1 and clathrin heavy

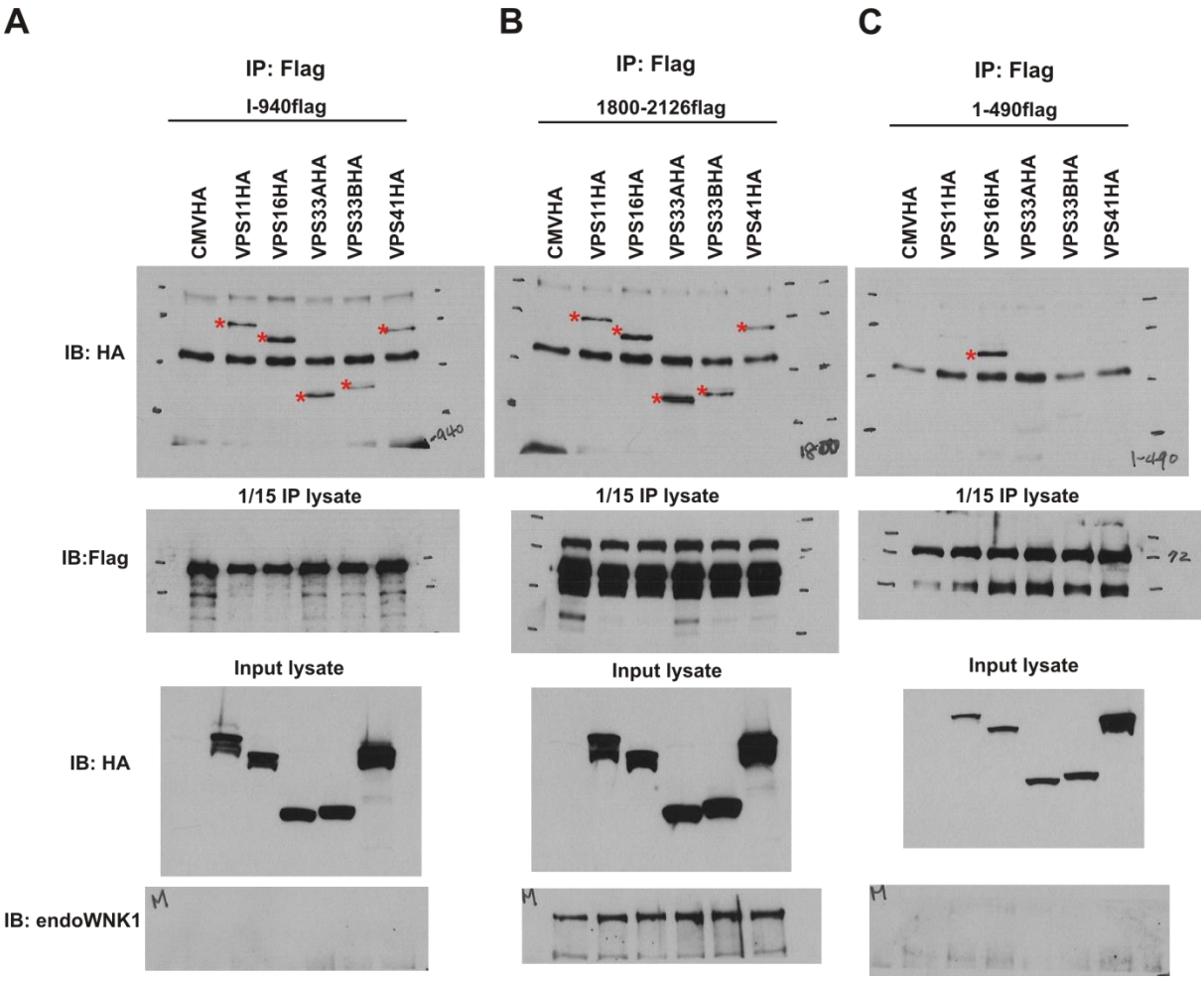

Figure 4-15. WNK1 1-940 and 1-490 is sufficient to interact with VPS33 and VPS16 respectively.

HEK 293 cells were co- transfected WNK1 1-940 flag (A) or 1800-2126 flag (B) or 1-490 flag (C) with plasmids encoding VPS subunits. Cell lysates were immunoprecipitated with anti-flag antibody and immunoblotted with anti-HA or anti-flag or anti-WNK1 antibodies. The interaction of the HOPS complex with WNK1 1-940 (shown in A, red stars) has similar pattern as WNK1 1800-2126 does (shown in B, red stars). Endogenous WNK1 was strongly pulled down by WNK1 1800-2126 (B). WNK1 1-490 is sufficient to interact with VPS16 but not VPS33 (C).

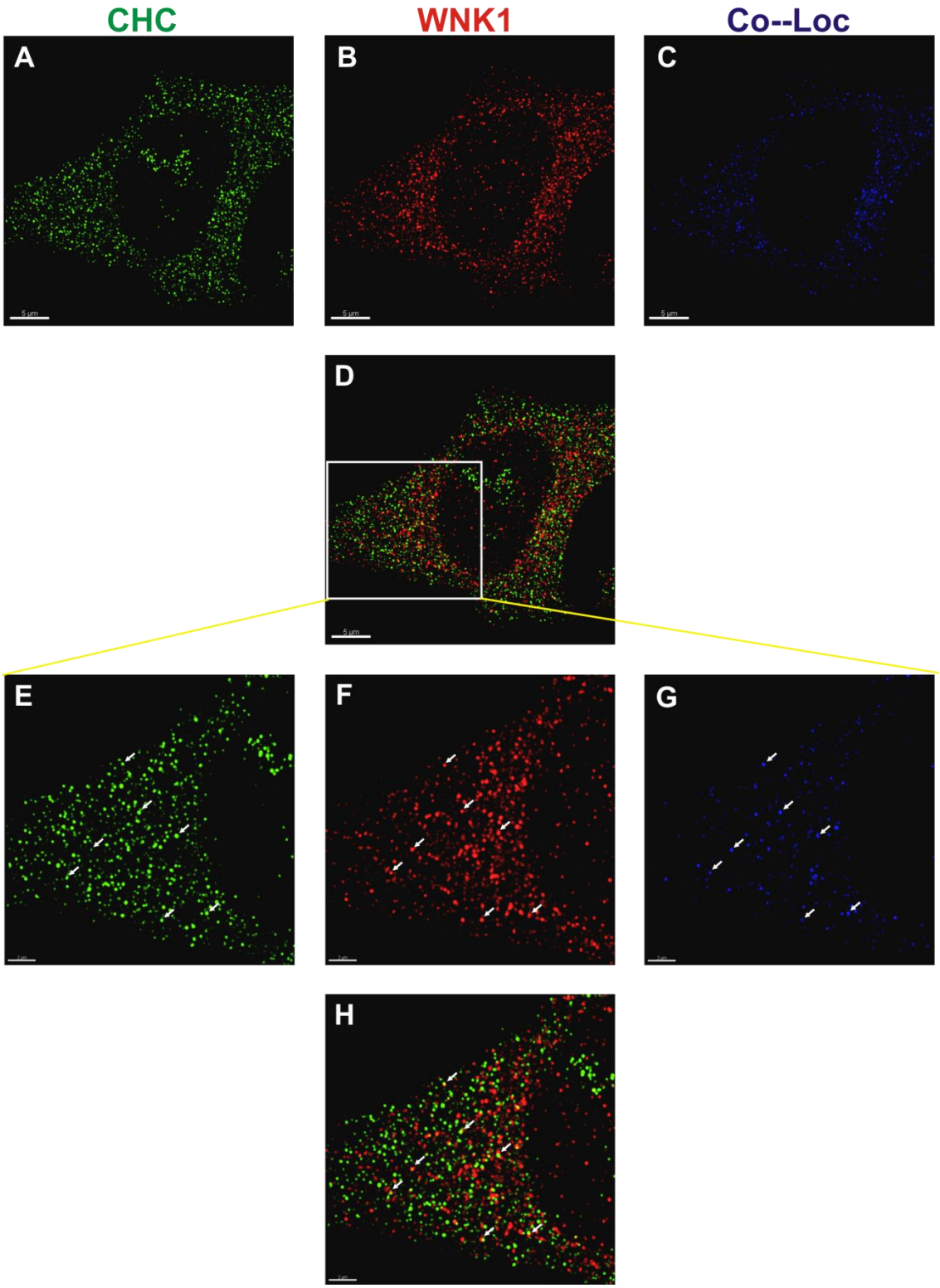

Figure 4-16. WNK1 co-localized with clathrin heavy chain. See next page for the legend.

Co- immnuostaining of HeLa cells with anti-clathrin heavy chain (CHC) (green) and anti-WNK1 (red) antibodies. The co-localization channel (blue) was generated by Imaris Co-Loc module. White arrowheads indicate the co-localized spots. Fig. F to H is a zoomed in picture from D. The pearson correlation coefficient is 0.3 from the image presented above (A to C).

chain showed co-localization spots (Fig. 4-16 C, blue channel generated by Imaris Co-Loc module). Fig. 4-16 E to G, zoomed in pictures from Fig. 4-16 D, demonstrated the co-localized spots (white arrowheads). The Pearson correlation coefficient is 0.3 from one image analyzed. Co-immunolocalization for WNK1 and AP-3 showed better co-localization pattern than that with clathrin heavy chain (Fig. 4-17 C and F, white arrowheads). The Pearson correlation coefficient is 0.53 from 4 images analyzed and two of them are shown in Fig. 4-17 A to F.

Depletion of WNK1 caused the defect of lysosomes and lysosome-related structures under normal culture and serum starvation condition

Disruption of lysosomal structures by Lamp1 staining is shown in WNK1-depleted cells. To further investigate organelle membrane formation in RNAi of WNK1 condition, I employed serum starvation to induce more lysosomal structures and observed them by electron microscopy or lysotracker staining, which is high selectivity for acidic organelles and typically concentrate in the intact spherical organelles. I performed double knockdown of WNK1 expression and serum starvation as the same protocol for the EGF receptor degradation assay. One set of samples was used for immunostaining of endogenous WNK1 and the other set was used for electron microscopy analysis. Silencing of WNK1 expression was achieved by 70% (Fig. 4-18 B and D). When observed by electron microscopy, serum starvation induced lysosomes - like structures (Fig. 4-18 G, yellow arrowheads) whereas the induction of lysosomes-like structures was abolished in WNK1-depleted cell (Fig. 4-18 H). The characteristics of WNK1-depleted cells show elongated and flat cell shapes (shown in chapter 2 and 3). Fig. 4-18 I showed that a cell with the aforementioned phenotypic morphology (yellow arrowhead) had little or no induction of

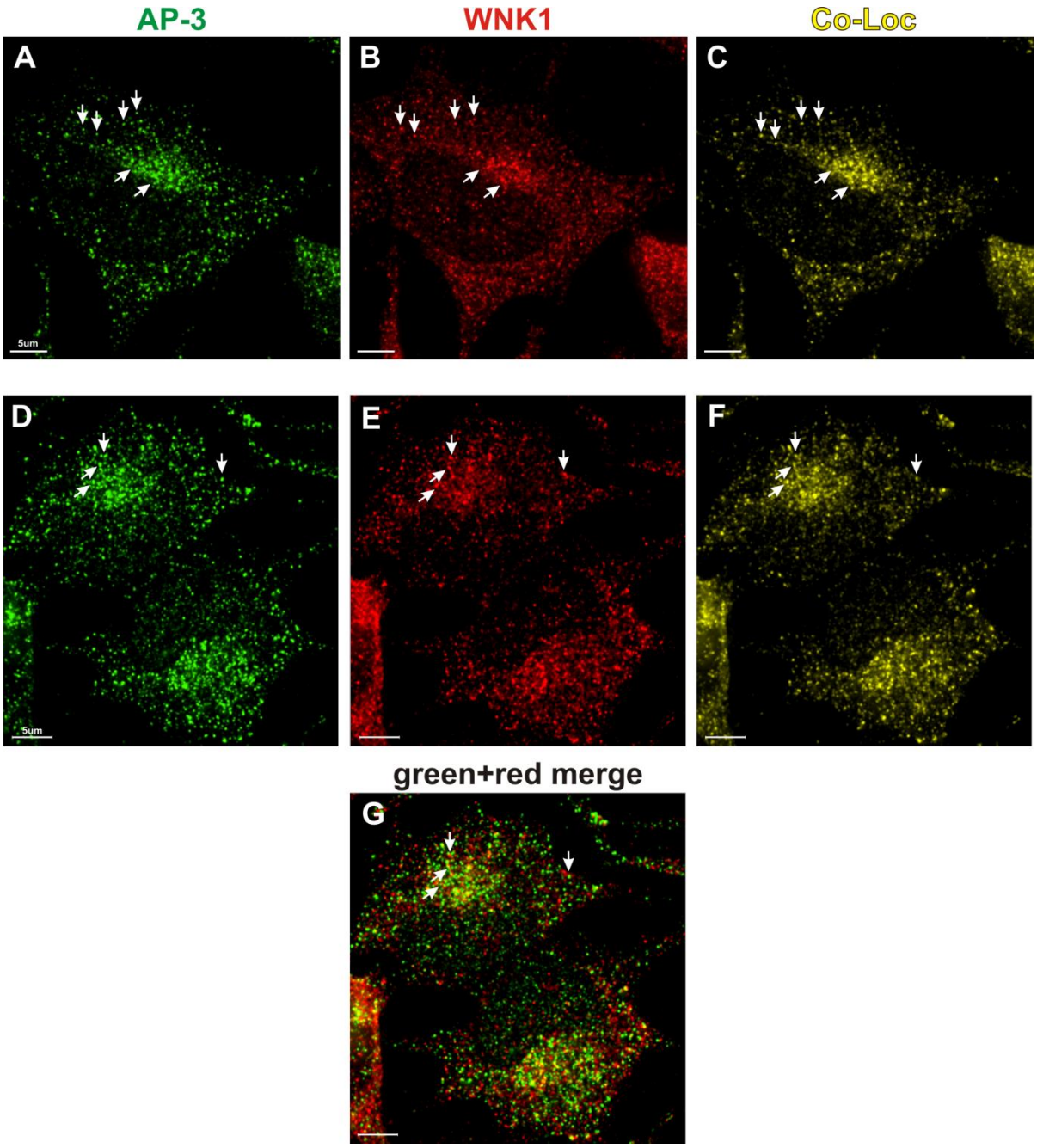

Figure 4-17. WNK1 co-localized with AP-3.

Co- immunostaining of HeLa cells with anti- adaptin δ, one of AP-3 subunits (green) and anti-WNK1 (red) antibodies. The co-localized yellow spots were generated by Imaris Co-Loc

module. The pearson correlation coefficient is 0.53 from 4 images analyzed. White arrowheads indicate co-localized spots.

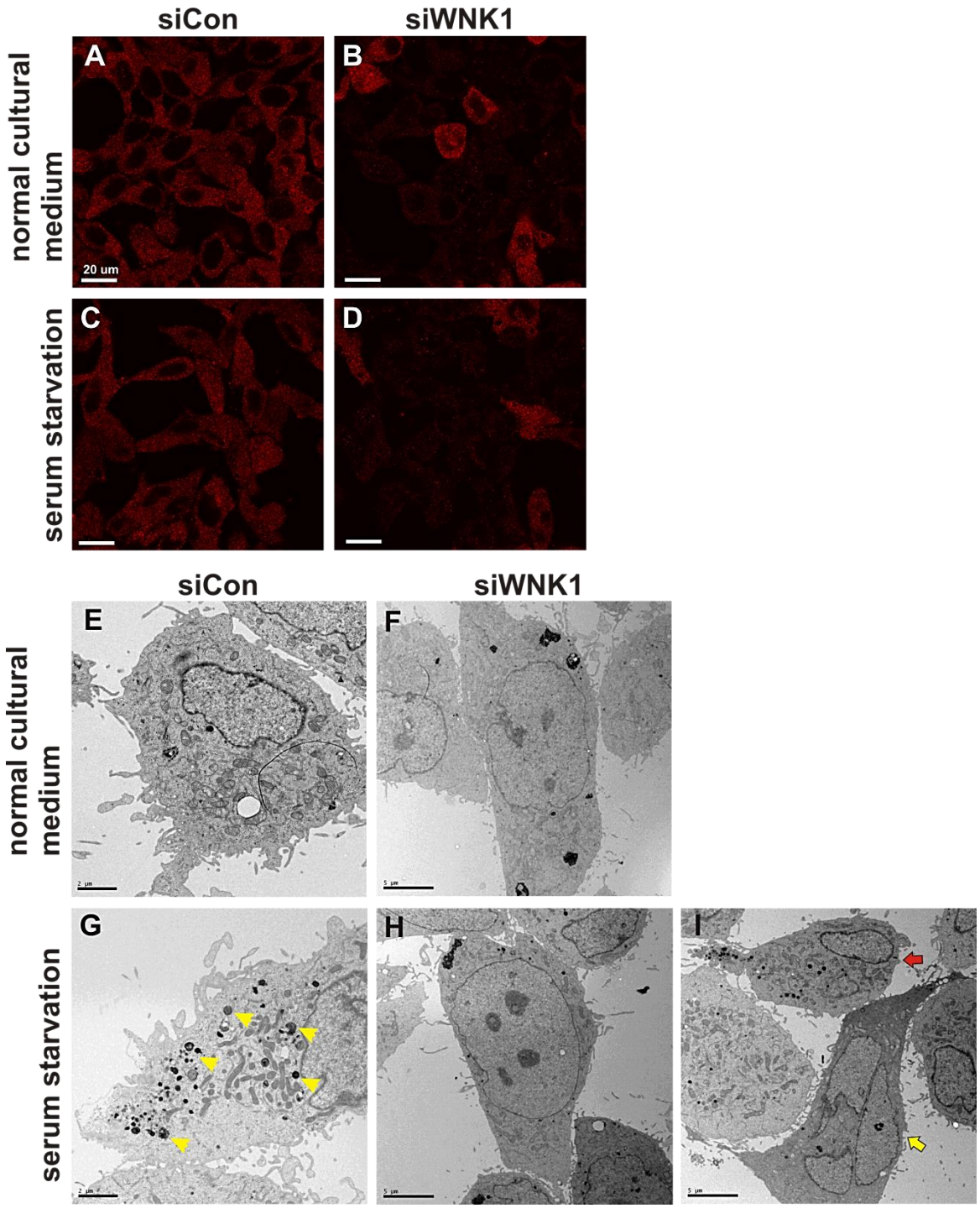

Figure 4-18. Depletion of WNK1 caused less induction of lysosomes-like structures under serum starvation observed by electron microscopy. See next page for the legend.

HeLa cells were transfected with WNK1 or control oligonucleotides as described in Fig. 4-3. Cells were serum starvation or in regular culture medium for 12 hours. One set of samples was immunostained with anti-WNK1 antibody (A to D), the other set was observed by electron microscopy (E to I). The depletion of WNK1 was about 70 % judging from the fluorescent intensity of WNK1 staining (B and D). The induction of lysosome-like structures was observed under serum starvation in control cells (shown in G, yellow arrowheads). Silencing of WNK1 expression seemed to diminish the biogenesis of lysosome- like structures (H). Figure I indicate that a cell with WNK1-depleted morphological shapes (yellow arrowhead) had little induction of lysosomes- like structures while the other cell with relative morphology (red arrowhead) showed several lysosome-like structures.

lysosomes-like structures whereas the other cell with relative normal morphology (red arrowhead) displayed several ones under serum starvation condition.

To confirm and quantify what I have observed in electron microscopy, lysotracker staining was performed. In normal culture condition, the intensity of lysotracker fluorescence was lower in WNK1-depleted cells (Fig 4-19 A, C and I), statistical results show that the difference between control and RNAi of WNK1 cells is significant (Fig. 4-19 I). Treating cells with 12 hours serum starvation, lysosomes and its related structures were strongly induced and clustered in the perinuclear region (Fig. 4-19 B) whereas cells depleted of WNK1 had much less lysotracker intensity and showed dispersion of lysosomes (Fig. 4-19 D). When compared the difference of the intensity between control and WNK1-depleted condition under serum starvation, statistical results also show highly significant (Fig. 4-19 I). It is noticed that the fold of induction of lysotracker intensity under serum starvation did not change between control and WNK1-depleted cells. These data suggested that the defect of lysosomal biogenesis could occur in normal culture condition.

Depletion of WNK1 caused the defect of the maturation of autophagosomes

One of the HPOS complex-mediated functions is to regulate the maturation of autophagosomes. The conversion of LC3 I to II is an indication of the maturation of autophagosomes. It was observed that cells had decreased amount of LC3II in WNK1-depleted cells even in normal culture medium (Fig. 4- 20, yellow arrowhead).

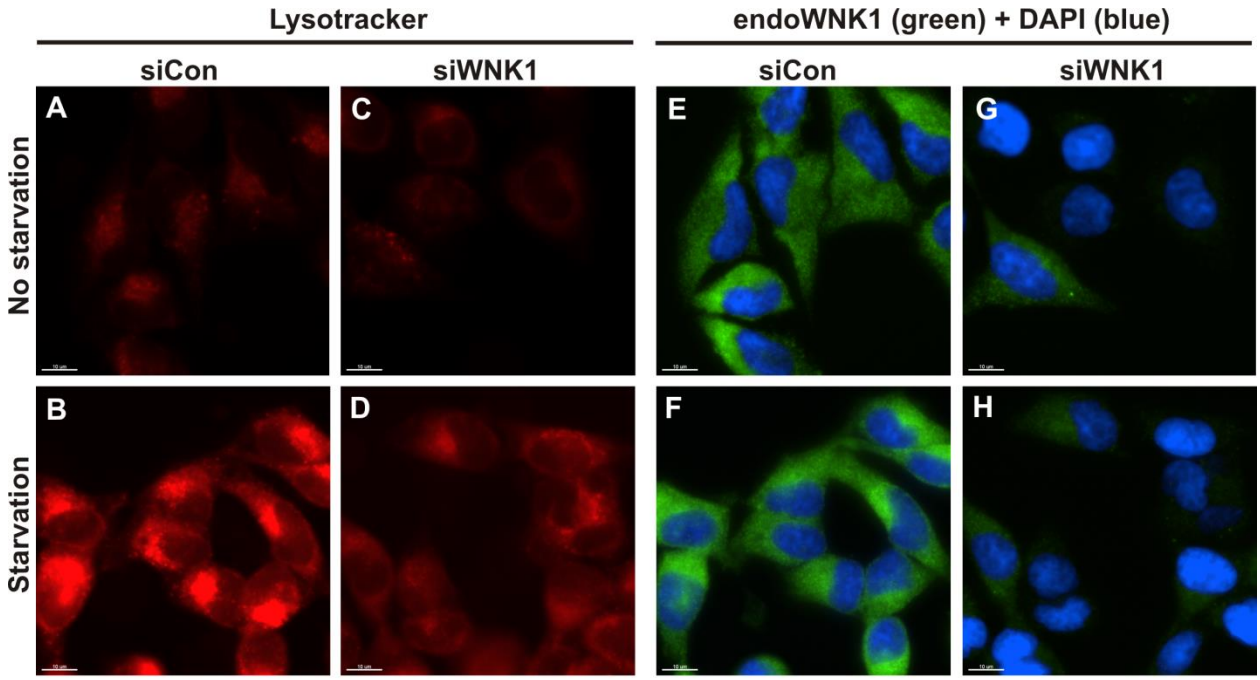
Lysotracker
endoWNK1 (green) + DAPI (blue)
siCon
siWNK1
siCon
siWNK1
No starvation
Starvation
A
B
C
D
E
F
G
H

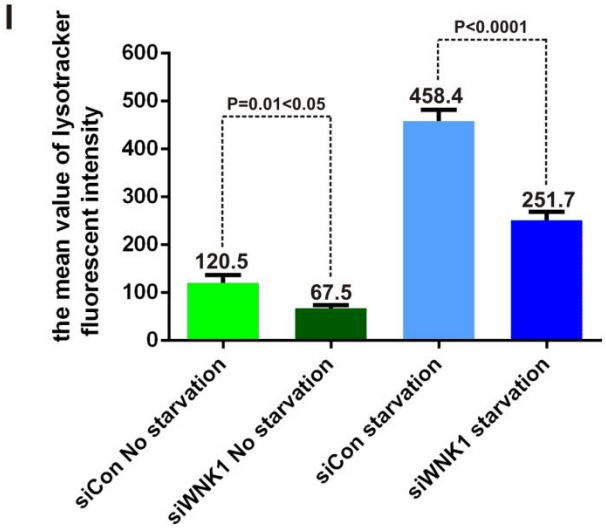
I
the mean value of lysotracker fluorescent intensity
600
500
400
300
200
100
0
P=0.01<0.05
P<0.0001
120.5
67.5
458.4
251.7
siCon No starvation
siWNK1 No starvation
siCon starvation
siWNK1 starvation

Figure 4-19. Depletion of WNK1 caused the defect of biogenesis of lysosomes and lysosome – related organelles.

HeLa cells were transfected with WNK1 or control oligonucleotides as described in Fig. 4-3. Cells were treated with serum starvation or no starvation for 12 hours. Lysotracker staining was performed (see methods) and cells were imaged (A to D). The position of each field was recorded. Cells were then immunostained with anti-WNK1 antibody and DAPI staining (E to H). Images were analyzed by Image J. 9 optical fields of siCon No starvation, 9 optical fields of siWNK1 No starvation, 8 optical fields of siCon starvation and 18 optical fields of siWNK1 starvation were analyzed to get the mean fluorescent intensity of lysotracker. Data were plotted and statistics was performed by unpaired t-test with Welch's correction (I). The experiment was done once.

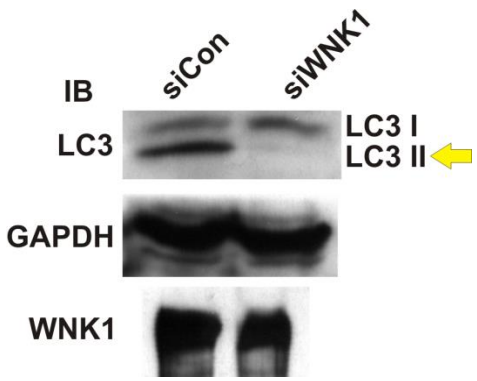

Figure 4-20. Depletion of WNK1 caused the defect of the maturation of autophagosomes in normal culture medium.

HeLa cells were transfected with WNK1 or control oligonucleotides as described in Fig. 4-3. Cells were harvested and prepared as described in the method section of " EGFR degradation assay". Lysates were used for Western blotting by anti- LC3, WNK1 and GAPDH antibodies. Yellow arrowheads indicate the conversion of LC3I to LC3 II, an indication of the maturation of autophagosomes.

Discussion

The phenotypic result of EGF receptor degradation assay in WNK1-depleted cells suggested that the internalization of clathrin-coated vesicle- mediated EGF-EGF receptor complex is not affected. A report (*28*) showed that WNK1 could affect the endocytosis of ROMK by interacting with intersectin, a scaffold protein for clathrin-coated vesicle machinery. It is not known what the EGF receptor degradation phenotype would present if intersectin expression was silenced. Perhaps there might be other important scaffold proteins involved so that intersectin alone would not affect the EGF receptor internalization in HeLa cells. It has been suggested that the EGF receptor could be recycled back to plasma membrane through early endosomes or recycling endosomes. WNK1 may not affect the recycling process as accumulation of initial amount of receptors remained the same observed in control and WNK1-depleted cells. Thus, higher amount of remaining receptors at later time in WNK1-depleted cells suggested the possible defect in later steps of endocytic pathway.

Further investigation revealed that the defect of lysosomes and lysosome-related organelles occurred in WNK1-depleted cells. Through biochemical and immunofluorescence studies, it appeared that WNK1 could interact with active Rab7-effector complexes. Though the initial candidate- motility complex-dynactin-RILP-ORP1L-Rab7 could not be detected in WNK1 immunocomplexes, the HOPS complex showed the interaction with WNK1. To pursue whether WNK1 affect Rab GTPase recognition or membrane fusion, co-expression of each HOPS subunit and WNK1 was performed. The data suggested that WNK1 preferred to associate with VPS16-VPS33 complex, two main subunits bridging the SNARE complex-mediated membrane fusion. VAMP7, one of the SNARE complex subunits, has been shown to play essential roles in cell abscission and homotypic membrane fusion in the assembly of pre-autophagosome

structures. In WNK1-depleted cells, the defect of abscission and decreased amount of basal LC3 II signals were shown. These data implied that WNK1 might affect homotypic (the assembly of phagophores) or heterotypic (late endosomes and lysosomes or late endosomes and the TGN) membrane fusion.

Mass spectrometry results suggested that WNK1 could pull down vacuolar ATPase (V-ATPase) (Table 3-1). In the study of mechanistic insight for how SNAREs complex could mediate membrane fusion in the yeast, it has been shown that V-ATPase acted at the downstream of SNARE complex-mediated membrane fusion (*130*). In neuronal cells, live cell imaging of neuronal degradation by microglia demonstrated a role for V-ATPase in phagosomal fusion in vivo (*131*). A recent report by Williamson et al. (*132*) also suggested that V-ATPase provides an endolysosomal degradation mechanism in *Drosophila melanogaster* photoreceptors. As mentioned in chapter one, in plants, AtWNK8 has been shown to bind to and phosphorylate V-ATPase subunit C (*15*). It would be interesting to investigate whether WNK1 could directly bind to and phosphorylate V-ATPase in mammalian cells.

In addition to SNARE-mediated membrane fusion, the adaptor protein complex (AP-3) - coated vesicles also served as an important regulation between the TGN and late endosomes. Mass spectrometry data suggested that WNK1 could associate with clathrin-heavy chain and AP-3 subunit β. Immunocolocalization study revealed that WNK1 co-localized with AP-3 in a high Pearson correlation coefficient. Inheritable genetic defects of AP-3 and VPS 33A cause the HPS syndrome showing an obvious defect in lysosomal related organelles. In melanocyte, the maturation of melanosomes is highly dependent on the AP-3 protein trafficking. It would be interesting to see if WNK1 could affect the formation of melanosomes in melanocyte cells. Moreover, there are growing data showing cargoes of AP-3- dependent protein trafficking.

Among them are V-ATPase, PI4KIIα, VAMP7 and tyrosinase (*133*). These are all promising subjects to investigate how WNK1 might affect the TGN and endolysosomal pathways. Eventually, it may help us understand the pathology of the HPS syndrome and provide a candidate therapeutic target for it.

Besides endolysosomal trafficking, several evidences suggested that WNK1 might affect the Golgi apparatus. It has been suggested that pericentrosomal – positioning of the Golgi is mediated by the minus-end directed dynein motor. However, the detailed mechanism is still unknown (*108*). Several possible interactors have been proposed to play such roles in the connection between the membrane of the Golgi and the dynein motor. One of them is dynein-dynactin-BICD2-Rab6. The other candidate- Golgin 160 has been shown to be important in directed secretion, cell polarity and wound healing (*134*). Following this report, the same group (*135*) demonstrated that Golgin 160 recruits dynein motor to position the Golgi apparatus. Mass spectrometry results suggested that WNK1 could pull down Golgin 160 (Table 3-1). The dynactin-BICD2 could not be detected in WNK1-immunocomplexes though WNK1 indeed interact with active Rab6-effector complexes. These data raised the possibility that WNK1 might affect positioning of the Golgi and cell migration through dynein - Golgi 160 complex.

CHAPTER 5

CONCLUSIONS AND FUTURE DIRECTIONS

In the final chapter, I will summarize the data presented in previous chapters and propose the direction for the future study of WNK1 and microtubules, WNK1 and membrane trafficking and one more observation regarding WNK1 and ion transporters.

WNK1 and microtubules

Immunofluorescence study suggested that WNK1 could localize on both interphase and spindle microtubules. Silencing of WNK1 expression caused both interphase and spindle microtubule defects. For mitosis, the identification of potential interactors might reveal more mechanistic insight on how WNK1 regulates mitosis. The WNK1 immunoprecipitation kinase assay shown in Fig. 2-10 suggested that WNK1 could associate with specific unknown proteins under nocodazole or taxol synchronized HeLa S3 cells. It may be possible to perform the same experiment as described in Fig. 2-10 to identify the interactors by mass spectrometry. Preliminary result from Fig. 2-10 suggests a specific radioactive band (green arrowhead), molecular weight close to 170 to 200 kDa. This could be centrosomal protein 170 kDa as shown in Table 3-1 and will be discussed below.

On the other hand, the defect of interphase microtubules and centrosome structures suggested that WNK1 also interacts with proteins whose function might affect both interphase and spindle microtubules. Mass spectrometry analysis by immunoprecipitating WNK1 1-940 or 1-2126 in the interphase cells revealed two potential candidates- Cep 70 and Cep 170. Both of them are centrosomal proteins. It has been shown that Cep 70 interacts with γ-tubulin to localize

on the centrosome. Through WNK1 rescue experiments, the kinase activity of WNK1 is required for the interphase microtubule phenotype. Therefore, Cep 70 could be a potential substrate for WNK1. The interaction of WNK1 and Cep 70 is also needed to be confirmed by co-immunoprecipitation assay. If the phosphorylation of Cep 70 could be shown by WNK1, the mapping of the phosphorylation site will be the next step to further reveal how the phosphorylation of Cep 70 could affect the binding with γ-tubulin and maintain the integrity of centrosomal structures.

The other candidate, Cep 170 is also a centrosomal protein. It has been shown that Cep 170 interacted with Polo-like kinase 1 (Plk1) and could be phosphorylated by Plk1 during mitosis. Depletion of Cep 170 by small interfering RNA resulted in disruption of interphase microtubules and elongated cell shape. These phenotypes were observed in WNK1-depleted cells too. Whether WNK1 could phosphorylate Plk1 could be tested. The interaction between WNK1 and Plk1 might be investigated as depletion of WNK1 caused multiple-polar spindles. Overexpression of Plk1 leads to the same phenotype. The localization of WNK1 on the mitotic spindles is similar to that of Plk1 during mitosis. WNK1 could be a negative regulator for Plk1 or Plk1-mediated signaling events.

WNK1 and membrane trafficking

Immunostaining of endogenous WNK1 displays a punctate pattern. However, the nature of these punctate structures remained unknown. Mass spectrometry revealed that WNK1 could pull down two kinds of vesicle- associated proteins – one is clathrin heavy chain and the adaptor protein complex 3 (AP-3); the other is coat protein complex (COP) I vesicles.

Identification of one of Rab7-effector complexes- the HOPS complex suggested the possible mechanism by which WNK1 affects membrane fusion between late endosome and lysosomes and its related structures. Subsequent analysis revealed that WNK1 might interact with the HOPS complex through VPS16 and 33. It is still not clear whether WNK1 kinase activity is required for the receptor degradation. If kinase activity is needed, it will be worth to test whether WNK1 could phosphorylate VPS16 or 33. Though VPS16 and 33 are obviously important for late endosome and lysosomes fusion, silencing of the HOPS complex still needs to be tested to see how it might affect the receptor degradation phenotype. As mentioned earlier, AP-3 vesicle trafficking is one of the HOPS complex- mediated vesicular trafficking. There are growing data showing cargoes of AP-3- dependent protein trafficking. Among them are vacuolar ATPase (V-ATPase), PI4KIIα, VAMP7 and tyrosinase. Tyrosinase is the rate limiting enzyme for controlling the production of melanin. As melanocyte is a good model system for studying AP-3 dependent cargo trafficking, it would be interesting to see if WNK1 could affect the formation of the melanosomes in melanocyte cells.

Another cargo, V-ATPase is also shown in mass spectrometry analysis (Table 3-1). As vacuolar ATPase has been implicated with the SNAREs complex and *Arabidopsis* WNK8 has been shown to phosphorylate V-ATPase, it would be interesting to test whether WNK1 could directly interact with vacuolar ATPase and phosphorylate it in mammalian cells.

WNK1 might act on membrane trafficking through COPI vesicles. COPI vesicles mediate intra-Golgi vesicular trafficking and play vital roles in maintaining membrane homeostasis between the Golgi and the ER. Mass spectrometry data revealed that WNK1 could pull down the subunits of COPI complex including α, β, and γ subunit. The other observation involved in the Golgi membrane dynamics was that WNK1 could interact with active Rab6-effector complexes.

The effector complexes for Rab6 are more than 15 characterized thus far. A recent report suggested that Rab6 is essential to the trafficking of the TGN-derived clathrin and COPI-coated vesicles revealed by electron tomography study (*136*). It is likely that WNK1 might interact with COPI complex directly. Future investigation for how WNK1 could affect COPI vesicles and trafficking between the Golgi and the ER is warranted.

In addition to AP-3 and COPI vesicles, I have observed that WNK1 could co-localize with GFP-caveolin 1 (Fig. 5-1). Endogenous WNK1 distribution could be re-distributed to plasma membranes when GFP-caveolin 1 is overexpressed. This data suggested that WNK1 has ability to involve in lipid raft membrane dynamics. Biochemical analysis also showed that WNK1 could remain in the pellet when cell lysates were extracted by 0.1 % Triton X-100. The possible involvement of WNK1 in caveolae-mediated membrane trafficking will be another future area to look into.

Immuno-co-localization study for WNK1 suggested that WNK1 could localize on interphase and spindle microtubules. Analysis through Imaris Co-Loc module for co-localization WNK1 with dynein intermediate chain or dynactin yields a high pearson correlation coefficient (0.46 and 0.53 respectively). The pearson correlation coefficient for WNK1 and AP-3 or clathrin heavy chain is 0.5 and 0.3. Perhaps WNK1 interacts with AP-3-mediated trafficking and this vesicular trafficking could be carried out by dynein motor complex. WNK1 also co-localizes with OSR1 (*112*). Another interesting result is that WNK1 co-localizes with constitutively active Rab 6 forming- vacuolar structures with a high pearson correlation coefficient (0.46). WNK1 shows no significant co-localization with Rab 5, M6PR, Lamp1 and VPS4. These data suggests that WNK1 could distribute in a variety of protein complexes and exerts its function through

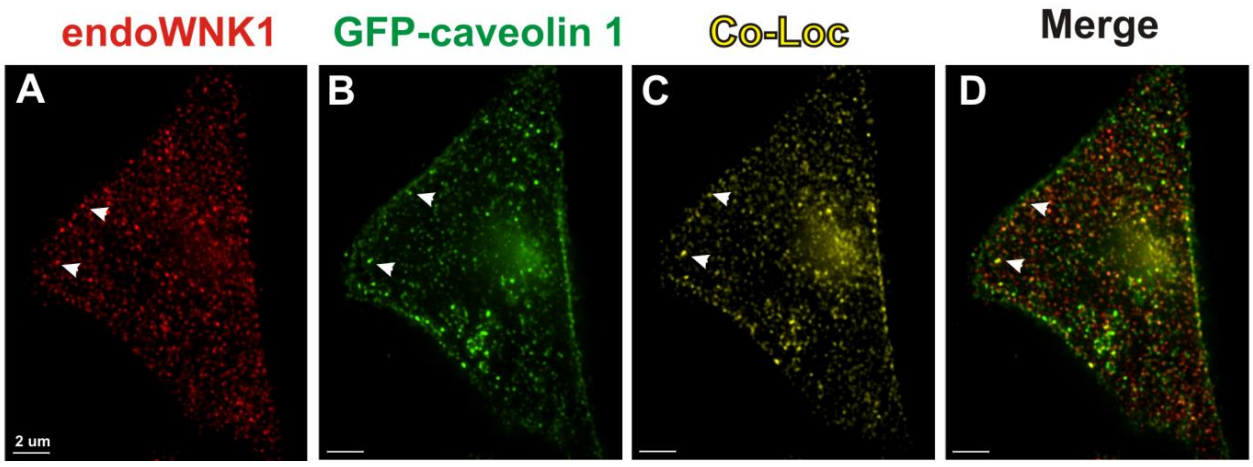

Figure 5-1. WNK1 could co-localize with GFP-caveolin 1.

HeLa cells were transfected with GFP-caveolin 1 for 24 hours. Cells were immunostained with anti-WNK1 antibody. (A) WNK1 (red) (B) GFP-caveolin (C) Co-localizd spots (generated by Imaris Co-Loc module). (D) Merge of A, B, and C. scale bar, 2μm. The pearson correlation coefficient is 0.42 analyzed from the image above. White arrowheads indicate co-localized spots.

either catalytic or non-catalytic activity. Taken together, WNK1 could affect a variety of vesicular trafficking with evidences regarding AP-3 vesicles and might worth to investigate further for COPI vesicles and caveolae-mediated endocytosis.

WNK1 and ion co-transporters

While investigating lysosomes and lysosome- related structures by electron microscopy, obvious dense dark structure was observed in WNK1- depleted cells (Fig. 5-2) and only very few in control cells. The dense dark structures appeared to be glycogen structures shown by Fridman et al. (*137*). In the future, the confirmation of glycogen structures could be performed by Periodic acid-Schiff (PAS) staining, a method used for detecting polysaccharides. The mechanism underlying induction of possible glycogen granules caused by depletion of WNK1 remained unknown. The characterization of glycogen granules cluster by Fridman et al. suggests that induction of the structures are involved in cardiac steroids (CS)- inhibition of Na^+, K^+ -ATPase activity. Mass spectrometry data suggested that WNK1 could pull down Na^+, K^+ -ATPase (Table 3-1). The similar phenotype observed in WNK1-depleted cells raised a possibility that WNK1 might be a positive regulator for Na^+, K^+ -ATPase. Depletion of Na^+, K^+ -ATPase could lead to induction of glycogen granules. If WNK1 indeed could enhance the activity of Na^+, K^+ -ATPase, it is possible that higher activity of Na^+, K^+ -ATPase caused by WNK1 expression could lead to increased pumping of Na^+ into basolateral lumen in the distal nephron, hence contributing to hypertension. In the future, co-expression of WNK1 and Na^+, K^+ -ATPase in *Xenopus* Oocyte system for recording the current might reveal whether WNK1 could affect Na^+, K^+ -ATPase. In addition, WNK1 might affect Na^+, K^+ -ATPase through its downstream effector- OSR1 / SPAK. Depletion of OSR1 or SPAK could be performed to see whether induction of glycogen granules

occurs. These finding will contribute to our understanding on how WNK1 affects ion co-transporters, thus the imbalance of the ion regulation in PHAII syndrome.

.

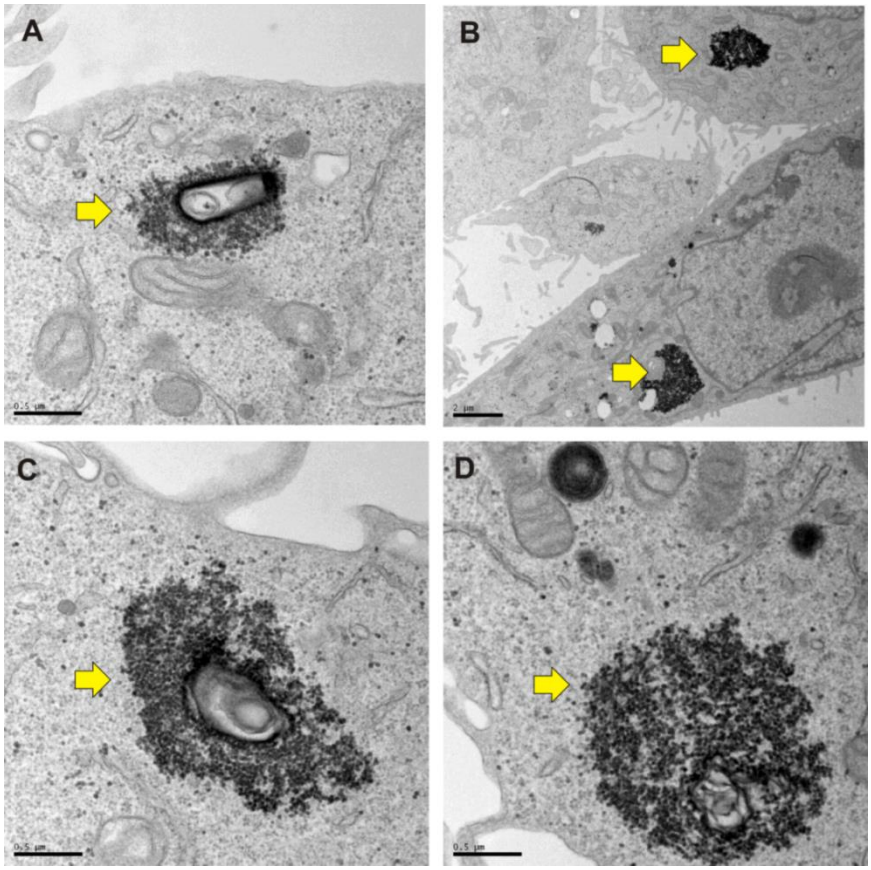

Figure 5-2. Dense dark structures induced by depletion of WNK1 in HeLa cells.

HeLa cells were treated with RNAi as described in Fig. 4-18 and imaged by electron microscopy (yellow arrowheads indicate glycogen granule - like structures). Scar bars: 0.5 µm in A, C and D. 2 µm in B.

REFERENCE

1. B. Xu *et al.*, WNK1, a novel mammalian serine/threonine protein kinase lacking the catalytic lysine in subdomain II. *The Journal of biological chemistry* **275**, 16795 (Jun 2, 2000).
2. F. Verissimo, P. Jordan, WNK kinases, a novel protein kinase subfamily in multi-cellular organisms. *Oncogene* **20**, 5562 (Sep 6, 2001).
3. G. Manning, D. B. Whyte, R. Martinez, T. Hunter, S. Sudarsanam, The protein kinase complement of the human genome. *Science* **298**, 1912 (Dec 6, 2002).
4. F. H. Wilson *et al.*, Human hypertension caused by mutations in WNK kinases. *Science* **293**, 1107 (Aug 10, 2001).
5. L. M. Boyden *et al.*, Mutations in kelch-like 3 and cullin 3 cause hypertension and electrolyte abnormalities. *Nature* **482**, 98 (Feb 2, 2012).
6. H. Louis-Dit-Picard *et al.*, KLHL3 mutations cause familial hyperkalemic hypertension by impairing ion transport in the distal nephron. *Nature genetics* **44**, 456 (Apr, 2012).
7. A. Ohta *et al.*, The CUL3-KLHL3 E3 ligase complex mutated in Gordon's hypertension syndrome interacts with and ubiquitylates WNK isoforms: disease-causing mutations in KLHL3 and WNK4 disrupt interaction. *The Biochemical journal* **451**, 111 (Apr 1, 2013).
8. K. A. Choate, K. T. Kahle, F. H. Wilson, C. Nelson-Williams, R. P. Lifton, WNK1, a kinase mutated in inherited hypertension with hyperkalemia, localizes to diverse Cl- -transporting epithelia. *Proceedings of the National Academy of Sciences of the United States of America* **100**, 663 (Jan 21, 2003).
9. M. O'Reilly, E. Marshall, H. J. Speirs, R. W. Brown, WNK1, a gene within a novel blood pressure control pathway, tissue-specifically generates radically different isoforms with and without a kinase domain. *Journal of the American Society of Nephrology : JASN* **14**, 2447 (Oct, 2003).
10. C. Delaloy *et al.*, Multiple promoters in the WNK1 gene: one controls expression of a kidney-specific kinase-defective isoform. *Molecular and cellular biology* **23**, 9208 (Dec, 2003).

11. E. Vidal-Petiot *et al.*, A new methodology for quantification of alternatively spliced exons reveals a highly tissue-specific expression pattern of WNK1 isoforms. *PloS one* **7**, e37751 (2012).
12. M. Shekarabi *et al.*, Mutations in the nervous system--specific HSN2 exon of WNK1 cause hereditary sensory neuropathy type II. *The Journal of clinical investigation* **118**, 2496 (Jul, 2008).
13. K. T. Kahle *et al.*, WNK4 regulates apical and basolateral Cl- flux in extrarenal epithelia. *Proceedings of the National Academy of Sciences of the United States of America* **101**, 2064 (Feb 17, 2004).
14. S. Holden, J. Cox, F. L. Raymond, Cloning, genomic organization, alternative splicing and expression analysis of the human gene WNK3 (PRKWNK3). *Gene* **335**, 109 (Jun 23, 2004).
15. A. Hong-Hermesdorf, A. Brux, A. Gruber, G. Gruber, K. Schumacher, A WNK kinase binds and phosphorylates V-ATPase subunit C. *FEBS letters* **580**, 932 (Feb 6, 2006).
16. B. E. Xu *et al.*, Regulation of WNK1 by an autoinhibitory domain and autophosphorylation. *The Journal of biological chemistry* **277**, 48456 (Dec 13, 2002).
17. X. Min, B. H. Lee, M. H. Cobb, E. J. Goldsmith, Crystal structure of the kinase domain of WNK1, a kinase that causes a hereditary form of hypertension. *Structure* **12**, 1303 (Jul, 2004).
18. D. R. Knighton *et al.*, Crystal structure of the catalytic subunit of cyclic adenosine monophosphate-dependent protein kinase. *Science* **253**, 407 (Jul 26, 1991).
19. S. S. Taylor, E. Radzio-Andzelm, Three protein kinase structures define a common motif. *Structure* **2**, 345 (May 15, 1994).
20. D. R. Knighton *et al.*, Structure of a peptide inhibitor bound to the catalytic subunit of cyclic adenosine monophosphate-dependent protein kinase. *Science* **253**, 414 (Jul 26, 1991).
21. H. L. De Bondt *et al.*, Crystal structure of cyclin-dependent kinase 2. *Nature* **363**, 595 (Jun 17, 1993).
22. T. S. Lewis, P. S. Shapiro, N. G. Ahn, Signal transduction through MAP kinase cascades. *Advances in cancer research* **74**, 49 (1998).

23. J. A. Frost, A. Khokhlatchev, S. Stippec, M. A. White, M. H. Cobb, Differential effects of PAK1-activating mutations reveal activity-dependent and -independent effects on cytoskeletal regulation. *The Journal of biological chemistry* **273**, 28191 (Oct 23, 1998).
24. L. Y. Lenertz *et al.*, Properties of WNK1 and implications for other family members. *The Journal of biological chemistry* **280**, 26653 (Jul 22, 2005).
25. T. M. Moon *et al.*, Solution Structure of the WNK1 Autoinhibitory Domain, a WNK-Specific PF2 Domain. *Journal of molecular biology* **425**, 1245 (Apr 26, 2013).
26. J. O. Thastrup *et al.*, SPAK/OSR1 regulate NKCC1 and WNK activity: analysis of WNK isoform interactions and activation by T-loop trans-autophosphorylation. *The Biochemical journal* **441**, 325 (Jan 1, 2012).
27. B. K. Kay, M. P. Williamson, M. Sudol, The importance of being proline: the interaction of proline-rich motifs in signaling proteins with their cognate domains. *FASEB journal : official publication of the Federation of American Societies for Experimental Biology* **14**, 231 (Feb, 2000).
28. G. He, H. R. Wang, S. K. Huang, C. L. Huang, Intersectin links WNK kinases to endocytosis of ROMK1. *The Journal of clinical investigation* **117**, 1078 (Apr, 2007).
29. M. Raman, W. Chen, M. H. Cobb, Differential regulation and properties of MAPKs. *Oncogene* **26**, 3100 (May 14, 2007).
30. J. Avruch, MAP kinase pathways: the first twenty years. *Biochimica et biophysica acta* **1773**, 1150 (Aug, 2007).
31. B. E. Xu *et al.*, WNK1 activates ERK5 by an MEKK2/3-dependent mechanism. *The Journal of biological chemistry* **279**, 7826 (Feb 27, 2004).
32. X. Wang, C. Tournier, Regulation of cellular functions by the ERK5 signalling pathway. *Cellular signalling* **18**, 753 (Jun, 2006).
33. X. Sun, L. Gao, R. K. Yu, G. Zeng, Down-regulation of WNK1 protein kinase in neural progenitor cells suppresses cell proliferation and migration. *Journal of neurochemistry* **99**, 1114 (Nov, 2006).
34. S. Moniz *et al.*, Protein kinase WNK2 inhibits cell proliferation by negatively modulating the activation of MEK1/ERK1/2. *Oncogene* **26**, 6071 (Sep 6, 2007).
35. J. A. Frost *et al.*, Cross-cascade activation of ERKs and ternary complex factors by Rho family proteins. *The EMBO journal* **16**, 6426 (Nov 3, 1997).

36. M. Shaharabany *et al.*, Distinct pathways for the involvement of WNK4 in the signaling of hypertonicity and EGF. *The FEBS journal* **275**, 1631 (Apr, 2008).
37. B. Zhou *et al.*, WNK4 inhibits NCC protein expression through MAPK ERK1/2 signaling pathway. *American journal of physiology. Renal physiology* **302**, F533 (Mar 1, 2012).
38. A. C. Vitari *et al.*, WNK1, the kinase mutated in an inherited high-blood-pressure syndrome, is a novel PKB (protein kinase B)/Akt substrate. *The Biochemical journal* **378**, 257 (Feb 15, 2004).
39. Z. Y. Jiang *et al.*, Identification of WNK1 as a substrate of Akt/protein kinase B and a negative regulator of insulin-stimulated mitogenesis in 3T3-L1 cells. *The Journal of biological chemistry* **280**, 21622 (Jun 3, 2005).
40. B. E. Xu, S. Stippec, A. Lazrak, C. L. Huang, M. H. Cobb, WNK1 activates SGK1 by a phosphatidylinositol 3-kinase-dependent and non-catalytic mechanism. *The Journal of biological chemistry* **280**, 34218 (Oct 7, 2005).
41. C. J. Heise *et al.*, Serum and glucocorticoid-induced kinase (SGK) 1 and the epithelial sodium channel are regulated by multiple with no lysine (WNK) family members. *The Journal of biological chemistry* **285**, 25161 (Aug 13, 2010).
42. A. M. Ring *et al.*, An SGK1 site in WNK4 regulates Na+ channel and K+ channel activity and has implications for aldosterone signaling and K+ homeostasis. *Proceedings of the National Academy of Sciences of the United States of America* **104**, 4025 (Mar 6, 2007).
43. D. J. Rozansky *et al.*, Aldosterone mediates activation of the thiazide-sensitive Na-Cl cotransporter through an SGK1 and WNK4 signaling pathway. *The Journal of clinical investigation* **119**, 2601 (Sep, 2009).
44. B. N. Armbruster, B. L. Roth, Mining the receptorome. *The Journal of biological chemistry* **280**, 5129 (Feb 18, 2005).
45. P. San-Cristobal *et al.*, Angiotensin II signaling increases activity of the renal Na-Cl cotransporter through a WNK4-SPAK-dependent pathway. *Proceedings of the National Academy of Sciences of the United States of America* **106**, 4384 (Mar 17, 2009).
46. S. W. An *et al.*, WNK1 promotes PIP(2) synthesis to coordinate growth factor and GPCR-Gq signaling. *Current biology : CB* **21**, 1979 (Dec 6, 2011).

47. M. J. Rebecchi, S. N. Pentyala, Structure, function, and control of phosphoinositide-specific phospholipase C. *Physiological reviews* **80**, 1291 (Oct, 2000).
48. X. H. Feng, R. Derynck, Specificity and versatility in tgf-beta signaling through Smads. *Annual review of cell and developmental biology* **21**, 659 (2005).
49. L. L. Hoover, S. W. Kubalak, Holding their own: the noncanonical roles of Smad proteins. *Science signaling* **1**, pe48 (2008).
50. R. H. Jenkins, J. Martin, A. O. Phillips, T. Bowen, D. J. Fraser, Transforming growth factor beta1 represses proximal tubular cell microRNA-192 expression through decreased hepatocyte nuclear factor DNA binding. *The Biochemical journal* **443**, 407 (Apr 15, 2012).
51. Y. Liang, D. Ridzon, L. Wong, C. Chen, Characterization of microRNA expression profiles in normal human tissues. *BMC genomics* **8**, 166 (2007).
52. E. Elvira-Matelot *et al.*, Regulation of WNK1 expression by miR-192 and aldosterone. *Journal of the American Society of Nephrology : JASN* **21**, 1724 (Oct, 2010).
53. B. H. Lee, W. Chen, S. Stippec, M. H. Cobb, Biological cross-talk between WNK1 and the transforming growth factor beta-Smad signaling pathway. *The Journal of biological chemistry* **282**, 17985 (Jun 22, 2007).
54. H. Kasai, N. Takahashi, H. Tokumaru, Distinct initial SNARE configurations underlying the diversity of exocytosis. *Physiological reviews* **92**, 1915 (Oct, 2012).
55. B. H. Lee *et al.*, WNK1 phosphorylates synaptotagmin 2 and modulates its membrane binding. *Molecular cell* **15**, 741 (Sep 10, 2004).
56. E. Oh, C. J. Heise, J. M. English, M. H. Cobb, D. C. Thurmond, WNK1 is a novel regulator of Munc18c-syntaxin 4 complex formation in soluble NSF attachment protein receptor (SNARE)-mediated vesicle exocytosis. *The Journal of biological chemistry* **282**, 32613 (Nov 9, 2007).
57. J. Xu, T. Mashimo, T. C. Sudhof, Synaptotagmin-1, -2, and -9: Ca(2+) sensors for fast release that specify distinct presynaptic properties in subsets of neurons. *Neuron* **54**, 567 (May 24, 2007).
58. S. H. Hu, C. F. Latham, C. L. Gee, D. E. James, J. L. Martin, Structure of the Munc18c/Syntaxin4 N-peptide complex defines universal features of the N-peptide

binding mode of Sec1/Munc18 proteins. *Proceedings of the National Academy of Sciences of the United States of America* **104**, 8773 (May 22, 2007).

59. E. Oh, D. C. Thurmond, The stimulus-induced tyrosine phosphorylation of Munc18c facilitates vesicle exocytosis. *The Journal of biological chemistry* **281**, 17624 (Jun 30, 2006).
60. B. Ke, E. Oh, D. C. Thurmond, Doc2beta is a novel Munc18c-interacting partner and positive effector of syntaxin 4-mediated exocytosis. *The Journal of biological chemistry* **282**, 21786 (Jul 27, 2007).
61. A. I. Mendes, P. Matos, S. Moniz, P. Jordan, Protein kinase WNK1 promotes cell surface expression of glucose transporter GLUT1 by regulating a Tre-2/USP6-BUB2-Cdc16 domain family member 4 (TBC1D4)-Rab8A complex. *The Journal of biological chemistry* **285**, 39117 (Dec 10, 2010).
62. J. Stockli *et al.*, Regulation of glucose transporter 4 translocation by the Rab guanosine triphosphatase-activating protein AS160/TBC1D4: role of phosphorylation and membrane association. *Molecular endocrinology* **22**, 2703 (Dec, 2008).
63. C. P. Miinea *et al.*, AS160, the Akt substrate regulating GLUT4 translocation, has a functional Rab GTPase-activating protein domain. *The Biochemical journal* **391**, 87 (Oct 1, 2005).
64. T. Soldati, M. Schliwa, Powering membrane traffic in endocytosis and recycling. *Nature reviews. Molecular cell biology* **7**, 897 (Dec, 2006).
65. C. J. Cheng, C. L. Huang, Activation of PI3-kinase stimulates endocytosis of ROMK via Akt1/SGK1-dependent phosphorylation of WNK1. *Journal of the American Society of Nephrology : JASN* **22**, 460 (Mar, 2011).
66. S. K. Cha, T. Wu, C. L. Huang, Protein kinase C inhibits caveolae-mediated endocytosis of TRPV5. *American journal of physiology. Renal physiology* **294**, F1212 (May, 2008).
67. S. K. Cha, C. L. Huang, WNK4 kinase stimulates caveola-mediated endocytosis of TRPV5 amplifying the dynamic range of regulation of the channel by protein kinase C. *The Journal of biological chemistry* **285**, 6604 (Feb 26, 2010).
68. M. Anitei, T. Wassmer, C. Stange, B. Hoflack, Bidirectional transport between the trans-Golgi network and the endosomal system. *Molecular membrane biology* **27**, 443 (Nov, 2010).

69. A. P. Golbang *et al.*, Regulation of the expression of the Na/Cl cotransporter by WNK4 and WNK1: evidence that accelerated dynamin-dependent endocytosis is not involved. *American journal of physiology. Renal physiology* **291**, F1369 (Dec, 2006).
70. H. Cai *et al.*, WNK4 kinase regulates surface expression of the human sodium chloride cotransporter in mammalian cells. *Kidney international* **69**, 2162 (Jun, 2006).
71. A. R. Subramanya, J. Liu, D. H. Ellison, J. B. Wade, P. A. Welling, WNK4 diverts the thiazide-sensitive NaCl cotransporter to the lysosome and stimulates AP-3 interaction. *The Journal of biological chemistry* **284**, 18471 (Jul 3, 2009).
72. B. Zhou *et al.*, WNK4 enhances the degradation of NCC through a sortilin-mediated lysosomal pathway. *Journal of the American Society of Nephrology : JASN* **21**, 82 (Jan, 2010).
73. A. M. Johnston *et al.*, SPAK, a STE20/SPS1-related kinase that activates the p38 pathway. *Oncogene* **19**, 4290 (Aug 31, 2000).
74. M. Tamari, Y. Daigo, Y. Nakamura, Isolation and characterization of a novel serine threonine kinase gene on chromosome 3p22-21.3. *Journal of human genetics* **44**, 116 (1999).
75. K. Piechotta, N. Garbarini, R. England, E. Delpire, Characterization of the interaction of the stress kinase SPAK with the Na+-K+-2Cl- cotransporter in the nervous system: evidence for a scaffolding role of the kinase. *The Journal of biological chemistry* **278**, 52848 (Dec 26, 2003).
76. K. Piechotta, J. Lu, E. Delpire, Cation chloride cotransporters interact with the stress-related kinases Ste20-related proline-alanine-rich kinase (SPAK) and oxidative stress response 1 (OSR1). *The Journal of biological chemistry* **277**, 50812 (Dec 27, 2002).
77. A. N. Anselmo *et al.*, WNK1 and OSR1 regulate the Na+, K+, 2Cl- cotransporter in HeLa cells. *Proceedings of the National Academy of Sciences of the United States of America* **103**, 10883 (Jul 18, 2006).
78. A. C. Vitari, M. Deak, N. A. Morrice, D. R. Alessi, The WNK1 and WNK4 protein kinases that are mutated in Gordon's hypertension syndrome phosphorylate and activate SPAK and OSR1 protein kinases. *The Biochemical journal* **391**, 17 (Oct 1, 2005).

79. T. Moriguchi *et al.*, WNK1 regulates phosphorylation of cation-chloride-coupled cotransporters via the STE20-related kinases, SPAK and OSR1. *The Journal of biological chemistry* **280**, 42685 (Dec 30, 2005).
80. M. Glover, M. O'Shaughnessy K, SPAK and WNK kinases: a new target for blood pressure treatment? *Current opinion in nephrology and hypertension* **20**, 16 (Jan, 2011).
81. E. J. Hoorn, D. H. Ellison, WNK kinases and the kidney. *Experimental cell research* **318**, 1020 (May 15, 2012).
82. B. E. Xu *et al.*, WNK1 activates SGK1 to regulate the epithelial sodium channel. *Proceedings of the National Academy of Sciences of the United States of America* **102**, 10315 (Jul 19, 2005).
83. C. Richardson *et al.*, Activation of the thiazide-sensitive Na+-Cl- cotransporter by the WNK-regulated kinases SPAK and OSR1. *Journal of cell science* **121**, 675 (Mar 1, 2008).
84. C. Richardson *et al.*, Regulation of the NKCC2 ion cotransporter by SPAK-OSR1-dependent and -independent pathways. *Journal of cell science* **124**, 789 (Mar 1, 2011).
85. B. F. Dowd, B. Forbush, PASK (proline-alanine-rich STE20-related kinase), a regulatory kinase of the Na-K-Cl cotransporter (NKCC1). *The Journal of biological chemistry* **278**, 27347 (Jul 25, 2003).
86. S. S. Yang *et al.*, Molecular pathogenesis of pseudohypoaldosteronism type II: generation and analysis of a Wnk4(D561A/+) knockin mouse model. *Cell metabolism* **5**, 331 (May, 2007).
87. M. Chiga *et al.*, Phenotypes of pseudohypoaldosteronism type II caused by the WNK4 D561A missense mutation are dependent on the WNK-OSR1/SPAK kinase cascade. *Journal of cell science* **124**, 1391 (May 1, 2011).
88. B. P. Zambrowicz *et al.*, Wnk1 kinase deficiency lowers blood pressure in mice: a gene-trap screen to identify potential targets for therapeutic intervention. *Proceedings of the National Academy of Sciences of the United States of America* **100**, 14109 (Nov 25, 2003).
89. C. Delaloy *et al.*, Cardiovascular expression of the mouse WNK1 gene during development and adulthood revealed by a BAC reporter assay. *The American journal of pathology* **169**, 105 (Jul, 2006).

90. J. Xie *et al.*, Endothelial-specific expression of WNK1 kinase is essential for angiogenesis and heart development in mice. *The American journal of pathology* **175**, 1315 (Sep, 2009).
91. S. S. Yang *et al.*, SPAK-knockout mice manifest Gitelman syndrome and impaired vasoconstriction. *Journal of the American Society of Nephrology : JASN* **21**, 1868 (Nov, 2010).
92. J. Xie, J. Yoon, S. S. Yang, S. H. Lin, C. L. Huang, WNK1 Protein Kinase Regulates Embryonic Cardiovascular Development through the OSR1 Signaling Cascade. *The Journal of biological chemistry* **288**, 8566 (Mar 22, 2013).
93. M. Boutros *et al.*, Genome-wide RNAi analysis of growth and viability in Drosophila cells. *Science* **303**, 832 (Feb 6, 2004).
94. N. Mausbacher, T. B. Schreiber, H. Daub, Glycoprotein capture and quantitative phosphoproteomics indicate coordinated regulation of cell migration upon lysophosphatidic acid stimulation. *Molecular & cellular proteomics : MCP* **9**, 2337 (Nov, 2010).
95. C. Hong *et al.*, Epigenome scans and cancer genome sequencing converge on WNK2, a kinase-independent suppressor of cell growth. *Proceedings of the National Academy of Sciences of the United States of America* **104**, 10974 (Jun 26, 2007).
96. J. Luders, T. Stearns, Microtubule-organizing centres: a re-evaluation. *Nature reviews. Molecular cell biology* **8**, 161 (Feb, 2007).
97. S. V. Costes *et al.*, Automatic and quantitative measurement of protein-protein colocalization in live cells. *Biophysical journal* **86**, 3993 (Jun, 2004).
98. H. Y. Yamada, G. J. Gorbsky, Spindle checkpoint function and cellular sensitivity to antimitotic drugs. *Molecular cancer therapeutics* **5**, 2963 (Dec, 2006).
99. R. Kuriyama, G. Keryer, G. G. Borisy, The mitotic spindle of Chinese hamster ovary cells isolated in taxol-containing medium. *Journal of cell science* **66**, 265 (Mar, 1984).
100. K. B. Gagnon, R. England, E. Delpire, Volume sensitivity of cation-Cl- cotransporters is modulated by the interaction of two kinases: Ste20-related proline-alanine-rich kinase and WNK4. *American journal of physiology. Cell physiology* **290**, C134 (Jan, 2006).

101. A. R. Conery, E. Harlow, High-throughput screens in diploid cells identify factors that contribute to the acquisition of chromosomal instability. *Proceedings of the National Academy of Sciences of the United States of America* **107**, 15455 (Aug 31, 2010).
102. M. Carmena, S. Ruchaud, W. C. Earnshaw, Making the Auroras glow: regulation of Aurora A and B kinase function by interacting proteins. *Current opinion in cell biology* **21**, 796 (Dec, 2009).
103. V. Archambault, D. M. Glover, Polo-like kinases: conservation and divergence in their functions and regulation. *Nature reviews. Molecular cell biology* **10**, 265 (Apr, 2009).
104. M. do Carmo Avides, A. Tavares, D. M. Glover, Polo kinase and Asp are needed to promote the mitotic organizing activity of centrosomes. *Nature cell biology* **3**, 421 (Apr, 2001).
105. M. M. Donaldson, A. A. Tavares, H. Ohkura, P. Deak, D. M. Glover, Metaphase arrest with centromere separation in polo mutants of Drosophila. *The Journal of cell biology* **153**, 663 (May 14, 2001).
106. M. De Luca, P. Lavia, G. Guarguaglini, A functional interplay between Aurora-A, Plk1 and TPX2 at spindle poles: Plk1 controls centrosomal localization of Aurora-A and TPX2 spindle association. *Cell cycle* **5**, 296 (Feb, 2006).
107. P. S. Vaughan, P. Miura, M. Henderson, B. Byrne, K. T. Vaughan, A role for regulated binding of p150(Glued) to microtubule plus ends in organelle transport. *The Journal of cell biology* **158**, 305 (Jul 22, 2002).
108. J. R. Kardon, R. D. Vale, Regulators of the cytoplasmic dynein motor. *Nature reviews. Molecular cell biology* **10**, 854 (Dec, 2009).
109. W. L. Lee, M. A. Kaiser, J. A. Cooper, The offloading model for dynein function: differential function of motor subunits. *The Journal of cell biology* **168**, 201 (Jan 17, 2005).
110. J. R. Kardon, S. L. Reck-Peterson, R. D. Vale, Regulation of the processivity and intracellular localization of Saccharomyces cerevisiae dynein by dynactin. *Proceedings of the National Academy of Sciences of the United States of America* **106**, 5669 (Apr 7, 2009).
111. A. Zagorska *et al.*, Regulation of activity and localization of the WNK1 protein kinase by hyperosmotic stress. *The Journal of cell biology* **176**, 89 (Jan 1, 2007).

112. S. Sengupta *et al.*, Interactions with WNK (with no lysine) family members regulate oxidative stress response 1 and ion co-transporter activity. *The Journal of biological chemistry* **287**, 37868 (Nov 2, 2012).
113. X. Shi *et al.*, CEP70 protein interacts with gamma-tubulin to localize at the centrosome and is critical for mitotic spindle assembly. *The Journal of biological chemistry* **286**, 33401 (Sep 23, 2011).
114. X. Shi *et al.*, Cep70 contributes to angiogenesis by modulating microtubule rearrangement and stimulating cell polarization and migration. *Cell cycle* **11**, 1554 (Apr 15, 2012).
115. G. Guarguaglini *et al.*, The forkhead-associated domain protein Cep170 interacts with Polo-like kinase 1 and serves as a marker for mature centrioles. *Molecular biology of the cell* **16**, 1095 (Mar, 2005).
116. S. W. Tu, A. Bugde, K. Luby-Phelps, M. H. Cobb, WNK1 is required for mitosis and abscission. *Proceedings of the National Academy of Sciences of the United States of America* **108**, 1385 (Jan 25, 2011).
117. A. Sorkin, M. Von Zastrow, Signal transduction and endocytosis: close encounters of many kinds. *Nature reviews. Molecular cell biology* **3**, 600 (Aug, 2002).
118. H. Stenmark, Rab GTPases as coordinators of vesicle traffic. *Nature reviews. Molecular cell biology* **10**, 513 (Aug, 2009).
119. M. Johansson *et al.*, Activation of endosomal dynein motors by stepwise assembly of Rab7-RILP-p150Glued, ORP1L, and the receptor betalll spectrin. *The Journal of cell biology* **176**, 459 (Feb 12, 2007).
120. C. C. Hoogenraad *et al.*, Mammalian Golgi-associated Bicaudal-D2 functions in the dynein-dynactin pathway by interacting with these complexes. *The EMBO journal* **20**, 4041 (Aug 1, 2001).
121. C. C. Hoogenraad *et al.*, Bicaudal D induces selective dynein-mediated microtubule minus end-directed transport. *The EMBO journal* **22**, 6004 (Nov 17, 2003).
122. C. Brocker, S. Engelbrecht-Vandre, C. Ungermann, Multisubunit tethering complexes and their role in membrane fusion. *Current biology : CB* **20**, R943 (Nov 9, 2010).
123. T. Wang, Z. Ming, W. Xiaochun, W. Hong, Rab7: role of its protein interaction cascades in endo-lysosomal traffic. *Cellular signalling* **23**, 516 (Mar, 2011).

124. N. Nakamura, A. Hirata, Y. Ohsumi, Y. Wada, Vam2/Vps41p and Vam6/Vps39p are components of a protein complex on the vacuolar membranes and involved in the vacuolar assembly in the yeast Saccharomyces cerevisiae. *The Journal of biological chemistry* **272**, 11344 (Apr 25, 1997).
125. D. F. Seals, G. Eitzen, N. Margolis, W. T. Wickner, A. Price, A Ypt/Rab effector complex containing the Sec1 homolog Vps33p is required for homotypic vacuole fusion. *Proceedings of the National Academy of Sciences of the United States of America* **97**, 9402 (Aug 15, 2000).
126. A. E. Wurmser, T. K. Sato, S. D. Emr, New component of the vacuolar class C-Vps complex couples nucleotide exchange on the Ypt7 GTPase to SNARE-dependent docking and fusion. *The Journal of cell biology* **151**, 551 (Oct 30, 2000).
127. M. A. Akbar, S. Ray, H. Kramer, The SM protein Car/Vps33A regulates SNARE-mediated trafficking to lysosomes and lysosome-related organelles. *Molecular biology of the cell* **20**, 1705 (Mar, 2009).
128. S. M. Di Pietro, E. C. Dell'Angelica, The cell biology of Hermansky-Pudlak syndrome: recent advances. *Traffic* **6**, 525 (Jul, 2005).
129. M. L. Wei, Hermansky-Pudlak syndrome: a disease of protein trafficking and organelle function. *Pigment cell research / sponsored by the European Society for Pigment Cell Research and the International Pigment Cell Society* **19**, 19 (Feb, 2006).
130. Q. S. Qiu, V-ATPase, ScNhx1p and yeast vacuole fusion. *Journal of genetics and genomics = Yi chuan xue bao* **39**, 167 (Apr 20, 2012).
131. F. Peri, C. Nusslein-Volhard, Live imaging of neuronal degradation by microglia reveals a role for v0-ATPase a1 in phagosomal fusion in vivo. *Cell* **133**, 916 (May 30, 2008).
132. W. R. Williamson, D. Wang, A. S. Haberman, P. R. Hiesinger, A dual function of V0-ATPase a1 provides an endolysosomal degradation mechanism in Drosophila melanogaster photoreceptors. *The Journal of cell biology* **189**, 885 (May 31, 2010).
133. E. C. Dell'Angelica, AP-3-dependent trafficking and disease: the first decade. *Current opinion in cell biology* **21**, 552 (Aug, 2009).
134. S. Yadav, S. Puri, A. D. Linstedt, A primary role for Golgi positioning in directed secretion, cell polarity, and wound healing. *Molecular biology of the cell* **20**, 1728 (Mar, 2009).

135. S. Yadav, M. A. Puthenveedu, A. D. Linstedt, Golgin160 recruits the dynein motor to position the Golgi apparatus. *Developmental cell* **23**, 153 (Jul 17, 2012).
136. B. Storrie *et al.*, Electron tomography reveals Rab6 is essential to the trafficking of trans-Golgi clathrin and COPI-coated vesicles and the maintenance of Golgi cisternal number. *Traffic* **13**, 727 (May, 2012).
137. E. Fridman, D. Lichtstein, H. Rosen, Formation of new high density glycogen-microtubule structures is induced by cardiac steroids. *The Journal of biological chemistry* **287**, 6518 (Feb 24, 2012).